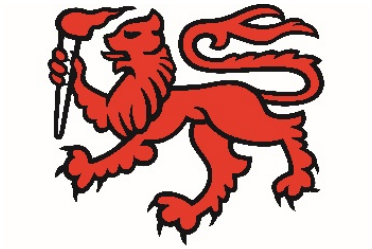

The cells of the oligodendrocyte lineage are differentially altered by tau accumulation and amyloidosis

Solène Clémence Aurélie Ferreira

Master of Sciences

Menzies Institute for Medical Research

Submitted in fulfilment of the requirements for the

Degree of Doctor of Philosophy

University of Tasmania, November 2019

Declaration of Originality

This thesis contains no material which has been accepted for a degree or diploma by the Institute or any other University or institution, except by way of background information duly acknowledged in the thesis, and to the best of my knowledge and belief no material previously published or written by another person except where due acknowledgement is made in the text of the thesis, nor does the thesis contain any material that infringes copyright.

Solène Ferreira

Authority of Access

This thesis may be made available for loan and limited copying and communication in accordance with the Copyright Act 1968.

Solène Ferreira

Statement of Co-Authorship

All of the work included in this thesis was carried out by Solène Ferreira, with the exception of the electrophysiological data presented in **Figure 4.3** and **Figure 4.4**, which was provided by Dr Kimberley Pitman and Associate Professor Kaylene Young.

The following people and institutions contributed to the publication of work undertaken as part of this thesis:

Candidate – Solène Ferreira, Menzies Institute for Medical Research, University of Tasmania

Author 1 – Kimberley A Pitman, Menzies Institute for Medical Research, University of Tasmania

Author 2 – Carlie L Cullen, Menzies Institute for Medical Research, University of Tasmania

Author 3 – Kaylene M Young, Menzies Institute for Medical Research, University of Tasmania

Author 4 – Shiwei Wang, Menzies Institute for Medical Research, University of Tasmania

Author 5 – Nicole Bye, School of Medicine, University of Tasmania

Author 6 – Benjamin S Summers, Menzies Institute for Medical Research, University of Tasmania

Contribution of work by co-authors for each paper:

Paper 1: Located in chapter 3

Solène Ferreira, Kimberley A Pitman, Benjamin S Summers, Shiwei Wang, Kaylene M Young and Carlie L Cullen. Oligodendrogenesis increases in hippocampal grey and white matter prior to locomotor or memory impairment in an adult mouse model of tauopathy. Article published in the *European Journal of Neuroscience*, 17th March 2020.

Author contributions:

Developed the project: Author 2, Author 3.

Carried out the experiments: Candidate, Author 2, Author 3, Author 4, Author 6.

Performed statistical analysis and generated the figures: Candidate, Author 1, Author 2, Author 3.

Wrote the paper: Candidate, Author 1, Author 2, Author 3.

Provided supervision: Author 1, Author 2, Author 3.

Obtained the funding: Author 1, Author 2, Author 3.

Paper 2: Located in chapter 4

Solène Ferreira, Kimberley A Pitman, Shiwei Wang, Nicole Bye, Benjamin S Summers, Kaylene M Young and Carlie L Cullen. Amyloidosis is associated with the formation of thicker myelin in development and increased adult oligodendrogenesis. Submitted to the *Journal of Neuroscience Research,* 23rd January 2020.

Author contributions:

Developed the project: Author 2, Author 3.

Carried out the experiments: Candidate, Author 1, Author 3, Author 4, Author 5, Author 6.

Performed statistical analysis and generated the figures: Candidate, Author 1, Author 2, Author 3.

Wrote the paper: Candidate, Author 1, Author 2, Author 3.

Provided supervision: Author 1, Author 2, Author 3.

Obtained the funding: Author 1, Author 2, Author 3.

We, the undersigned, endorse the above stated contribution of work undertaken for each of the published (or submitted) peer-reviewed manuscripts contributing to this thesis:

Signed:

_____	_____
Solène Ferreira	Associate Professor Kaylene Young
Candidate	Primary Supervisor
Menzies Institute for Medical Research	Menzies Institute for Medical Research
University of Tasmania	University of Tasmania
Date: 28.11.2019	**Date: 02.12.2019**

_____

Professor Alison Venn

Head of School

Menzies Institute for Medical Research

University of Tasmania

Date: 02.12.2019

Statement regarding Published Work contained in Thesis

The publishers of the papers comprising Chapters 3 and 4 hold the copyright for that content and access to the material should be sought from the respective journals. The remaining non

published content of the thesis may be made available for loan and limited copying and communication in accordance with the Copyright Act 1968.

Solène Ferreira

Statement of Ethical Conduct

The research associated with this thesis abides by the international and Australian codes on human and animal experimentation, the guidelines by the Australian Government's Office of the Gene Technology Regulator and the rulings of the Safety, Ethics and Institutional Biosafety Committees of the University. Ethics Approval No/s 13741 and 16151.

Solène Ferreira

Acknowledgements

First, I would like to express my appreciation to the funding bodies that provided my scholarship and allowed this project to happen.

I would like to express my immense gratitude to my supervisors, Associate Professor Kaylene Young, Dr Kimberley Pitman and Dr Carlie Cullen for their support during the past four years. I cannot thank you enough for your guidance and assistance. I would like to thank Associate Professor Kaylene Young for giving me the opportunity to be a PhD student in the "glial mutant ninja turtles" lab. I would like to thank Dr Kimberley Pitman for her support during the first year of my PhD. Finally, I would like to particularly thank Dr Carlie Cullen for sharing her expertise, wisdom and great taste in music. You are an amazing mentor, thank you!

I must acknowledge all the members of the Young, Foa, Lin and Small labs for their support and feedback during my PhD. I would also like to express my gratitude for their technical help to Dr Olivier Bibari, Dr Nicole Bye and the staff of the animal facility at the Menzies Institute for Medical Research and the Cambridge facility – especially Peta Lawrie, Lynda Mahoney, Lisa Harding and Keri Smith.

I would like to thank my fellow PhD students and friends. Sarah, Emma, Cassie, Isabel, Kirianne, Raphael, Andy and the rest of the 'Vanilla team' – it was great to share this adventure with you.

I would also like to thank my friends and family back home and in Australia for their fantastic support. Camille, Stefan and Lilie – thank you for your visits while I was far away from

everyone else. To my housemates – thank you for your tremendous encouragement throughout my PhD. Louise – thank you for your support during the first year of my PhD. Jordie – thank you for keeping me sane with your occasional ‘Are you okay?’, being a great housemate and a fantastic friend! Last but not least, I would like to thank the original lab gang – Macarena and Yilan - without you girls, this journey would have been completely different. I am happy we pulled through this experience together as out of this I gained two fabulous friends. From New-Zealand to China, stopping by Chile and France; this is only the beginning!

Table of Contents

List of Figures and Tables

List of Abbreviations

Aβ	Amyloid beta
AD	Alzheimer's disease
AMPA	α-amino-3-hydroxy-5-methyl-4-isoxazole propionate
ANOVA	Analysis of Variance
APC	Adenomatous polyposis coli
APP	Amyloid precursor protein
ASPA	Aspartoacylase
BCAS1	Breast Carcinoma Amplified Sequence 1
BrdU	Bromodeoxyuridine
CA1	Cornu Ammonis field 1
CA2	Cornu Ammonis field 2
CNP	2',3'-cyclic nucleotide 3'-phosphodiesterase
CNQX	6-cyano-7-nitroquinoxaline-2,3-dione
CNS	Central nervous system
CY5	Cyanine 5
DAPI	4',6-diamidino-2-phenylindole
DNA	Deoxyribonucleic acid
EdU	5-ethynyl-2'-deoxyuridine
ENPP6	Ectonucleotide Pyrophosphatase Phosphodiesterase 6
FCS	Fetal Calf Serum / Fetal Bovine Serum
FITC	Fluorescein isothiocyanate
GA	Glutaraldehyde
GABA	Gamma-aminobutyric acid

GFP	Green fluorescent protein
HRP	Horseradish peroxidase
Iba1	Ionized calcium-binding adapter molecule 1
KA	Kainate
LINGO-1	Leucine rich repeat and Ig domain containing NOGO receptor interacting protein 1
MAG	Myelin-Associated Glycoprotein
MAPT	Microtubule-Associated Protein Tau gene
MBP	Myelin Basic Protein
MOG	Myelin Oligodendrocyte Glycoprotein
MyRF	Myelin Regulatory Factor
NG2	Neural / Glial antigen 2
OPC	Oligodendrocyte Progenitor Cell
P30, P60, etc.	Postnatal day 30, 60, etc.
PBS	Phosphate Buffer Saline
PCR	Polymerase Chain Reaction
PDGFβ	Platelet Derived Growth Factor-beta chain
PDGFRα	Platelet-Derived Growth Factor Receptor alpha
PFA	Paraformaldehyde
PLP	Proteolipid protein
PSEN1	Presenilin 1
PSEN2	Presenilin 2
PTX	Picrotoxin
PVDF	Polyvinylidene fluoride
RIPA	Radioimmunoprecipitation assay

RMP	Resting membrane potential
SD	Standard deviation
SDS	Sodium dodecyl sulfate
SEM	Standard error of the mean
TAE	Tris-Acetate EDTA
Tau	Microtubule-Associated Protein Tau
TBS-T	0.2% Tween-20 in Tris Buffered Saline
TEM	Transmission electron microscopy
TRITC	Tetramethylrhodamine isothiocyanate
WT	Wildtype
YFP	Yellow Fluorescent Protein

Abstract

Oligodendrocytes produce and wrap an insulating, fatty substance called myelin around axons to increase the conduction velocity of action potentials along these axons and to provide them with critical metabolic support. Highly myelinated white matter regions are amongst the first to be damaged in Alzheimer's disease (AD), and early oligodendrocyte damage has been detected in transgenic mice carrying human genetic variants associated with the development of AD. In diseases such as multiple sclerosis, immature brain cells called oligodendrocyte progenitor cells (OPCs) proliferate and differentiate into myelinating oligodendrocytes in an attempt to replace oligodendrocytes lost to the disease, restore action potential conduction speed and protect neurons from further damage. However, OPC fate in the early stages of AD-like pathology is unknown.

In this thesis, I have shown that the cells of the oligodendrocyte lineage respond differently to hyperphosphorylated microtubule-associated protein tau (tau) (Chapter 3) and amyloidosis (Chapter 4), two major pathological features of AD, respectively recapitulated in transgenic mice by the overexpression in neurons of a human genetic variant of *microtubule-associated protein tau* (*MAPT)* or the *amyloid precursor protein* (*APP*). Overexpression of *MAPT* in neurons indirectly increased new oligodendrocyte addition throughout the brain; however, this was not associated with a change in total oligodendrocyte number, proportion of myelinated axons and myelin thickness in *MAPT* mice compared to WT (Chapter 3). The OPC response to glutamate and GABA was unchanged in pre-symptomatic *MAPT* mice; however, OPC responded more robustly to GABA in early amyloid pathology. By overexpressing *APP* in neurons and oligodendrocytes throughout life, developmental myelin thickness was increased, but amyloid plaque formation was also coincident with an increase in oligodendrogenesis between 5 and 6 months of age in *APP* mice (Chapter 4). Together, this thesis suggests that

oligodendrocyte turnover is an early feature of both tau and amyloid pathology, while myelin remodelling only occurs in amyloid pathology, which may result from neurotransmitter or excitatory-inhibitory signalling imbalance within the neuronal network.

My data suggest that OPCs and oligodendrocytes are affected by both tauopathy and amyloidosis, which are critical aspects of pathology in people diagnosed with AD. More specifically, my data suggest that oligodendrocytes are particularly susceptible to undergo cell death in response to these pathological insults. The lost oligodendrocytes are replaced by OPCs early on, suggesting that early interventions that promote oligodendrocyte survival and oligodendrogenesis could be very beneficial for preserving neural circuit function in people with AD, and slowing neurodegeneration in other tauopathies.

Chapter 1: Introduction

The central nervous system (CNS) includes the brain, spinal cord and optic nerve; and is responsible for cognition and executive function. The CNS is composed of neurons, which are the electrically active cells critical for neurotransmission (reviewed by Yuste, 2015); vascular cells, which regulate blood flow (reviewed by Mazurek et al., 2017); and three major types of glial cells - microglia, astrocytes and oligodendrocytes. Microglia are critical for maintaining brain homeostasis through their role in clearing cellular debris (Ayata et al., 2018; Villani et al., 2019) and pruning synapses (Paolicelli et al., 2011). By contrast, astrocytes ensure brain homeostasis through neurotransmitters reuptake (Voutsinos-Porche et al., 2003; Cho et al., 2018), delivery of nutrients from blood-vessels to the electrically conducting parts of neurons known as axons (García-Cáceres et al., 2016) and maintenance of ion balance at the synapse (Sibille et al., 2015). The third glial cell type, the oligodendrocytes, create and wrap a lipid and protein rich substance known as myelin around axons, which facilitates their rapid saltatory conduction of action potentials (reviewed by Hughes and Appel, 2016). Small myelinic channels in the myelin sheath also allow oligodendrocytes to provide critical metabolic support to axons (Fünfschilling et al., 2012; Lee et al., 2012; Meyer et al., 2018). Each glial cell type is critical for CNS function and the dysregulation or loss of these cells has been shown to cause or exacerbate a number of pathological conditions.

Oligodendrocyte death and the associated myelin loss, known as demyelination, are key pathological feature of multiple sclerosis (Traka et al., 2015; Way et al., 2015), and can also be observed in various types of dementia, including frontotemporal dementia (Kovacs et al., 2008; Zhang et al., 2009) and Alzheimer's disease (AD: Zhang et al., 2009; Gagyi et al., 2012). This thesis will explore the impact that the expression of two human pathological proteins, that

are known to result in frontotemporal dementia or AD, have on the behaviour of oligodendrocytes and their precursor cells, the oligodendrocyte progenitor cells (OPCs).

1.1. Developmental oligodendrogenesis

OPCs also known as NG2 (neural / glial antigen 2) glia or polydendrocytes are immature precursor cells that give rise to mature myelinating oligodendrocytes in the developing (Zhu et al., 2008, 2011) and mature (Dimou et al., 2008; Rivers et al., 2008; Kang et al., 2010; Zhu et al., 2011; Young et al., 2013) CNS. OPC can be identified *in situ* by their expression of the chondroitin sulphate proteoglycan NG2 (Nishiyama et al., 1996), the mitogenic receptor platelet-derived growth factor receptor α (PDGFRα; Pringle et al., 1992) and the transcription factor OLIG2 (Ligon et al., 2004, 2006). During mouse development OPCs are produced from neural stem cells located in the ventricular zone of the brain (Kessaris et al., 2006) and spinal cord (Fu et al., 2002; Masahira et al., 2006). In the brain, OPCs are generated in three waves: the first involves OPC production from neural stem cells located in the medial ganglionic eminence at embryonic day 12.5; the second comprises OPC production from the lateral and caudal ganglionic eminence at embryonic day 15.5, and the third wave of OPC generation occurs after birth, with OPCs being produced from neural stem cells in the ventricular zone of the cortex (Kessaris et al., 2006).

Once formed, OPC undergoes symmetric or asymmetric division resulting in two OPCs or an OPC and a differentiating oligodendrocyte (Sugiarto et al., 2011; Zhu et al., 2011; Hill et al., 2014; Boda et al., 2015), or alternatively directly differentiates to produce an oligodendrocyte. In rodents, OPCs start to differentiate into mature myelinating oligodendrocytes after birth with the peak period of oligodendrogenesis observed between postnatal day (P)7 and P21 in the optic nerve (Barres et al., 1992). OPC production, differentiation and oligodendrocyte

maturation in the human CNS follow a similar pattern, with OPCs being observed from 9 weeks of gestation; however, they commence differentiation prior to birth (Back et al., 2001; Jakovcevski and Zecevic, 2005), with the first myelin sheaths being produced by oligodendrocytes at approximately 18 weeks of gestation (Jakovcevski and Zecevic, 2005; Jakovcevski et al., 2007, 2009).

OPC differentiation is associated with significant changes in gene transcription (Copray et al., 2006; Maire et al., 2010; Hornig et al., 2013; Zhu et al., 2014; **Figure 1.1**). NG2 and PDGFRα expression are downregulated (Zhou et al., 2000, 2001; Lu et al., 2002; Zhou and Anderson, 2002; Jakovcevski and Zecevic, 2005) as an OPC becomes a premyelinating oligodendrocyte, which can be identified by the expression of ectonucleotide pyrophosphatase phosphodiesterase 6 (ENPP6; Zhang et al., 2014; Xiao et al., 2016), breast carcinoma amplified sequence 1 (BCAS1; Fard et al., 2017) and the transcription factor critical for oligodendrocyte maturation, myelin regulatory factor (MyRF; Cahoy et al., 2008; Emery et al., 2009; Bujalka et al., 2013; Hornig et al., 2013). MyRF expression in premyelinating oligodendrocytes triggers the expression of myelin proteins leading to their maturation into myelinating oligodendrocytes (Emery et al., 2009).

In the developing CNS, cell death allows the removal of unnecessary oligodendrocytes (Barres et al., 1992; Trapp et al., 1997). In the rat optic nerve, cell death peaks in the first 10 days of postnatal life with 0.25% of all cells dying, but decreases drastically by P45 (Barres et al., 1992). Between P4 and P12, ~15% of all propidium iodide-labelled cells with pyknotic nuclei co-labelled with the oligodendrocyte-specific RIP antigen (Berger and Frotscher, 1994; Butt et al., 1995; Watanabe et al., 2006), suggesting that a substantial number of oligodendrocytes die in the rat optic nerve. As the RIP antigen is an an intracellular protein that might be digested

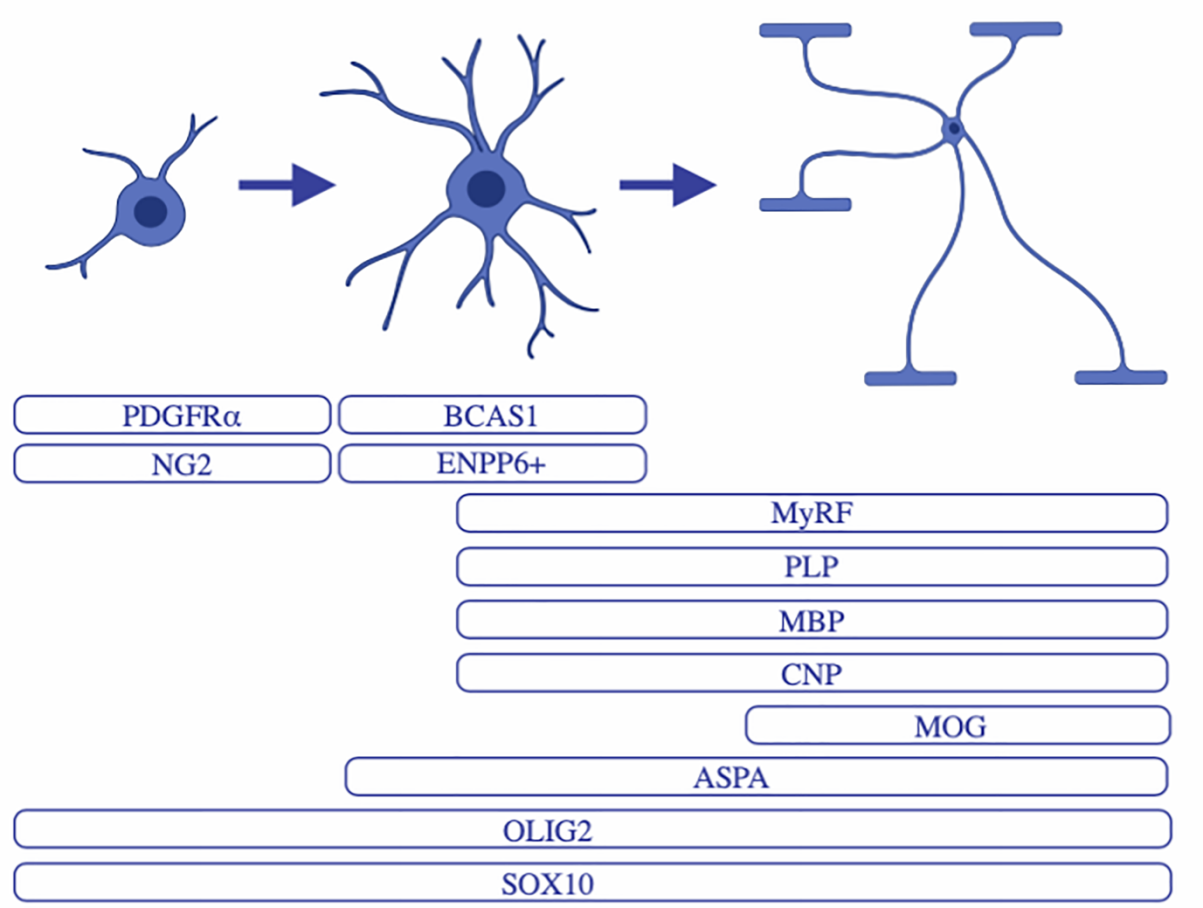

Figure 1.1. Schematic of OPC differentiation

OPC can be identified by their expression of the mitogenic receptor PDGFRα and the proteoglycan NG2. As they differentiate into premyelinating oligodendrocytes, the expression of these markers is downregulated, and expression of BCAS1, ENPP6, ASPA, MyRF, PLP, MBP and CNP are induced. As premyelinating oligodendrocytes mature into myelinating oligodendrocytes, expression of BCAS1 and ENPP6 is lost, and expression of MOG is induced. All the cells of the oligodendrocyte lineage can be identified by their expression of the transcription factors OLIG2 and SOX10. Figure created with Biorender.

rapidly during cell death, it is unlikely to allow the detection of oligodendrocytes in late stages of programmed cell death. To address this, hybridoma cells that secreted antibodies against an extracellular oligodendrocyte antigen (galactocerebroside) were injected into the subarachnoid space of P2 rats. This approach allowed the comprehensive and long-lived labelling of these cells and revealed that ~91% of cells that were dying in the P5 rat optic nerve were oligodendrocytes (Barres et al., 1992). Furthermore, injection of bromodeoxyuridine (BrdU) in the optic nerve at P15 revealed that oligodendrocytes die within 2 to 3 days after being generated (Barres et al., 1992). In the developing rat cerebral cortex, ~20% of premyelinating oligodendrocytes undergo cell death between P7 and P21; and by P28 it increases to ~37% (Trapp et al., 1997) as premyelinating oligodendrocytes that are not necessary for myelination degenerate during development (Barres et al., 1992; Trapp et al., 1997). However, the majority of premyelinating oligodendrocytes undergo further transcriptional and morphological changes to become mature myelinating oligodendrocytes (Fitzner et al., 2006; Emery et al., 2009).

As oligodendrocytes differentiate into mature myelinating oligodendrocytes, they extend many new cellular processes (Fitzner et al., 2006). This process is supported by alterations to the cytoskeleton (Wilson and Brophy, 1989). Process outgrowth requires the transport of mRNAs that code for the synthesis of myelin-specific proteins such as myelin basic protein (MBP), to the cellular extensions (Ainger et al., 1993, 1997; Carson et al., 1997; Smith, 2004). MBP mRNA translocation in oligodendrocytes depends on intact microtubules and kinesins (Carson et al., 1997), which require expression of microtubule-associated proteins such as microtubule-associated protein 2 and microtubule-associated protein tau (tau) to stabilize and organize the microtubule network (Al-Bassam et al., 2002; Kadavath et al., 2015; Shigematsu et al., 2018). Microtubule-associated protein 2 and tau are expressed by oligodendrocytes *in vitro* (Müller et

al., 1997; Richter-Landsberg and Gorath, 1999) and facilitate oligodendrocyte process outgrowth as well as the formation and maintenance of myelin sheaths.

1.2. Myelination

During the early stages of myelin formation also called myelination or myelinogenesis, oligodendrocytes produce a cholesterol-rich membrane (Saher et al., 2005) looped around axons that progressively forms a compact multilamellar spiral structure (Aggarwal et al., 2013; Snaidero et al., 2014). Each oligodendrocyte ensheathes multiple selected axon segments (Matthews and Duncan, 1971; Chong et al., 2012). The ensheathment process occurs over a brief time window. For example, ensheathment is completed within 12-18 hours in rat cortical cultures (Downes and Mullins, 2014), while oligodendrocytes produce new myelin internodes during a period of 5 hours in zebrafish (Czopka et al., 2013). In zebrafish, a small proportion of the myelin sheaths is subsequently rapidly retracted over the following 2 days after which oligodendrocyte morphology and myelin sheath number remain stable.

The myelin sheath is composed of various lipids and proteins (**Figure 1.2a**). By transmission electron microscopy (TEM), the myelin sheath appears to have alternative major dense lines, or dark and light layers (reviewed by Simons and Nave, 2016). Myelin is 40% water and its dry mass includes 70% lipid and 30% protein (O'Brien and Sampson, 1965), which form the different dark and light layers observed using TEM (**Figure 1.2b**). Myelin contains cholesterol, phospholipids and glycolipids, and is particularly rich in glycosphingolipids, including galactocerebrosides (Raff et al., 1978; Zalc et al., 1981). MBP and proteolipid protein (PLP) represent 30% and 50% of myelin proteins respectively. Other proteins, such as 2',3'-cyclic nucleotide 3'-phosphodiesterase (CNP), myelin-associated glycoprotein (MAG)

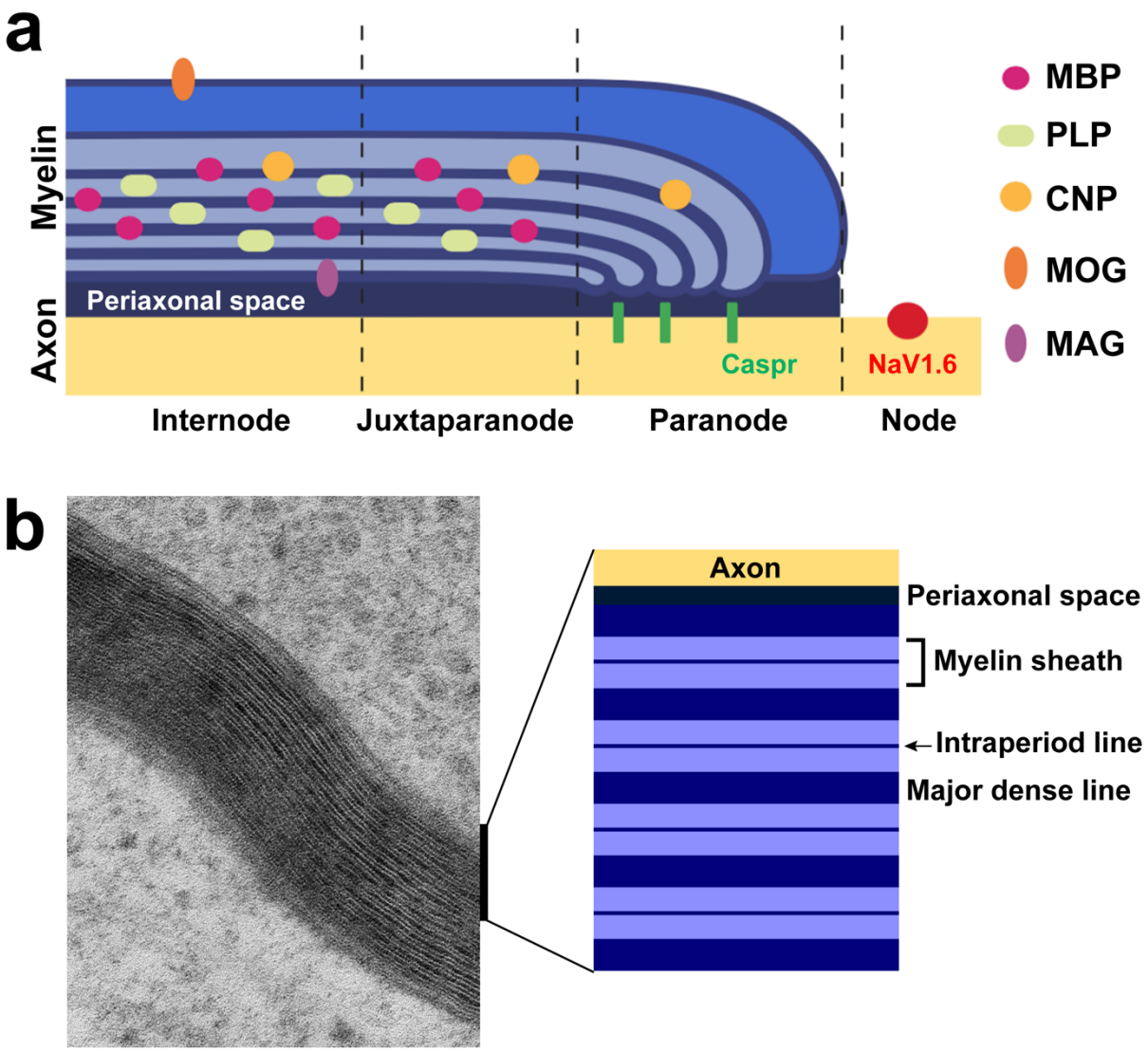

Figure 1.2. Schematic of myelin structure

a) *Myelin is composed of various lipids and proteins including MBP, PLP, CNP, MOG and MAG. These proteins regulate myelin formation, compaction and maintenance.* ***b)*** *As myelin sheaths are wrapped around the axon, they form concentric myelin layers, and each layer is separated by a major dense line. Figure partially created with Biorender.*

and myelin oligodendrocyte glycoprotein (MOG) are also present (Scolding et al., 1989; Yin et al., 1998; Marques et al., 2016; Snaidero et al., 2017).

Proteins within the myelin membrane regulate myelin sheath compaction and stability, and the appropriate compaction of myelin is required for the fast transmission of action potentials as well as the ability of oligodendrocytes to offer long-term metabolic support to axons (Gutiérrez et al., 1995; Griffiths et al., 1998; Lappe-Siefke et al., 2003). To provide an example, MBP is required for the compaction and maintenance of the myelin sheath (Allinquant et al., 1991; Weil et al., 2016), with the *MBP* gene deleted shiverer mice showing myelin decompaction (Allinquant et al., 1991), and MBP loss causing myelin breakdown and ultimately axonal degeneration (Weil et al., 2016). The ratio of CNP to MBP protein is also important, as it determines the level of myelin compaction (Snaidero et al., 2017), with CNP counteracting the MBP-driven myelin compaction (Snaidero et al., 2017) and allowing oligodendrocyte process outgrowth (Lee et al., 2005) and the formation of the axo-myelinic channels necessary for axonal support (Lappe-Siefke et al., 2003). Consequently, mice overexpressing CNP have impaired MBP accumulation and reduced myelin compaction (Gravel et al., 1996; Yin et al., 1997). PLP is largely required for myelin maintenance, as *Plp*-deficient mice develop myelin decompaction in the optic nerve (Boison and Stoffel, 1994; Klugmann et al., 1997; Rosenbluth et al., 2006), which is ultimately associated with axonal mitochondrial dysfunction and axon degeneration (Yin et al., 2016a). Premature oligodendrocyte death observed from P4 in the spinal cord, P12 in the optic nerve and P16 in the corpus callosum of jimpy mice expressing a *plp* mutation has been associated with gross myelin deficit observed in these mice (Knapp et al., 1986). Similarly, within 6 months of gene deletion, tamoxifen-inducible *Plp*-deficient mice also show myelin disassembly and outfoldings of the sheath, as well as axonal sprouting and spheroid formation in the optic nerve (Lüders et al., 2019).

Once generated, oligodendrocytes and their myelin internodes are remarkably stable throughout life (Tripathi et al., 2017; Auer et al., 2018; Hill et al., 2018; Hughes et al., 2018). For example, in the mouse corpus callosum, ~90% of developmentally born oligodendrocytes survive for over 8 months, compared with ~70% in the motor cortex, and ~60% in the spinal cord and optic nerve (Tripathi et al., 2017). While the oligodendrocytes themselves largely survived long-term, a subset of myelin internodes was found to extend or retract (Auer et al., 2018; Hill et al., 2018), indicating that mature myelinating oligodendrocytes may retain some level of plasticity. Indeed the level of myelin plasticity observed in the adult CNS is quite significant, as in addition to plastic changes made by existing mature oligodendrocytes, it has been demonstrated that new oligodendrocytes are added to the brain of adult rodents (Rivers et al., 2008; Young et al., 2013; Hill et al., 2018; Hughes et al., 2018) and humans (Yeung et al., 2014) throughout life.

1.3. Oligodendrogenesis occurs in the healthy adult brain

Following developmental oligodendrogenesis, OPCs are maintained in the adult CNS (Wren et al., 1992). In the rodent brain, OPCs represent 5-8% of all cells (Dawson et al., 2003; Dimou et al., 2008; Rivers et al., 2008) and the population is maintained in the brain parenchyma through a process of self-renewal (Wren et al., 1992; Menn et al., 2006); however, a small number of new OPCs are generated from stem cells in the subventricular zone (Nait-Oumesmar et al., 1999; Picard-Riera et al., 2002; Menn et al., 2006). Like their developmental counterparts, adult OPCs express the chondroitin sulphate proteoglycan NG2, the mitogenic receptor PDGFRα and the O4 glycolipid antigen, and while they proliferate less frequently, and differentiate more slowly (Wolswijk et al., 1989, 1990; Wren et al., 1992; Psachoulia et al., 2009), they continue to generate new oligodendrocytes throughout life. Of the premyelinating oligodendrocytes produced in the mouse cortex between ~8-14 months of age,

Hughes et al. (2018) demonstrated that only ~22% survived to form mature myelinating oligodendrocytes. These data suggest that more cells are born than are required for oligodendrocyte addition. However, as adult parenchymal OPCs increasingly express senescence markers (Kujuro et al., 2010) and show reduced proliferation with increasing age (Lasiene et al., 2009; Young et al., 2013), the steady supply of immature premyelinating oligodendrocytes is diminished with aging.

1.4. Oligodendrocyte loss with aging and injury

White and grey matter volumes reduce with aging in human (Giorgio et al., 2010; Gogniat et al., 2018), and rhesus monkey brain (Wisco et al., 2008), and this pattern of tissue loss is also seen in senescence accelerated mice (Tanaka et al., 2005). Senescence accelerated mice experience oligodendrocyte loss from the hippocampus, but have normal numbers of oligodendrocytes in the cerebral cortex and optic nerve at 10 months of age (Tanaka et al., 2005). With normal aging, mice experience cortical oligodendrocyte loss from approximately 2 years of age (Hill et al., 2018). In aging, increased oxidative stress (Dröge and Schipper, 2007), neuroinflammation (Mecha et al., 2012) and changes in cytokine production (Chen et al., 2008) may stress oligodendrocytes, which have a high metabolic demand, and this may render them susceptible to cell death. However, oligodendrocytes can also switch their energy consumption in response to nutrient deprivation to prioritise cell survival (Rone et al., 2016). This ability may explain discrepancy between the decreased oligodendrocyte density in mice and increased oligodendrocyte population in rhesus monkeys (Peters, 2004) but relatively stable oligodendrocyte population in humans during aging (Yeung et al., 2014). Indeed to promote their survival following metabolic stress, human oligodendrocytes have the ability to reduce glycolytic ATP production leading to myelin process withdrawal and demyelination (Rone et al., 2016).

Demyelination is a process inducing the degeneration and loss of myelin sheaths, and is a key pathological feature of multiple sclerosis (Haider et al., 2016; Schirmer et al., 2019). Multiple sclerosis is an autoimmune disease in which peripheral immune cells invade the CNS and cause myelin loss from discrete regions referred to as lesions. Lesions develop in the brain, spinal cord and optic nerve, and lead to motor and cognitive impairment (Manrique-Hoyos et al., 2012; Hulst et al., 2013; Sbardella et al., 2013). People are generally diagnosed with multiple sclerosis between 20 and 45 years of age and the disease affects three times as many women as men (Evans et al., 2013). A variety of immunomodulatory drugs can be effective reducing immune cell infiltration of the CNS (reviewed by Goldenberg, 2012); however, no treatment is currently available to prevent oligodendrocyte death and demyelination or promote oligodendrogenesis and remyelination.

1.5. Remyelination is mediated by oligodendrocyte addition to the brain

Remyelination is the process by which OPCs form new oligodendrocytes that elaborate new myelin sheaths on previously demyelinated axons (Franklin et al., 1997; Gensert and Goldman, 1997; **Figure 1.3**). Parenchymal OPCs and OPCs newly formed in the subventricular zone of the adult mouse brain successfully produce new oligodendrocytes involved in the spontaneous remyelination process following demyelination (Nait-Oumesmar et al., 1999; Menn et al., 2006; Serwanski et al., 2018). OPCs from the subventricular zone have been shown to remyelinate more efficiently in the short-term, while parenchymal OPCs have been shown to produce long-term repair following cuprizone-induced demyelination (Brousse et al., 2015). New oligodendrocytes may be added to a lesion site following demyelination through migration of neural progenitors from the subventricular zone, which produce OPCs that later

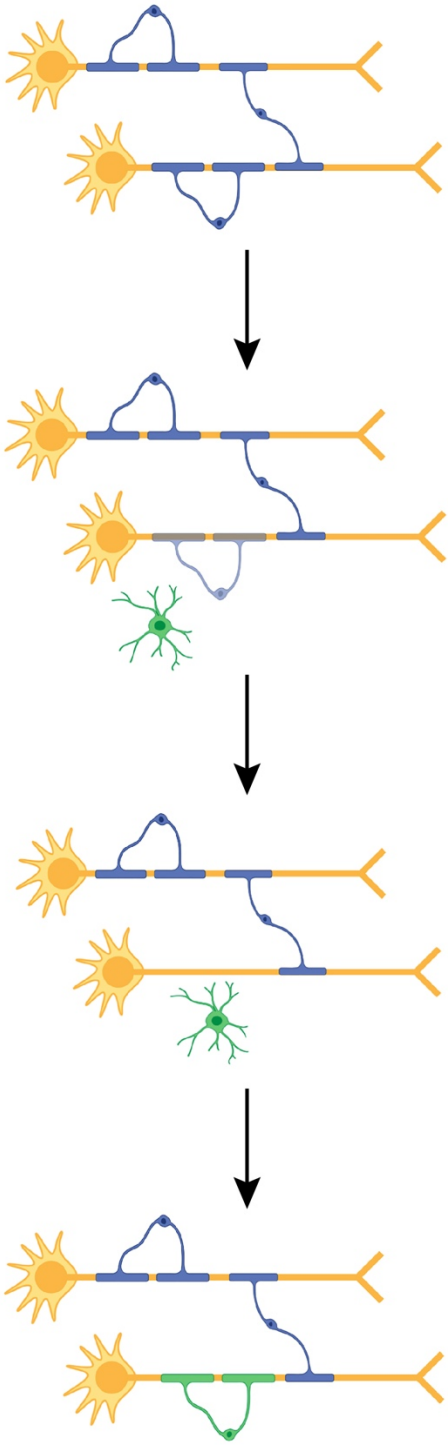

Figure 1.3. Schematic of remyelination by new oligodendrocyte addition

When an oligodendrocyte dies (grey), an OPC or premyelinating oligodendrocyte (green) can contact the demyelinated axon and differentiate into a new mature, myelinating oligodendrocyte and wrap new myelin sheaths around the axon. Figure created with Biorender.

proliferate and differentiate into immature and mature myelinating oligodendrocytes (Xing et al., 2014). Following 4 weeks of cuprizone-induced demyelination in mice, OPC number tripled in the corpus callosum, the oligodendrocyte population was replaced within 1 week of recovery, and remyelination was completed within 6 weeks (Baxi et al., 2017). While OPCs can differentiate into oligodendrocytes or astrocytes *in vitro* (Raff et al., 1983) and *in vivo* (Zhu et al., 2007), they preferentially differentiate into oligodendrocytes following induced demyelination in the corpus callosum (Nait-Oumesmar et al., 1999) and spinal cord (Kang et al., 2010; Tripathi et al., 2010) of transgenic mice.

The myelin formed during remyelination is thinner and shorter than myelin formed during development but can still protect axons (Duncan et al., 2017). Axonal conduction is improved by new myelin internode addition as it restores saltatory conduction; however, axonal conduction is not as rapid following remyelination as it was prior to demyelination (Brill et al., 1977; Blakemore and Murray, 1981). Using TEM, remyelinated axons can be distinguished from developmentally myelinated axons (Gledhill and McDonald, 1977; Prineas and Connell, 1979; Blakemore and Murray, 1981) with the exception of smaller diameter axons (Stidworthy et al., 2003). However, Powers et al. (2013) showed that 6 months after contusion-induced partial spinal cord demyelination, remyelinated and developmentally myelinated axons are indistinguishable with the exception of the largest diameter axons.

In advanced demyelinating diseases, oligodendrocytes establish contact with axons but fail to myelinate, which result in axonal dystrophy, swelling and degeneration (Chang et al., 2002). OPCs and premyelinating oligodendrocytes have been identified in demyelinated regions (Boyd et al., 2013; Fard et al., 2017) when mature oligodendrocytes are rare (Chang et al., 2002; Kuhlmann et al., 2008). For successful remyelination, OPC proliferation,

oligodendrocyte differentiation and survival must be promoted. In the past decade, various factors have been identified that can enhance remyelination *in vitro* and *in vivo* including the neuregulin, neurotrophin-3 and the brain-derived neurotrophic factor, which promote OPC proliferation, differentiation and remyelination (Vondran et al., 2011; Lundgaard et al., 2013; Wong et al., 2013; McTigue et al., 2018).

Myelin loss is observed in a number of conditions that are not classically thought of as demyelinating diseases. For example, myelin loss has been detected in multiple system atrophy (Wakabayashi et al., 1998), amyotrophic lateral sclerosis (Philips et al., 2013), traumatic brain injury (Flygt et al., 2013, 2016), perinatal white matter injury (Back and Rosenberg, 2014), neuropsychiatric diseases (Tkachev et al., 2003) and other neurodegenerative disorders including frontotemporal dementia (Zhang et al., 2009) and AD (Bartzokis et al., 2004; Zhan et al., 2014; Dean et al., 2017). However, the extent of oligodendrocyte loss and replacement has been poorly characterised in many of these conditions.

1.6. Alzheimer's disease

AD is a neurodegenerative disease and the most common form of dementia. It is characterized by significant brain atrophy (Jack et al., 2010), memory loss and executive function decline (Garcia-Alvarez et al., 2019). Personality and behavioural changes such as enhanced paranoia, aggression, delusions, hallucinations, apathy, elevated fear and sleep disturbances are often observed in AD patients (McKhann et al., 1984). Clinically, AD can be partially diagnosed using multiple tests and the medical history of each patient but the diagnosis always has to be confirmed post-mortem by brain tissue analysis with assessment of amyloid beta (Aβ) and tau biomarkers in the cerebrospinal fluid (Andreasen et al., 2001). The formation of amyloid plaques (amyloid pathology, accumulated Aβ) and neurofibrillary tangles (tau pathology,

aggregated tau) were first described in 1906 by German psychiatrist and neurologist Alois Alzheimer (translation of original paper by Stelzmann et al., 1995; Graeber and Mehraein, 1999); and are now known as the main pathological features of AD. However, more than a century after this discovery, the underlying cause of AD in the majority of patients remains unclear (reviewed by Selkoe, 2001).

AD patients are generally classified as having familial or sporadic AD depending on the presence or absence of an inherited genetic mutation known to precipitate the disease (Haass et al., 1995; Lemere et al., 1996; Cruchaga et al., 2012; Jin et al., 2012; Hatami et al., 2017). Familial AD has been the main form studied in the past decades while sporadic AD actually represents about 99% of all AD cases (Goedert and Spillantini, 2006). It is not possible to produce faithful mouse models of sporadic AD without knowing the precise cause of this disease in humans; however, some mouse models have been developed that produce age-related deficits in memory, that are being used in this context. For example, high-cholesterol diet models were generated to investigate lipid mechanism disorders associated with AD, while senescence-accelerated models were developed to define aging implication on AD progression (reviewed by Zhang et al., 2020). None of these models are a true model of sporadic AD, but allow instead specific investigation of defective mechanisms observed in human sporadic AD cases. Most research studies instead use mouse models of familial AD, which cannot be used to study the cause of sporadic AD, but can be used to gain insight into the molecular and cellular changes that are common to both familial and sporadic forms of AD. It has been established that the pathological phenotype produced by both forms of AD is very similar and can often be mistaken if the age of the patient is unknown by the neuropathologist studying the case (McKhann et al., 1984). The vast majority of genetic mutations known to cause familial AD

are found within the *amyloid precursor protein* (*APP)* gene, or genes coding for proteins known to alter APP expression and activity (Blauwendraat et al., 2019; Giau et al., 2019).

1.6.1. Amyloid pathology

Amyloid pathology is mainly characterized by the extracellular aggregation of Aβ peptides forming amyloid plaques also called senile plaques, which disrupt synapses and cause neuronal loss (reviewed by Selkoe and Hardy, 2016; Kashyap et al., 2019). The Aβ peptides result from the cleavage of the single transmembrane APP by beta secretase and gamma secretase (Kang et al., 1987; Vassar et al., 1999; Takasugi et al., 2003). The main peptides obtained from this cleavage are the $A\beta_{40}$ and $A\beta_{42}$ oligomers (Citron et al., 1996; Qiang et al., 2017). $A\beta_{42}$ is more likely to aggregate and form amyloid plaques while $A\beta_{40}$ is the main form of circulating Aβ in the plasma, cerebrospinal fluid and brain interstitial fluid (Roher et al., 2009).

The primary physiological function of APP is unclear; however, many roles have been proposed, including the facilitation of intracellular and extracellular signalling, gene regulation and activity as a trophic factor (reviewed by Dawkins and Small, 2014). Interestingly, APP levels are elevated at sites of axonal damage and in dystrophic neurites around amyloid plaques suggesting that physiological APP might participate in synaptic repair and homeostasis (Cras et al., 1991; Joachim et al., 1991; Yasuhara et al., 1994). However, mutations in the *APP* gene can affect the ratio of $A\beta_{40}/A\beta_{42}$ and increase the production of $A\beta_{42}$ as well as its aggregation in the extracellular milieu in AD (Levy et al., 1990; Citron et al., 1992; Haass et al., 1995; Cheng et al., 2004). The *APP* gene is located on chromosome 21 and patients with Down syndrome (trisomy 21) have an extra copy of the *APP* gene, which causes an increased risk of developing AD (Potter et al., 2016). Goate et al. (1991) identified the first mutation of the *APP* gene involved in AD as a missense mutation in codon 717 leading to the replacement of a

valine by an isoleucine (Val-Ile), this mutation is now known as the London mutation (Goate et al., 1991). At present, only one mutation of the *APP* gene has been identified as being protective against the development of AD (Hashimoto and Matsuoka, 2014) despite the identification of numerous pathological mutations in *APP* and its associated regulators.

Presenilins are transmembrane proteins involved in the cleavage of APP and genetic mutations affecting the function of these proteins can impact the ratio of $A\beta_{40}/A\beta_{42}$ (Jankowsky et al., 2004). Presenilins 1 (PSEN1) and 2 (PSEN2) are subunits of the protease gamma secretase and mutations of both *PSEN1* and *PSEN2* have been associated with an accelerated AD phenotype development (Steiner et al., 1999; McMillan et al., 2000; Lou et al., 2017; Giau et al., 2019). Notably, Scheuner et al. (1996) showed that mutations of the *PSEN1* gene (on chromosome 14) and *PSEN2* gene (on chromosome 1) led to the increased cleavage of APP to produce more $A\beta_{42}$ and less $A\beta_{40}$ in human plasma, consequently leading to increased amyloid plaque formation in the brain. Jankowsky et al. (2004) showed that decreased $A\beta_{40}/A\beta_{42}$ ratio following $A\beta_{42}$ increase, and subsequent accelerated amyloid pathology were associated with *PSEN1* overexpression rather than *PSEN1* loss of function.

Various AD associated mutations detected in the *APP*, *PSEN1* and *PSEN2* genes have been expressed in transgenic mice to study AD progression (reviewed by Elder et al., 2010). These mutations mostly induce an amino acid substitution, which is called a missense mutation. Commonly studied *APP* mutations include the mutant human *APP* Swedish (K670N, M671L; Mullan et al., 1992), Indiana (V717F; Murrell et al., 1991), London (V717I, Goate et al., 1991) and Florida (I716V; Eckman et al., 1997) AD mutations. In addition, common *PSEN1* mutations used include M146L, L286V, L166P and deltaE9; and finally, the main *PSEN2* mutation used is N141I. By transgenically expressing these pathological mutations, it has been

possible to study disease progression and evaluate the effect of Aβ production and plaque formation on neuronal survival, gliosis, synaptic function and cognitive impairment.

Some of the most commonly used mouse models of amyloid pathology include the J20 (*APP* Swedish and *APP* Indiana mutations; Mucke et al., 2000), APP/PS1 (*APP* Swedish, *PSEN1* L166P; Radde et al., 2006), and 5xFAD (*APP* Swedish, *APP* Florida, *APP* London, *PSEN1* M146L and *PSEN1* L286V mutations; Oakley et al., 2006) mouse lines. All these models present with different pathological time courses and are influenced by the mutations but also the genetic background of the mouse line. The J20 mouse line expressing a three point mutation in the *APP* gene exhibits cognitive impairment at approximately 4 months of age in the radial arm maze (Wright et al., 2013), and which is severe enough to be detected in the Morris water maze at 6-7 months of age (Palop et al., 2003). The cognitive phenotype appears prior to amyloid plaque formation (Hong et al., 2016) and reactive gliosis (Wright et al., 2013), which are detected from 5-6 months of age. By contrast the APP/PS1 mice exhibit amyloid plaque and gliosis at approximately 1 month of age (Radde et al., 2006), synaptic loss from 2 months of age (Bittner et al., 2012), and cognitive impairment from 7 months of age in the Morris water maze (Serneels et al., 2009). On a hybrid background (C57BL/6 x SJL), 5xFAD mice develop amyloid plaques and gliosis at 2 months of age (Oakley et al., 2006), synaptic deficits from 4 months of age and spatial working memory impairment by 4-5 months of age in the Y maze, prior to neuronal loss (Oakley et al., 2006; Devi and Ohno, 2010). On a C57BL/6 background, 5xFAD mice still develop amyloid plaques (Richard et al., 2015) and gliosis (Giannoni et al., 2016) at 2 months of age, yet synaptic deficits (Buskila et al., 2013) are also observed at 2 months of age, followed by synapse loss (Crowe and Ellis-Davies, 2014) and working memory impairment in the cross-maze at 6 months of age and neuronal loss at 12

months of age (Jawhar et al., 2012). Transgenic mice have become precious tools to understand AD development and the progression of the amyloid but also the tau pathology.

1.6.2. Tau pathology

In the healthy brain, tau proteins promote microtubule network integrity (Weingarten et al., 1975; Qiang et al., 2018). There are six isoforms of tau, which are encoded by the *microtubule-associated protein tau* (*MAPT)* gene located on chromosome 17 (Neve et al., 1986; Goedert et al., 1989). These six isoforms are divided in two main groups: those with 3 (3R-tau) or 4 (4R-tau) microtubule binding repeats (Goode et al., 2000; reviewed by Venkatramani and Panda, 2019). Tau isoform composition determines the effectiveness of microtubule assembly; 4R-tau strongly stabilises microtubules and effectively prevents disassembly compared to 3R-tau repeats (Panda et al., 2003). In frontotemporal dementia with parkinsonism-17, *MAPT* mutations shift the 3R:4R ratio, promoting microtubule disassembly (D'Souza et al., 1999). The phosphorylation of tau regulates microtubule assembly (Utton et al., 1997) and tau hyperphosphorylation leads to microtubule disassembly (Alonso et al., 1994) and the formation of neurofibrillary tangles inside neurons (Grundke-Iqbal et al., 1986; Alonso et al., 1996, 2001), which is a pathological characteristic of tauopathies.

In AD, tau can be found in the brain as toxic oligomers that accumulate into neurofibrillary tangles, which are less toxic (D'Orange et al., 2018). Elevated tau and phosphorylated tau levels have been reported in the cerebrospinal fluid of AD patients and those with other tauopathies (Arai et al., 1995, 1997). Khatoon et al. (1992) reported that total tau was four to eight-fold higher in the brain of AD patients relative to age-matched controls due to a significant increase in hyperphosphorylated tau. Köpke et al. (1993) reported that 40% of tau found in the AD brain was hyperphosphorylated oligomeric tau, which is highly toxic *in vitro*

(Gómez-Ramos et al., 2006). The oligomeric toxic form of tau can be removed from the cerebrospinal fluid by promoting protein aggregation into neurofibrillary tangles, which promotes neuronal survival (D'Orange et al., 2018). Phosphorylation of tau at phosphorylation sites Ser262 and Ser214, required for tau detachment from microtubules, protects against its aggregation (Schneider et al., 1999). It has been suggested that neurofibrillary tangles observed in neurons are formed to be cleared but this process would be overwhelmed at some stages, notably due to tau slower turnover rate following acetylation (Noack et al., 2014). Tau aggregates are mainly found in neurons; however, tau inclusions can also be found in astrocytes and oligodendrocytes (Hashimoto et al., 2003; Lin et al., 2003a; Ren et al., 2014). Clearance of abnormal tau aggregates can occur via two main pathways: the ubiquitin-proteasome and the autophagy-lysosomal pathways (Krishnamurthy et al., 2011; Leyk et al., 2015; Guo et al., 2016). However, phosphorylation and acetylation can lead to the malfunction of these two pathways (reviewed by Richter-Landsberg, 2016).

Mutations of the *MAPT* gene have been discovered and linked to various neurodegenerative diseases with AD-like phenotypes; yet, while *MAPT* genetic risk variants have been described in AD (Myers et al., 2005; Laws et al., 2007; Jin et al., 2012; Allen et al., 2014), no mutations have been associated with AD pathology (reviewed by Cacace et al., 2016; Blauwendraat et al., 2019). Mutations that induce the hyperphosphorylation of tau have been identified in patients with frontotemporal dementia (Bugiani et al., 1999), frontotemporal dementia parkinsonism linked to chromosome 17 (Hutton et al., 1998), corticobasal degeneration and multiple system atrophy (Spillantini et al., 1998).

The overexpression of missense mutations such as *MAPT*P301S* (Yoshiyama et al., 2007) or *MAPT*P301L* (Lewis et al., 2000) in transgenic mice have been used to study tau pathology

progression. PS19 transgenic mice overexpress the *MAPT*P301S* mutation in neurons under the control of the prion protein promoter, and exhibit early gliosis and synapse loss at 3 months of age followed by cognitive impairment by 6 months of age in the Morris water maze (Takeuchi et al., 2011) coincident with the formation of neurofibrillary tangles prior to neuron loss (Yoshiyama et al., 2007). The JNPL3 transgenic mice overexpress *MAPT*P301L* in neurons under the control of the prion protein promoter, and develop neurofibrillary tangles by 4.5 months, while gliosis and neuronal loss have not been observed prior to 10 months of age (Lewis et al., 2000). When this variant is overexpressed in CamKIIa^{+} neurons, spatial memory impairment (Ramsden et al., 2005; Santacruz et al., 2005) and gliosis (Helboe et al., 2017) are observed from 2.5 months of age followed by neurofibrillary tangle formation at 4 months of age and subsequent neuron loss (Ramsden et al., 2005; Santacruz et al., 2005). Surprisingly, deletion of the endogenous *Mapt* in transgenic mice either resulted in motor deficits (Ikegami et al., 2000; Lei et al., 2012; Morris et al., 2013), or produced no overt motor and cognitive deficits (Van Hummel et al., 2016; Tan et al., 2018).

1.7. Progressive white and grey matter loss lead to cognitive deficit in Alzheimer's disease

In addition to the two main pathological features, the amyloid and tau pathology, AD is characterised by white and grey matter diminution (Defrancesco et al., 2014). White and grey matter loss occur in aging as observed using magnetic resonance imaging (Ge et al., 2002); however, brain atrophy is more severe in AD and mostly prevalent in frontal and temporal lobes (Van Der Flier et al., 2002) leading to memory impairment (Di Paola et al., 2007; Irish et al., 2014; Rémy et al., 2015). Using magnetic resonance imaging, it was demonstrated that first brain areas affected in AD are the entorhinal cortex and the hippocampus (Du et al., 2001; Pennanen et al., 2004), which are two key regions involved in learning and memory (Hyman

et al., 1984). Like grey matter, degenerated white matter was observed in the parietal, frontal and temporal lobes of people diagnosed with AD using both diffusion tensor (Zhang et al., 2009) and T1-weighted (Baron et al., 2001) magnetic resonance imaging, and occurs in early AD suggesting it may participate in pathology development (reviewed by Nasrabady et al., 2018).

White matter damage is found in many brain regions in AD starting in regions defined as late-myelinating (Stricker et al., 2009; Gao et al., 2011; Benitez et al., 2014) in accordance with the retrogenesis model (Reisberg et al., 1999; Brickman et al., 2012). Loss of white matter occurs in the parietal, frontal and temporal regions and affects the corpus callosum tracts (Hampel et al., 1998; Dean et al., 2017), uncinate fasciculus tracts and cingulum tracts in AD patients (Rose et al., 2000; Zhang et al., 2009). Using diffusion tensor imaging, Stricker et al. (2009) showed white matter loss was more pronounced in late-myelinating fibre tracts including the inferior and the superior longitudinal fasciculi fibre pathways compared to early myelinating-tracts. Additionally, Benitez et al. (2014) characterized white matter tract metrics using diffusional kurtosis imaging and showed a correlation between the decrease in late-myelinating tracts integrity (superior and inferior longitudinal fasciculi) and patient semantic verbal fluency decline, a cognitive function affected in AD (Benitez et al., 2014). Moreover, early disruption of fronto-hippocampal white matter connectivity initiates episodic memory impairment in people diagnosed with AD (Rémy et al., 2015).

White matter degeneration is associated with myelin alterations and oligodendrocyte loss in late AD (Ihara et al., 2010; Nielsen et al., 2014; Ota et al., 2019), and oligodendrocytes are particularly absent in amyloid plaque vicinity in post-mortem AD brain tissue (Mitew et al., 2010). AD-related myelin decrease correlates with increased phosphorylated tau and amyloid

levels in late myelinating regions Notably, cholesterol and myelin protein levels, including CNP, MBP and PLP, are reduced in the white matter of people with AD, analysed post-mortem (Roher et al., 2002). Additionally, oligodendrocytes have shrunken nuclei (Gagyi et al., 2012), and increased DNA damage has been associated with increased oligodendrocyte death (Tse et al., 2018).

White matter loss is also observed in transgenic mouse models of AD (**reviewed in Table 1.1**); and is associated with cognitive impairment. Myelin pathology in transgenic mouse models of AD includes the focal loss of myelin from the vicinity of amyloid plaques (Mitew et al., 2010), the development of myelin aberrations such as myelin outfoldings (Behrendt et al., 2013), the abnormal expression of MBP in the nuclei of oligodendrocytes (Desai et al., 2011), and decreased MBP expression (Desai et al., 2010). White matter pathology often develops prior to the onset of cognitive deficits in AD transgenic mouse models (**see Table 1.1**), and the progressive loss of oligodendrocytes and myelin seem to precipitate learning and memory impairment.

1.8. Oligodendrocytes contribute to learning and memory

Cognitive changes in AD have been largely attributed to synaptic deficits and neuronal loss; however, it may also be exacerbated by changes in oligodendrogenesis and myelin levels (reviewed by Bartzokis, 2011). Social isolation during rodent development reduces myelin levels and impairs working memory (Makinodan et al., 2012; Yang et al., 2017). Similarly, induced-oligodendrocyte loss and demyelination in the rat hippocampus (Xu et al., 2017) or mouse prefrontal cortex (Xu et al., 2010) impairs working memory; but preventing cuprizone-induced demyelination in mice can rescue working memory (Xiao et al., 2008). Furthermore,

Mouse	Mutations	Myelin and oligodendrocyte pathology	Cognition	References
APP/PS1	*APP*^{K670N,M671L} *PSEN1*^{L166P}	- Myelin aberrations - Myelin loss in amyloid plaque core - Increased OPC proliferation and differentiation → age: 6 months, brain region: cortical grey and white matter	- Spatial learning and memory deficit in Morris water maze at 7 months of age	Behrendt et al., 2013 Serneels et al., 2009
APPSwe / PSEN1dE9	*APP*^{K670N,M671L} *PSEN1*^{dE9}	- Decreased g-ratio and internode length - Increased MBP, NG2 and CNPase relative density → age:2 months, brain region: hippocampus - Downregulation of MBP mRNA (from 3 months, more advanced at 6 months) - Increase in NG2^{+} cells → age: 6 months, brain region: temporal lobe	- Spatial learning deficit in Morris water maze at 12 months of age	Wu et al., 2017 Dong et al., 2018 Lalonde et al., 2005
APPSwe / PSEN1^{M146L}	*APP*^{K670N,M671L} *PSEN1*^{M146L}	- Decreased myelin levels in amyloid plaque vicinity → age: 13 months	- Spatial learning normal at 5-7 months but deteriorates by 15-17 months in water maze and radial arm maze	Mitew et al., 2010 Arendash et al., 2001
Tg2576	*APP*^{K670N,M671L}	- Decreased myelin levels in amyloid plaque vicinity → age: 13 months	- Impaired spatial learning and working memory develops between 6 to 12 months of age NB: Mice subject to blindness	Mitew et al., 2010 Hsiao et al., 1996
3xTG	*PSEN1*^{M146V} *MAPT*^{P301L} *APP*^{K670N,M671L}	- Myelin abnormalities → age: 2 and 6 months, brain region: hippocampus and entorhinal cortex - Decreased myelin level - Decreased number of myelinated processes - Increased CC1^{+} oligodendrocytes - No change in OLIG2^{+} cells → age: 6 months, brain region: hippocampus (CA1) - Aberrant expression of MBP within oligodendrocyte nuclei – mature oligodendrocytes are non-myelinating. → age: 9 months, brain region: entorhinal cortex	- Memory retention deficit from 4 months of age in Morris water maze - Spatial learning deficit from 6 months of age in Morris water maze	Desai et al., 2009 Desai et al., 2010 Desai et al., 2011 Billings et al., 2005

Table 1.1. Overview of myelin and oligodendrocyte pathology in commonly used transgenic mouse models of AD.

Mouse	Mutations	Myelin and oligodendrocyte pathology	Cognition	References
5xFAD	*APP*^{K670N,M671L} *APP*^{I716V} *APP*^{V7171} *PSEN1*^{M146L} *PSEN1*^{L286V}	- Myelin aberrations - Increased g-ratio due to decreased myelin thickness, and progressive decrease of axon calibre with age → age: 1, 2, 3 and 5 months, brain region: prelimbic area, retrosplenial granular cortex, CA1, entorhinal cortex	- Spatial learning deficit in Morris Water Maze from 1 month of age - Motor deficits from 12 months of age (females)	Gu et al., 2018 Chu et al., 2017 Tang et al., 2016 O'Leary et al., 2018
PS19	*MAPT*^{P301S}	Not reported	- Increased hyperactivity in open field test, Y-maze and elevated plus maze at 6-7 months of age - Decreased anxiety-like behaviour in elevated plus maze at 6,7 and 10 months of age - Spatial memory retention deficit in Barnes Maze and Morris Water Maze from 6 months of age - Spatial learning deficit at 10 months of age	Takeuchi et al., 2011 Dumont et al., 2011 Chalermpalanupap et al., 2017.
J20	*APP*^{K670N,M671L} *APP*^{V717F}	Not reported	- Hyperactivity from 2 months of age reported in multiple tests (e.g. open field, elevated plus maze) - Decreased anxiety-like behaviour in elevated plus maze from 2 months of age - Spatial learning and memory deficit observed in radial arm maze from 4 months of age, in Morris water maze from 3-4 months of age, in Barnes Maze from 5 months of age	Wright et al., 2013 Cheng et al., 2007 Harris et al., 2010 Cissé et al., 2011 Murakami et al., 2011 Sanchez et al., 2012 Dubal et al., 2015 Nunes et al., 2015 Mably et al., 2015 Mesquita et al., 2015 Fujikawa et al., 2017 Flores et al., 2018

Table 1.1. Overview of myelin and oligodendrocyte pathology in commonly used transgenic mouse models of AD. (continued)

white matter ultrastructure changes have been reported in humans following complex-motor skill training (Scholz et al., 2009; Sampaio-Baptista et al., 2013), and recent evidences demonstrate that new oligodendrocyte addition and myelination are required throughout life for motor-skill learning (Mckenzie et al., 2014; Xiao et al., 2016).

Learning is the ability to acquire, modify or reinforce new knowledge, behaviours and skills. It can be active or passive, associative or non-associative, and involves the acquisition of pure data or the formation of an association between, for example, a place and an emotion (reviewed by Milner et al., 1998). Learning stimulates short and long-term memory creation. Short-term memory includes sensory and working memory (Cowan, 2009). Long-term memory is characterized as either declarative/explicit and includes the recollection of facts (semantic memory) and events (episodic-like or spatial memory) (Squire and Zola, 1996), or as non-declarative/implicit and includes the recollection of learned skills (procedural memory) and reflexes to an event (classical conditioning) (Milner et al., 1998). Learning and memory processes are associated with measurable changes in brain microstructure.

Learning is associated with ultrastructural changes in grey and white matter regions of the CNS in humans (Gaser and Schlaug, 2003; Scholz et al., 2009; Jiang et al., 2016) and rodents (Sampaio-Baptista et al., 2013; Mckenzie et al., 2014). Changes in white matter architecture were also described in the healthy human brain in the intraparietal sulcus following juggling training (Scholz et al., 2009). Healthy aged individuals trained in a single (reasoning) or multi-domain cognitive training (reasoning, memory, visual and motor) twice per week for 12 weeks experienced cortical thickness changes in correlation with the type of cognitive task performed (Jiang et al., 2016). For example, improvement in immediate memory was correlated with an increase in cortical thickness in the entorhinal cortex following single-domain cognitive

training. Correspondingly, brain structure differences were observed between musicians, non-professional musicians and non-musician controls proving that experience and training can modify the brain structure in a training dependent-manner as grey matter volume correlates with training intensity (Gaser and Schlaug, 2003). Motor-dependent training tasks showed that learning is associated with alteration in white and grey matter regions including but not limited to corpus callosum, primary motor and somatosensory cortex, which could either be associated with myelin, neuronal changes or both. By performing transgenic lineage tracing of OPCs and delivery of 5-ethynyl-2'-deoxyuridine (EdU), Mckenzie et al. (2014) showed that motor skill training stimulates OPC proliferation and increases the number of new oligodendrocytes added to the adult mouse brain. Furthermore, rats trained to perform a skilled reaching task demonstrated an increase in myelination in the cingulum, external capsule and corpus callosum subjacent to the sensorimotor cortex contralateral to the trained limb relative to control groups including unskilled reaching and caged controls (Sampaio-Baptista et al., 2013). Adult oligodendrogenesis and myelination are required for learning and memory acquisition, and in turn neuronal activity changes occurring during learning regulate new oligodendrocyte addition and myelination; however, neuronal activity is altered in AD.

1.9. Neuronal activity changes in Alzheimer's disease

Neuronal activity is impeded in AD by neurotransmitters or excitatory-inhibitory signalling imbalance leading to Aβ-induced neuronal hyperactivity followed by neuron loss. Glutamate accumulates in the synaptic cleft as transporters fail its reuptake (Masliah et al., 1996; Scott et al., 2002; Potier et al., 2010), particularly in close vicinity of amyloid plaques (Hefendehl et al., 2016), which overexcite the neuronal network in early AD. Glutamate-induced overactivation becomes toxic and progressively induces synaptic deficits and neuron death in late AD (reviewed by Ong et al., 2013). As a consequence of excitatory-inhibitory signalling

imbalance, theta oscillations are boosted in early AD (Montez et al., 2009), while their decrease in late AD correlates with cognitive deficit reported by mini-mental state examination (Engels et al., 2016). Alterations of neural oscillations associated with amyloid plaque burden (Mander et al., 2015) lead to cognitive deficit (Verret et al., 2012; Bender et al., 2016) and increase the risk of epileptic seizures associated with abnormal neuronal activity in people diagnosed with AD (Amatniek et al., 2006; reviewed by Kitchigina, 2018). Nonetheless, rescuing gamma-aminobutyric acid (GABA) levels in cell cultures (Velasco and Tapia, 2002) and enhancing $GABA_A$ receptors activity in rodents (Paula-Lima et al., 2005; Brito-Moreira et al., 2011) can protect against glutamate-induced neuron damage.

Abnormal neuronal network connectivity and disproportion of excitatory-inhibitory signalling (Palop et al., 2007; Busche et al., 2008, 2012; Sun et al., 2009; Verret et al., 2012; Van Groen et al., 2014) alter neuron status to hypoactive or hyperactive based on amyloid plaque vicinity in AD transgenic mice (Busche et al., 2008), resulting in epileptic-seizures and behavioural abnormalities (Palop et al., 2007; Sanchez et al., 2012; Verret et al., 2012). Neuronal hyperactivity has been associated with progressive amyloid accumulation in the brain (Busche et al., 2012; Lerdkrai et al., 2018) starting with early hippocampal hyperactivity following soluble Aβ accumulation (Busche et al., 2012), while neuronal hypoactivity occurs only after amyloid plaque formation (Busche et al., 2012). By contrast, human *MAPT* overexpression in transgenic mice leads to an increase in hypoactive or silent neurons (Busche et al., 2008), and *MAPT* overexpression overlooks amyloid-induced hyperactivity in mice recapitulating both the amyloid and tau pathology leading to an increase in silent neuron population following soluble tau accumulation (Busche et al., 2019). This suggests an early Aβ-induced overexcitation of neuronal activity followed by the loss of neuronal function as observed in early and late AD, respectively.

Soluble Aβ accumulation triggers the loss of white matter integrity in the fimbria/fornix and perforant pathways (Van Groen et al., 2014) highly involved in memory processing (Amaral et al., 2014, 2018). Amyloidosis induces astrocytic glutamate release, associated with early neuronal hyperactivity and neuronal hypoactivity in advanced AD (reviewed by Findley et al., 2019), and reduces synaptic density (Talantova et al., 2013). Glutamate promotes tau phosphorylation (Sindou et al., 1994) and tau accumulation reduces dendritic length and synapse number (Yin et al., 2016b) leading to neuron hypoactivity and loss. Neuronal activity is regulated by APP and tau accumulation, and can in turn regulate amyloid burden (Bero et al., 2011; Zhen et al., 2017) and extracellular tau level released in mice (Yamada et al., 2014) consequently worsening AD pathology. However, as early AD pathology is associated with an increase in neuronal activity, this could result in an increased rate of oligodendrocyte addition to the brain.

1.10. Neuronal activity promotes new oligodendrocyte addition

Oligodendrocyte addition and adaptive myelination are promoted by neuronal activity. Optogenetic stimulation of layer V projection neurons in the premotor cortex of awake and behaving *Thy1::ChR2* mice rapidly enhanced OPC proliferation. Within 4 weeks post-stimulation oligodendrogenesis and myelin thickness were boosted in the premotor cortex and corpus callosum, which was associated with motor performance improvement in the CatWalk gait test relative to controls (Gibson et al., 2014). Similarly, pharmacological increase of neuronal activity of some somatosensory axons using h3MDq-DREADD (designer receptor exclusively activated by a designer drug) and clozapine-N-oxide injection in the somatosensory cortex of *Pdgfrα-CreER^{T2}::Tau-mGFP* mice led to an increase in PDGFRα^{+} OPC density, PDGFRα^{+} EdU^{+} proliferating OPCs, aspartoacylase (ASPA)$^{+}$ EdU^{+} newly added

oligodendrocytes and an increase in the proportion of green fluorescent protein $(GFP)^+$ myelinated axons in the corpus callosum (Mitew et al., 2018). While electrically active axons are preferentially myelinated, a decrease of neuronal activity does not result in oligodendrocyte and myelin degeneration but in myelination adjustment. Overexpression of Kir2.1 to reduce neuron excitability in mice did not alter OPC density, proliferation and differentiation but the number of GFP^+ myelinated axons was decreased in the corpus callosum (Mitew et al., 2018). Neuronal activity regulates myelination, and myelination regulates neural synchronicity. Overexpression of *PLP* in PLP-tg mice (Kagawa et al., 1994) result in motor learning impairment, reduced oligodendrogenesis and MBP mRNA expression relative to controls following motor training (Kato et al., 2019). Decreased task-related and spontaneous Ca^{2+} transients were observed in PLP-tg mice compared to controls during motor learning suggesting an incapacity of myelin to regulate excitatory signalling as parvalbumin-positive inhibitory interneurons functioned normally (Kato et al., 2019). Optogenetic stimulation of thalamic cell bodies in PLP-tg mice, 3 weeks post-injection with AAV2/1-Syn-ChR2 (H134R)-EYFP into the thalamus, increased spike latency, spike volley duration and number of spikes; and rescued motor learning during the pull lever task indicating a potential compensation for thalamic activity by input adjustment (Kato et al., 2019). New oligodendrocyte addition and myelination are enhanced by neuronal activity and in turn myelination regulates neural synchronicity required for learning and memory acquisition but the continuous role of oligodendrogenesis in memory maintenance in the healthy CNS and in pathological conditions is unknown.

1.11. Amyloidosis affects the cells of the oligodendrocyte lineage

Human studies suggest that amyloid alters mature oligodendrocyte morphology (Roher et al., 2002), and *in vitro* evidences found that Aβ peptides are toxic for oligodendrocytes (Xu et al.,

2001; Horiuchi et al., 2012). Xu et al. (2001) indicated that $A\beta_{40}$ as well as its truncated fragment $A\beta_{25-35}$ led to oligodendrocyte death in cultures obtained from the cortex of P1-2 rats. Horiuchi et al. (2012) later showed that $A\beta_{1-42}$ oligomers are cytotoxic for mature myelinating oligodendrocytes and inhibit myelin sheaths formation *in vitro*. Aβ-induced oligodendrocyte dysfunction was reported to be increased by *PSEN1* mutation, using the 3xTg transgenic mouse line (Desai et al., 2011). Desai et al. (2011) showed that MBP distribution was impaired in mature myelinating oligodendrocytes, which consequently were not able to produce myelin sheaths. Increase in MBP degradation and formation of myelin vesicles was observed in the periventricular white matter of AD patients using immunohistochemical staining of AD brain tissue post-mortem (Zhan et al., 2014), and degraded MBP was found to colocalize with $A\beta_{1-42}$ peptides in the core of amyloid plaques (Zhan et al., 2015).

The main myelin protein MBP binds to Aβ peptides and inhibits Aβ fibrils formation (Hoos et al., 2009; Liao et al., 2009; Ou-Yang et al., 2015). Using cell culture, Liao et al. (2009) demonstrated that purified human MBP and recombinant human MBP could bind and degrade $A\beta_{40}$ and $A\beta_{42}$ peptides *in vitro*. In addition, using a mouse line expressing the APP Swedish mutation (Tg2576), they reported that MBP could degrade assembled fibrillar Aβ *in situ*. These data are consistent with results reported by Hoos et al. (2009) showing that MBP could interact with Aβ peptides and inhibit Aβ fibril formation *in vitro*. The N-terminal domain of MBP and particularly four residues (K54, R55, G56, and K59) found between residues 54 and 64 of MBP_{1-64} (Kotarba et al., 2013) mediates Aβ fibrillar aggregation inhibition (Liao et al., 2010). Transgenic mice Tg-MBP1-EGFP overexpressing MBP_{1-64} in neurons via the Thy1.2 promoter crossed with 5xFAD mice (Oakley et al., 2006) presented a decrease in insoluble Aβ and fibrillar amyloid following a decrease in the size of amyloid plaques rather than a decrease in number, which led to an improved spatial memory in the Barnes maze (Ou-Yang et al., 2015).

Aβ directly interacts with OPCs (NG2 cells) and can affect their morphology. Human NG2 cells exposed to Aβ oligomer or fibril enriched preparation *in vitro* experienced morphological changes and fibrillar $A\beta_{1-42}$ decreased NG2 concentrations (Nielsen et al., 2013). AD patients presented lower cerebrospinal fluid NG2 levels compared to controls that was correlated to AD-related biomarkers including Aβ, consequently a prolonged exposure to Aβ might actually be toxic for OPCs (Nielsen et al., 2013). While decrease in NG2 levels were observed in diagnosed AD patients with advanced AD stages, the ratio of NG2 cells in the temporal lobe was increased in concomitance with early loss of myelin in the corpus callosum at 6 months of age in APPSwe/PSEN1dE9 mice (Dong et al., 2018). NG2 cell clusters around amyloid plaques were observed between 6 and 15 months of age in APPSwe/PSEN1dE9 mice and NG2 cells cleared $A\beta_{42}$ peptides in OPC cultures derived from Sprague-Dawley rats at P1-2; and Aβ clearance by NG2 cells occurred via endocytosis and autophagy (Li et al., 2013). Processes by which OPCs can promote homeostasis and remyelination and consequently delay neurodegeneration are still unclear. However, the increase in OPC ratio following demyelination suggests that OPCs could promote repair in AD as observed in multiple sclerosis (Keirstead et al., 1998; Chang et al., 2000; Girolamo et al., 2010).

Oligodendrocyte and myelin alterations can be rescued in amyloid-like pathology. In APP/PS1 mouse model, an increase in total $OLIG2^+$ oligodendrocyte population and the proportion of proliferating $OLIG2^+$ cells were observed at 6 and 11 months of age in APP/PS1 mice compared to controls (Behrendt et al., 2013). The increase in $OLIG2^+$ cells corresponded to a significant increase in proliferating $NG2^+$ $BrdU^+$ OPCs and $GST\pi^+$ $BrdU^+$ newly differentiated oligodendrocytes in cortical grey and white matter at 6 months of age. The increase in OPC proliferation and differentiation was associated with myelin aberration repair between 6 and 9

months of age, which was observed by Gallyas impregnation and MAG immunostaining (Behrendt et al., 2013). APP/PS1 mice showed focal myelin loss around amyloid plaques, which was previously reported by Mitew et al. (2010) in APPSwe/PSEN1^{M146L} mice and AD brain tissue post-mortem. The amyloid pathology seems to initially increase oligodendrocyte addition in rodents; however, a similar effect was not observed in humans. Nielsen et al. (2013) observed a decrease in NG2 immunoreactivity in the molecular layer of the hippocampus in post-mortem brain specimens from clinically diagnosed and post-mortem verified AD patients compared to non-demented controls (Nielsen et al., 2013). These findings were in accordance with the reported decreased OLIG2^{+} oligodendrocyte population in grey and white matter of the sensory motor cortex, superior temporal gyrus and the mid frontal gyrus in AD brain tissue post-mortem (Behrendt et al., 2013). As brain tissue samples used in human studies were obtained from mild to severe AD patients, the decrease in oligodendrocytes may only correspond to advanced stages of the disease, consequently the fate of the cells of the oligodendrocyte lineage in early AD remains unclear and further investigations are required.

1.12. Tau alterations disturb the cells of the oligodendrocyte lineage

Tau modifications alter oligodendrocyte differentiation and process outgrowth. Seiberlich et al., (2015) showed that oligodendrocytes lacking tau following siRNA knockdown of *MAPT* *in vitro* remained in a progenitor state rather than differentiate due to a lack of MBP transport from the soma to the processes, which resulted in shorter processes and an incapacity to form appropriate contact with neurons to differentiate into oligodendrocytes and form myelin internodes. A transient tau dephosphorylation in oligodendrocytes following hydrogen peroxide exposure resulted in a loss of oligodendrocyte cellular processes in OPC cultures prepared from primary mixed glial cultures established from rat neonate brains (LoPresti and Konat, 2001). Tau expression and phosphorylation modulate oligodendrocyte differentiation,

process outgrowth and myelination; yet, the fate of oligodendrocytes in presence of hyperphosphorylated tau remains unknown.

Overexpression of human *MAPT* in transgenic mouse models leads to oligodendrocyte and myelin loss associated with cognitive and motor impairment. In transgenic mice overexpressing *Prnp-MAPT*P301L* mutation, motor impairment was associated with increased tau levels and dying TUNEL^{+} and Caspase3^{+} cells in females and males compared to non-transgenic controls (Zehr et al., 2004). Oligodendrocytes were found to be apoptotic while neurons and astrocytes did not colocalized with TUNEL^{+} and Caspase3^{+} cells (Zehr et al., 2004). Overexpression of a *MAPT*P301L* mutation driven in oligodendrocytes by the CNP promoter in transgenic mice engendered impaired axonal transport prior to myelin and axon degeneration and the appearance of Thioflavin-S^{+} tau inclusions in oligodendrocytes, oligodendrocyte death and motor impairment (Higuchi et al., 2005). Overexpression of the three 3R human isoforms via overexpression of *MAPT*P301L* mutation, associated with frontotemporal dementia parkinsonism linked to the chromosome 17, expressed in neurons, astrocytes and oligodendrocytes under the control of the mouse α-tubulin promoter resulted in tau inclusions in oligodendrocytes and astrocytes by 6 months of age, myelin and glial degeneration and motor deficits by 24-25 months of age. Significant age-related loss of oligodendrocytes in the basal ganglia, cerebellum and brain stem; and loss of myelin associated with neuronal loss in the spinal cord were found between 1 and 24 months of age in these mice (Higuchi et al., 2002). The conditional overexpression of *MAPT*P301L* in CamKIIa^{+} neurons resulted in myelin thinning of myelinated axons from the perforant pathway, a widespread myelin damage of myelinated axons from the ammonic path in the para-ventricular alveus near the Cornu Ammonis field 2 (CA2) region of the hippocampus; and myelin remodelling in the optic nerve with no signs of demyelination but associated with a transient decrease in neuronal

excitability at 1 month post induction, which recovered by 6 months post-induction (Jackson et al., 2018). Brain regions can react differently to *MAPT* overexpression and some areas may be prone to oligodendrocyte and myelin replacement in tauopathy.

MAPT overexpression may enhance OPC differentiation. Following focal lysolecithin-induced demyelination of the spinal cord ventral funiculus of 2-months old *Thy1.2-MAPT*^{P301S} mice, OPC density ($Sox2^+$ / $OLIG2^+$ cells per mm^2) is maintained within the lesion (Ossola et al., 2016). However, mature oligodendrocyte density (Adenomatous polyposis coli $(APC)^+$ / $OLIG2^+$ cells per mm^2; and PLP^+ cells per mm^2) and expression of MBP was increased in *Thy1.2-MAPT*^{P301S} mice relative to controls within the lesioned area. A three-fold increase in mature oligodendrocyte density (MBP^+ / $OLIG2^+$ cells per mm^2) was additionally observed in OPC cultures from P10-12 *Thy1.2-MAPT*^{P301S} mice compared to controls suggesting that OPC enhanced ability to proliferate and differentiate was acquired from microenvironment priming as OPCs did not directly expressed the *MAPT* mutation but yet retained their enhanced ability *in vitro*. Nevertheless, in accordance with previous findings, the interaction of tau with the cells of the oligodendrocyte lineage is evident. However, OPC response to *MAPT* overexpression in early tauopathy such as AD remains unclear.

1.13. Hypothesis & Aims

OPCs generate new oligodendrocytes throughout life in the healthy brain, and can increase oligodendrocyte production in response to demyelination to promote myelin replacement and maintain neuronal activity. Myelin loss is observed in late AD, but whether OPCs have the ability to increase new oligodendrocyte addition to replace oligodendrocytes and myelin early in AD is unclear. A recent study showed that OPCs produced larger numbers of new oligodendrocytes in response to a focal, demyelination injury in the spinal cord of transgenic mice that overexpress a dementia-associated pathogenic variant of human *MAPT* (Ossola et al., 2016); and that new oligodendrocyte addition can also be enhanced by the overexpression of human pathogenic versions of *APP* and *PSEN1* (Behrendt et al., 2013). However, it is not known whether the overexpression of pathogenic *MAPT* or *APP* is sufficient to affect cells of the oligodendrocyte lineage early in AD development. I hypothesise that the overexpression of pathological human *MAPT* and *APP*, primarily in neurons, will be sufficient to induce oligodendrocyte damage and that this will result in elevated oligodendrogenesis.

I will evaluate this hypothesis, by achieving the following aims:

Aim 1: To determine whether the overexpression of *MAPT* has a pathological effect on cells of the oligodendrocyte lineage

I will assess cognitive performances of *Prnp-MAPT*^{P301S} transgenic mice, that primarily overexpress hyperphosphorylated human tau in neurons in the CNS, by performing a series of behavioural assessments to ensure that these mice do not experience significant memory impairment prior to 6 months of age, in order to define the pre-symptomatic period. I will then use Cre-lox lineage tracing technology to label OPCs and follow their fate over time,

quantifying oligodendrogenesis in the hippocampus, entorhinal cortex and fimbria of control and *Prnp-MAPT*^{P301S} transgenic mice. I will use histological approaches and transmission electron microscopy to determine the impact of any change in oligodendrogenesis on myelination in the hippocampus.

Aim 2: To determine whether the overexpression of a human AD-associated variant of *APP* has a pathological effect on cells of the oligodendrocyte lineage

I will determine the pre-symptomatic period of *PDGFβ-APP*^{Sw,Ind} mice, overexpressing human *APP* Swedish and Indiana mutations in neurons and oligodendrocytes, using a battery of behavioural assessments. I will assess PDGFRα^{+} OPC density in the hippocampus, entorhinal cortex and fimbria of *PDGFβ-APP*^{Sw,Ind} transgenic mice and WT littermates over time, using immunohistochemistry. I will compare the electrophysiological properties of OPCs in control, *Prnp-MAPT*^{P301S} and *PDGFβ-APP*^{Sw,Ind} mice, in order to determine whether amyloid pathology influences the membrane properties of these cells or their ability to respond to neurotransmitter signalling. I will use transmission electron microscopy to determine if myelin thickness is altered in the hippocampus of *PDGFβ-APP*^{Sw,Ind} mice during the pre-symptomatic period. Using Cre-lox lineage tracing technology and histological approaches, I will quantify oligodendrogenesis in control and *PDGFβ-APP*^{Sw,Ind} mice, and determine whether amyloid pathology impacts the total number of oligodendrocytes.

This research will provide critical insight into the impact that AD pathology has on cells of the oligodendrocyte lineage. I will particularly study the impact that AD pathology has on these cells prior to the onset of behavioural symptoms in order to understand some of the earliest cellular changes that underpin neurodegeneration, and identify potential early targets for therapeutic intervention.

Chapter 2: General methods

2.1. Transgenic mice

Male and female mice were housed in individually ventilated cages (Optimice) on a 12h light / dark cycle (07:00-19:00) with food and water available *ad libitum*. All animal experiments were approved by the Animal Ethics Committee of the University of Tasmania (13741 and 16151) and carried out in accordance with the Australian code of practice for the care and use of animals in science. Details of animal experiments are reported in accordance with the ARRIVE guidelines. *Rosa26-YFP* Cre-sensitive reporter mice (Srinivas *et al.*, 2001) were purchased from the Jackson Laboratory (B6.129X1-Gt(ROSA)26Sortm1(EYFP)Cos/J, stock #006148) and backcrossed onto a C57BL/6 background in house for >10 generations. *PDGFβ-APP^{Sw,Ind}* mice (referred to here as *APP* mice, but also known as J20 mice; Mucke *et al.*, 2000) expressing a three point mutation (Swedish and Indiana) driven in neurons by the *platelet derived growth factor-beta chain* (*PDGFβ*) were purchased from the Jackson Laboratory [B6.Cg-Zbtb20Tg(PDGFB-APPSwInd)20Lms/2Mmjax, stock #006293]. *Prnp-MAPT^{P301S}* transgenic mice (referred to here as *MAPT* mice, but also known as PS19 mice, Yoshiyama *et al.*, 2007), that express a human variant of *MAPT* driven in neurons by the *prion protein* promoter, were purchased from the Jackson Laboratory (B6;C3-Tg(Prnp-MAPT*P301S)PS19Vle/J, stock #008169) and backcrossed onto a C57BL/6 background for >20 generations. *Pdgfrα-CreER^{T2}* transgenic mice (Rivers et al., 2008) were a kind gift from Prof. William D Richardson (University College London, UK). *Pdgfrα–H2BGFP* mice (Hamilton et al., 2003) were purchased from the Jackson Laboratory (B6.129S4-Pdgfratm11(EGFP)Sor/J, stock # 007669). Mice were maintained on a C57BL/6 background and bred to generate experimental mice that were heterozygous for each transgene. Mouse used for each aim in this study are listed below (**Appendix 2. Table 1**).

We performed cre-lox lineage tracing (Metzger et al., 1995; Leone et al., 2003) to fluorescently label adult OPCs and trace their generation of new oligodendrocytes over time. When tamoxifen is delivered to *Pdgfrα-CreER^{T2} :: Rosa26-YFP* transgenic mice, it binds to a form of cre-recombinase that is fused to the estrogen-receptor type II, only in OPCs, causing it to translocate to the nucleus. In the nucleus, Cre recombinase recognises and recombines the loxp-sites that flank a stop codon in the *Rosa26-YFP* transgene, excising the stop codon and enabling expression of the yellow fluorescent protein (YFP) reporter. YFP expression is permanently turned on in the OPCs and retained by their progeny (as per Rivers et al., 2008) In this system, Cre activation and OPC labelling has been shown to be strictly dependent on tamoxifen delivery (Rivers et al., 2008; Clarke et al., 2012; Young et al., 2013). Mouse lines expressing an *APP* or *MAPT* mutation were selected due to reported cognitive decline prior to amyloid plaque (Palop et al., 2003; Wright et al., 2013) and neurofibrillary tangle (Yoshiyama et al., 2007; Takeuchi et al., 2011) formation allowing us to evaluate the effect of early stages AD-like pathology on the cells of the oligodendrocyte lineage.

2.2. Genotyping transgenic mice tissue sample

2.2.1. Genomic DNA extraction from ear clips

To determine and confirm the genotype of each transgenic mouse, genomic deoxyribonucleic acid (DNA) was extracted from a small tissue biopsy. Mice ear clips or tail samples were collected at ~ P30 and post-mortem. Each sample was sealed in a DNAse free 1.5ml microcentrifuge tube and incubated with 250µl of DNA extraction buffer containing 6µl Proteinase K (stock solution 20mg/ml) at 55°C overnight on a heat block. On the next day, they were briefly vortexed and centrifuged to avoid cross-contamination. Subsequently, 6M Ammonium Acetate (100µl, Sigma) was added into samples using p200 Barrier Tip for cell lysis. Samples were then vortexed, placed on ice for 15 min and centrifugated for 10 min at

13,200 rpm and 4°C to separate cellular debris from the DNA. The supernatant containing the DNA was poured into a fresh tube. Isopropanol (250µL, Sigma) was added into the supernatant to precipitate the DNA. Tubes were vortexed and spun at 13,200 rpm for 3 min at room temperature. The supernatant was quickly poured off and the precipitated DNA was washed using 70% ethanol (125µL, Sigma). Most of ethanol was removed after 3 min centrifugation. The DNA pellet was centrifuged for 1 min in the remaining solution, which was then removed. 50µl of Milli-Q water were added and the DNA pellet resuspended at 55°C for 15 min or overnight at room temperature. The DNA was quantified by spectrophotometry using a NanoDrop UV-Vis Spectrophotometer (Thermo Fisher Scientific, Waltham, USA). The DNA was then stored at -20°C or used to perform genotyping by polymerase chain reaction (PCR; see below).

2.2.2. Amplification by Polymerase Chain Reaction of genomic DNA

PCR was applied to genotype transgenic mice by a 25µl PCR reaction. For most transgenes, 0.5 to 2µl depending on concentration of extracted DNA was used as template in PCR reaction together with 12.5µl of GoTaq, 0.5µl of each primer, and 9.5 to 11µl of Milli-Q water to complete the 25µl required volume. For the *APP* and *MAPT* transgenes, a Taq DNA polymerase with standard Taq (Mg-free) buffer (New England Biolabs) was used and included 0.1µl of Taq, 2.5µl of standard buffer, 2.0µl of MgCl2, 0.5µl of deoxynucleotide solution mix (New England Biolabs), 0.2µl of each primers, and 17.5 to 19µl of Milli-Q water to complete the 25µl required volume. The DNA sequence was initially amplified at 94°C for 4 min then for a various number of cycles; depending on the transgene of interest (**Appendix 2. Table 2**); at 94°C for 30 seconds, 57˚C or 62°C for 45 seconds and 72°C for 1 min, followed by 10 min at 72°C and hold at 4°C.

2.2.3. Gel electrophoresis

Following PCR, the DNA product was visualized by gel electrophoresis, which separates DNA based on its size. 1% and 2% (w/v) agarose gels were made by dissolving agarose powder (Biorad) in 1X Tris-Acetate EDTA (TAE) (LifeTechnologies). The solution was heated in a microwave until the powder dissolved. 100mL of molten agarose were added to a gel cast containing 1µl of SybrSafe (Invitrogen) for DNA detection. Once set the gel was transferred into a gel tank containing 1X TAE (Life Technologies). The gel comb was removed, and 15µl of PCR product was loaded into each well. 5µl of Hyperladder I (Biorad) was loaded into one well as a reference to determine the size of the PCR product. The gel was run at 100 volts for 15 to 30 min depending on the gel concentration, 1 to 2 % respectively. The gel was then removed from the gel tank and excited at 470nm using an Image Station Amersham™ Imager 600 (GE Healthcare Life Sciences) and bands were detected with an emission filter set at 600nm.

2.2.4. Genotyping by light to reveal fluorescence

To confirm the *Histone-GFP* transgene expression in *Pdgfrα–H2BGFP* mice, pups were placed under a light after birth (P1-P2) to reveal brain fluorescence prior to skull skin thickening (Hamilton et al., 2003).

2.3. Tamoxifen preparation and delivery

Tamoxifen (Sigma) was dissolved in corn oil (40mg/ml) by sonication (Ultrasonic cleaner FXP 8M, Unisonics Australia) at 21˚C for 2 hours and administered to adult mice (P60) to activate Cre-recombinase and induce expression of yellow fluorescent protein (YFP). Control, *MAPT* and *APP* adult mice (P60) carrying the *Pdgfrα-CreER*^{T2} and *Rosa26-YFP* transgenes received 300mg tamoxifen/kg body weight daily for four consecutive days by oral gavage as previously

described (O'Rourke et al., 2016). Mice were analysed 7, 60, 90 or 120 days after their first dose of tamoxifen, and are referred to as P60+7, P60+60, P60+90 and P60+120, respectively.

2.4. Western blot

Mice were terminally anaesthetized with sodium pentobarbital (i.p.60mg/kg). Toe pinch-response method was used to determine depth of anaesthesia. Once mice were unresponsive, they were placed onto a shallow tray and a longitudinal incision was made to open the chest; the heart was exposed and carefully trimmed. An incision was made to the mice's right atrium with iris scissors, and mice were transcardially perfused with 0.01M phosphate buffer saline (PBS). The brain was placed inside a coronal brain matrix (Agar Scientific, Essex, UK) and scalpel blades placed at Bregma -1.06 and -2.06. The hippocampi were dissected from this brain slice and protein lysates produced in radioimmunoprecipitation assay (RIPA) cell lysis buffer (50mM Tris-HCL, 150mM NaCl, 1% NP-40, 1% sodium deoxycholate, 0.1% Sodium dodecyl sulfate (SDS) and one phosphatase inhibitor tablet per 10mL in autoclaved MilliQ water). Samples were centrifuged for 10 min at 13,200 rpm and 4˚C before the supernatant was collected and stored at -80°C. Protein quantification by Bradford assay and western blotting was performed as previously described (Auderset et al., 2016). The western gel was run for 1 hour at 21˚C and 90 V and 20 min at 165 V and the proteins transferred onto an ethanol-activated polyvinylidene fluoride (PVDF) membrane (Biorad) over a 60 min period at 20 V and 4°C. Each membrane was placed in blocking solution [5% (w/v) skim milk powder in 0.2% Tween-20 in Tris Buffered Saline (TBS-T)] and incubated on the orbital shaker for 1 hour at 21°C, before being transferred into blocking solution containing primary antibodies (**Appendix 3. Table 3**) and incubated on a rotator overnight at 4°C. The membrane was then washed by agitation in TBS-T (3 x 10 min) at 21°C. The relevant horseradish peroxidase

(HRP) conjugated secondary antibodies were diluted in 1% (w/v) skim milk powder in TBS-T and applied for 1 hour at 21°C. The membrane was again washed in TBS-T and exposed to 1:1 Immobilon Western™ HRP Peroxidase Solution (Millipore) and Luminol Reagent (Millipore) for visualisation of the protein bands on an Image Station Amersham™ Imager 600 (GE Healthcare Life Sciences).

Membranes were washed with PBS, TBS-T and a blot stripping buffer (ThermoScientific) and incubated in blocking solution for 1 hour before exposure to mouse anti-β-actin (1:1000 in blocking solution) for 1 hour at 21˚C. The membrane was washed in TBS-T (3 x 10 min) before application of goat anti-mouse HRP (1:10000). The membrane was washed in TBS-T (2 x 8 min) before band visualisation as describe above. Western blot band intensity was calculated by measuring integrated density and normalized to actin protein expression levels.

2.5. Behavioural assessment

Mice cognitive performance was assessed using a battery of behavioural tests, which involved the activation of our brain regions of interest that are highly involved in memory function and greatly affected in AD, the hippocampus and the entorhinal cortex. Behavioural testing was carried out over 17 days (**Figure 2.1a**) for *MAPT* (*Prnp-MAPT*^{P301S}) transgenic mice, *APP* (*PDGFβ- APP*^{Sw,Ind}) transgenic mice and their wildtype (WT) littermates (C57BL/6 mice) in separate cohorts at 60, 90 and 180 days of age. All behavioural testing was carried out during the dark phase of the light-dark cycle. Mice were moved to the testing room 2 hours prior to the light cycle change, and habituated to the room for 3 hours. All testing was carried out within the same 5-hour window of the dark phase. Sodium lights were used in the room, and bright lights were used above the maze as needed. All trials were video recorded and animal

movement tracked using automated tracking software (EthoVision XT 11, Noldus, Netherlands). Males were tested prior to females but the order of testing was otherwise randomised between sessions. All equipment was cleaned with 70% ethanol between trials to avoid olfactory cues. To avoid any flaw due to fear or stress, mice were handled fifteen times prior to any behaviour assessment (5 min per day).

2.5.1. Barnes Maze

First, mice underwent a shortened version of the Barnes maze protocol, adapted from Attar et al. (2013) over seventeen days (**Figure 2.1b**). On day 1, mice were placed in the brightly lit centre (120 lux) of an elevated (30cm above the ground), circular maze (100cm diameter) that contained 20 holes evenly spaced around the circumference. After 1 min, the mice were gently directed to an escape box located underneath one of the holes in the circumference and left to habituate to the box for 5 min. On days 2 and 3, the maze was raised to 70cm, and light intensity in the centre of the maze increased to 160 lux. Distinct patterns were placed on each wall surrounding the maze, acting as spatial reference points that remained consistent throughout all trials. At the start of each trial, each mouse was placed at the centre of the maze under a covered start box for 15-30 sec before the box was removed, and the mouse left to explore until they found the escape box or 5 min elapsed. If a mouse did not find the escape box prior to the end of trial, it was given direction to the box and allowed to enter it. After entering the escape box, each mouse was left for 1 min before being returned to the home cage to await the next trial. Mice were trained to learn the location of the escape box across three trials per day with an inter-trial interval of 30-45 min. During training, approaching any hole that did not lead to the escape box was considered a primary error, and the number of primary errors made during a trial was measured as an indicator of learning (reviewed by Gawel *et al.*, 2019).

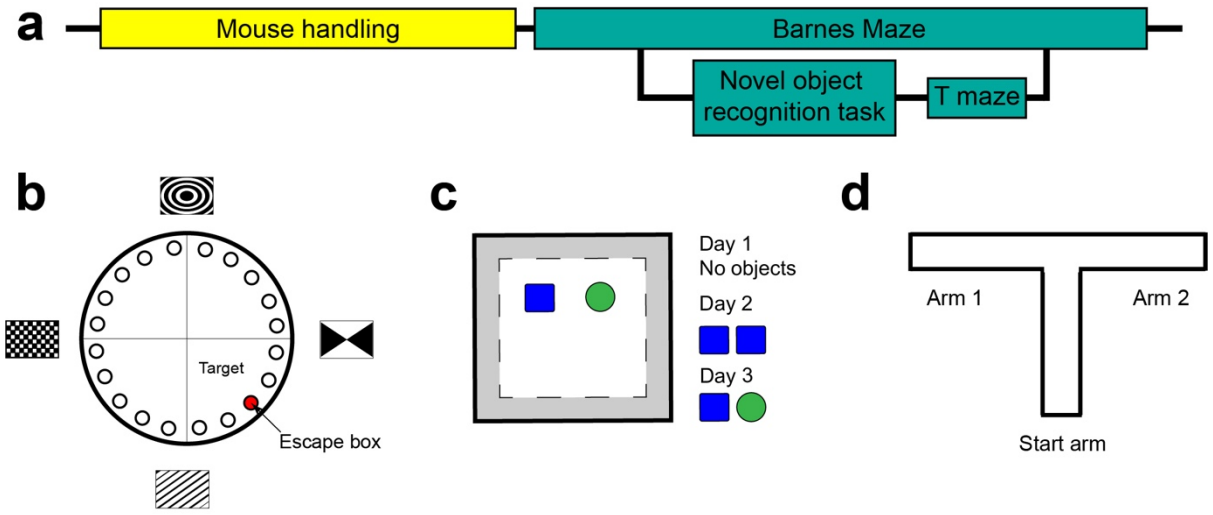

Figure 2.1. Behavioural testing to evaluate spatial learning, recognition, short- and long-term memory

a*) Each experimental mouse was handled for 5 minutes per day for 15 consecutive days prior to starting behaviour testing and cognitive tests were performed in the order shown.* ***b****) The Barnes maze was used to evaluate spatial learning, recognition, short-term and long-term memory.* ***c****) The novel object recognition task was performed to examine recognition and short-term memory, and the first day of the novel object recognition task was used as an open field task to measure activity.* ***d****) The T-maze was performed to evaluate working memory.*

Short-term and long-term memory were assessed 1-day and 2-weeks after initial training, respectively. For each memory probe trial, mice were returned to the maze but with the escape box removed and left to explore the maze for 5 min. The maze was divided into four quadrants within the tracking software (EthoVision XT 11) and the quadrant containing the hole that previously led to the escape hole was designated the target zone. The proportion of time spent within the target zone during the probe trial was measured as an indicator of intact memory for the location of the escape box.

2.5.2. Open field and novel object recognition task

The novel object recognition task was performed over 3 days (**Figure 2.1c**) to evaluate recognition memory and short-term memory. On day 1, we carried out an open field assessment using a protocol adapted from Wang et al. (2013), to assess locomotor and anxiety-like behaviour. Each mouse was placed in an open square arena (30cm^2, with walls of 20cm in height) lit (200 lux) to create a bright centre and dark perimeter, and the speed of movement and total distance moved was measured over a 10 min period. On day 2, the arena was uniformly illuminated (50 lux) and contained two identical objects (multi-coloured green and blue Lego towers), equidistant from the box edges (7.5cm away from the box edges). Each mouse was left to explore the arena and familiarise themselves with the identical objects for 10 min. On Day 3, one of the familiarised objects was replaced by a novel object (a multi-coloured green and blue Lego man) that was of similar size and colour, but a different shape and texture. Each mouse was returned to the arena and left to explore for 5 min. The time spent exploring each object was recorded and the proportion of time exploring the novel object was calculated as an indication of short-term recognition memory.

2.5.3. T Maze

The final test used was the T maze, which was performed over a day (**Figure 2.1d**). The T maze was used to evaluate mice working memory using a protocol adapted from Deacon and Rawlins (2006). A mouse was placed in the start arm and once they chose to explore the left or right arm of the maze, retreat from that arm was blocked for 1 min. The mouse was then returned to the start arm and allowed to make another choice. This was repeated 10 times. Mice naturally exhibit exploratory behaviour and tend to choose the arm not visited in the previous trial, therefore, returning to the same arm in successive trials was recorded as an error.

2.6. Tissue perfusion fixation and cryoprotection

Mice were anaesthetized with sodium pentobarbital (i.p.60mg/kg) and depth of anaesthesia testing were performed as described above (see 2.4.). 4% (w/v) paraformaldehyde (PFA) in PBS was injected into left ventricle using a perfusion needle. Once the blood was removed and the fixation was finished, the brain was taken out, sectioned coronally (1mm thick sections) using a brain matrix, immersion fixed into 4 % PFA at room temperature for 90 min and stored in 20% (w/v) sucrose in PBS overnight at 4°C. The following day, brain sections were embedded with Thermofisher™ Cryomatrix™ medium and stored at -80°C until use.

2.7. Immunohistochemistry and amyloid plaque detection

30µm coronal brain cryosections containing the hippocampus, entorhinal cortex and fimbria (Bregma -1.34 to -2.54; Franklin & Paxinos, 2007) were collected and processed as floating sections. Cryosections were incubated for 1 hour at 21°C in blocking solution [10% Fetal Calf Serum (FCS) / 0.1% triton x-100 in PBS] before being placed on an orbital shaker overnight at 4˚C in blocking solution containing primary antibodies (**Appendix 3. Table 4**). Sections were washed thrice in PBS before being placed on an orbital shaker at 4˚C overnight, in blocking

solution containing secondary antibodies, conjugated to Alexa Fluors (**Appendix 3. Table 4**). Cell nuclei were visualised by the inclusion of Hoechst 33342 (**Appendix 3. Table 4**). To detect amyloid plaques, 40µm coronal brain cryosections were transferred into 0.1% (w/v) Thioflavin-S (Sigma) / 60% (v/v) ethanol / 40% (v/v) PBS, and agitated on a shaker for 3 min at 21°C. Sections were de-stained by washing twice in 50% ethanol (v/v) in PBS and thrice in PBS. Floating sections were mounted onto glass slides and the fluorescence preserved by the application of fluorescent mounting medium (Dako Australia Pty. Ltd., Campbellfield, Australia).

2.8. EdU administration and detection

EdU (Invitrogen) was administered to P175 mice via their drinking water (0.2 mg/ml, as per Young et al., 2013) for 5 consecutive days. EdU-labelled cells were visualised using the AlexaFluor-647 Click-iT EdU kit (Invitrogen). Briefly, 30µm floating cryosections were incubated for 15 min in 0.5% Triton X-100 (v/v) in PBS at room temperature before being transferred into the EdU developing cocktail and incubated for 45 min in the dark. Cryosections were washed twice in PBS before carrying out immunohistochemistry as described above.

2.9. Confocal microscopy

Confocal images (3µm spacing) were collected from the hippocampus, entorhinal cortex and fimbria, using a 20x air, 40x air or 100x oil objective and standard excitation and emission filters for 4',6-diamidino-2-phenylindole (DAPI), Fluorescein isothiocyanate (FITC; Alexa Fluor-488), Tetramethylrhodamine isothiocyanate (TRITC; Alexa Fluor-568) and Cyanine 5 (CY5; Alexa Fluor-647). A minimum of n=3 images were collected per area from each hemisphere, across n=3 brain sections and n=3 mice on an Andor Confocal microscope with

Nikon Software (Andor Technology Ltd., Belfast, Northern Ireland) or UltraView Spinning Disk Confocal microscope with Volocity Software (Perkin Elmer, Waltham, USA). Brain regions of interests were delimited based on the Mouse Brain Atlas (Franklin and Paxinos, 2007). Measurements to determine cell density, g-ratio and nodes length were performed manually using Fiji software (NIH, Washington DC, USA). All measurements were made blind to the genotype and time-point being analysed.

2.10. Electrophysiology

Control, *MAPT* and *APP* mice carrying the *Pdgfrα–H2BGFP* transgene, in which OPCs express GFP, were used for the electrophysiological characterisation of OPCs. Following cervical dislocation, P30 (P30-P35) and P100 (P100-P114) mice were decapitated and their brains transferred into ice cold slicing solution (124 mM NaCl, 26 mM $NaHCO_3$, 1 mM NaH_2PO_4, 2.5 mM KCl, 2 mM $MgCl_2$, 2.5 mM $CaCl_2$, 10 mM glucose, and 1 mM Na-kynurenate) saturated with 95% O_2 / 5% CO_2. Horizontal brain slices (300 µm), prepared using a VT1200s vibratome (Leica), were incubated at 21°C in slicing solution that lacked Na-kynurenate. Whole cell patch clamp recordings were made at 21°C from GFP^+ cells situated amongst the Schaffer collaterals in Cornu Ammonis field 1 (CA1) of the hippocampus. Recordings were made using an Axopatch200B or HEKA patchclamp EPC800 amplifier, collected using PClamp9.2 or PClamp10.5 software (Molecular Devices), sampled at a rate of 50 kHz and filtered at 10 kHz. The perfusion solution contained 144 mM NaCl, 2.5 mM KCl, 2.5 mM $CaCl_2$, 10 mM HEPES, 1 mM NaH_2PO_4 and 10 mM glucose set to pH 7.4 and saturated with O_2. Electrodes were prepared from glass capillaries with a resistance of 3-6 MΩ when filled with an internal solution containing 130 mM K-gluconate, 4 mM NaCl, 0.5 mM $CaCl_2$, 10 mM HEPES, 10 mM BAPTA, 4 mM MgATP, 0.5 mM Na_2GTP set to pH of 7.2- 7.4, and an osmolarity of 290 ± 5 mOsm/kg.

Upon breakthrough, resting membrane potential (RMP), capacitance, membrane resistance, and the magnitude of the voltage-gated inward (sodium) current, elicited by a voltage step from -60 mV to 20 mV, were recorded as previously described (Clarke et al., 2012). Cells with a voltage gated sodium channel current < 60 pA were classified as newly differentiated oligodendrocytes (Clarke et al., 2012) and were consequently removed from analysis. Access resistance was measured before and after each recording and was between 12-25.0 MΩ (mean 19.18 ± 0.42 MΩ). Data were not included if the access resistance changed by ≥ 20% over the course of the recording or exceeded 25 MΩ. To determine the effect of bath applied 100 μM kainate (KA; Abcam), cells were voltage clamped at -60 mV and currents elicited by 200 ms voltage steps from -100 to 20 mV (20 mV increments). To measure the effect of bath-applied 100 μM GABA (Sigma), cells were voltage clamped at 0 mV and currents elicited by 200 ms voltage steps from -80 to +80 mV (20 mV increments). The average steady state current magnitude in the last 50 ms of the voltage step was measured using clampfit 10.5 (molecular devices) and the evoked current (current in the presence of drug minus baseline current) reported. After recording the KA- or GABA-evoked current, 6-cyano-7-nitroquinoxaline-2,3-dione (CNQX; α-amino-3-hydroxy-5-methyl-4-isoxazole propionate (AMPA)/KA receptor antagonist, 10 μM, Sigma) or picrotoxin (PTX, $GABA_A$ receptor antagonist, 100 μM, Sigma) was bath applied for 2 minutes before reapplication of KA or GABA.

2.11. Transmission electron microscopy

2.11.1. Perfusion fixation and dehydration steps

Mice were terminally anaesthetised using sodium pentobarbital (i.p. 60mg/kg) and transcardially perfused with Karnovsky's fixative [0.8% (v/v) glutaraldehyde (GA) / 2% (w/v) PFA / 0.25mM CaCl2 / 0.5mM MgCl2 in 0.1M sodium-cacodylate buffer]. Brains were sliced

into 2mm thick coronal slices using a rodent brain matrix (Agar Scientific, Essex, UK) and immersion fixed at 21ºC for 2h, before being stored in 0.1M sodium-cacodylate buffer overnight at 4°C. The stratum lacunosum moleculare of the CA1 of the hippocampus was dissected and immersed in 1% osmium tetroxide / 1.5% potassium ferricyanide in 0.065M sodium-cacodylate buffer, in the dark, for 2h at 4˚C. Tissue was washed five times in Milli-Q water, before being dehydrated in: 70% ethanol (v/v) in Milli-Q water overnight at 21ºC; 80% ethanol (2 x 10 min); 85% ethanol (2 x 10 min); 90% ethanol (2 x 10 min); 95% ethanol (2 x 10 min) and 100% ethanol (4 x 10 min). Tissue was embedded by serial exposure to: 100% propylene oxide (2 x 5 min); 75% propylene oxide / 25% epon (4h); 67% propylene oxide / 33% epon (4h); 50% propylene oxide / 50% epon (overnight); 33% propylene oxide / 67% epon (4h); 25% propylene oxide / 75% epon (4h), and 100% epon (overnight). Tissue was transferred to fresh 100% epon for 4h before being polymerised at 60˚C for 72h. Blocks containing the samples were stored at room temperature until use.

2.11.2. Sectioning and grid staining

Embedded sample size was reduced using an ultramicrotome (Ultracut, Leica) to hold the sample in position and razor blades to remove excess resin. Glass-knifes were made using a knifemaker (7800 knifemaker, Leica). Using an ultramicrotome (Reichert Ultracut S, Leica) and a glass knife, 1µm sections were cut to polish the samples. Once the tissue was visible, a glass knife with a boat (fixed to the glass knife using nail polish and filled with water) was placed on the ultramicrotome to cut and collect floating sections with a perfect loop (Diatome). Sections were placed on a slide and stained with toluidine blue for 30s on a heat plate at 60˚C to locate the region of interest visualised with an optical microscope (Zeiss). The glass knife was then replaced with a diamond knife (Diatome) and ultrathin floating sections (70nm thick) were cut and similarly collected with a perfect loop. Ultrathin sections were placed on a gold

grid with formvar (ProSciTech). The next day, sections were stained on the grid with Reynolds' stain [Reynolds, 1963; lead citrate made from lead nitrate (Sigma) and trisodium citrate dihydrate (Merck)] and 4% uranyl acetate (filtered, Serva) in 50% ethanol to enhance the contrast.

2.11.3. Imaging

Electron micrographs of the stratum lacunosum moleculare were collected using a HT7700 (Hitachi) transmission electron microscope. Axons were identified based on their microtubule organisation (reviewed by Stassart et al., 2018) and individual myelin lamella (wrap) by the presence of major dense lines (reviewed by Simons & Nave, 2016). The g-ratio was measured for a minimum of 95 myelinated axons per mouse, and the number of myelin wraps for a minimum of 27 myelinated axons per mouse. Quantification was performed by an experimenter blind to genotype for n=3-4 mice per group.

2.12. Statistical analyses

Statistical analyses were performed using GraphPad Prism 8.0 (La Jolla CA, USA). The distribution of each data set was evaluated to determine whether the data were normally distributed using the D'Agostino & Pearson normality test or Shapiro-Wilk normality test where $n \geq 5$. Data that were normally distributed were analysed by a parametric test [one-way analysis of variance (ANOVA) or two-way ANOVA for groups comparison with a Bonferroni post-hoc test], and data that were not normally distributed were analysed using a non-parametric text [Mann-Whitney U test or Kolmogorov-Smirnoff test]. For experiments where n=3, a normal distribution was assumed, and data were analysed using an unpaired two-tailed t-test. Survival curve comparisons were performed using a Log-Rank (Mantel-Cox) test.

Statistical significance was established as $p<0.05$. Statistical details are reported in corresponding figure legend and individual data points are presented on each graph. Behavioural and electrophysiological data are presented as mean ± standard error of the mean (SEM). Western blot, immunohistochemical or TEM data are presented as mean ± standard deviation (SD).

Chapter 3: Grey and white matter oligodendrogenesis is increased prior to locomotor or memory impairment in an adult mouse model of tauopathy

3.1. Introduction

In physiological aging, white matter damage can be detected in brain regions that are critical for cognitive and emotional processing, including the hippocampus, neocortex and frontal white matter tracts, and the extent of white matter damage closely correlates with cognitive decline (Charlton et al., 2006; Hirsiger et al., 2017; Fan et al., 2019). White matter degeneration is exacerbated in people diagnosed with a tauopathy. For example, diffusion tensor imaging evaluations of people with frontotemporal dementia indicate that fractional anisotropy is reduced in frontal and temporal white matter regions including the anterior corpus callosum, anterior cingulum tracts and uncinate tracts, when compared with healthy controls (Zhang et al., 2009; Lu et al., 2014; Kassubek et al., 2018). Similar studies show that people with AD have reduced fractional anisotropy in parietal, temporal and frontal regions including the corpus callosum, cingulum and uncinate tracts, compared to controls (Choi et al., 2005; Stricker et al., 2009; Zhang et al., 2009; O'Dwyer et al., 2011; Benitez et al., 2014; Brueggen et al., 2019). In these tauopathies, the observed white matter degeneration likely reflects a combination of myelin breakdown and axon degeneration.

Tauopathies are a group of diseases characterised by the aggregation of hyperphosphorylated tau in neurons and glial cells, including myelinating oligodendrocytes (reviewed by Ferrer, 2018). Tau aggregates in cells of the oligodendrocyte lineage are referred to as coiled bodies and threads, and have been identified in post-mortem tissue from people diagnosed with Pick's

disease (Komori, 1999; Arai et al., 2001; Mimuro et al., 2010), progressive supranuclear palsy (Nishimura et al., 1995b; Arima et al., 1997; Komori, 1999; Arai et al., 2001; Jin et al., 2006), corticobasal degeneration (Wakabayashi et al., 1994; Feany and Dickson, 1995; Komori, 1999; Arai et al., 2001) frontotemporal lobar degeneration associated with variants in *MAPT* (Higuchi et al., 2005) and AD (Nishimura et al., 1995a). In Frontotemporal dementia, myelin degenerates in the frontal white matter, and in AD white matter cholesterol and myelin proteins such as MBP, PLP and CNP (Roher et al., 2002) are progressively lost. CNP expression is reduced in the frontal cortex in AD (Vlkolinský et al., 2001), and impaired myelin lipid synthesis occurs in the temporal grey matter, hippocampus and frontal grey matter in AD (Couttas et al., 2016). Myelin degeneration is also detected post-mortem in the frontal and periventricular white matter regions of people with AD (Ihara et al., 2010; Zhan et al., 2014), and a recent proteomics study revealed that myelin sheath components are significantly reduced in the frontal cortex of people with sporadic AD (Zhang et al., 2018).

Tauopathy-like oligodendrocyte pathology can be induced in mice by the injection of brain tissue homogenates from sporadic AD primary age-related tauopathy, aging-related tau astrogliopathy, globular glial tauopathy, progressive supranuclear palsy, Pick's disease and frontotemporal lobar degeneration (linked to the $MAPT^{P301L}$ variant) into the corpus callosum. Phospho-tau deposits developed inside cells of the oligodendrocyte lineage and myelin disruption was evident within 6 months after injection (Ferrer et al., 2019). However, a separate study found that tau-inclusions were rarely seen in mice inoculated with AD homogenates but were a common feature following inoculation with corticobasal degeneration homogenates (Boluda et al., 2015).

Transgenic mice that express human tauopathy-associated variants in *MAPT*, primarily the *MAPT*^{P301L} and *MAPT*^{P301S} variants, also recapitulate many of the aspects of human tauopathy, including the development of gliosis, the formation of neurofibrillary tangles, neuron loss, and motor and cognitive impairment (Lewis et al., 2000; Lin et al., 2003b, 2003a; Ramsden et al., 2005; Santacruz et al., 2005; Yoshiyama et al., 2007; Takeuchi et al., 2011; Ren et al., 2014). In the spinal cord of the *Prnp-MAPT*^{P301L} transgenic mice, oligodendrocytes also undergo apoptosis (Zehr et al., 2004). Furthermore, when three human tauopathy *MAPT* variants are expressed under the control of the mouse α-tubulin promoter, in the absence of endogenous *Mapt*, coiled bodies form inside spinal cord oligodendrocytes, and oligodendrocyte number is reduced by 6 months of age - prior to neuron loss (Higuchi et al., 2002). Consistent with these findings, the expression of *MAPT*^{P301L} in *CamKIIa*$^{+}$ neurons was associated with myelin thinning within perforant pathway axons that project from the entorhinal cortex to the hippocampus (Jackson et al., 2018), and when expression of this variant was restricted to oligodendrocytes (*CNP* promoter) myelin degeneration and axon loss from the spinal cord was detected prior to the development of tau aggregates in oligodendrocytes or oligodendrocyte loss (Higuchi et al., 2005).

OPCs have the ability to proliferate and differentiate to produce new oligodendrocytes in response to oligodendrocyte loss and demyelination (Picard-Riera et al., 2002; Zawadzka et al., 2010; Assinck et al., 2017; Baxi et al., 2017), making it possible that oligodendrogenesis occurs alongside oligodendrocyte loss in tauopathy. Following a focal, lysolecithin-induced demyelination of the spinal cord ventral funiculus in young adult *Thy1.2-MAPT*^{P301S} mice, OPC density is maintained, but the density of oligodendrocytes and expression of MBP is elevated at the lesion site, compared with demyelinated WT mice (Ossola et al., 2016), suggesting that

in the presence of *MAPT*^{P301S}, demyelination can be more effectively countered by oligodendrogenesis.

In this study, we demonstrate that overexpression of the *MAPT*^{P301S} variant, primarily in neurons, results in a large number of new oligodendrocytes accumulating in the hippocampus, entorhinal cortex and fimbria between 5 and 6 months of age. This increase in oligodendrocyte addition occurred prior to axon loss or the development of overt cognitive deficits but did not increase the total number of oligodendrocytes detected in these regions, suggesting that new oligodendrocyte addition facilitates oligodendrocyte and myelin maintenance as early pathology develops in the CNS of *MAPT* transgenic mice.

3.2. Results

3.2.1. *MAPT* transgenic mice do not develop overt locomotor or memory impairment by P180

Prior to examining the response of cells of the oligodendrocyte lineage to the earliest stages of tauopathy, we confirmed that human tau was expressed in brain tissue from *MAPT* mice (**Figure 3.1**). Western blot analysis of the dorsal hippocampus indicated that human tau (**Figure 3.1a, c**) and phosphorylated human tau (phosphorylated at threonine 231; **Figure 3.1b, d**) was expressed by *MAPT* transgenic mice, but not their WT littermates, at P30, P60, P90 and P180. By comparing the relative expression of human tau (upper band, **Figure 3.2a**) and endogenous mouse tau (lower band, **Figure 3.2a**), we determined that human tau expression was 2- to 5-fold more abundant than mouse tau in the hippocampus of *MAPT* mice (**Figure 3.2c**). We also found that phosphorylated human tau (upper band, **Figure 3.2b**) was 7- to

Figure 3.1. MAPT mice do not develop overt locomotor or memory impairment by P180

***a-b**) Western blots probing for tau (a; human ~55kDa; mouse ~51kDa) and phosphorylated tau (pTau) (b; human ~55kDa, mouse ~51kDa) in hippocampal brain lysates from P30 wildtype (WT; open circles, black bars) and MAPT (black squares, open bars) mice. **c**) Human tau expression relative to β-actin in P30, P60, P90 and P180 WT and MAPT mice [Two-way ANOVA, genotype: $F (1, 16) = 110$, $p < 0.0001$; age: $F (3, 16) = 1.034$, $p = 0.4040$; interaction: $F (3, 16) = 0.9767$, $p = 0.4282$]. **d**) Human phosphorylated tau relative to β-actin in MAPT and WT mice at P30, P60, P90 and P180 [Two-way ANOVA, genotype: $F (1, 16) = 148.4$, $p < 0.0001$; age: $F (3, 16) = 2.078$, $p = 0.1434$; interaction: $F (3, 16) = 2.004$, $p = 0.1540$]. **e-f**) Track visualisation (EthoVision XT) showing movement (white lines) of P180 WT (**e**) and MAPT (**f**) mice in the open field locomotor task. **g**) The total distance travelled by WT and MAPT mice in the open field task at P60, P90 and P180 [Two-way ANOVA, genotype: $F (1, 94) = 3.536$, $p = 0.0631$; age: $F (2, 94) = 1.180$, $p = 0.3119$; interaction: $F (2, 94) = 0.767$, $p = 0.4671$]. **h**) Quantification of the average movement velocity of WT and MAPT mice during the open field task at P60, P90 and P180 [Two-way ANOVA, genotype: $F (1, 94) = 3.466$, $p = 0.0658$; age: $F (2, 94) = 1.253$, $p = 0.2904$; interaction: $F (2, 94) = 0.8427$, $p = 0.4338$]. **i**) Schematic of the T-maze. **j**) Quantification of the proportion incorrect arm choices (errors) made by P60, P90 and P180 WT and MAPT mice during the T-maze alternation task [Two-way ANOVA, genotype: $F (1, 96) = 4.317$, $p = 0.0404$; age: $F (2, 96) = 0.7271$, $p = 0.4859$; interaction: $F (2, 96) = 3.028$, $p = 0.0531$]. **k-l**) Heatmaps (EthoVision XT) showing the relative proportion of time P180 WT (**k**) and MAPT (**l**) mice spent exploring the familiar and novel objects in the novel object recognition task. Warmer colours represent a greater proportion of time in that area. **m**) Quantification of the proportion of time P60, P90, and P180 WT or MAPT mice spent exploring the novel object relative to the total time spent exploring either object [Two-way ANOVA, genotype: $F (1, 98) = 2.823$, $p = 0.0961$; age: $F (2, 98) = 2.506$, $p = 0.0868$; interaction: $F (2, 98) = 0.006544$, $p = 0.9935$]. **n-o**) Track visualisation images (EthoVision XT) showing movement (white lines) of P180 WT (**n**) and MAPT (**o**) mice during the Barnes maze long-term memory probe trial, carried out 2 weeks after mice learned the expected location of an escape box (red arrows). Yellow shading indicates the quadrant defined as the target zone. **p**) The proportion of time P60, P90, and P180 WT or MAPT mice spent within the target zone during the long-term memory probe trial [Two-way ANOVA, genotype: $F (1, 98) = 3.708$, $p = 0.0570$; age: $F (2, 98) = 0.5633$, $p = 0.5711$; interaction: $F (2, 98) = 2.623$, $p = 0.0777$]. Western blot data are presented as mean ± SD, n = 3 mice per group. Behaviour data are presented as mean ± SEM, n= 9-24 mice per group. Asterisks denote significant differences identified by Bonferroni post hoc analysis, $^{**}p < 0.01$, $^{***}p < 0.001$, $^{****}p < 0.0001$. Scale bars represent 10cm (e-f, i, k-l) and 25cm (n-o).*

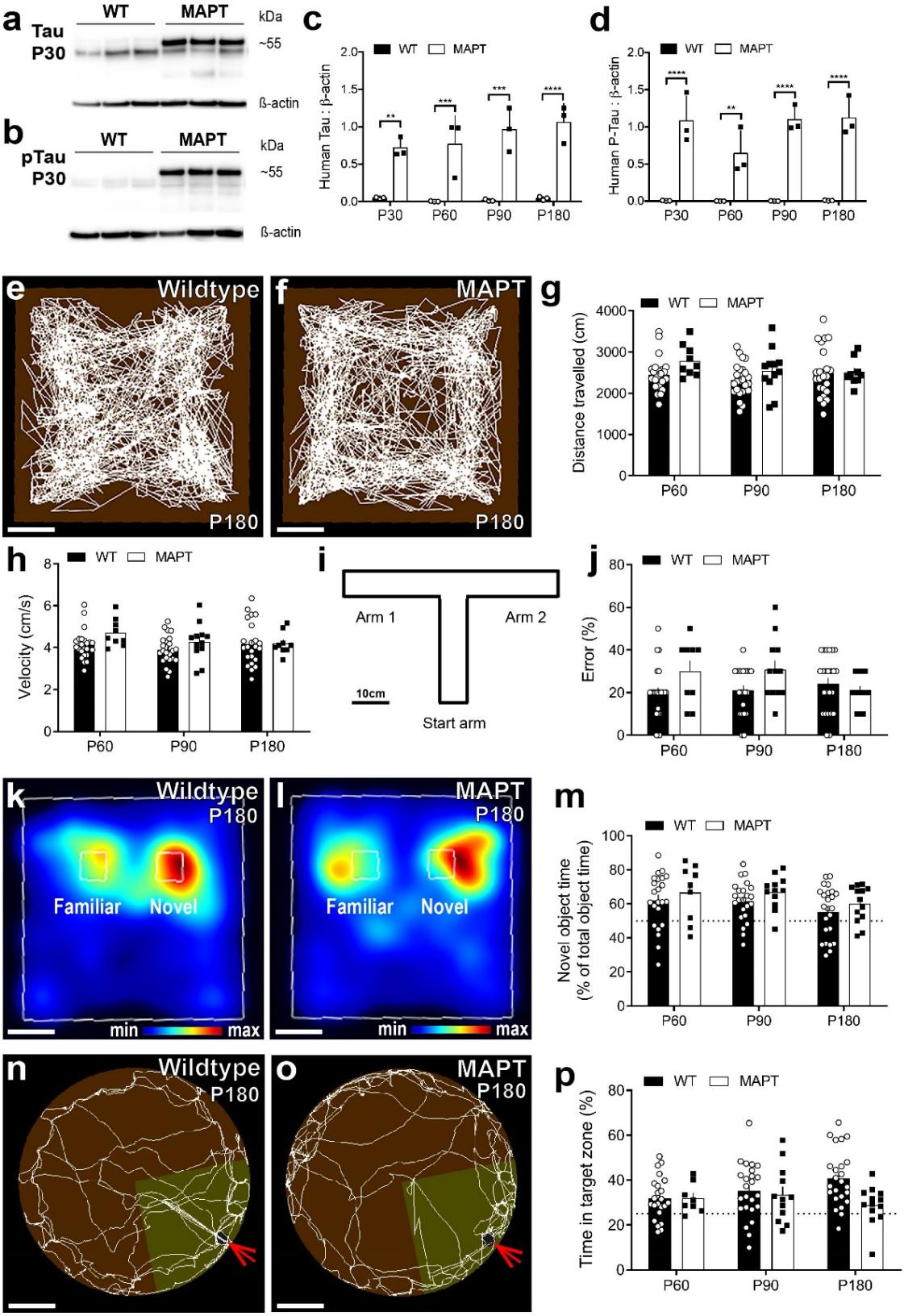
a
Tau
P30
WT
MAPT
kDa
~55
ß-actin
b
pTau
P30
WT
MAPT
kDa
~55
ß-actin
c
WT
MAPT
Human Tau : β-actin
P30
P60
P90
P180
d
WT
MAPT
Human P-Tau : β-actin
P30
P60
P90
P180
e
Wildtype
P180
f
MAPT
P180
g
WT
MAPT
Distance travelled (cm)
P60
P90
P180
h
WT
MAPT
Velocity (cm/s)
P60
P90
P180
i
Arm 1
Arm 2
10cm
Start arm
j
WT
MAPT
Error (%)
P60
P90
P180
k
Wildtype
P180
Familiar
Novel
min
max
l
MAPT
P180
Familiar
Novel
min
max
m
WT
MAPT
Novel object time
(% of total object time)
P60
P90
P180
n
Wildtype
P180
o
MAPT
P180
p
WT
MAPT
Time in target zone (%)
P60
P90
P180

Figure 3.2. Human tau protein expression is 2- to 5-fold higher than endogenous mouse tau in MAPT mice

***a**) Representative images of western blots probing for human (~55kDa) and mouse (~51kDa) tau in hippocampal brain lysates from P60, P90 and P180 WT and MAPT mice (one western blot per time point).* ***b**) Representative images of western blots probing for human (~55kDa) and mouse (~51kDa) tau phosphorylated on Threonine 231 site in hippocampal brain lysates from P60, P90 and P180 WT and MAPT mice (one western blot per time point).* ***c**) Fold change between human tau and mouse tau in MAPT mice at P30, P60, P90 and P180.* ***d**) Fold change between human phosphorylated tau and mouse phosphorylated tau in MAPT mice at P30, P60, P90 and P180. Results are presented as mean ± SD, n = 3 mice per genotype.* ***e**) 86% of MAPT mice (n = 39) survived to P200 against 98% of WT mice (n = 73). Survival curves comparison: Log-Rank (Mantel-Cox), p = 0.0390.*

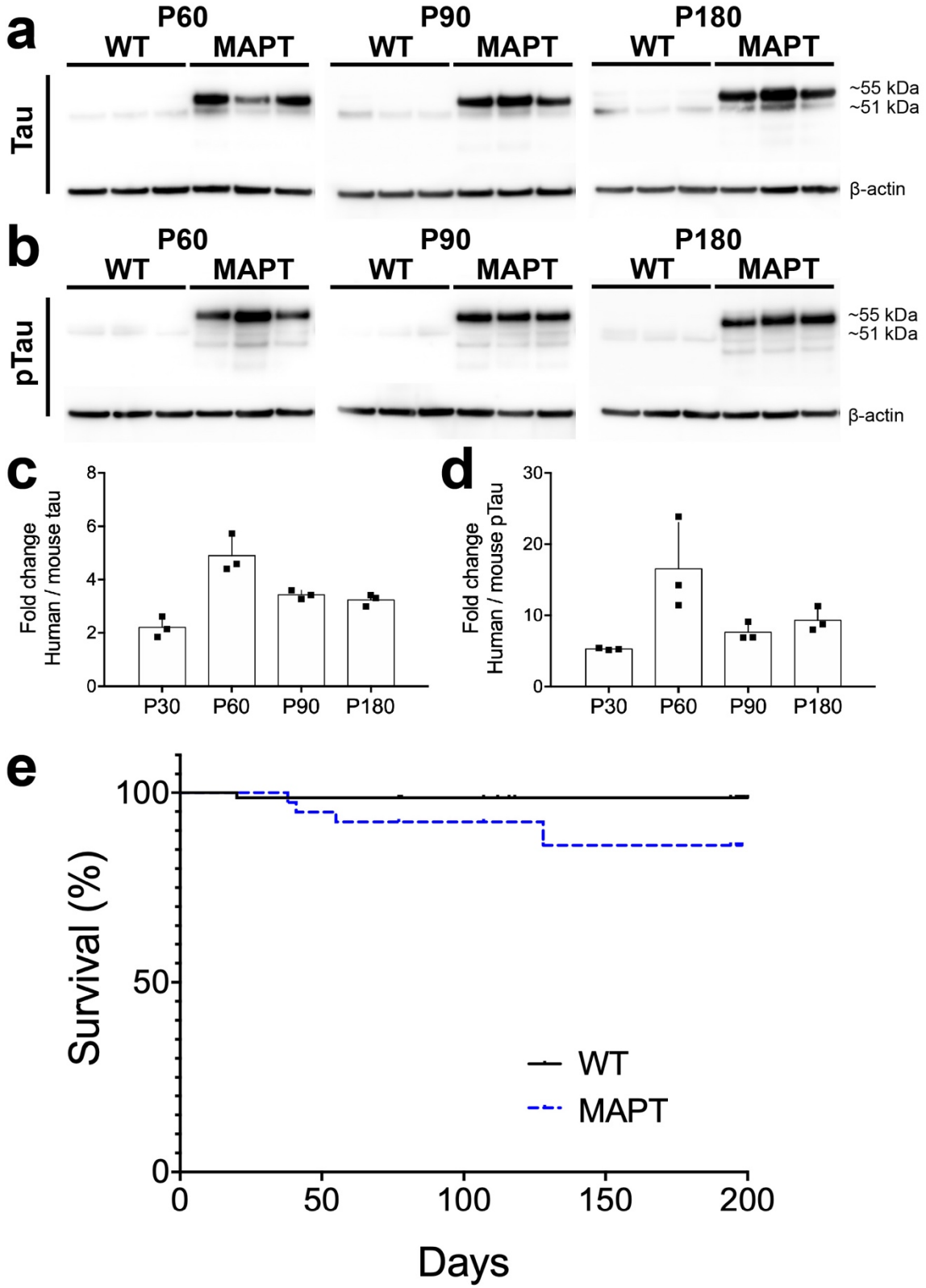
a
P60
P90
P180
WT
MAPT
Tau
~55 kDa
~51 kDa
β-actin
b
pTau
c
Fold change
Human / mouse tau
P30
P60
P90
P180
d
Fold change
Human / mouse pTau
e
Survival (%)
Days
WT
MAPT

10-fold more abundant than phosphorylated mouse tau (lower band, **Figure 3.2b**) in the hippocampus of *MAPT* mice (**Figure 3.2d**). This transgenic overexpression of human *MAPT* was associated with the impaired survival of *MAPT* transgenic mice, relative to their WT littermates (**Figure 3.2e**), and reactive microgliosis by P180, that was primarily observed in the hippocampus and entorhinal cortex (**Figure 3.3**). To determine whether the overexpression of human tau impacted gross locomotor or cognitive performance over this time period, *MAPT* and WT mice were subjected to a battery of behavioural tasks. WT (**Figure 3.1e**) and *MAPT* (**Figure 3.1f**) mice were placed in an open field arena, and the distance that each mouse travelled (**Figure 3.1g**), and the velocity of that movement (**Figure 3.1h**), was mapped over a 10 min period. The overexpression of human tau did not alter the distance travelled (**Figure 3.1g**) or the velocity of movement (**Figure 3.1h**) at P60, P90 or P180. *MAPT* and WT mice also spent a similar proportion of time in the central area of the open field [P60: WT 31.9 ± 2.0 %, *MAPT* 38.2 ± 3.8 %; P90: WT 32.2 ± 2.0 %, *MAPT* 32.3 ± 3.5 %; P180: WT 35.8 ±1.9 %, *MAPT* 35.1 ± 3.3 %, mean ± SEM; Two-way ANOVA, genotype: $F(1, 94) = 0.6999$, $p = 0.4049$; age: $F(2, 94) = 0.8799$, $p = 0.4182$; interaction: $F(2, 94) = 0.9449$, $p = 0.3924$].

Working-memory was evaluated by assessing spontaneous alternation in the T-maze (**Figure 3.1i**). We found that the performance of WT and *MAPT* mice was equivalent for this task, with mice of each genotype making an equivalent number of errors at P60, P90 and P180 (**Figure 3.1j**). Short-term recognition memory was evaluated for WT (**Figure 3.1k**) and *MAPT* (**Figure 3.1l**) mice using the novel object recognition task. Both WT and *MAPT* mice spent a larger proportion of their time exploring the novel object, compared to the familiar object, and we found that the overexpression of human tau did not affect the ability of mice to discriminate between the objects at P60, P90 or P180 (**Figure 3.1m**). The spatial learning ability, as well

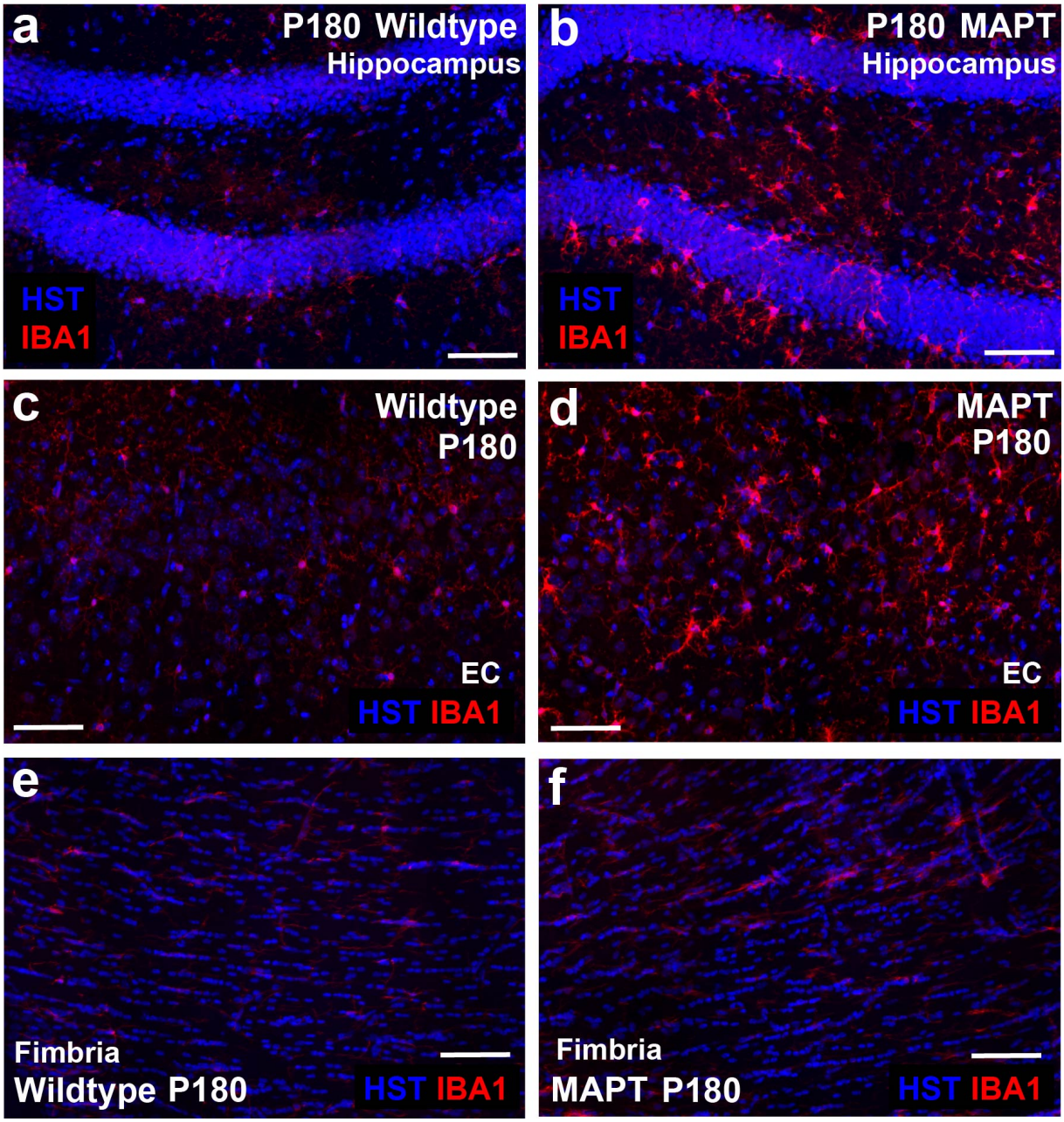

Figure 3.3. Reactive microglia are visible in MAPT mice at P180

a-f) *Representative confocal images of Iba1 (red) and Hoechst 33342 (blue) in the hippocampus (**a-b**), entorhinal cortex (EC; **c-d**) and fimbria (**e-f**) of WT (**a, c, e**) and MAPT (**b, d, f**) mice at P180. Scale bars represent 60µm.*

as the short- and long-term memory performance of WT (**Figure 3.1n**) and *MAPT* (**Figure 3.1o**) mice was assessed using a Barnes maze spatial learning task (**Figure 3.4a**). We found that at P60, P90 and P180, WT and *MAPT* mice made fewer visits to incorrect holes (primary errors) on day 2 of training, compared with day 1, suggesting that mice of both genotypes learned the location of the escape box (**Figure 3.4b-d**). One day after training, during the short-term memory probe phase, P180 WT and *MAPT* mice spent an equivalent amount of time in the target quadrant of the maze, and both groups spent more time in the target quadrant compared with all other quadrants (**Figure 3.4e**). During the long-term memory probe phase, two weeks after initial training, WT mice spent more time in the target quadrant, relative to other maze quadrants, while *MAPT* mice spent an equivalent amount of time in all 4 quadrants (**Figure 3.4f**). While these data may suggest that *MAPT* mice are beginning to experience long-term memory impairment, this was not a robust phenotype, as the time that *MAPT* mice spent in the target quadrant was equivalent to that of WT mice (**Figure 3.1p**). Overall, these data indicate that human tau overexpression does not induce overt cognitive impairment in mice by P180.

3.2.2. The number of new YFP$^+$ cells produced by OPCs is elevated in P180 *MAPT* mice

To determine whether the overexpression of human hyperphosphorylated tau in neurons could indirectly influence adult oligodendrogenesis, prior to the onset of a behavioural change, we performed cre-lox lineage tracing of PDGFRα$^+$ OPCs in the hippocampus, entorhinal cortex and fimbria of control and *MAPT* mice. The hippocampus and entorhinal cortex were selected, as they are among the first regions affected in human tauopathy associated with AD (Xu et al., 2000; Du et al., 2001; Pennanen et al., 2004), and the fimbria is part of the major white matter

Figure 3.4. Learning and memory performance in the Barnes maze

a) *Schematic diagram of the Barnes maze depicting the location of the escape box (red) relative to the spatial cues surrounding the maze and quadrant divisions.* ***b)*** *Quantification of the average number primary errors committed by P60 WT (open circles, black bars) and MAPT (black squares, open bars) mice during the first and second day of learning [Two-way ANOVA, genotype: F (1, 60) = 0.24, p = 0.6233; learning day: F (1, 60) = 12.46, p = 0.0008; interaction: F (1, 60) = 0.39, p = 0.5307].* ***c)*** *Quantification of the average number primary errors committed by P90 WT and MAPT mice during the first and second day of learning [Two-way ANOVA, genotype: F (1, 68) = 6.30, p = 0.0144; learning day: F (1, 68) = 13.37, p = 0.0005; interaction: F (1, 68) = 0.25, p = 0.6166].* ***d)*** *Quantification of the average number primary errors committed by P180 WT and MAPT mice during the first and second day of learning [Two-way ANOVA, genotype: F (1, 70) = 2.569, p = 0.1135; learning day: F (1, 70) = 13.91, p = 0.0004; interaction: F (1, 70) = 0.5959, p = 0.4428].* ***e)*** *Quantification of the time spent by P180 WT and MAPT mice in each quadrant of the maze during the short-term memory probe phase [Two-way ANOVA, genotype: F (1, 140) = 6.558e-006, p = 0.9980; maze quadrant: F (3, 140) = 35.37, p < 0.0001; interaction: F (3, 140) = 1.959, p = 0.1230].* ***f)*** *Quantification of the time spent by P180 WT and MAPT mice in each quadrant of the maze during the long-term memory probe phase [Two-way ANOVA, genotype: F (1, 140) = 0.033, p = 0.8550; maze quadrant: F (3, 140) = 14.14, p < 0.0001; interaction: F (3, 140) = 6.737, p = 0.0003]. Data are presented as mean ± SEM, n= 9-24 mice per group.*

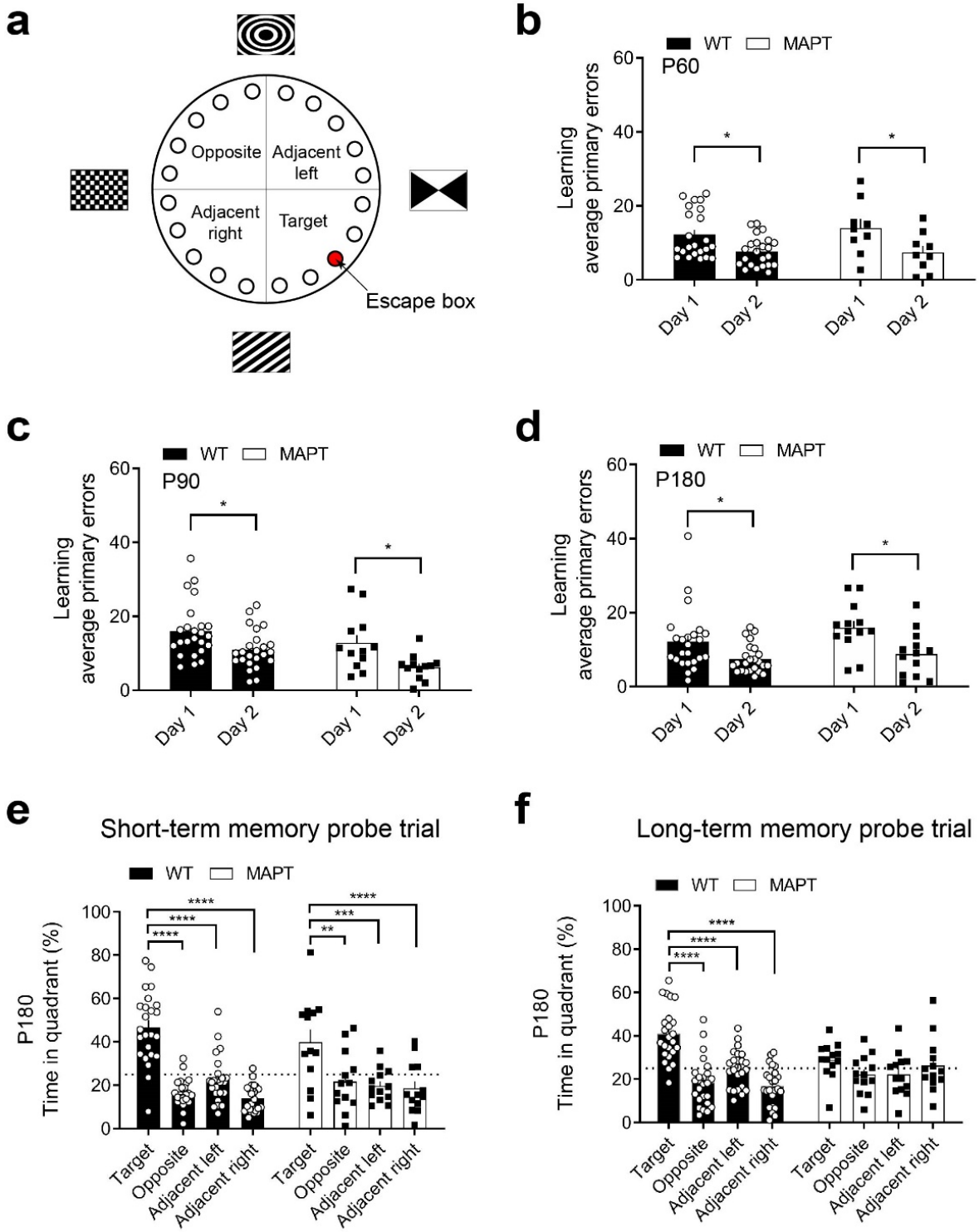
a
Opposite
Adjacent left
Adjacent right
Target
Escape box
b
WT
MAPT
P60
Learning average primary errors
Day 1
Day 2
c
P90
d
P180
e
Short-term memory probe trial
P180 Time in quadrant (%)
Target
Opposite
Adjacent left
Adjacent right
f
Long-term memory probe trial

tract that connects the hippocampi of both hemispheres, and each hippocampus with other subcortical structures of the brain (Fimbria-fornix-commissural pathway; Wyss *et al.*, 1980; reviewed by Kesner & Rolls, 2015). Tamoxifen was administered to P60 control (*Pdgfrα-CreER^{T2}::Rosa26-YFP*) and *MAPT* (*Pdgfrα-CreER^{T2}::Rosa26-YFP::Prnp-MAPT^{P301S}*) mice, and brain tissue was collected at P60+7, 90 or 120 days (**Figure 3.5**). Immunohistochemistry was performed on coronal cryosections, to allow detection of PDGFRα^{+} OPCs (red) and YFP (green) tracer in the hippocampus (**Figure 3.5a-d**), entorhinal cortex (**Figure 3.5e-h**) and fimbria (**Figure 3.5i-l**). By quantifying the proportion of OPCs that expressed YFP, we determined that ~40% of OPCs had undergone recombination in all brain regions examined in control and *MAPT* mice (**Figure 3.5m-o**). Furthermore, these YFP-labelled OPCs gave rise to YFP^{+} PDGFRα-negative presumptive oligodendrocytes over time (arrows, **Figure 3.5a-l**). However, between P60+90 and P60+120, the proportion of YFP^{+} cells that were PDGFRα-negative significantly increased in the hippocampus (**Figure 3.5p**), entorhinal cortex (**Figure 3.5q**) and fimbria (**Figure 3.5r**) of *MAPT* mice, despite being largely unchanged in controls. This equated to a doubling in the density of new YFP^{+} oligodendrocytes present in each region over a 1-month period, such that by P60+120 *MAPT* mice had significantly more new oligodendrocytes in the hippocampus (**Figure 3.5s**), entorhinal cortex (**Figure 3.5t**) and fimbria (**Figure 3.5u**), than control mice.

3.2.3. Fimbria OPC proliferation is increased in P180 *MAPT* mice

To determine whether human hyperphosphorylated tau influenced new oligodendrocyte number by modulating OPC proliferation, we next evaluated PDGFRα^{+} OPC density in the hippocampus (**Figure 3.6a-c**), entorhinal cortex (**Figure 3.6d**) and fimbria (**Figure 3.6e**) of control and *MAPT* mice, at P60+7, P60+90 and P60+120. OPC density was equivalent in

Figure 3.5. New oligodendrocyte addition is increased in the hippocampus, entorhinal cortex and fimbria of MAPT mice at P180

***a-l**) Representative confocal images showing PDGFRα (red), YFP (green), and Hoechst (blue) in the hippocampus (**a-d**), entorhinal cortex (**e-h**) and fimbria (**i-l**) of PDGFRα-CreER^{T2} :: Rosa26-YFP (control; **a-b, e-f, i-j**) and PDGFRα-CreER^{T2} :: Rosa26-YFP :: Prnp-MAPT^{P301S} (MAPT; **c-d, g-h, k-l**) mice at 90 (P60+90) and 120 (P60+120) days post tamoxifen administration (P60). **m-o**) Quantification of the proportion of recombined OPCs (YFP + PDGFRα + / PDGFRα +) in the hippocampus [(**m**) : Two-way ANOVA, genotype: F (1, 23) = 1.272, p = 0.2710; age: F (2, 23) = 0.8038, p = 0.4598; interaction: F (2, 23) = 0.04821, p = 0.9530], the entorhinal cortex [(**n**) : Two-way ANOVA, genotype: F (1, 25) = 3.13, p = 0.0891; age: F (2, 25) = 0.982, p = 0.3885; interaction: F (2, 25) = 0.169, p = 0.8455] and the fimbria [(**o**) : Two-way ANOVA, genotype: F (1, 23) = 3.469, p = 0.0753; age: F (2, 23) = 0.3587, p = 0.7024; interaction: F (2, 23) = 0.02172, p = 0.9785] of control (open circles, black bars) and MAPT (black squares, open bars) mice at 7, 90 and 120 days post tamoxifen administration (P60). **p-r**) Quantification of the proportion of recombined OPCs that differentiated into new oligodendrocytes (PDGFRα negative YFP+ / YFP+) over 7, 90 and 120 days in the hippocampus [(**p**) : Two-way ANOVA, genotype: F (1, 23) = 18.33, p = 0.0003; age: F (2, 23) = 20.33, p < 0.0001; interaction: F (2, 23) = 11.70, p = 0.0003], the entorhinal cortex [(**q**) : Two-way ANOVA, genotype: F (1, 25) = 9.489, p = 0.0050; age: F (2, 25) = 34.13, p < 0.0001; interaction: F (2, 25) = 15.42, p < 0.0001] and the fimbria [(**r**) : Two-way ANOVA, genotype: F (1, 23) = 10.18, p = 0.0041; age: F (2, 23) = 58.20, p < 0.0001; interaction: F (2, 23) = 10.49, p = 0.0006] of control and MAPT mice. **s-u**) Quantification of the density of new oligodendrocytes (PDGFRα-negative YFP+ / mm^2) added to the hippocampus [(**s**) : Two-way ANOVA, genotype: F (1, 23) = 23.09, p < 0.0001; age: F (2, 23) = 20.88, p < 0.0001; interaction: F (2, 23) = 15.26, p < 0.0001], the entorhinal cortex [(**t**) : Two-way ANOVA, genotype: F (1, 25) = 14.94, p = 0.0007; age: F (2, 25) = 18.28, p < 0.0001; interaction: F (2, 25) = 14.37, p < 0.0001] and the fimbria [(**u**) : Two-way ANOVA, genotype: F (1, 23) = 26.15, p < 0.0001; age: F (2, 23) = 35.02, p < 0.0001; interaction: F (2, 23) = 21.65, p < 0.0001]. Data are presented as mean ± SD, n=4-6 mice per group. Asterisks indicate significant differences identified by Bonferroni post hoc analysis, ****p < 0.0001. Scale bars represent 30 μm. Arrows indicate YFP+ PDGFRα+ recombined OPCs. Arrow heads indicate YFP+ PDGFRα-negative newly added oligodendrocytes.*

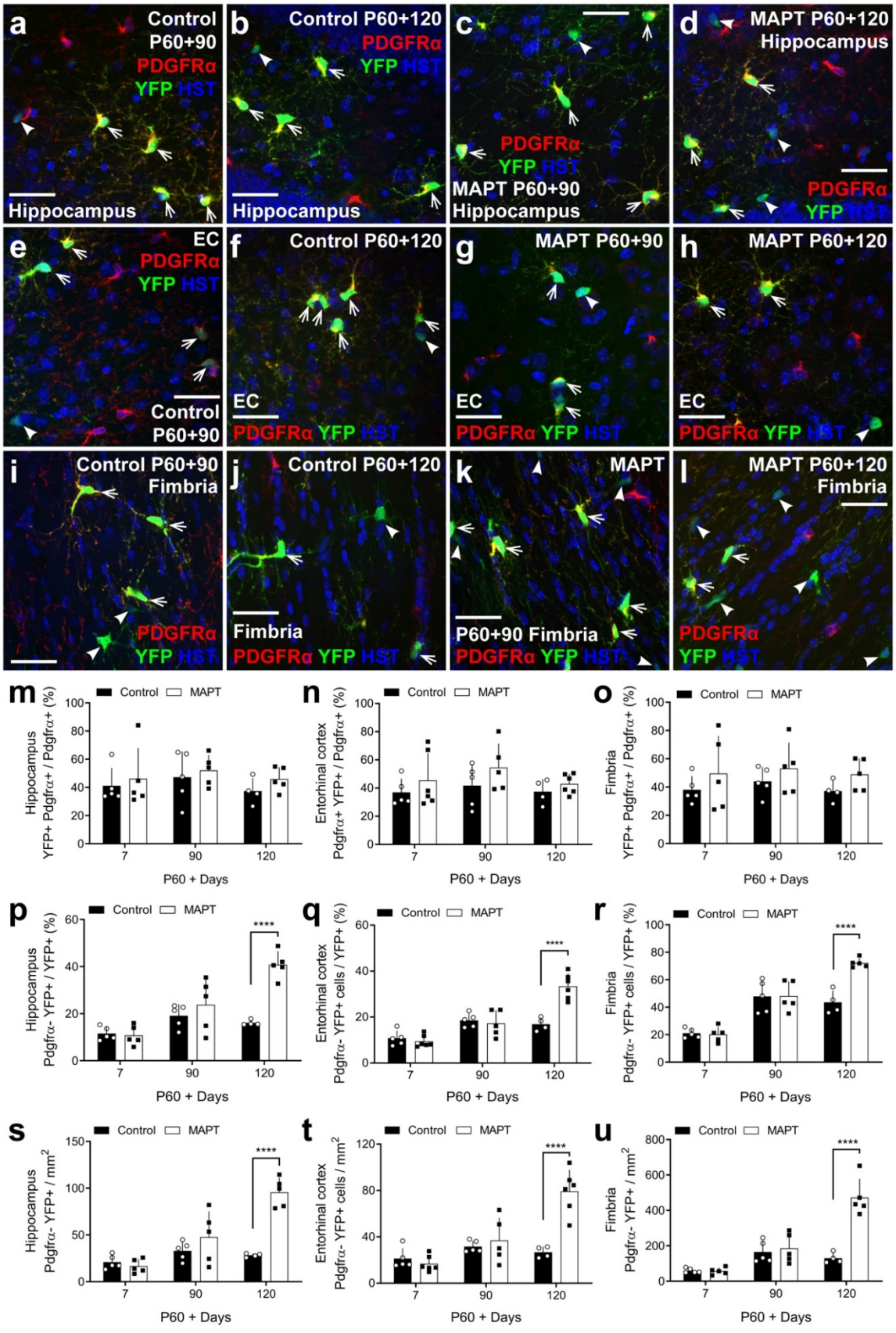
a
Control
P60+90
PDGFRα
YFP HST
Hippocampus
b
Control P60+120
PDGFRα
YFP HST
Hippocampus
c
PDGFRα
YFP HST
MAPT P60+90
Hippocampus
d
MAPT P60+120
Hippocampus
PDGFRα
YFP HST
e
EC
PDGFRα
YFP HST
Control
P60+90
f
Control P60+120
EC
PDGFRα YFP HST
g
MAPT P60+90
EC
PDGFRα YFP HST
h
MAPT P60+120
EC
PDGFRα YFP HST
i
Control P60+90
Fimbria
PDGFRα
YFP HST
j
Control P60+120
Fimbria
PDGFRα YFP HST
k
MAPT
P60+90 Fimbria
PDGFRα YFP HST
l
MAPT P60+120
Fimbria
PDGFRα
YFP HST
m
Control
MAPT
Hippocampus
YFP+ Pdgfrα+ / Pdgfrα+ (%)
P60 + Days
n
Control
MAPT
Entorhinal cortex
Pdgfrα+ YFP+ / Pdgfrα+ (%)
P60 + Days
o
Control
MAPT
Fimbria
YFP+ Pdgfrα+ / Pdgfrα+ (%)
P60 + Days
p
Control
MAPT
****
Hippocampus
Pdgfrα- YFP+ / YFP+ (%)
P60 + Days
q
Control
MAPT
****
Entorhinal cortex
Pdgfrα- YFP+ cells / YFP+ (%)
P60 + Days
r
Control
MAPT
****
Fimbria
Pdgfrα- YFP+ cells / YFP+ (%)
P60 + Days
s
Control
MAPT
****
Hippocampus
Pdgfrα- YFP+ / mm2
P60 + Days
t
Control
MAPT
****
Entorhinal cortex
Pdgfrα- YFP+ cells / mm2
P60 + Days
u
Control
MAPT
****
Fimbria
Pdgfrα- YFP+ / mm2
P60 + Days

Figure 3.6. OPC proliferation is increased in the fimbria of MAPT mice at P180

***a-b**) Representative confocal image stacks showing PDGFRα labelling in the hippocampus of PDGFRα-CreER^{T2} :: Rosa26-YFP (control; **a**) and PDGFRα-CreER^{T2} :: Rosa26-YFP :: Prnp-MAPT^{P301S} (MAPT; **b**) mice at 120 days post tamoxifen administration (P60). **c-e**) Quantification of OPC density (PDGFRα+ / mm^2) in the hippocampus [(**c**): Two-way ANOVA, genotype: F (1, 23) = 1.938, p = 0.1772; age: F (2, 23) = 0.3121, p = 0.7349; interaction: F (2, 23) = 2.015, p = 0.1562], the entorhinal cortex [(**d**): Two-way ANOVA, genotype: F (1, 25) = 1.188, p = 0.2861; age: F (2, 25) = 1.162, p = 0.3292; interaction: F (2, 25) = 3.189, p = 0.0584] and the fimbria [(**e**): Two-way ANOVA, genotype: F (1, 23) = 0.5396, p = 0.4700; age: F (2, 23) = 12.37, p = 0.0002; interaction: F (2, 23) = 0.2118, p = 0.8107] of control (open circles, black bars) and MAPT (black squares, open bars) mice. **f-k**) Representative confocal image stacks showing PDGFRα (red), EdU (green) and Hoechst 33342 (blue) labelling in the hippocampus (**f-g**), entorhinal cortex (**h-i**) and fimbria (**j-k**) of P180 wildtype (WT; open circles, black bars) and MAPT (black squares, open bars) mice following 5 days of EdU administration. **l**) Quantification of the proportion of EdU+ OPCs (EdU+ PDGFRα+ / PDGFRα+) in the hippocampus, entorhinal cortex and fimbria of WT and MAPT mice [(**l**): Two-way ANOVA, genotype: F (1, 20) = 11.98, p = 0.0025; brain region: F (2, 20) = 121.7, p < 0.0001; interaction: F (2, 20) = 5.997, p = 0.0091]. **m-n**) Representative confocal images showing cells expressing PDGFRα (red) and Ki67 (green) in the fimbria of P180 WT (**m**) and MAPT (**n**) mice. (**o**) Quantification of the proportion of Ki67+ OPCs (Ki67+ PDGFRα+ / PDGFRα+) at P180 within the fimbria (Two tailed, unpaired t-test, p = 0.798). Data are presented as mean ± SD for n=3-6 mice per group. Arrows indicate PDGFRα+ OPCs. Arrow heads indicate recently divided OPCs (EdU+ PDGFRα+). Scale bars represent 80µm (**a-b**); 40µm (**f-k**); 20µm (**m-n**).*

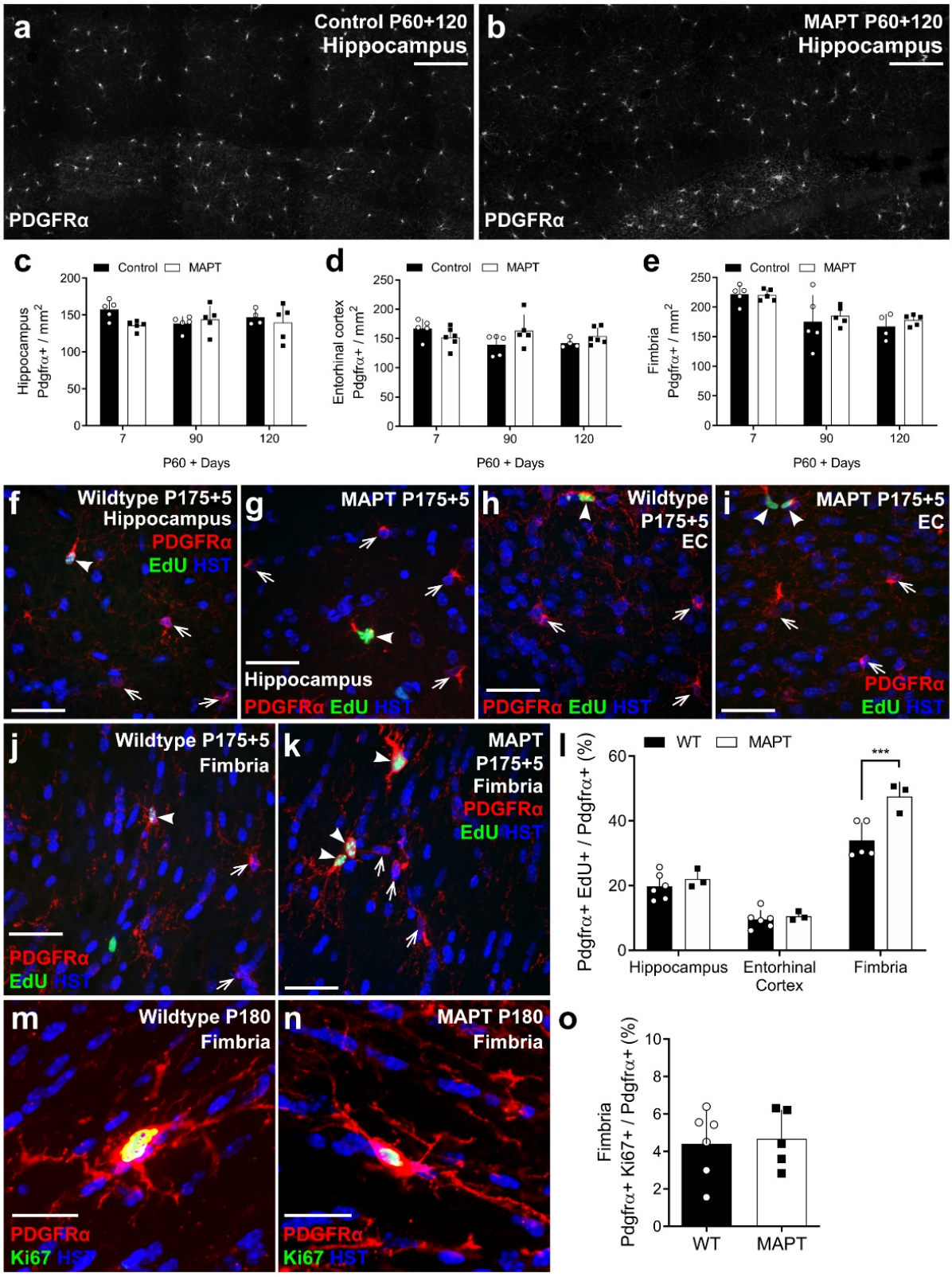
a
Control P60+120
Hippocampus
PDGFRα
b
MAPT P60+120
Hippocampus
PDGFRα
c
Control
MAPT
Hippocampus
Pdgfrα+ / mm2
P60 + Days
d
Control
MAPT
Entorhinal cortex
Pdgfrα+ / mm2
P60 + Days
e
Control
MAPT
Fimbria
Pdgfrα+ / mm2
P60 + Days
f
Wildtype P175+5
Hippocampus
PDGFRα
EdU HST
g
MAPT P175+5
Hippocampus
PDGFRα EdU HST
h
Wildtype
P175+5
EC
PDGFRα EdU HST
i
MAPT P175+5
EC
PDGFRα
EdU HST
j
Wildtype P175+5
Fimbria
PDGFRα
EdU HST
k
MAPT
P175+5
Fimbria
PDGFRα
EdU HST
l
WT
MAPT
***
Pdgfrα+ EdU+ / Pdgfrα+ (%)
Hippocampus
Entorhinal
Cortex
Fimbria
m
Wildtype P180
Fimbria
PDGFRα
Ki67 HST
n
MAPT P180
Fimbria
PDGFRα
Ki67 HST
o
Fimbria
Pdgfrα+ Ki67+ / Pdgfrα+ (%)
WT
MAPT

control and *MAPT* mice and did not change with age in any region (**Figure 3.6c-e**). To determine whether OPC proliferation was affected by hyperphosphorylated tau, P175 WT and *MAPT* mice were given the thymidine-analogue EdU via their drinking water for 5 consecutive days, and coronal cryosections processed to detect PDGFRα (red) and EdU (green) (**Figure 3.6f-k**). The proportion of OPCs that proliferated to incorporate EdU (EdU^+ $PDGFR\alpha^+$ / $PDGFR\alpha^+$ x 100) was equivalent in the hippocampus (**Figure 3.6f, g, l**) and entorhinal cortex (**Figure 3.6h, i, l**) of WT and *MAPT* mice. By contrast, we detected a small but significant increase in OPC proliferation in the fimbria of *MAPT* mice, compared with WT mice (**Figure 3.6j-l**), but this was not a large enough change in proliferation to overtly alter the proportion of OPCs that expressed the proliferative marker Ki67 at P180 (**Figure 3.6m-n**). Consequently, this small increase in fimbria OPC proliferation appears unable to explain the large increase in new oligodendrocyte number noted across the hippocampus, entorhinal cortex and fimbria of *MAPT* mice at P60+120 (**Figure 3.5**).

3.2.4. Oligodendrocyte density is normal in *MAPT* mice

To determine whether the increase in new oligodendrocyte addition was accompanied by an overall increase in oligodendrocyte number in the hippocampus (**Figure 3.7a-d**), entorhinal cortex (**Figure 3.7e-h**) or fimbria (**Figure 3.7i-l**), we performed immunohistochemistry on coronal brain cryosections from P120 and P180 WT and *MAPT* mice, to detect the oligodendrocyte marker ASPA. We found that the density of $ASPA^+$ oligodendrocytes was unchanged between P120 and P180 in the hippocampus (**Figure 3.7m**), entorhinal cortex (**Figure 3.7n**) and fimbria (**Figure 3.7o**) of WT or *MAPT* mice, and that the overexpression of hyperphosphorylated tau did not influence total oligodendrocyte density in any region. However, as only 284 ± 36 (mean ± SD) oligodendrocytes are present per mm^2 in the

Figure 3.7. Oligodendrocyte population is not altered in MAPT mice at P120 and P180

***a-l**) Representative confocal images of ASPA (red) and Hoechst 33342 (blue) in the hippocampus (**a-d**), entorhinal cortex (EC; **e-h**) and fimbria (**i-l**) of WT and MAPT mice at P120 and P180. **m-o**) Quantification of total oligodendrocyte density (ASPA+ / mm^2) in the hippocampus [(**m**): Two-way ANOVA, genotype: F (1, 17) = 0.417, p = 0.526; age: F (1, 17) = 0.849, p = 0.369; interaction: (1, 17) = 1.100, p = 0.308], the entorhinal cortex [(**n**): Two-way ANOVA, genotype: F (1, 18) = 0.004, p = 0.948; age: F (1, 18) = 0.0254, p = 0.875; interaction: F (1, 18) = 0.397, p = 0.536] and the fimbria [(**o**): Two-way ANOVA, genotype: F (1, 14) = 0.594, p = 0.453; age: F (1, 14) = 1.145, p = 0.302; interaction: F (1, 14) = 0.080, p = 0.781] of WT (open circles, black bars) and MAPT (black squares, open bars) mice at P120 and P180. Data are presented as mean ± SD, n=3-5 mice per group. Scale bars represent 40µm.*

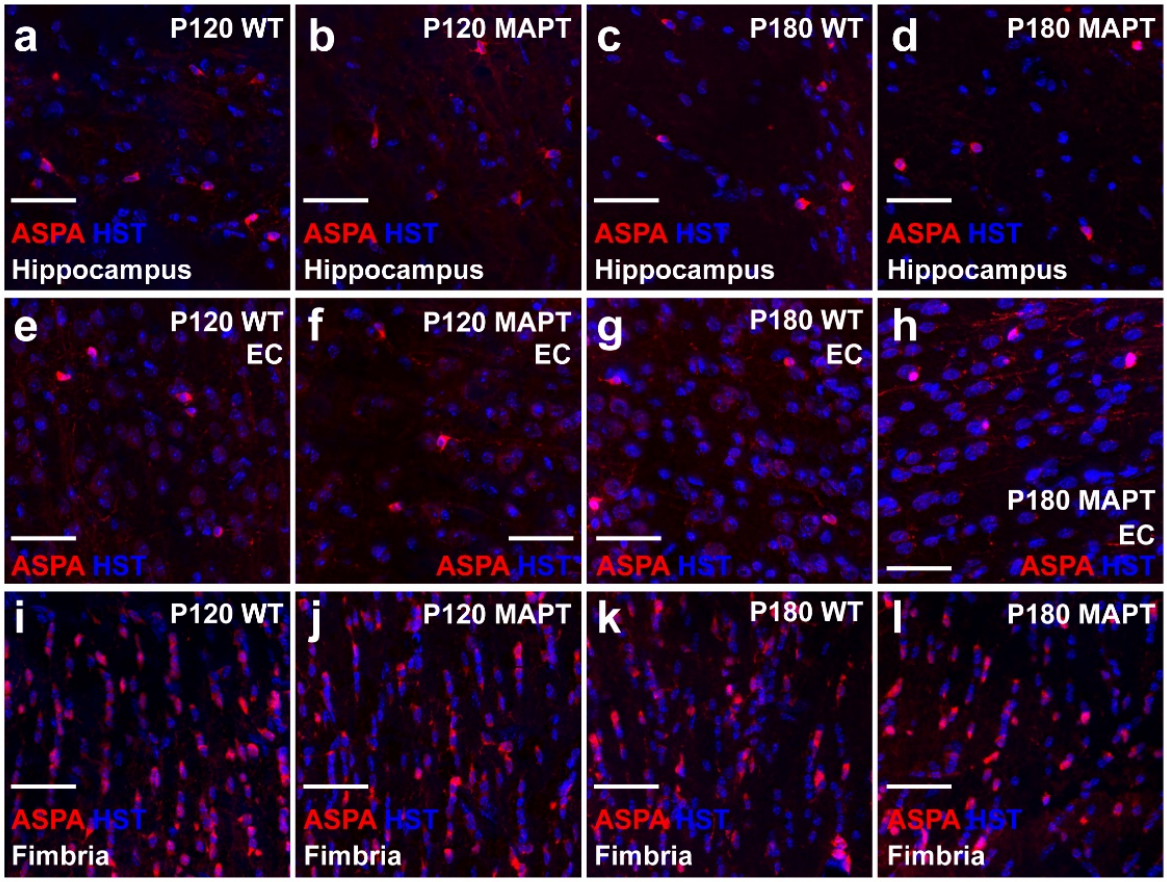
a
P120 WT
ASPA HST
Hippocampus
b
P120 MAPT
ASPA HST
Hippocampus
c
P180 WT
ASPA HST
Hippocampus
d
P180 MAPT
ASPA HST
Hippocampus
e
P120 WT
EC
ASPA HST
f
P120 MAPT
EC
ASPA HST
g
P180 WT
EC
ASPA HST
h
P180 MAPT
EC
ASPA HST
i
P120 WT
ASPA HST
Fimbria
j
P120 MAPT
ASPA HST
Fimbria
k
P180 WT
ASPA HST
Fimbria
l
P180 MAPT
ASPA HST
Fimbria

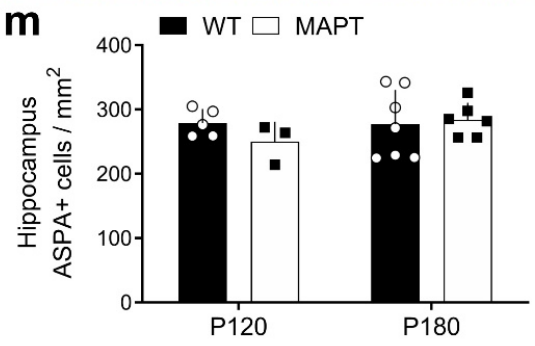
m
WT
MAPT
Hippocampus
ASPA+ cells / mm2
400
300
200
100
0
P120
P180

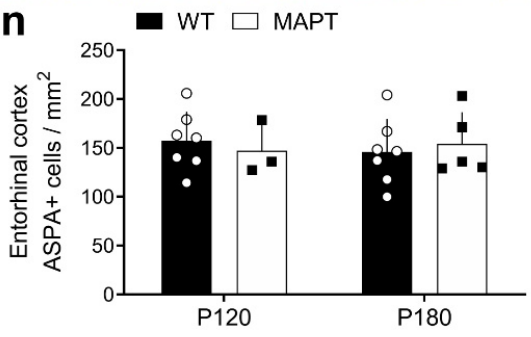
n
WT
MAPT
Entorhinal cortex
ASPA+ cells / mm2
250
200
150
100
50
0
P120
P180

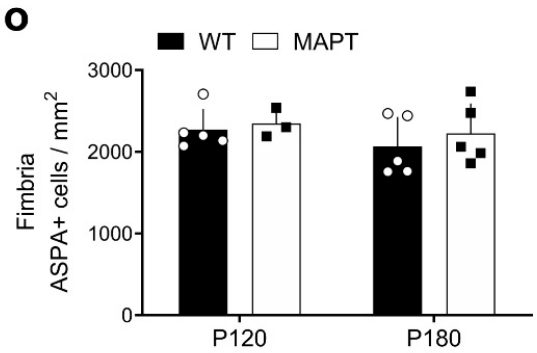
o
WT
MAPT
Fimbria
ASPA+ cells / mm2
3000
2000
1000
0
P120
P180

hippocampus of P180 *MAPT* mice, and 95 ± 15 (mean ± SD) cells/mm^2 are newborn oligodendrocytes, these data suggest that ~33% of oligodendrocytes present in the P180 *MAPT* hippocampus are newborn oligodendrocytes. In the entorhinal cortex and fimbria, it equates to ~51 and 21%, respectively. As the new oligodendrocytes comprise such a large proportion of all oligodendrocytes in the hippocampus, entorhinal cortex and fimbria of the P180 *MAPT* mice, but do not increase total oligodendrocyte density beyond that seen in WT mice, it is likely that oligodendrocyte addition is accompanied by oligodendrocyte loss in the *MAPT* mouse brain.

To determine whether new oligodendrocytes added to the brains of P60+120 controls and *MAPT* mice are mature oligodendrocytes, we immunolabelled coronal cryosections, containing the hippocampus and fimbria, to detect PDGFRα$^+$ (blue), YFP$^+$ (green) and ASPA (red) (**Figure 3.8a-h**). We found that the density of YFP$^+$ ASPA$^+$ mature oligodendrocytes was increased in the hippocampus (**Figure 3.8.i**) and fimbria (**Figure 3.8.j**) of *MAPT* mice relative to controls, while the density of YFP$^+$ PDGFRα-negative ASPA-negative presumptive premyelinating oligodendrocytes was equivalent between *MAPT* mice and controls. Therefore, new oligodendrocytes may be added to replace myelin.

3.2.5. Myelination is not altered in *MAPT* mice

To further explore the possibility of oligodendrocyte turnover, we next quantified myelination in the stratum lacunosum moleculare of the CA1 region of the hippocampus in P180 WT and *MAPT* mice by TEM (**Figure 3.9**). We found that total axon density (**Figure 3.9a-c**) and myelinated axon density (**Figure 3.9d**) were equivalent between WT and *MAPT* mice. Looking more closely at the myelinated axons, we found that the g-ratio [axon diameter / (axon+myelin diameter)], a measure of myelin thickness relative to axon size, was the same

Figure 3.8. MAPT mice add more ASPA$^+$ mature oligodendrocytes to the hippocampus and fimbria than control mice between 5 and 6 months of age.

***a-h**) Confocal images showing ASPA (red), PDGFRα (blue) and YFP (green) in the hippocampus of P60 + 120 Pdgfrα-CreERT2:: Rosa26-YFP (control; **a-d**) and Pdgfrα-CreERT2:: Rosa26-YFP:: Prnp-MAPT^{P301S} (MAPT; **e-h**) mice. **i**) Quantification of the density of all YFP$^+$ cells that are PDGFRα-negative in the hippocampus of P60 + 120 control and MAPT mice, including those that are YFP$^+$ PDGFRα-negative ASPA-negative premyelinating oligodendrocytes versus YFP$^+$ PDGFRα-negative ASPA$^+$ mature oligodendrocytes. [two-way ANOVA, genotype: $F(1, 12) = 120.5$, $p < .0001$; cell type: $F(2, 12) = 79.72$, $p < .0001$; interaction: $F(2, 12) = 25.19$, $p < .0001$]. **j**) Quantification of the density of all YFP$^+$ cells that are PDGFRα-negative in the fimbria of P60 + 120 control and MAPT mice, including those that are YFP$^+$ PDGFRα-negative ASPA-negative premyelinating oligodendrocytes versus YFP$^+$ PDGFRα-negative ASPA$^+$ mature oligodendrocytes. [two-way ANOVA, genotype: $F(1, 12) = 40.81$, $p < .0001$; cell type: $F(2, 12) = 15.27$, $p = .0005$; interaction: $F(2, 12) = 5.46$, $p = .02$]. Asterisks indicate significant differences identified by Bonferroni post hoc analysis, **p < .01, ***p < .001, ****p < .0001. White arrows indicate newborn oligodendrocytes (YFP$^+$ ASPA$^+$ cells). Scale bars represent 35μm.*

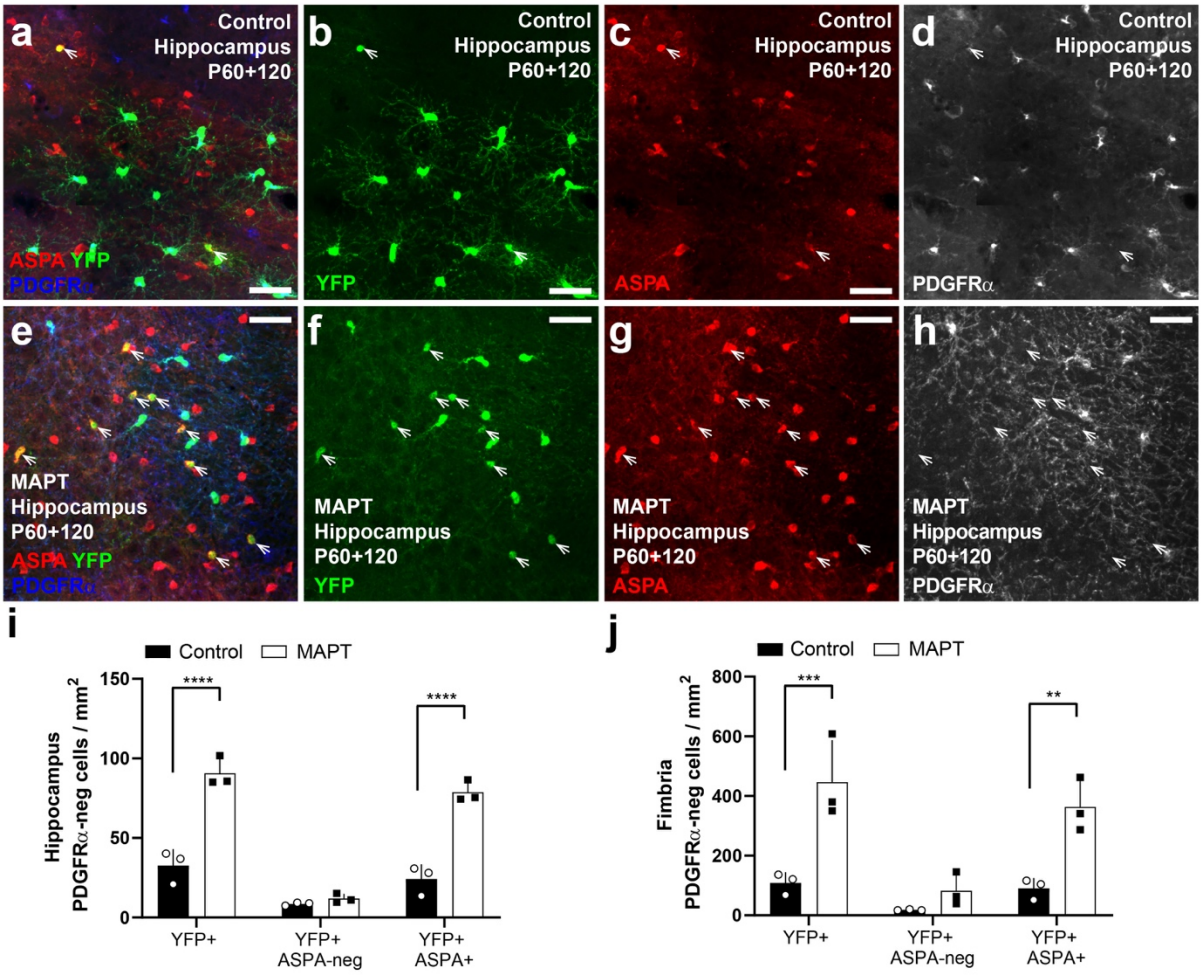
a
Control
Hippocampus
P60+120
ASPA YFP
PDGFRα
b
Control
Hippocampus
P60+120
YFP
c
Control
Hippocampus
P60+120
ASPA
d
Control
Hippocampus
P60+120
PDGFRα
e
MAPT
Hippocampus
P60+120
ASPA YFP
PDGFRα
f
MAPT
Hippocampus
P60+120
YFP
g
MAPT
Hippocampus
P60+120
ASPA
h
MAPT
Hippocampus
P60+120
PDGFRα

i
Control
MAPT
Hippocampus
PDGFRα-neg cells / mm2
150
100
50
0
****
****
YFP+
YFP+
ASPA-neg
YFP+
ASPA+

j
Control
MAPT
Fimbria
PDGFRα-neg cells / mm2
800
600
400
200
0
***
**
YFP+
YFP+
ASPA-neg
YFP+
ASPA+

Figure 3.9. Axon density, proportion of myelinated axons and myelin thickness are not altered in the hippocampus of MAPT mice at P180

***a-b**) Representative electron micrographs from the CA1 region of the hippocampus of WT (**a**) and MAPT (**b**) mice at P180. **c**) Quantification of axon density (axons/mm^2) in WT (open circles) and MAPT (black squares) mice (Two-tailed, unpaired t-test: t=0.2567, df=5, p =0.8076). **d**) Quantification of the proportion of myelinated axons in the CA1 of WT and MAPT mice at P180 (Two-tailed, unpaired t-test: t=0.1780, df=5, p = 0.8657). **e**) Graphical representation of the g-ratio distribution based on axon diameter (Kolmogorov-Smirnoff test, K-S D = 0.06307, p = 0.2825; n = 98-190 myelinated axons per mouse). **f-i**) Representative high magnification electron micrographs through a single myelinated axon within the CA1 region of the number of myelin wraps in WT (**f-g**) and MAPT mice (**h-i**) at P180. **j**) Quantification of average g-ratio per animal in WT and MAPT mice at P180 (Two-tailed, unpaired t-test: t=0.5232, df=5, p = 0.6232). **k**) Quantification of average myelin wraps per animal in WT and MAPT mice at P180 (Two-tailed, unpaired t-test: t=1.112, df=5, p = 0.3167). Scale bars represent: 1µm (**a-b**), 300nm (**f, h**) and 100nm (**g, i**). Results are presented as mean ± SD, n = 3-4 mice per genotype.*

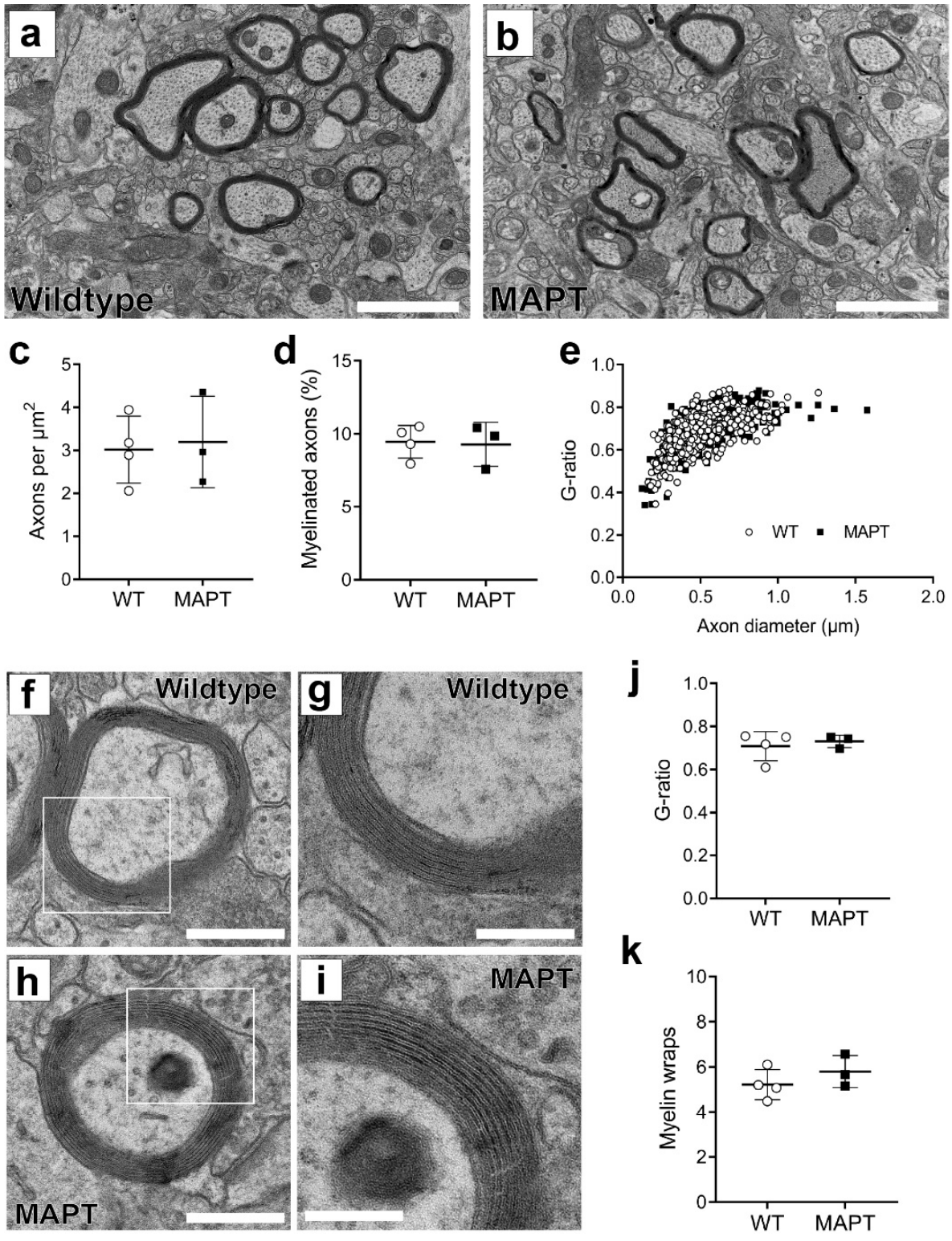
a
Wildtype
b
MAPT
c
Axons per µm²
WT
MAPT
d
Myelinated axons (%)
WT
MAPT
e
G-ratio
WT
MAPT
Axon diameter (µm)
f
Wildtype
g
Wildtype
h
MAPT
i
MAPT
j
G-ratio
WT
MAPT
k
Myelin wraps
WT
MAPT

for axons in the hippocampus of WT and *MAPT* mice (**Figure 3.9e-i**) and that across individual mice, the average g-ratio (**Figure 3.9j**) and average number of myelin wraps per sheath (**Figure 3.9k**) was also unaffected by genotype. These data suggest that myelination is normal in the hippocampus of P180 *MAPT* mice, or that newborn oligodendrocytes act to maintain a normal level of myelination.

3.3. Discussion

Myelin and axon loss are associated with cognitive decline and is exacerbated in people diagnosed with tauopathy. However, the behaviour of OPCs early in the disease process, and the potential for myelin repair remains unclear. Herein, by tracing the fate of OPCs in *MAPT* transgenic mice we show that the number of adult-born oligodendrocytes increases in the hippocampus, entorhinal cortex and fimbria between 5 and 6 months of age, prior to the onset of overt cognitive symptoms. This increase in new oligodendrocyte addition cannot be explained by an equivalent increase in OPC proliferation and was not associated with a change in total oligodendrocyte density, or myelination within the hippocampus.

3.3.1. *MAPT* mice do not develop overt motor or cognitive deficits by 6 months of age.

MAPT transgenic mice overexpress the T34 isoform of human *MAPT* (1N4R) with the P301S mutation under the regulation of the mouse prion promotor, leading to human tau being expressed in the brain at levels that are 5-times above that of the endogenous mouse protein (Yoshiyama et al., 2007). To determine whether the relative expression of human tau within the hippocampus changed with age, we performed Western blot analysis of hippocampal lysates from P30, P60, P90 and P180 mice. We found that human tau and hyperphosphorylated human tau were not detected in WT mice, but were abundantly expressed in *MAPT* mice, and

the level of expression remained stable over time (**Figure 3.1**). *MAPT* mice, maintained on a B6C3H background, exhibit prominent microglial activation, prior to the formation of neurofibrillary tangles at 6 months of age (Yoshiyama et al., 2007). We observed microglial activation at 6 months of age (**Figure 3.3**), and neurofibrillary tangles are reported to develop at 10 months of age when *MAPT* mice are backcrossed onto a C57BL/6 background (Dumont et al., 2011). The more severe phenotype of *MAPT* mice on a B6C3H background is further supported by poorer survival outcomes with ~25% dying by 6 months of age (Yoshiyama et al., 2007) compared with only ~15% of mice dying within the first 6 months when they are crossed onto a C57BL/6 background (Merchán-Rubira *et al.*, 2019; **Figure 3.2**).

Tauopathies are associated with progressive motor degeneration and cognitive impairment (Lewis *et al.*, 2000; Ramsden *et al.*, 2005; Santacruz *et al.*, 2005; Yoshiyama *et al.*, 2007; Takeuchi *et al.*, 2011; reviewed by Ferrer, 2018). To determine whether *MAPT* mice had impaired locomotor or cognitive performance, they were subjected to a battery of behavioural tests at 2, 3 and 6 months of age. We found that locomotion in an open field task was not affected by overexpression of $MAPT^{P301S}$ up to 6 months of age (**Figure 3.1)**, suggesting there was no overt impairment in motor function. There was also no effect of $MAPT^{P301S}$ overexpression on working memory performance in the T-maze, short term recognition memory in the novel object recognition task, or spatial learning and memory in the Barnes maze at any age (**Figure 3.1**), suggesting that these mice do not exhibit a decline in cognitive performance until after 6 months of age. Overexpression of the P301L mutation of human *MAPT* under the mouse prion promotor results in a rapid decline in motor function from as early as 4.5 months of age in homozygous and 6.5 months in heterozygous mice (Lewis et al., 2000). However, motor decline is not observed in mice overexpressing the P301S mutation under the same promotor (Dumont *et al.*, 2011; Takeuchi *et al.*, 2011; Chalermpalanupap *et*

al., 2017; **Figure 3.1**). Instead, transient increases in locomotor behaviour in an open field arena have been reported that are either only seen between 30 and 90 min of a 2-hour observation time (Takeuchi et al., 2011), or present at 7 months of age but not at 10 months (Dumont et al., 2011). For *MAPT* mice raised on the B6CH3 background, spatial memory and contextual fear conditioning have been reported at 6 (Takeuchi et al., 2011) and 7.5 (Lasagna-Reeves et al., 2016) months of age. However, consistent with our data, when *MAPT* mice are backcrossed onto a C57BL/6 background the onset of memory impairment is delayed until after 10 months of age (Dumont et al., 2011; Chalermpalanupap et al., 2017), such that performance in a Barnes maze is equivalent to WT mice at 6 months of age (Takeuchi et al., 2011). These data indicated that cellular changes identified in *MAPT* mice ≤ 6 months of age occur prior to the onset of cognitive decline.

3.3.2. The number of new oligodendrocytes added to the brain of *MAPT* mice increases between 5 and 6 months of age

OPCs continue to generate new oligodendrocytes at different rates in the adult mouse brain grey and white matter (Dimou *et al.*, 2008; Rivers *et al.*, 2008; Hill *et al.*, 2013; Young *et al.*, 2013; Fukushima *et al.*, 2015). While the rate of OPC proliferation and oligodendrocyte addition slows with aging in the mouse CNS (reviewed by Wang & Young, 2014), experimental interventions that produce demyelination have been shown to stimulate OPC proliferation and result in the rapid replacement of oligodendrocytes and remyelination (Tripathi et al., 2010; Zawadzka et al., 2010; Assinck et al., 2017; Baxi et al., 2017). To determine whether the expression of the human $MAPT^{P301S}$ variant in neurons was associated with a change in OPC behaviour and new oligodendrocyte addition, we fluorescently labelled OPCs and followed their fate over time (**Figure 3.5**). We found that a small number of newborn YFP-labelled oligodendrocytes accumulated in the hippocampus, entorhinal cortex

and fimbria of control and *MAPT* transgenic mice between P60 and P150, and that the rate of oligodendrocyte addition was not affected by *MAPT*^{P301S} expression. However, between P150 and P180, when oligodendrocyte addition was negligible in control mice, the number of YFP-labelled oligodendrocytes increased significantly in *MAPT* transgenic mice, in each of the brain regions examined. Previous studies have not examined oligodendrogenesis in *MAPT* transgenic mice; however, there is some evidence that oligodendrogenesis is increased in P60 adult *Thy1.2-MAPT*^{P301S} transgenic mice following toxin-induced focal demyelination of the ventral funiculus in the spinal cord (Ossola et al., 2016). 14 days after demyelination, the density of APC^{+} OLIG2^{+} oligodendrocytes was increased in the lesion site of *Thy1.2-MAPT*^{P301S} transgenic mice compared to WT lesioned mice (Ossola et al., 2016), confirming the capacity for OPCs to efficiently remyelinate the injured CNS in the early stages of tau pathology.

A large increase in oligodendrocyte generation is often accompanied by an increase in OPC proliferation, as OPC differentiation stimulates the proliferation of adjacent OPCs to sustain the OPC population (Hughes et al., 2013). To determine whether expression of the human *MAPT*^{P301S} variant, and the associated increase in new oligodendrocyte number, was associated with elevated OPC proliferation, dividing OPCs were EdU labelled in the brain of 6-month old control and *MAPT* transgenic mice (**Figure 3.6**). While OPC proliferation was elevated in the fimbria of *MAPT* transgenic mice, when compared with WT littermates, it was not elevated in the hippocampus or entorhinal cortex. These data could be explained by an increase in oligodendrogenesis occurring close to P150, such that OPC proliferation has returned to normal by P180. We have previously shown that new oligodendrocyte number can be increased without increasing OPC proliferation, as this can be achieved by enhancing the survival of the newborn cells (Cullen et al., 2019). It is therefore possible that oligodendrocyte loss or other stimuli could increase the number of new oligodendrocytes detected by enhancing newborn

oligodendrocyte survival in the *MAPT* transgenic mice. Indeed, a combination of increased cell generation and improved survival would likely be needed to account for the substantial increase in new oligodendrocyte number observed over a one month-period in the *MAPT* transgenic mice.

3.3.3. Is oligodendrocyte turnover increased in *MAPT* mice?

To determine whether the large number of new oligodendrocytes added to the hippocampus, entorhinal cortex and fimbria of *MAPT* transgenic mice increased the total number of oligodendrocytes, or acted to replace oligodendrocytes lost to pathology, we quantified oligodendrocyte density in each region (**Figure 3.7**) and determined whether newborn oligodendrocytes added to the brains were mature oligodendrocytes (**Figure 3.8**). Oligodendrocyte density was significantly higher in the fimbria than in the hippocampus or entorhinal cortex but was equivalent between WT and *MAPT* transgenic mice in each region (**Figure 3.7**). However, a larger proportion of new oligodendrocytes were added and matured between 5 and 6 months of age in *MAPT* mice compared to controls (**Figure 3.8**), suggesting that oligodendrocyte turnover had occurred. To confirm that this phenotype was not associated with neuron loss, we quantified axon density and the proportion of axons that are myelinated (**Figure 3.9**) in the hippocampus at 6 months of age. Axon density in the CA1 subfield of the hippocampus was normal in 6-month-old *MAPT* transgenic mice, and the proportion of axons that were myelinated, and their myelin thickness was also equivalent to that of WT mice. As the newborn oligodendrocytes comprise a large proportion of all oligodendrocytes detected in the grey matter regions of *MAPT* transgenic mice, it would not be possible for their addition to result in no change in total oligodendrocyte addition or the proportion of axons that are myelinated without an increase in oligodendrocyte death and myelin loss. Therefore, we suggest that oligodendrocyte addition between P150 and P180 is driven by the need for

oligodendrocyte replacement in the *MAPT* transgenic mice and propose that these oligodendrocytes act to maintain myelin at this early stage of tauopathy.

Hyperphosphorylated tau can directly affect oligodendrocytes as they express tau proteins (Müller et al., 1997; Seiberlich et al., 2015), and can develop tau inclusions (Ikeda et al., 1998; Arai et al., 2001), which leads to oligodendrocyte degeneration in transgenic mice overexpressing human $MAPT^{P301L}$ variant throughout the CNS under the mouse α-tubulin promoter (Higuchi et al., 2002). However, the human $MAPT^{P301S}$ variant is primarily expressed in neurons by the prion protein promoter (Bailly et al., 2004; Tremblay et al., 2007) in our study; therefore, the oligodendrocyte phenotype observed is likely to be a secondary outcome of neuronal tauopathy.

Chapter 4: Amyloidosis is associated with the formation of thicker myelin in development and increased adult oligodendrogenesis

4.1. Introduction

In the aging human brain, white matter degeneration occurs in regions critical for cognitive and emotional processing, including the hippocampus, neocortex and frontal white matter tracts, and the extent of white matter degeneration correlates with the degree of cognitive impairment and loss of information processing speed (Charlton et al., 2006; Hirsiger et al., 2017; Chopra et al., 2018; Fan et al., 2019). However, the degree of white matter degeneration is exacerbated in AD (Choi et al., 2005; Stricker et al., 2009; Zhang et al., 2009; O'Dwyer et al., 2011; Benitez et al., 2014; Brueggen et al., 2019). AD is a progressive neurodegenerative disease characterized post-mortem by the presence of extracellular plaques of aggregated amyloid β (Miller et al., 1993; Roher et al., 1993; Burgold et al., 2011; reviewed by Selkoe and Hardy, 2016), and the detection of neurofibrillary tangles, form by the intracellular aggregation of cytoskeletal proteins, mainly hyperphosphorylated tau (Goedert et al., 1989; Schmidt et al., 1990; Braak and Braak, 1996; Iseki et al., 2006). Oligodendrocyte loss and demyelination has also been detected in post-mortem AD brain at the site of pathological inclusions throughout the brain (Mitew et al., 2010; Behrendt et al., 2013; Tse et al., 2018). As diffusion tensor imaging studies, examining individuals in the preclinical stages of disease, have determined that the extent to which fractional anisotropy increases and mean diffusivity decreases for white matter regions including the fornix, cingulum and corpus callosum, correlates with amyloid β42 load (Gold et al., 2014; Racine et al., 2014; Shi et al., 2015), early white matter degeneration may be associated with amyloidosis. This idea is further supported by the fact that in preclinical individuals carrying gene mutations associated with increased risk of AD,

lower cerebral spinal fluid concentration of amyloid β42 correlated with a greater severity of white matter hyperintensities identified by magnetic resonance imaging (Scott et al., 2015; Lee et al., 2016). Decreased concentration of amyloid β42 in cerebral spinal fluid are associated with increased amyloid plaque deposition in the brain of AD patients (Grimmer et al., 2009) and white matter hyperintensity volume increases after the reduction of cerebral spinal fluid amyloid β42 concentration, but prior to symptom onset in preclinical patients (Lee et al., 2016) indicating that amyloid induced changes in white matter integrity may be an early feature of AD pathophysiology.

A number of studies have demonstrated that oligodendrocyte function is impaired by exposure to amyloid, with cultured rat oligodendrocytes exposed to amyloid β1-42 or amyloid β25-35, experiencing oxidative stress and undergoing cell death (Xu et al., 2001; Lee et al., 2004), and exposed to amyloid β1-42 showing impaired myelin sheath formation (Horiuchi et al., 2012). Additionally, exposure of a mouse oligodendrocyte progenitor cell line to amyloid β1-42 has been shown to induce cell death in the differentiated and undifferentiated cells (Desai et al., 2010). However, when the undifferentiated cells also carried pathological variant of human *PSEN1*^{M146V}, exposure to amyloid β1-42 increased the number of CC1^{+} MBP-negative premyelinating oligodendrocytes, an effect that was not observed in cells carrying human *PSEN1* (Desai et al., 2011), suggesting that pathological variants of *PSEN1* can modulate the response of OPCs to amyloid pathology.

A small number of studies have examined the influence of amyloid pathology on OPC and oligodendrocyte function *in vivo*, and these studies have largely examined the combined effect of human pathological variants in *APP* and *PSEN1*. In APP/PS1 transgenic mice, amyloid

plaques form by 2 months of age (Radde et al., 2006), and are associated with focal demyelination at 6 months of age (Behrendt et al., 2013). However, OPCs and oligodendrocytes appear to respond early to pathology, as expression of the OPC proteoglycan NG2 and the oligodendrocyte proteins CNP and MBP are already elevated in the hippocampus by 2 months of age (Wu et al., 2017). Despite an increase in OPC density and proliferation and GSTpi^{+} oligodendrocyte number at 6 months of age, myelin aberrations can also be clearly detected, including double ensheathment, excess cytoplasm in the inner loop, myelin out-folding, degenerating sheaths and myelin ballooning (Behrendt et al., 2013). In 3xTg mice, that carry human pathological variants in APP^{Sw}, $PSEN1^{M146V}$ and $MAPT^{P301L}$, amyloid β1-42 is increased by 6 months of age (Desai et al., 2010); however, Schaffer collateral axons are already dystrophic and have granulated myelin by 2 months of age, and myelin protein expression is reduced in the CA1 region of the hippocampus (Desai et al., 2009), which manifests as fewer myelinated CA1 axons by 6 months of age (Desai et al., 2010). As the viral delivery of intracellular targeted anti-Aβ antibodies to 3xTg mice at 2 months of age, to prevent Aβ aggregation, can restore myelination at 6 months of age (Desai et al., 2010), amyloid pathology appears to be the primary driver of oligodendrocyte damage in these mice.

Herein, we show that mice carrying the Swedish and Indiana mutations in *APP* transgenic mice maintain a normal density of OPCs and oligodendrocytes in the hippocampus from P60 to P180; however, OPC behaviour is altered by amyloid pathology. In young adulthood (P100), OPCs in the hippocampus of *APP* transgenic mice have an increased response to GABA, becoming more depolarised upon bath application of the neurotransmitter. Oligodendrocyte maturation also appears to be affected in the hippocampus of these mice, as the nodes of Ranvier are shorter and the paranodes longer and this phenotype is associated with increased myelin thickness by P100. The number of new oligodendrocytes produced by adult OPCs

appeared normal in early adulthood, but increased in the hippocampus, entorhinal cortex and fimbria of *APP* transgenic mice as pathology developed. As total oligodendrocyte density was unchanged by P180, it is likely that the newborn oligodendrocytes replace oligodendrocytes lost to pathology.

4.2. Results

4.2.1. *APP* mice develop histopathological features of Alzheimer's disease by P180

To characterise the expression of human APP and the timeframe for the development of amyloid plaques in the brain of *APP* transgenic mice, we generated hippocampal brain lysates and coronal brain cryosections from WT, *MAPT* and *APP* mice at P30, P60, P90 and P180. By performing a series of Western blots to detect immature and mature human APP (6E10 antibody), we determined that human APP was already expressed by *APP* mice at P30, and expression was stable over time (**Figure 4.1a, b**). Human APP (~100kDa) was not detected in hippocampal lysates from WT or *MAPT* transgenic mice (**Figure 4.1b**), which acted as an additional control for this experiment. A smaller protein band (~55kDa) was detected in lysates from *MAPT* transgenic mice; however, this band does not correspond to human APP (Grant et al., 2019). We next performed a histological study to determine whether human APP expression resulted in amyloid plaque formation in *APP* transgenic mice. Coronal brain cryosections from P60, P90 and P180 WT and *APP* mice were stained with thioflavin S (**Figure 4.1c-i**, green), which binds to β-sheet structures identifying amyloid β plaques (Sun et al., 2002; Bussière et al., 2004). Sections were also co-labelled to detect the microglial marker Iba1 (**Figure 4.1c-i**, red). Plaques were absent from the hippocampus of WT and *APP* mice at P60 (**Figure 4.1c, d**) and P90 (**Figure 4.1e, f**). At P180, plaques had not formed in the hippocampus of WT mice (**Figure 4.1g**), but were present in the hippocampus of *APP* mice (**Figure 4.1h-i**).

Figure 4.1. APP transgenic mice have impaired survival compared with their wildtype littermates

a) *A Western blot utilising the anti-human APP 6E10 antibody reveals a protein band of ~100kDa in hippocampal protein lysates generated from P30 APP mice, that is absent from lysates generated from WT littermates and Prnp-MAPT^{P301S} (MAPT) transgenic mice. A protein band corresponding to β-actin (~42kDa) was detected in all brain lysates.* ***b)*** *Quantification of human APP expression, relative to β-actin expression, in brain lysates from P30, P60, P90 and P180 WT, MAPT and APP transgenic mice, indicated that human APP expression was significantly elevated in APP mice relative to WT and MAPT mice at all timepoints [Two-way ANOVA, genotype: $F(2, 24) = 112.0$, $p < 0.0001$; age: $F(3, 24) = 2.35$, $p = 0.097$; interaction: $F(6, 24) = 2.31$, $p = 0.066$]. P180 APP transgenic mice expressed more human APP than P30, P60 or P90 mice of the same genotype [Bonferroni post-test: 30 vs 180, $p = 0.040$; 60 vs 180, $p = 0.001$; 90 vs 180, $p = 0.030$].* ***c-h)*** *Coronal brain cryosections showing the hippocampus of P60, P90 and P180 WT and APP mice stained to detect the microglial marker Iba1 (red) and amyloid plaques (thioflavin S; green). White arrow heads indicate amyloid plaques.* ***i)*** *A thioflavin S labelled amyloid plaque (green) surrounded by microglia (Iba1; red) in the hippocampus of a P180 APP transgenic mouse.* ***j)*** *Quantification of the survival of WT and APP mice from birth until P241. [Log Rank (Mantel-Cox) test: Chi square = 40.97, df = 1, $p < 0.0001$]. Asterisks denote significant differences identified by Bonferroni post hoc analysis ****$p < 0.0001$. Scale bar represents 200µm (**c-h**) or 55µm (**i**).*

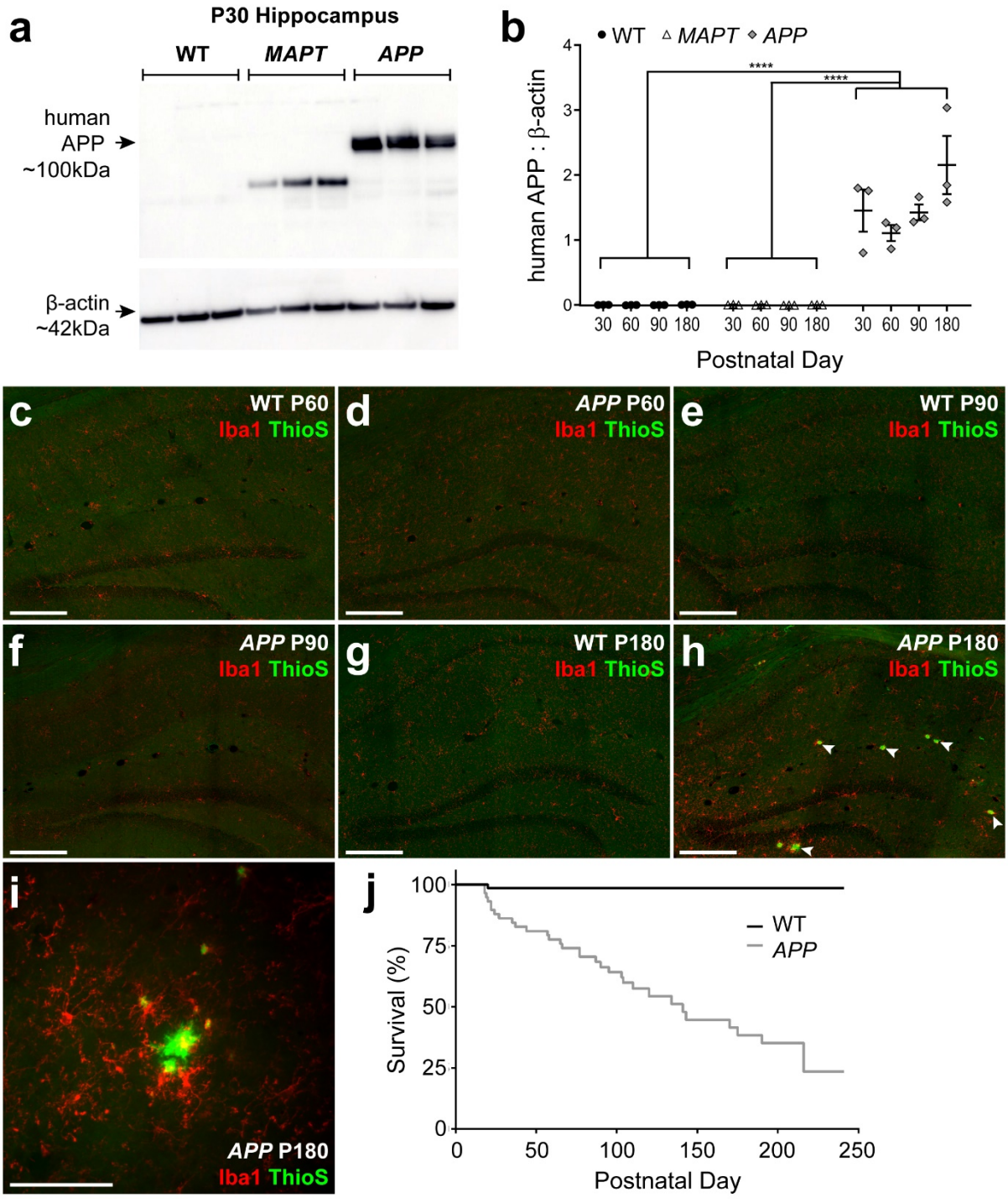
a
P30 Hippocampus
WT
MAPT
APP
human APP ~100kDa
β-actin ~42kDa
b
WT
MAPT
APP
human APP : β-actin
****
****
0
1
2
3
4
30 60 90 180 30 60 90 180 30 60 90 180
Postnatal Day
c
WT P60
Iba1 ThioS
d
APP P60
Iba1 ThioS
e
WT P90
Iba1 ThioS
f
APP P90
Iba1 ThioS
g
WT P180
Iba1 ThioS
h
APP P180
Iba1 ThioS
i
APP P180
Iba1 ThioS
j
Survival (%)
0
25
50
75
100
WT
APP
0 50 100 150 200 250
Postnatal Day

While microglia were present in the hippocampus of WT and *APP* mice at all ages examined, Iba1 expression increased noticeably by P180 in the *APP* mice, which is indicative of reactive microgliosis, and microglia were also found to accumulate around amyloid plaques (**Figure 4.1i**).

While *APP* transgenic mice developed amyloid plaques by P180, their survival was impaired prior to adulthood. By quantifying the survival of WT and *APP* transgenic mice from birth until P180, we determined that ~60% of *APP* transgenic mice die prior to P180, compared with only ~2% of WT mice [Log-rank (Mantel-Cox) test, $p < 0.0001$, **Figure 4.1j**]. As we next aimed to characterise the behavioural consequences of $APP^{Sw,Ind}$ overexpression, it should be noted that the impaired survival of *APP* transgenic mice introduces an unavoidable bias into our analyses, skewing our characterisation towards the less affected mice that survive to the older ages.

4.2.2. *APP* mice exhibit hyperactive behaviour by P60 but do not develop spatial learning deficits by P180

To compare the cognitive performance of WT and *APP* transgenic mice prior to and during plaque formation, WT and *APP* mice were subjected to a battery of behavioural tasks at P60, P90 or P180. WT (**Figure 4.2a**) and *APP* transgenic mice (**Figure 4.2b**) were placed into an open field arena for 10 minutes, over which time the total distance each mouse travelled (**Figure 4.2c**), and the average velocity of that movement (**Figure 4.1d**) was recorded. At all ages tested, *APP* mice travelled further (**Figure 4.2c**) and faster (**Figure 4.2d**) than their WT littermates, suggesting that these mice are hyperactive. Additionally, WT and *APP* mice spent a similar proportion of time in the brightly lit centre of the open field at P60 and P90; however,

Figure 4.2. APP transgenic mice are hyperactive but show no overt learning and memory deficit by 6 months of age

***a-b**) Representative track visualisation images (EthoVision XT) showing movement (black lines) of P180 WT (**a**) and APP (**b**) mice during the open field task. **c**) Quantification of the total distance travelled by WT and APP mice in the open field task at P60, P90 and P180 [Two-way ANOVA, genotype: $F(1, 53) = 48.59$, $p < 0.0001$; age: $F(2, 53) = 2.30$, $p = 0.109$; interaction: $F(2, 53) = 3.18$, $p = 0.049$]. **d**) Quantification of the average movement velocity of WT and APP mice during the open field task at P60, P90 and P180 [Two-way ANOVA, genotype: $F(1, 53) = 47.83$, $p < 0.0001$; age: $F(2, 53) = 2.27$, $p = 0.113$; interaction: $F(2, 53) = 3.21$, $p = 0.047$]. **e**) Quantification of the proportion of time spent in the centre of the open field of WT and APP mice during the open field task at P60, P90 and P180 [Two-way ANOVA, genotype: $F(1, 53) = 8.05$, $p = 0.006$; age: $F(2, 53) = 0.51$, $p = 0.59$; interaction: $F(2, 53) = 2.431$, $p = 0.097$]. **f**) Quantification of the proportion incorrect arm choices (errors) made by P60, P90 and P180 WT and APP mice during the T-maze alternation task [Two-way ANOVA, genotype: $F(1, 50) = 18.89$, $p < 0.0001$; age: $F(2, 50) = 1.20$, $p = 0.204$; interaction: $F(2, 50) = 0.064$, $p = 0.937$]. **g-h**) Representative track visualisation images (EthoVision XT) showing movement (black lines) of P180 WT (**g**) and APP (**h**) mice during the Barnes maze long-term memory probe trial, carried out 2 weeks after mice learned the expected location of an escape box (red arrows). Blue shading indicates the quadrant of the maze defined as the target zone. **i**) Quantification of the proportion of time P60, P90, and P180 WT or APP mice spent within the target zone during the long-term memory probe trial [Two-way ANOVA, genotype: $F(1, 52) = 1.93$, $p = 0.170$; age: $F(2, 52) = 3.06$, $p = 0.055$; interaction: $F(2, 52) = 0.16$, $p = 0.844$]. **j**) Quantification of the time spent by P180 WT and APP mice in each quadrant of the Barnes maze during the short-term memory probe phase [Two-way ANOVA, genotype: $F(1, 80) = 0.006$, $p = 0.935$; maze quadrant: $F(3, 80) = 41.96$, $p < 0.0001$; interaction: $F(3, 80) = 1.212$, $p = 0.310$]. **k**) Quantification of the time spent by P180 WT and APP mice in each quadrant of the Barnes maze during the long-term memory probe phase [Two-way ANOVA, genotype: $F(1, 80) = 0.004$, $p = 0.946$; maze quadrant: $F(3, 80) = 42.55$, $p < 0.0001$; interaction: $F(3, 80) = 1.77$, $p = 0.159$]. Data are presented as mean ± SEM, n= 8-11 mice per group. Asterisks denote significant differences identified by Bonferroni post hoc analysis, *$p < 0.05$, **$p < 0.01$, ****$p < 0.0001$. TA: target quadrant; OP: opposite quadrant; AL: adjacent left quadrant; AR: adjacent right quadrant. Scale bars represent 5cm (**a-b**) and 20cm (**g-h**).*

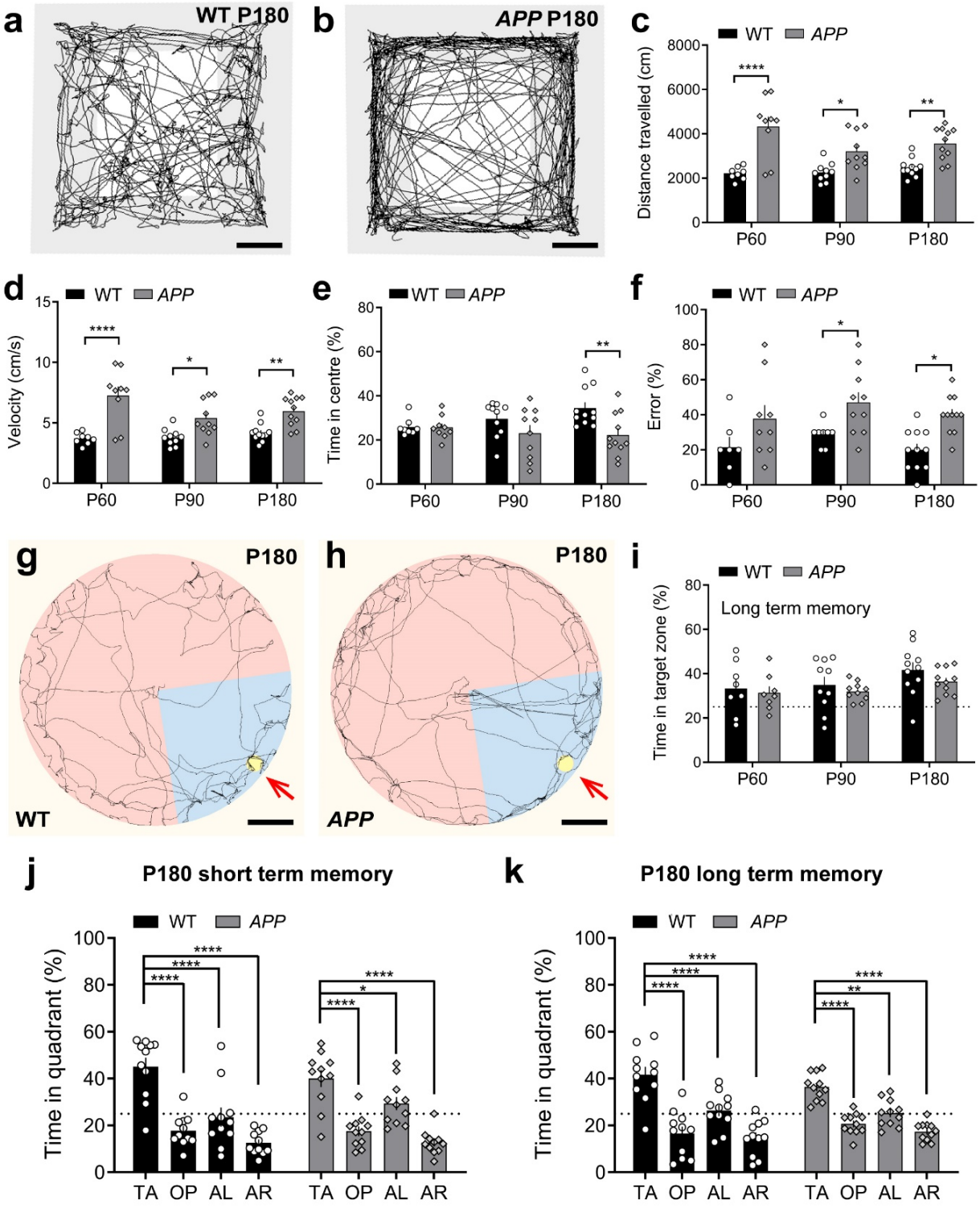
a
WT P180
b
APP P180
c
WT
APP
Distance travelled (cm)
8000
6000
4000
2000
0
****
*
**
P60
P90
P180
d
WT
APP
Velocity (cm/s)
15
10
5
0
****
*
**
P60
P90
P180
e
WT
APP
Time in centre (%)
80
60
40
20
0
**
P60
P90
P180
f
WT
APP
Error (%)
100
80
60
40
20
0
*
*
P60
P90
P180
g
P180
WT
h
P180
APP
i
WT
APP
Long term memory
Time in target zone (%)
80
60
40
20
0
P60
P90
P180
j
P180 short term memory
WT
APP
Time in quadrant (%)
100
80
60
40
20
0
****
****
****
****
*
****
TA
OP
AL
AR
TA
OP
AL
AR
k
P180 long term memory
WT
APP
Time in quadrant (%)
100
80
60
40
20
0
****
****
****
****
**
****
TA
OP
AL
AR
TA
OP
AL
AR

by P180 *APP* mice spent less of their time in the centre region (**Figure 4.2e**), which is indicative of an increase in anxiety-like behaviour.

Working-memory performance was subsequently evaluated by assessing spontaneous alternation in the T-maze. We found that WT and *APP* mice performed similarly at P60, but that by P90 *APP* mice persistently made more repeat arm entries (errors) than their WT littermates (**Figure 4.2f**) suggesting that these mice have impaired working memory or attentional processing that is likely associated with their hyperactivity (Kim et al., 2017; Montarolo et al., 2019). When evaluating short and long-term memory retention by WT (**Figure 4.2g**) and *APP* transgenic mice (**Figure 4.2h**) using the Barnes maze spatial navigation task, we found that regardless of age, *APP* mice and their WT littermates performed equally well in the short-term memory probe trial [P60: WT 35.11 ± 2.4, *APP* 34.02 ± 3.0; P90: WT 40.35 ± 6.0, *APP* 44.90 ± 3.9; P180: WT 45.10 ± 3.8, *APP* 40.02 ± 3.5; mean ± SEM, time in target zone (%)] one day after learning the location of the escape box, and again two-weeks later during the long-term memory probe trial (**Figure 4.2i**). This is highlighted by data showing that even at P180, WT and *APP* mice spend significantly more time in the target quadrant, compared to all other quadrants during the short-term (**Figure 4.2j**) and long-term (**Figure 4.2k**) memory trials, indicating that mice of both genotypes learned and remembered the location of the escape box.

4.2.3. OPC density and membrane properties are unchanged, but the response to GABA is increased at P100 in *APP* mice

To determine how OPC behaviour might be affected by amyloid pathology, we first quantified the density of PDGFRα$^+$ OPCs in the hippocampus, entorhinal cortex and fimbria of WT and

APP mice (**Figure 4.3a-i**). We found that OPC density was slightly reduced in the hippocampus of *APP* mice compared with control mice at P67; however, this difference was not maintained at later ages (**Figure 4.3g**). In the entorhinal cortex (**Figure 4.3h**) and fimbria (**Figure 4.3i**), OPC density was not affected by genotype and remained stable over time. To determine whether amyloid pathology affected the membrane properties of OPCs, we also performed whole cell patch clamp analysis of GFP^+ OPCs in the hippocampus of brain slices collected from WT, *MAPT* or *APP* transgenic mice carrying the *Pdgfrα–H2BGFP* transgene. We report that neither the overexpression of human $MAPT^{P301S}$ or $APP^{Sw,Ind}$ in neurons altered the OPC membrane capacitance (an approximate measure of cell size; **Figure 4.3j**), membrane resistance (**Figure 4.3k**) or RMP (**Figure 4.3l**), which were equivalent for WT, *MAPT* and *APP* transgenic mice at P30 and P100. Furthermore, the magnitude of the inwards voltage-gated sodium channel current recorded from P30 and P100 OPCs was equivalent for WT, *MAPT* and *APP* transgenic mice (**Figure. 4.3m**).

As *APP* mice are hyperactive by P60, which may reflect altered neurotransmitter signalling or inhibitory-excitatory balance in the brain (Palop et al., 2007; Sanchez et al., 2012; Verret et al., 2012; Snowden et al., 2019), we next used whole cell patch clamp electrophysiology to examine the ability of OPCs in the hippocampus of WT, *MAPT* and *APP* mice to respond to excitatory and inhibitory neurotransmitters. GFP^+ OPCs from WT mice were first held at -60 mV and KA (100 μM) was bath applied to activate the ionotropic AMPA/KA subtype of glutamate receptors. KA application evoked an inwards current that was sensitive to the AMPA/KA receptor antagonist CNQX (**Figure 4.4a-c**).

Figure 4.3. OPC density and membrane properties are normal in APP transgenic mice

a-f) *Coronal brain sections (30µm) from P120 WT and APP mice were stained to detect PDGFRα$^+$ OPCs in the hippocampus, entorhinal cortex and fimbria.* ***g)*** *Quantification of OPC density in the hippocampus of P60, P120, 150 and P180 WT and APP transgenic mice [Two-way ANOVA, genotype: F (1, 30) = 13.66, p = 0.0009; age: F (3, 30) = 0.14, p = 0.93; interaction: F (3, 30) = 0.91, p = 0.44].* ***h)*** *Quantification of OPC density in the entorhinal cortex of P60, P120 and P180 WT and APP transgenic mice [Two-way ANOVA, genotype: F (1, 18) = 0.85, p = 0.36; age: F (2, 18) = 0.22, p = 0.80; interaction: F (2, 18) = 0.20, p = 0.81].* ***i)*** *Quantification of OPC density in the fimbria of P60, P120, 150 and P180 WT and APP transgenic mice [Two-way ANOVA, genotype: F (1, 27) = 0.0009, p = 0.97; age: F (3, 27) = 4.49, p = 0.01; interaction: F (3, 27) = 1.23, p = 0.31]. .31]. Data are presented as mean ± SD, n=3-6 mice per group (**g-i**).* ***j)*** *The membrane capacitance of OPCs in the hippocampus of P30 and P100 WT, MAPT and APP mice [Two Two-way ANOVA, genotype: F (2, 77) = 3.748, p = 0.03; age: F (1, 77) = 0.03 p = 0.87; interaction: F (2, 77) = 0.45, p = 0.64, Bonferroni's post-test P30 or P100 WT vs APP or MAPT p>0.05].* ***k)*** *The membrane resistance of OPCs in the hippocampus of P30 and P100 WT, MAPT and APP mice [Two-way ANOVA, genotype: F (2, 67) = 1.173, p = 0.31; age: F (1, 67) = 0.24, p = 0.63; interaction: F (2, 67) = 0.49, p = 0.61].* ***l)*** *The resting membrane potential of OPCs in the hippocampus of P30 and P100 WT, MAPT and APP mice [Two-way ANOVA, genotype: F (2, 77) = 1.7166, p = 0.18; age: F (1, 77) = 1.35, p = 0.25; interaction: F (2, 77) = 0.75, p = 0.48].* ***m)*** *The voltage-gated sodium channel current (I_{Na}) recorded from OPCs in the hippocampus of P30 and P100 WT, MAPT and APP mice [Two-way ANOVA, genotype: F (2, 73) = 0.002, p = 0.998; age: F (1, 73) = 4.1, p = 0.047; interaction: F (2, 73) = 0.019, p = 0.98, Bonferroni's post-test P30 or P100 WT vs APP or MAPT p>0.05]. Data are presented as mean ± SEM, n=6-23 cells per group (**j-m**). Scale bars represent 185 µm (**a, b**) and 70 µm (**c-f**).*

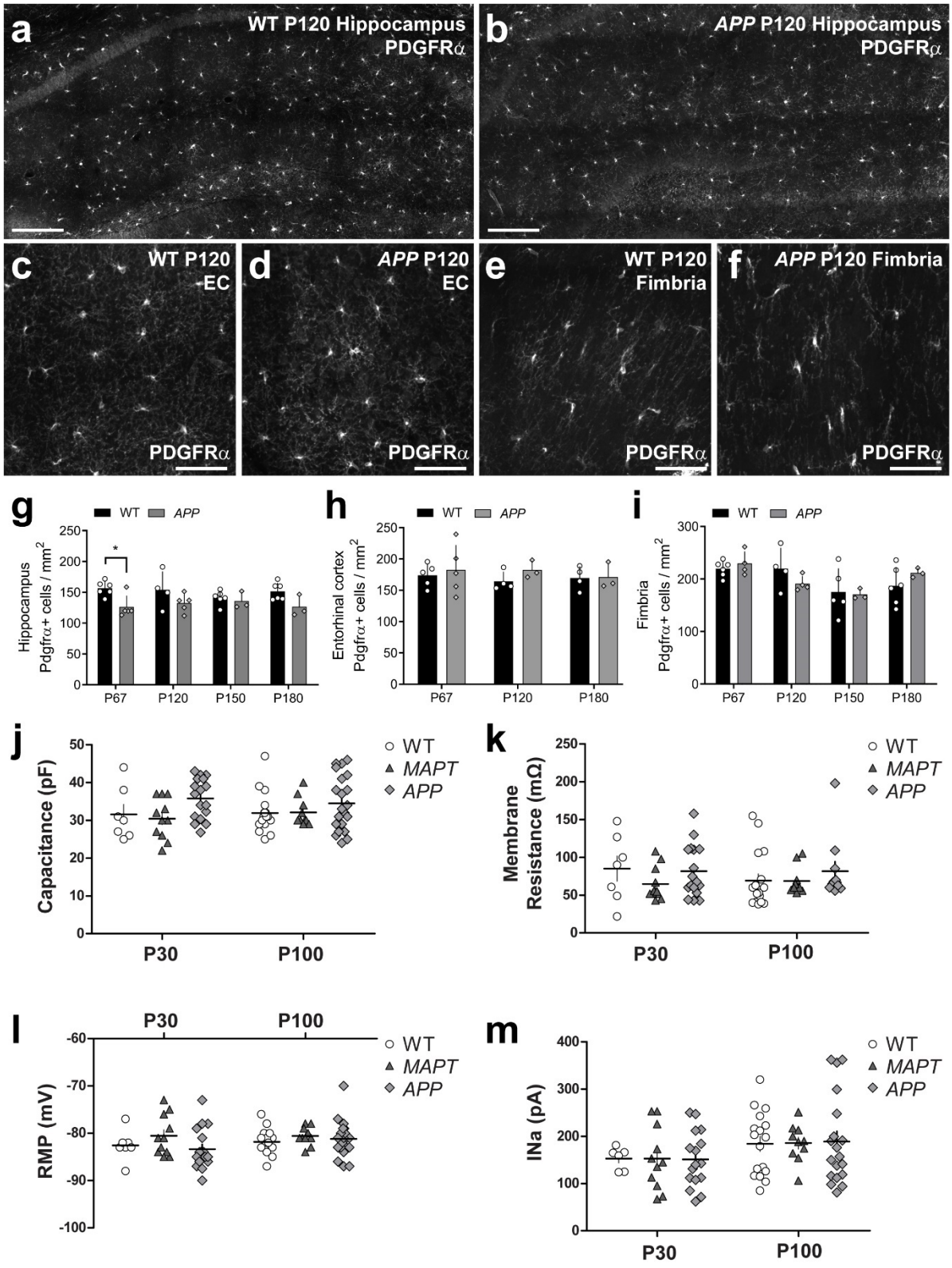
a
WT P120 Hippocampus
PDGFRα
b
APP P120 Hippocampus
PDGFRα
c
WT P120
EC
PDGFRα
d
APP P120
EC
PDGFRα
e
WT P120
Fimbria
PDGFRα
f
APP P120 Fimbria
PDGFRα
g
WT
APP
Hippocampus
Pdgfrα+ cells / mm2
P67
P120
P150
P180
h
Entorhinal cortex
i
Fimbria
j
Capacitance (pF)
MAPT
k
Membrane
Resistance (mΩ)
l
RMP (mV)
m
INa (pA)
P30
P100

Figure 4.4. OPCs from APP transgenic mice have a heightened response to GABA

a) *I-V relationship for the current evoked in hippocampal OPCs by the bath application of 100 µM KA (mean steady state baseline current was subtracted from the mean steady state current in the presence of KA) in P30 or P100 WT mice [Two-way ANOVA, genotype effect F (1,8) = 0.2372 p = 0.6393].* ***b)*** *Quantification of KA (100 µM) evoked currents when hippocampal OPCs are hyperpolarised to -100 mV in P30 or P100 WT mice in the presence or absence of CNQX (10 µM) [Two-way ANOVA, drug effect F (1,35) = 124.3 p < 0.0001, Bonferroni's post-hoc test P30 or P100 KA vs KA+CNQX p <0.001].* ***c)*** *Example traces show the baseline currents, currents in the presence of KA, or currents in the presence of KA + CNQX from OPCs of WT mice after a family of voltage steps from -100 to 20 mV (20 mV increments).* ***d)*** *Quantification of KA-evoked currents measured after a hyperpolarising pulse (to -100 mV) for OPCs in the hippocampus of P30 or P100 WT, MAPT or APP transgenic mice [Two-way ANOVA, genotype effect F (2,54) = 0.1375 p = 0.2616].* ***e)*** *Example traces showing KA-evoked currents (baseline current was subtracted from currents recorded in the presence of KA) after voltage steps form -100 mV to 20 mV (40 mV increments) in P30 or P100 WT, MAPT or APP mice.* ***f)*** *I-V relationship for the current evoked in hippocampal OPCs by the bath application of 100 µM GABA (mean steady state baseline current subtracted from the mean steady state current in the presence of GABA) in P30 or P100 WT mice [Two-way ANOVA, genotype effect F (1,14) = 0.002744 p = 0.9590].* ***g)*** *Quantification of the GABA-evoked current measured after hyperpolarising hippocampal OPCs to -80 mV in the absence or presence of picrotoxin (50 µM) [Two-way ANOVA, drug effect F (1,14) = 46.75 p = 0.0001, Bonferroni's post-hoc test P30 or P100 GABA vs GABA+PTX p <0.001].* ***h)*** *Example traces showing the baseline currents, currents in the presence of GABA, or currents in the presence of GABA + picrotoxin from OPCs in hippocampal slices from WT mice after a family of voltage steps from -80 to 80 mV (20 mV increments).* ***i)*** *Quantification of the GABA-evoked current measured after a hyperpolarising pulse to -80 mV in OPCs from P30 or P100 WT, MAPT or APP mice [Two-way ANOVA. genotype effect F (2,59) = 5.738 p = 0.0053, Bonferroni's post-hoc test P100 WT vs APP p <0.001].* ***j)*** *Example traces showing GABA-evoked currents (baseline current was subtracted from currents recorded in the presence of GABA) after voltage steps from -80 mV to 80 mV (40 mV increments) for hippocampal OPCs from P30 or P100 WT, MAPT or APP mice. Values represent mean ± SEM, n=4-16 cells per group.* *** *= p <0.001 Two-way ANOVA with Bonferroni's post-hoc test.*

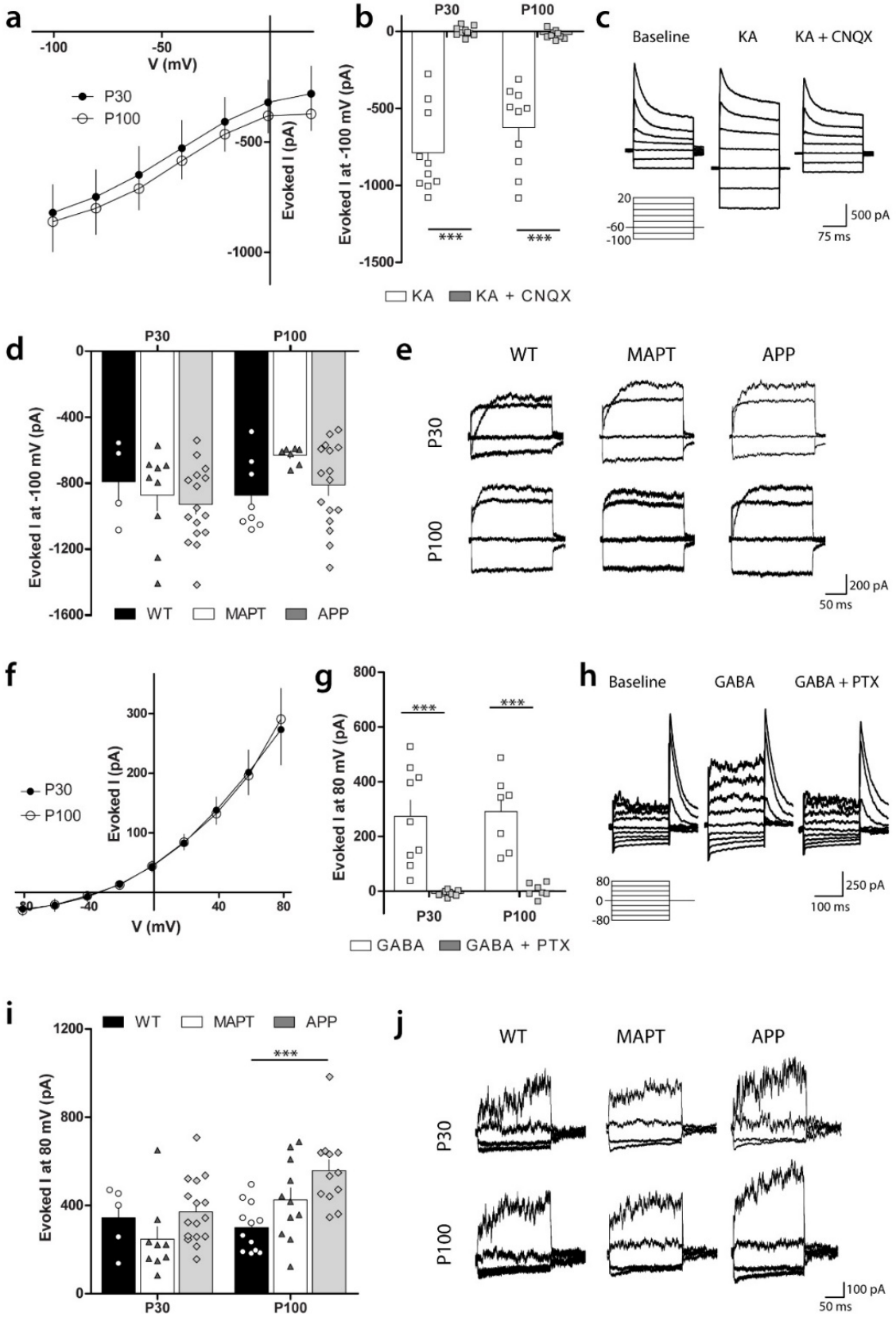
a
-100
-50
V (mV)
P30
P100
-500
-1000
Evoked I (pA)
b
P30
P100
0
-500
-1000
-1500
Evoked I at -100 mV (pA)
***
***
KA
KA + CNQX
c
Baseline
KA
KA + CNQX
20
-60
-100
500 pA
75 ms
d
P30
P100
0
-400
-800
-1200
-1600
Evoked I at -100 mV (pA)
WT
MAPT
APP
e
WT
MAPT
APP
P30
P100
200 pA
50 ms
f
300
200
100
Evoked I (pA)
P30
P100
-80
-40
40
80
V (mV)
g
800
600
400
200
0
Evoked I at 80 mV (pA)
***
***
P30
P100
GABA
GABA + PTX
h
Baseline
GABA
GABA + PTX
80
0
-80
250 pA
100 ms
i
WT
MAPT
APP
1200
800
400
0
Evoked I at 80 mV (pA)
***
P30
P100
j
WT
MAPT
APP
P30
P100
100 pA
50 ms

The KA-evoked current in OPCs at P30 and P100 was not linear and did not reverse (**Figure 4.4a**), which is consistent with previous reports showing that in OPCs sodium entry through AMPA/KA receptors inhibits the voltage gated potassium channel current at depolarised potentials (Borges and Kettenmann, 1995). We report that the amplitude of the KA-evoked current does not differ between P30 and P100, and is equivalent in WT, *MAPT* and *APP* transgenic mice (**Figure 4.4d, e**). To assess the response of OPCs to the inhibitory neurotransmitter GABA (100 μM), OPCs were held at 0 mV while GABA was bath applied. At P30 and P100, GABA evoked an outwardly rectifying current that was completely abolished in the presence of PTX (100 μM; **Figure 4.4f-h**), indicating that the evoked currents resulted from the activation of ionotropic $GABA_A$ receptors. There was no difference in the amplitude of current evoked by GABA in OPCs from P30 WT, *MAPT* and *APP* transgenic mice (**Figure 4.4i, j**). By contrast, OPCs in hippocampal slices generated from P100 *APP* transgenic mice responded more robustly to GABA at 80 mV than OPCs from P100 WT or *MAPT* mice (**Figure 4.4i, j**). These data suggest that early amyloid pathology is associated with a change in the subunit composition of $GABA_A$ receptors expressed by OPCs, or a change in the number of $GABA_A$ receptors expressed on the cell surface.

4.2.4. Node of Ranvier length is decreased and paranode length increased in the hippocampus of P180 *APP* mice

To determine whether myelin integrity was affected in young adult *APP* transgenic mice, we first examined the morphology of the nodes of Ranvier and their associated paranodes in P100 WT and *APP* transgenic mice (**Figure. 4.5**). Coronal brain cryosections containing the hippocampus (**Figure 4.5a, b**) and fimbria (**Figure 4.5c, d**) were immunolabelled to detect the nodal protein NaV1.6 (red) and the paranodal protein Caspr (green), and the length of each structure measured from confocal micrographs. We found that node of Ranvier length was

Figure 4.5. Nodes of Ranvier are shorter and paranodes longer in the hippocampus of APP transgenic mice

***a-d**) Coronal brain sections (30µm) from P107 WT and APP mice were stained to detect Caspr (green; paranodal marker) and Nav1.6 (red; used to mark nodes of Ranvier) in the hippocampus and fimbria. Magnified panels demonstrate measurement of nodes of Ranvier. **e**) Quantification of node length in the hippocampus of WT (n = 229 nodes) and APP (n = 142 nodes) mice (Mann Whitney test: U = 11990, p < 0.0001). **f**) Cumulative distribution plot on node length in the hippocampus of WT (open circles) and APP mice (grey diamonds) (Kolmogorov-Smirnov test: D = 0.2033, p = 0.0014). **g**) Quantification of mean hippocampal node length for each mouse in WT (n = 4) or APP (n = 3) mice (Two -tailed, unpaired t-test: t = 2.664, df = 5, p = 0.0447). **h**) Quantification of paranode length in the hippocampus of WT (n = 135 paranodes) and APP (n = 113 paranodes) mice (Mann Whitney test: U = 5568, p = 0.0003). **i**) Cumulative distribution plot on paranode length in the hippocampus of WT and APP mice (Kolmogorov-Smirnov test: D = 0.2507, p = 0.0009). **j**) Quantification of mean hippocampal paranode length for each mouse in WT (n = 4) or APP (n = 3) mice (Two-tailed, unpaired t-test: t = 2.799, df = 5, p = 0.038). **k**) Quantification of node length in the fimbria of WT (n = 278 nodes) and APP (n = 163 nodes) mice (Mann-Whitney test: U = 20500, p = 0.0947). **l**) Cumulative distribution plot of node length in the fimbria of WT and APP mice (Kolmogorov-Smirnov test: D = 0.1190, p = 0.1091). **m**) Quantification of mean hippocampal node length for each mouse in WT (n = 4) or APP (n = 3) mice (Two-tailed, unpaired t-test: t = 1.293, df = 5, p = 0.2526). **n**) Quantification of paranode length in the hippocampus of WT (n = 193 paranodes) and APP (n = 134 paranodes) mice (Mann-Whitney test: U = 12280, p = 0.4374). **o**) Cumulative distribution plot on paranode length in the hippocampus of WT and APP mice (Kolmogorov-Smirnov test: D = 0.08391, p = 0.6336). **p**) Quantification of mean hippocampal paranode length for each mouse in WT (n = 4) or APP (n = 3) mice (Two-tailed, unpaired t-test: t = 0.5096, df = 5, p = 0.6338). Results are presented as mean ± SD. Scale bars represent 2.8µm (**a-d**), 1.4µm (magnified insets).*

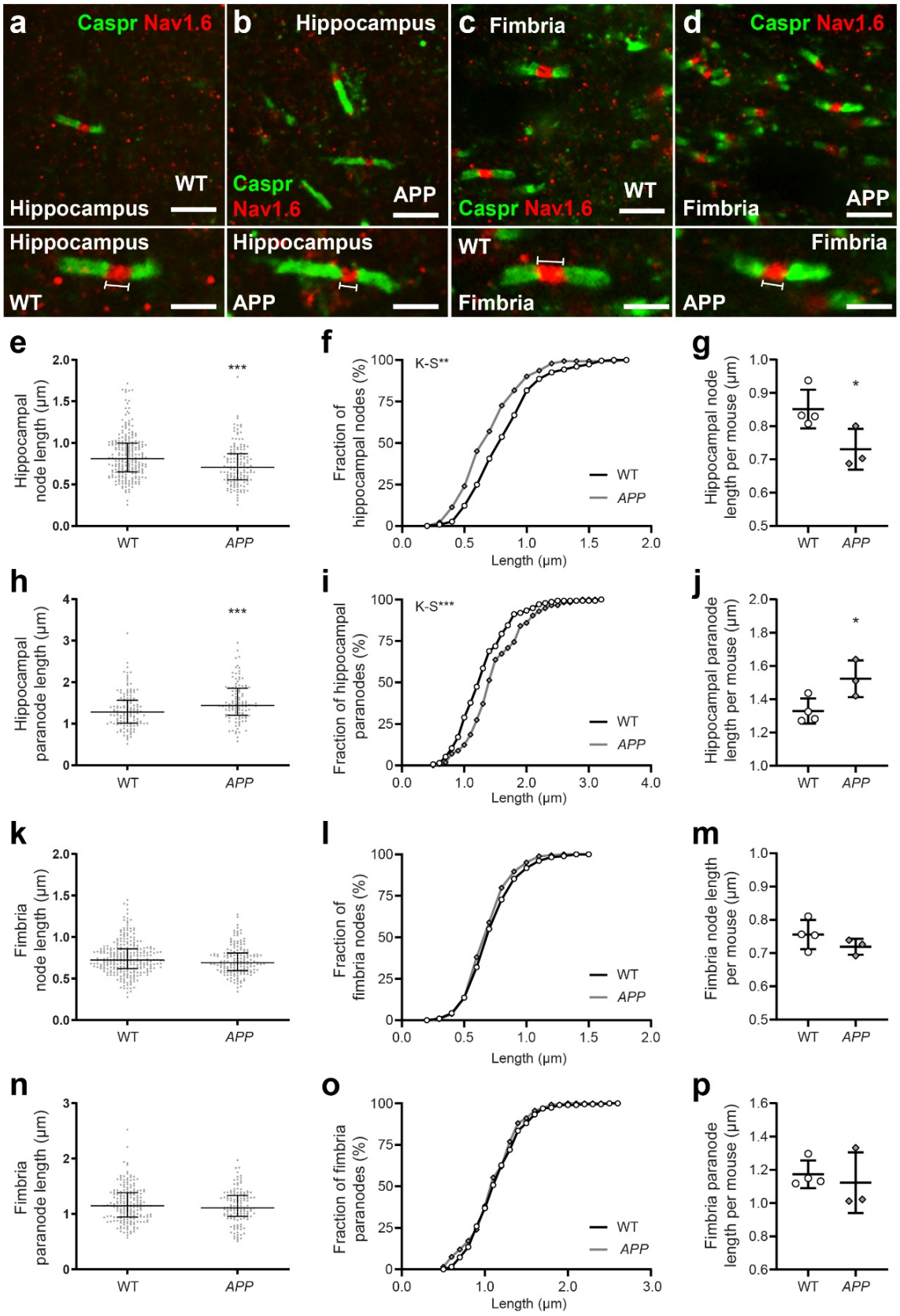
a
Caspr Nav1.6
Hippocampus
WT
b
Hippocampus
Caspr
Nav1.6
APP
c
Fimbria
Caspr Nav1.6
WT
d
Caspr Nav1.6
Fimbria
APP
Hippocampus
WT
Hippocampus
APP
WT
Fimbria
Fimbria
APP
e
Hippocampal node length (µm)
***
WT
APP
f
Fraction of hippocampal nodes (%)
K-S**
WT
APP
Length (µm)
g
Hippocampal node length per mouse (µm)
*
WT
APP
h
Hippocampal paranode length (µm)
***
WT
APP
i
Fraction of hippocampal paranodes (%)
K-S***
WT
APP
Length (µm)
j
Hippocampal paranode length per mouse (µm)
*
WT
APP
k
Fimbria node length (µm)
WT
APP
l
Fraction of fimbria nodes (%)
WT
APP
Length (µm)
m
Fimbria node length per mouse (µm)
WT
APP
n
Fimbria paranode length (µm)
WT
APP
o
Fraction of fimbria paranodes (%)
WT
APP
Length (µm)
p
Fimbria paranode length per mouse (µm)
WT
APP

shorter in the hippocampus of *APP* transgenic compared to WT mice (**Figure 4.5e**), with node length distribution being significantly shifted towards the formation of shorter nodes (**Figure 4.5f**). Furthermore, average node length per mouse was also reduced with $APP^{Sw,Ind}$ expression (**Figure 4.5g**). The observed change in node length was accompanied by a lengthening of the paranodes in the hippocampus of *APP* transgenic mice (**Figure 4.5h**), as paranode length distribution was shifted towards the generation of longer paranodes (**Figure 4.5i**). Within the hippocampus of *APP* transgenic mice, average paranode length was also increased per mouse (**Figure 4.5j**). By contrast, node of Ranvier length (**Figure 4.5k-m**) and paranode length (**Figure 4.5n-p**) was equivalent for WT and *APP* transgenic mice in the fimbria, suggesting that this phenotype is region specific.

4.2.5. Myelin thickness is increased in the hippocampus of P100 *APP* transgenic mice

As paranode lengthening can result from myelin decompaction (Howell et al., 2006; Stojic et al., 2018) or increasing myelin thickness following myelin sheath addition (Snaidero et al., 2014), we next examined the ultrastructure of hippocampal myelin in P100 WT (**Figure 4.6a**) and *APP* mice (**Figure 4.6b**) by TEM. We found that axon density (**Figure 4.6c**), myelinated axon density (**Figure 4.6d**), and the proportion of axons that are myelinated (**Figure 4.6e**) was equivalent between WT and *APP* mice, suggesting that developmental myelination was largely normal in these mice. However, the g-ratio [axon diameter / (axon + myelin diameter)] measured for myelinated axons in the hippocampus of *APP* mice was reduced compared to those measured in WT mice (**Figure 4.6f-g**), suggesting that *APP* mice have thicker myelin in this region. By further quantifying axon diameter and the number of myelin wraps per axon (**Figure 4.6h-k**), we confirmed that myelinated axon diameter was equivalent in the hippocampus of WT and *APP* transgenic mice (**Figure 4.6l**); however, the number of myelin lamellae (wraps) was increased in *APP* compared to WT mice (**Figure 4.6m**). These data

Figure 4.6. Myelin thickness is increased in APP transgenic mice

***a-b**) Representative electron micrographs from the CA1 region of the hippocampus of WT (**a**) and APP (**b**) mice at P90. **c**) Quantification of total axon density (axons / μm^2) in WT (open circles) and APP (grey diamonds) mice (Two-tailed, unpaired t-test: t = 2.46, df = 4, p = 0.06). **d**) Quantification of myelinated axon density (axons / μm^2) in WT and APP mice (Two-tailed, unpaired t-test: t = 1.69, df = 4, p = 0.16). **e**) Quantification of the proportion of myelinated axons in the CA1 of WT and APP mice at P90 (Two-tailed, unpaired t-test: t = 0.46, df = 4, p = 0.66). **f**) Graphical representation of the g-ratio distribution based on axon diameter (Kolmogorov-Smirnoff test, K-S D = 0.2926 p < 0.0001). **g**) Quantification of average g-ratio for WT and APP mice (Two-tailed, unpaired t-test: t = 4.18, df = 4, p = 0.013). **h-k**) Representative high magnification electron micrographs through a single myelinated axon within the CA1 region of WT (**h-i**) and APP mice (**j-k**) at P90. **l**) Quantification of average myelinated axon diameter within the CA1 region of WT and APP mice (Two-tailed, unpaired t-test: t = 2.27, df = 4, p = 0.085). **m**) Quantification of average number of myelin wraps for axons within the CA1 region of WT and APP mice at P90 (Two-tailed, unpaired t-test: t = 4.12, df = 4, p = 0.014). Scale bars represent: 1µm (**a-b**), 300nm (**h, j**) and 100nm (**i, k**). Results are presented as mean ± SD, n = 3 mice per genotype.*

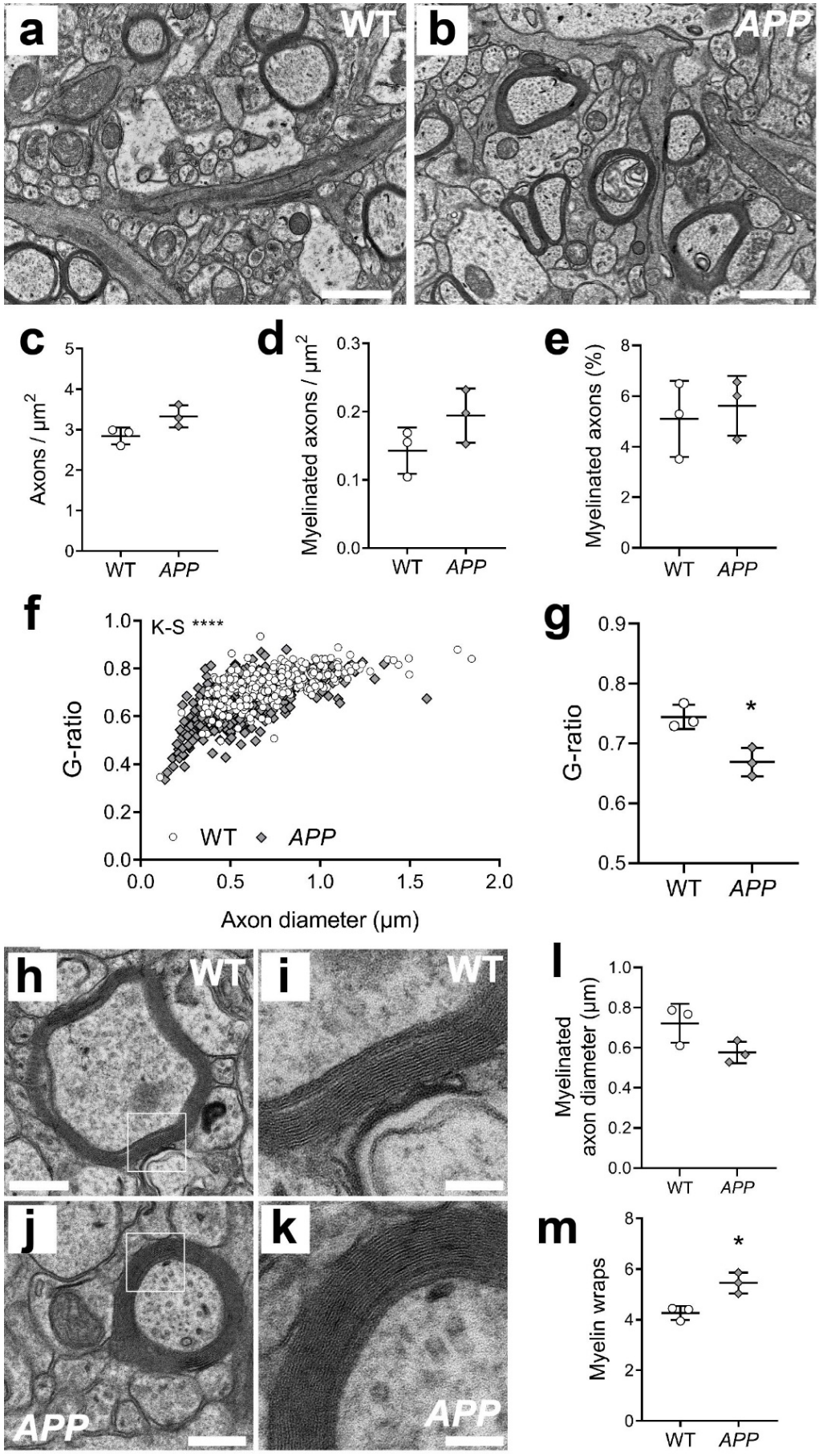
a
WT
b
APP
c
Axons / µm2
WT
APP
d
Myelinated axons / µm2
e
Myelinated axons (%)
f
K-S ****
G-ratio
Axon diameter (µm)
g
G-ratio
*
h
i
j
k
l
Myelinated axon diameter (µm)
m
Myelin wraps

indicate that early amyloid pathology influences the myelinating behaviour of oligodendrocytes in the hippocampus.

4.2.6. New oligodendrocyte number is elevated in the hippocampus, entorhinal cortex and fimbria of adult *APP* transgenic mice

To determine whether the ability of OPCs to generate new oligodendrocytes was affected by early amyloid pathology, we performed cre-lox lineage tracing of adult OPCs from P60, comparing oligodendrocyte generation in control (*Pdgfra-CreER^{T2}::Rosa26-YFP*) and *APP* (*Pdgfra-CreER^{T2}::Rosa26-YFP::PDGFβ-hAPP^{Sw,Ind}*) mice (**Figure 4.7**). Coronal brain cryosections from P60+7, P60+60, P60+90 and P60+120 control and *APP* transgenic mice, containing the hippocampus, entorhinal cortex and fimbria, were stained to detect YFP (green), PDGFRα (red) and Hoechst 33342 (blue) (**Figure 4.7a-l**). While PDGFRα$^+$ YFP$^+$ OPCs gave rise to new PDGFRα-neg YFP$^+$ cells over time, essentially all YFP-labelled cells expressed the transcription factor OLIG2, even at P60+120, confirming that they remained in the oligodendrocyte lineage. For example, at P60+120, ~97 ± 1% of YFP$^+$ cells in the hippocampus of control mice and ~96 ± 2% of YFP$^+$ cells in the hippocampus of *APP* transgenic mice were OLIG2$^+$ (mean ± SD). While we found that OPCs differentiated to produce new oligodendrocytes in the hippocampus (**Figure 4.7a-d**), entorhinal cortex **(Figure 4.7e-h**) and fimbria (**Figure 4.7i-l**) of adult control and *APP* mice, the proportion of YFP$^+$ cells that became new oligodendrocytes was significantly increased in the hippocampus of *APP* transgenic mice compared to control mice by P60+90 (**Figure 4.7m**). By P60+120, the proportion of YFP$^+$ cells that were new oligodendrocytes was also significantly higher in the entorhinal cortex (**Figure 4.7n**) and fimbria (**Figure 4.7o**) of *APP* transgenic mice compared to controls. This increase in cell addition resulted in an increase in the density of newborn

Figure 4.7. Adult oligodendrogenesis is elevated in the APP transgenic mouse brain

***a-d**) Confocal images of the hippocampus in coronal brain cryosections from P60+60 and P60+120 control and APP transgenic mice stained to detect YFP (green), PDGFRα (red) and Hoechst 33342 (blue). **e-h**) Confocal images of the entorhinal cortex in coronal brain cryosections from P60+60 and P60+120 control and APP transgenic mice stained to detect YFP (green), PDGFRα (red) and Hoechst 33342 (blue). **i-l**) Confocal images of the fimbria in coronal brain cryosections from P60+60 and P60+120 control and APP transgenic mice stained to detect YFP (green), PDGFRα (red) and Hoechst 33342 (blue). **m**) Quantification of the proportion of YFP^+ cells in the hippocampus of control and APP mice that have differentiated into PDGFRα-negative YFP^+ oligodendrocytes [Two-way ANOVA, genotype: $F(1, 30) = 21.35$, $p < 0.0001$; age: $F(3, 30) = 13.12$, $p < 0.0001$; interaction: $F(3, 30) = 3.62$, $p = 0.024$]. **n**) Quantification of the proportion of YFP^+ cells in the entorhinal cortex of control and APP mice that have differentiated into PDGFRα-negative YFP^+ oligodendrocytes [Two-way ANOVA, genotype: $F(1, 18) = 7.01$, $p = 0.016$; age: $F(2, 18) = 11.61$, $p = 0.0006$; interaction: $F(2, 18) = 2.03$, $p = 0.16$]. **o**) Quantification of the proportion of YFP^+ cells in the fimbria that have differentiated of control and APP mice that have differentiated into PDGFRα-negative YFP^+ oligodendrocytes [Two-way ANOVA, genotype: $F(1, 27) = 14.29$, $p = 0.0008$; age: $F(3, 27) = 45.15$, $p < 0.0001$; interaction: $F(3, 27) = 3.11$, $p = 0.042$]. **p**) Quantification of the density of YFP^+ PDGFRα-negative newborn oligodendrocytes in the hippocampus of control and APP transgenic mice (cells per mm^2 as adjusted for x-y area only) [Two-way ANOVA, genotype: $F(1, 30) = 16.92$, $p = 0.0003$; age: $F(3, 30) = 9.97$, $p = 0.0001$; interaction: $F(3, 30) = 3.41$, $p = 0.029$]. **q**) Quantification of the density of YFP^+ PDGFRα-negative newborn oligodendrocytes in the entorhinal cortex of control and APP transgenic mice (oligodendrocytes per mm^2 as adjusted for x-y area only) [Two-way ANOVA, genotype: $F(1, 18) = 16.16$, $p = 0.0008$; age: $F(2, 18) = 18.50$, $p < 0.0001$; interaction: $F(2, 18) = 4.41$, $p = 0.027$]. **r**) Quantification of the density of YFP^+ PDGFRα-negative newborn oligodendrocytes in the fimbria of control and APP transgenic mice (oligodendrocytes per mm^2 as adjusted for x-y area only) [Two-way ANOVA, genotype: $F(1, 27) = 24.73$, $p < 0.0001$; age: $F(3, 27) = 23.68$, $p < 0.0001$; interaction: $F(3, 27) = 8.55$, $p = 0.0004$]. White arrows indicate YFP^+ PDGFRα-negative newborn oligodendrocytes. Data are presented as mean ± SD, n=3-6 mice per group. Scale bar represents 25 μm (**a-h**) or 33 μm (**i-l**).*

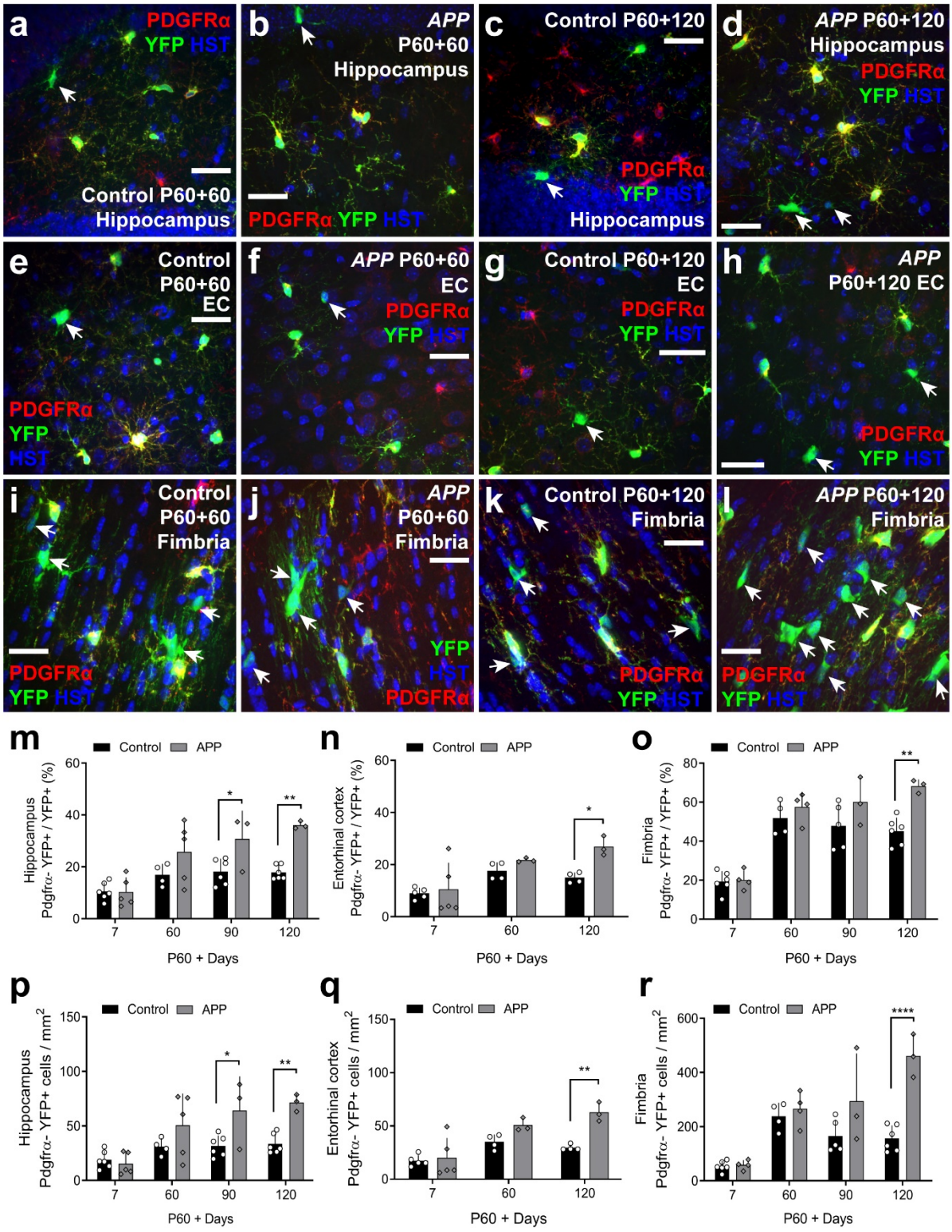
a
PDGFRα
YFP HST
Control P60+60
Hippocampus
b
APP
P60+60
Hippocampus
PDGFRα YFP HST
c
Control P60+120
PDGFRα
YFP HST
Hippocampus
d
APP P60+120
Hippocampus
PDGFRα
YFP HST
e
Control
P60+60
EC
PDGFRα
YFP
HST
f
APP P60+60
EC
PDGFRα
YFP HST
g
Control P60+120
EC
PDGFRα
YFP HST
h
APP
P60+120 EC
PDGFRα
YFP HST
i
Control
P60+60
Fimbria
PDGFRα
YFP HST
j
APP
P60+60
Fimbria
YFP
HST
PDGFRα
k
Control P60+120
Fimbria
PDGFRα
YFP HST
l
APP P60+120
Fimbria
PDGFRα
YFP HST
m
Control
APP
Hippocampus
Pdgfrα- YFP+ / YFP+ (%)
P60 + Days
n
Control
APP
Entorhinal cortex
Pdgfrα- YFP+ / YFP+ (%)
P60 + Days
o
Control
APP
Fimbria
Pdgfrα- YFP+ / YFP+ (%)
P60 + Days
p
Control
APP
Hippocampus
Pdgfrα- YFP+ cells / mm2
P60 + Days
q
Control
APP
Entorhinal cortex
Pdgfrα- YFP+ cells / mm2
P60 + Days
r
Control
APP
Fimbria
Pdgfrα- YFP+ cells / mm2
P60 + Days

YFP$^+$ oligodendrocytes detected in the hippocampus (**Figure 4.7p**), entorhinal cortex (**Figure 4.7q**) and fimbria (**Figure 4.7r**) of *APP* mice relative to controls.

Surprisingly, the addition of new oligodendrocytes did not alter the total density of oligodendrocytes detected in the hippocampus, entorhinal cortex or fimbria of control or *APP* mice (**Figure 4.8**). By performing immunohistochemistry on coronal brain cryosections from P120 or P180 WT and *APP* transgenic mice to detect the oligodendrocyte marker ASPA (**Figure 4.8 a-l)**, we determined that the density of ASPA$^+$ oligodendrocytes was higher in the fimbria (**Figure 4.8o**) and hippocampus (**Figure 4.8m**) than the entorhinal cortex (**Figure 4.8n**), but consistent across age and between WT and *APP* transgenic mice. However, as there are only 213 ± 65 (mean ± SD) oligodendrocytes per mm^2 of hippocampus in *APP* mice at P180 (**Figure 4.8m**) and 71 ± 7 (mean ± SD) cells per mm^2 are newborn oligodendrocytes (**Figure 4.7p**), these data suggest that ~33% of oligodendrocytes present in the hippocampus of P180 *APP* mice are newborn. This equates to ~49% and ~23% in the entorhinal cortex (**Figure 4.8n; Figure 4.7q**) and fimbria (**Figure 4.8o; Figure 4.7r**), respectively, which is a significant contribution to the total population and strongly suggests that amyloid pathology is associated with oligodendrocyte turnover by P180. To determine whether newborn oligodendrocytes are mature oligodendrocytes, we immunolabelled coronal sections containing the hippocampus and fimbria, to detect PDGFRα$^+$ (blue), YFP$^+$ (green) and ASPA$^+$ (red) (**Figure 4.9a-h**). We found that YFP$^+$ ASPA$^+$ mature oligodendrocyte addition was significantly increased at P60+120 in the hippocampus (**Figure 4.9.i**) and fimbria (**Figure 4.9.j**) of *APP* mice relative to controls, suggesting that new oligodendrocytes are added to replace myelin.

Figure 4.8. Oligodendrocyte number is normal in APP transgenic mice

***a-d**) Confocal images of the hippocampus in coronal brain cryosections (30µm) from P120 and P180 WT and APP transgenic mice stained to detect the oligodendrocyte marker ASPA (red) and Hoechst 33342 (blue).* ***e-h**) Confocal images of the entorhinal cortex in coronal brain cryosections from P120 and P180 WT and APP transgenic mice stained to detect the oligodendrocyte marker ASPA (red) and Hoechst 33342 (blue).* ***i-l**) Confocal images of the fimbria in coronal brain cryosections from P120 and P180 WT and APP transgenic mice stained to detect the oligodendrocyte marker ASPA (red) and Hoechst 33342 (blue).* ***m**) Quantification of the density of $ASPA^+$ oligodendrocytes in the hippocampus of WT (black bars, open circles) and APP (grey bars, grey diamonds) transgenic mice (oligodendrocytes per mm^2 as adjusted for x-y area only) [Two-way ANOVA, genotype: $F(1, 16) = 2.11$, $p = 0.16$; age: $F(1, 16) = 1.48$, $p = 0.24$; interaction: $F(1, 16) = 1.27$, $p = 0.27$].* ***n**) Quantification of the density of $ASPA^+$ oligodendrocytes in the entorhinal cortex of WT and APP transgenic mice (oligodendrocytes per mm^2 as adjusted for x-y area only) [Two-way ANOVA, genotype: $F(1, 18) = 2.08$, $p = 0.16$; age: $F(1, 18) = 0.95$, $p = 0.34$; interaction: $F(2, 53) = 0.02$, $p = 0.87$].* ***o**) Quantification of the density of $ASPA^+$ oligodendrocytes in the fimbria of WT and APP transgenic mice (oligodendrocytes per mm^2 as adjusted for x-y area only) [Two-way ANOVA, genotype: $F(1, 16) = 0.40$, $p = 0.53$; age: $F(1, 16) = 0.08$, $p = 0.77$; interaction: $F(1, 16) = 0.64$, $p = 0.43$]. Results are presented as mean ± SD, n = 3-6 mice per group. Scale bars represent 30 µm.*

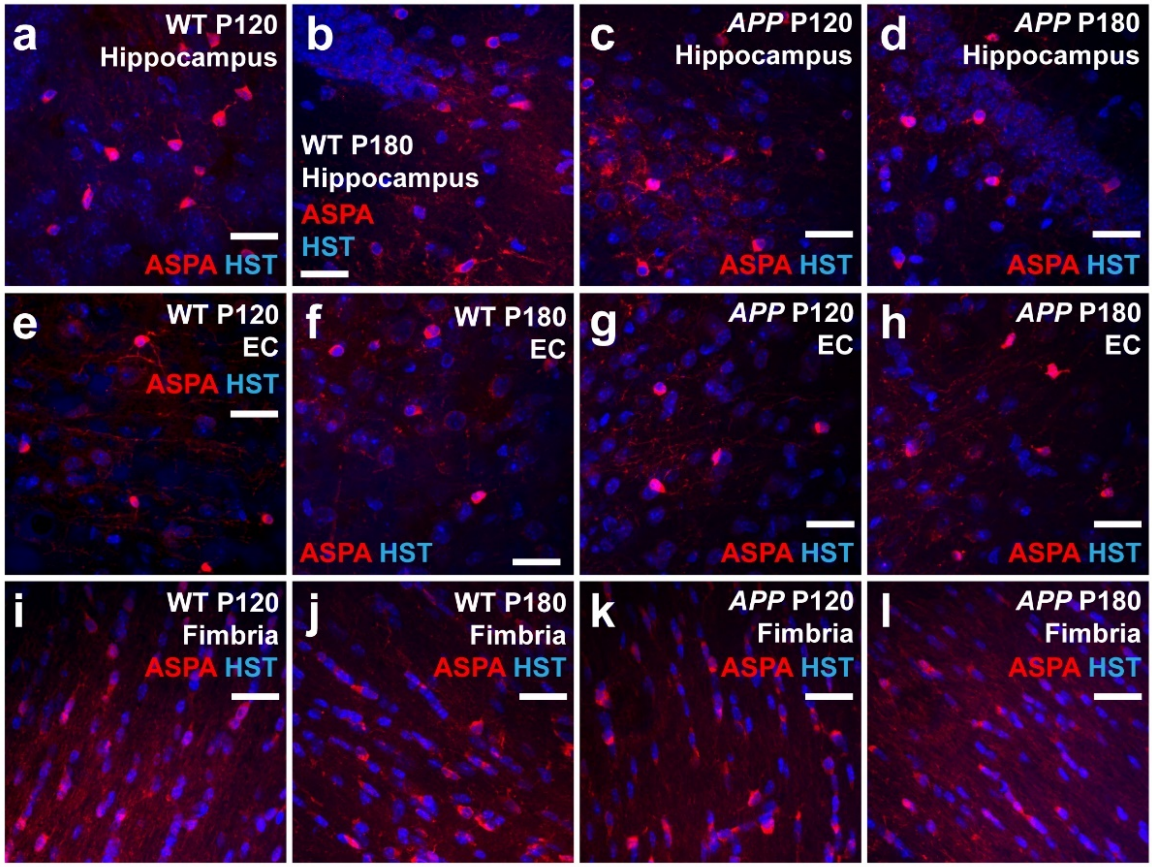
a
WT P120
Hippocampus
ASPA HST
b
WT P180
Hippocampus
ASPA
HST
c
APP P120
Hippocampus
ASPA HST
d
APP P180
Hippocampus
ASPA HST
e
WT P120
EC
ASPA HST
f
WT P180
EC
ASPA HST
g
APP P120
EC
ASPA HST
h
APP P180
EC
ASPA HST
i
WT P120
Fimbria
ASPA HST
j
WT P180
Fimbria
ASPA HST
k
APP P120
Fimbria
ASPA HST
l
APP P180
Fimbria
ASPA HST

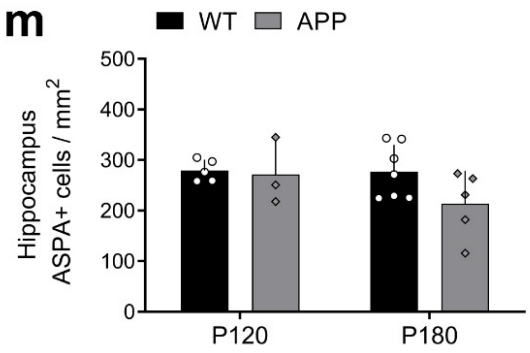
m
WT
APP
Hippocampus
ASPA+ cells / mm2
500
400
300
200
100
0
P120
P180

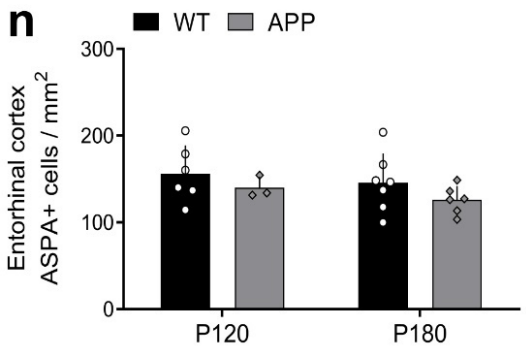
n
WT
APP
Entorhinal cortex
ASPA+ cells / mm2
300
200
100
0
P120
P180

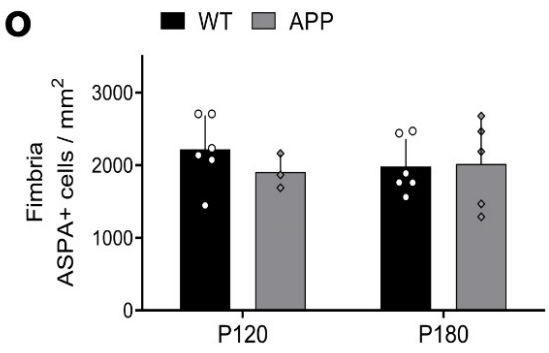
o
WT
APP
Fimbria
ASPA+ cells / mm2
3000
2000
1000
0
P120
P180

Figure 4.9. APP mice add more ASPA$^+$ mature oligodendrocytes to the hippocampus and fimbria than control mice by 6 months of age.

***a-h**) Confocal images showing ASPA (red), PDGFRα (blue) and YFP (green) in the hippocampus of P60 + 120 Pdgfrα-CreERT2:: Rosa26-YFP (control; **a-d**) and Pdgfrα-CreERT2:: Rosa26-YFP:: PDGFβ-APP^{Sw,Ind} (APP; **e-h**) mice. **i**) Quantification of the density of all YFP$^+$ cells that are PDGFRα-negative in the hippocampus of P60 + 120 control and APP mice, including those that are YFP$^+$ PDGFRα-negative ASPA-negative premyelinating oligodendrocytes versus YFP$^+$ PDGFRα-negative ASPA$^+$ mature oligodendrocytes. [two-way ANOVA, genotype: $F (1, 15) = 49.33$, $p < 0.0001$; cell type: $F (2, 15) = 80.29$, $p < 0.0001$; interaction: $F (2, 15)$, $p = 0.0029$]. **j**) Quantification of the density of all YFP$^+$ cells that are PDGFRα-negative in the fimbria of P60 + 120 control and APP mice, including those that are YFP$^+$ PDGFRα-negative ASPA-negative premyelinating oligodendrocytes versus YFP$^+$ PDGFRα-negative ASPA$^+$ mature oligodendrocytes. [two-way ANOVA, genotype: $F (1, 15) = 81.97$, $p < 0.0001$; cell type: $F (2,15) = 96.15$, $p < 0.0001$; interaction: $F (2, 15) = 21.21$, $p < 0.0001$]. Asterisks indicate significant differences identified by Bonferroni post hoc analysis, **p < .01, ***p < .001, ****p < .0001. White arrow heads indicate OPCs in which YFP expression has been enabled; yellow arrow head indicate YFP$^+$ cells that do not stain for either an OPC marker or a mature oligodendrocyte marker, suggesting that they are immature (premyelinating) oligodendrocytes. White arrows indicate YFP$^+$ (newborn) oligodendrocytes (ASPA$^+$ cells). Scale bars represent 35μm.*

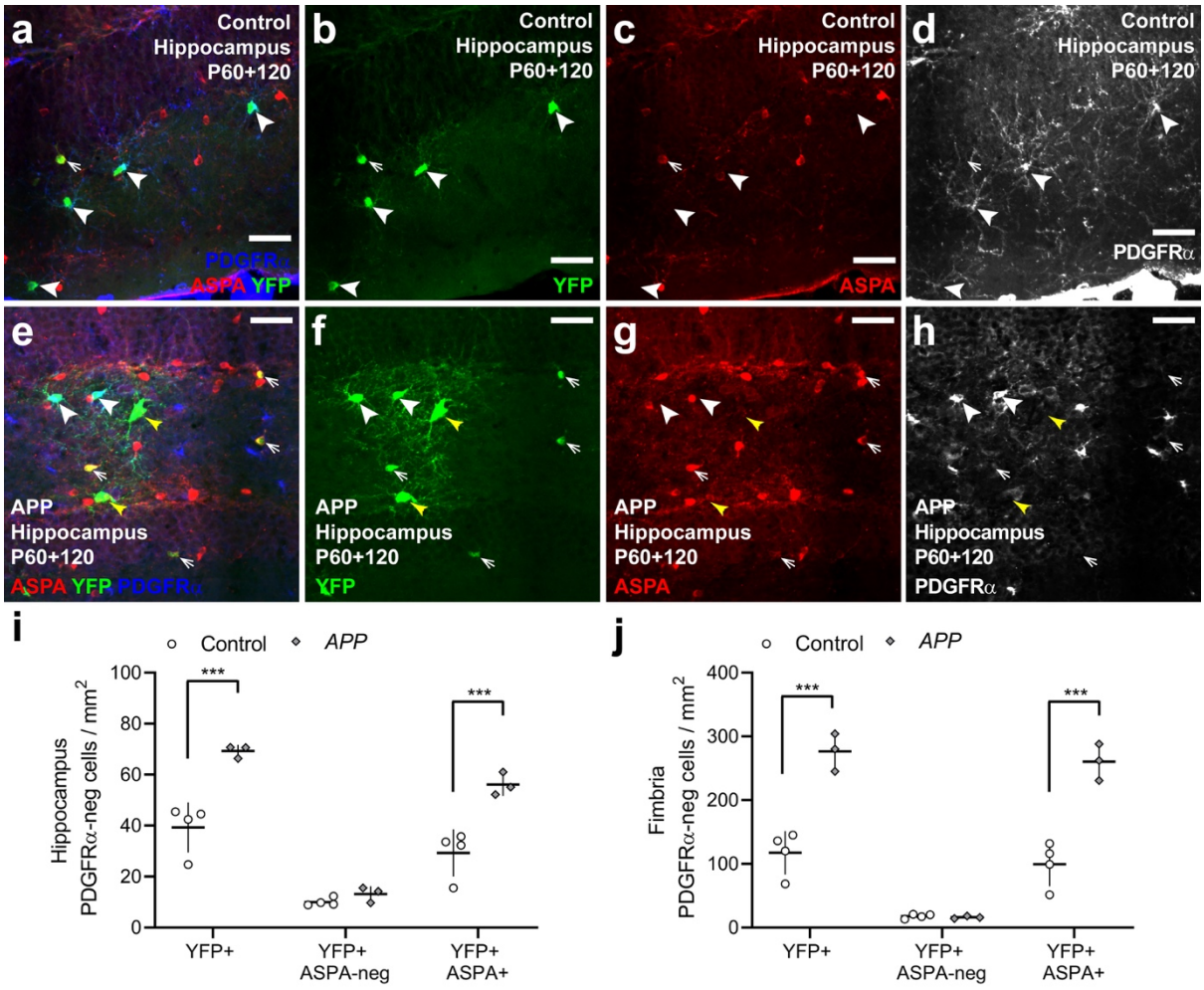
a
Control
Hippocampus
P60+120
PDGFRα
ASPA YFP
b
Control
Hippocampus
P60+120
YFP
c
Control
Hippocampus
P60+120
ASPA
d
Control
Hippocampus
P60+120
PDGFRα
e
APP
Hippocampus
P60+120
ASPA YFP PDGFRα
f
APP
Hippocampus
P60+120
YFP
g
APP
Hippocampus
P60+120
ASPA
h
APP
Hippocampus
P60+120
PDGFRα
i
Control
APP
Hippocampus
PDGFRα-neg cells / mm2
100
80
60
40
20
0
***
***
YFP+
YFP+
ASPA-neg
YFP+
ASPA+
j
Control
APP
Fimbria
PDGFRα-neg cells / mm2
400
300
200
100
0
***
***
YFP+
YFP+
ASPA-neg
YFP+
ASPA+

4.3. Discussion

Herein we show that *APP* transgenic mice have an increased level of human APP expression in the hippocampus at P180, which corresponds with their development of amyloid plaques (**Figure 4.1**). Behaviourally these mice were hyperactive by 2 months of age, which impacted their performance in other behavioural assessments; however, they did not develop spatial memory deficit by 6 months of age (**Figure 4.2**). OPCs within the hippocampus of *APP* transgenic mice are present at a normal density, but have an increased response to GABA by P100 (**Figure 4.3** and **Figure 4.4**). Additionally, developmental myelination was affected in *APP* transgenic mice, as the nodes of Ranvier along hippocampal axons were shorter and the paranodes longer in young adulthood, and this phenotype was associated with increased myelin thickness (**Figure 4.5** and **Figure 4.6**). OPCs in the hippocampus, entorhinal cortex and fimbria of young adult *APP* transgenic mice also produced a normal number of new oligodendrocytes; however, as pathology developed oligodendrogenesis increased (**Figure 4.7**). As this was not accompanied by a change in total oligodendrocyte number (**Figure 4.8**), but an increased addition of mature oligodendrocytes (**Figure 4.9**), we propose that *APP* transgenic mice have a higher level of oligodendrocyte turnover than their WT littermates by P180, which may be required to replace lost myelin.

4.3.1. *APP* mice are hyperactive prior to amyloid plaque deposition

APP or J20 mice express a human variant of *APP* containing the Swedish (K670N/M671L) and Indiana (V717F) familial AD-linked mutations, driven by the *PDGFβ* promoter (Mucke et al., 2000). By performing a western blot analysis of hippocampal protein lysates from P30, P60, P90 and P180 WT, *MAPT* and *APP* mice, detecting amino acids 1-16 of human APP using the 6E10 antibody, we found that human APP (~100kDa) was present in the hippocampus

of *APP* mice by P30 and was not present in WT mice (Mucke et al., 2000; Galvan et al., 2006). While a human APP band of ~100kDa was not present in the hippocampus of *MAPT* transgenic mice, the antibody bound to a protein of ~55kDa. As peptide inhibitors designed to target a 16-23 amino acid region of amyloid β to prevent its aggregation, can also prevent the aggregation of hyperphosphorylated tau, these two pathological proteins may share a common epitope (Griner et al., 2019). Therefore, we propose that the protein band detected in *MAPT* mice using the 6E10 antibody corresponds to tau, usually detected at ~55kDa (Kalani et al., 2017; Pu et al., 2018). While human APP was present in *APP* mice by P30, APP expression increased significantly by P180, which coincided with the appearance of amyloid plaques. Wright et al. (2013) similarly found that *APP* mice express an increasing concentration of amyloid proteins over time, leading to amyloid plaque formation at 6 months of age, while others have reported the presence of amyloid plaques developing between 4-6 (Meilandt et al., 2009) or 5-7 (Mucke et al., 2000) months of age, confirming that our *APP* mice follow the typical pattern of amyloid pathology reported for this strain. Premature mortality has also been widely reported for *APP* mice, and is often attributed to a susceptibility to spontaneous seizures (Palop et al., 2007); however, the longevity described for these mice is highly varied, with survival rates ranging from 65-90% by 6 months of age (Cheng et al., 2007; Cissé et al., 2011; Murakami et al., 2011; Verret et al., 2012; Dubal et al., 2015). We found that ~60% of *APP* mice died unexpectedly by 6 months of age, and it is reasonable to assume that the mice that died prematurely had developed greater pathology, such that the reduced survival of *APP* mice unavoidably biases our analyses, skewing our characterisation towards the less affected mice that survive to the older ages.

By subjecting *APP* mice to a battery of behavioural tasks at 2, 3 or 6 months of age, we determined that *APP* mice were hyperactive, travelling further and faster than their WT

littermates in the open field task at all ages examined. *APP* mice also developed episodic working memory deficits, observed in the T-maze spontaneous alternation task, by 3 months of age, and spent less time in the brightly lit centre of the open field by 6 months of age, which may suggest that these mice are developing anxiety-like behavioural traits. However, these phenotypes may also be an artefact of the hyperactivity of these mice. Hyperactivity is a consistent behavioural feature of *APP* mice (Cheng et al., 2007; Harris et al., 2010; Cissé et al., 2011; Murakami et al., 2011; Sanchez et al., 2012; Verret et al., 2012; Wright et al., 2013; Dubal et al., 2015; Fujikawa et al., 2017; Flores et al., 2018); however, to our knowledge, we are the first to show a tendency towards increased anxiety-like behaviour in this strain. Most studies report a decrease in anxiety-like behaviour, or a disinhibition of caution in *APP* mice demonstrated by an increase in open arm exploration time in the elevated plus maze as early as 2 months of age (Cheng et al., 2007; Harris et al., 2010; Cissé et al., 2011; Murakami et al., 2011; Sanchez et al., 2012; Dubal et al., 2015). However, others see no phenotype in the same test at 4, 6 or 11 months of age (Wright et al., 2013; Dekens et al., 2018) or no difference in performance in the light/dark emergence test at 5-8 months of age (Fujikawa et al., 2017). It is interesting to note that mice expressing the Swedish (K670N/M671L), Iberian (I716F) and Artic (E693G) mutations in human *APP* ($APP^{NL\text{-}G\text{-}F}$ mice) have been shown to simultaneously exhibit anxiogenic behaviour in the open field (less time in the centre) and anxiolytic behaviour in the elevated plus maze (more time in the open arms) at 7-8 months of age (Pervolaraki et al., 2019) which the authors suggest is reflective of altered decision making processes, rather than a core deficit in emotional motivation.

We report that *APP* mice were able to learn and remember the location of the escape box in the Barnes Maze task equally as well as their WT littermates for up to two weeks. Our finding that *APP* mice have unimpaired spatial learning and memory function, even at 6 months of age,

is seemingly at odds with the field. Numerous studies have reported spatial learning and memory deficits in the Morris water maze task from as early as 3-4 months of age in this mouse strain, but most studies show the deficit develops between 5-8 months of age (Cheng et al., 2007; Harris et al., 2010; Cissé et al., 2011; Sanchez et al., 2012; Mesquita et al., 2015). However, where other tests of spatial learning were used, the phenotype was less clear cut. Wright et al. (2013) reported that *APP* mice developed spatial learning deficits in the radial arm maze at 4 months of age, whereas Mably et al. (2015) did not see impairment in this task until 8 months of age. Similarly, Flores et al. (2018) reported that *APP* mice displayed spatial learning and memory impairment in the Barnes maze task from 5 months of age, while others reported no deficit in this task before 12 months of age (Nunes et al., 2015; Fujikawa et al., 2017), suggesting that the Morris water maze has a greater sensitivity for identifying early spatial learning impairments in the *APP* mouse model. Despite this, our data indicate that the cellular changes we observe in cells of the oligodendrocyte lineage before 6 months of age occur prior to the onset of overt amyloid pathology or cognitive decline.

4.3.2. OPCs from P100 *APP* transgenic mice have a heightened response to GABA

OPCs remained largely unchanged in *APP* transgenic mice, for example, their density, basic membrane properties and response to the AMPA/KA receptor agonist, KA, was unchanged; however, hippocampal OPCs from P100 *APP* mice responded more robustly to the bath application of the inhibitory neurotransmitter GABA. APP is a synaptic protein and has been shown to modulate GABAergic signalling, predominantly modulating presynaptic metabotropic $GABA_B$ receptors or the reversal potential of chloride (reviewed by Tang, 2019). APP can bind to the $GABA_{B1a}$ subunit of presynaptic $GABA_B$ receptors, with secreted APP acting as a ligand at presynaptic $GABA_B$ receptors to modulate neurotransmission (Rice et al., 2019); and the deletion of *APP* result in a deficit in $GABA_B$ mediated neurotransmitter release

(Dinamarca et al., 2019). OPCs do express $GABA_B$ receptors (Luyt et al., 2003, 2007; Serrano-Regal et al., 2019), but the currents evoked in OPCs by GABA application were completely antagonised by a selective $GABA_A$ receptor antagonist; however, it is possible that APP could modulate $GABA_B$ receptor activity on neurons to have a secondary effect on $GABA_A$ receptor expression or composition in OPCs, as the ability for $GABA_B$ to influence currents mediated by ion channels on OPCs has not been explored (Larson et al., 2016).

APP has also been shown to affect the reversal potential for chloride in neurons via modulation of chloride transporters, particularly KCC2 (*SLC12A5*; Chen et al., 2017; Doshina et al., 2017), which, in turn, alters signalling through ionotropic $GABA_A$ receptors. Within the CNS, NKCC1 (*SlC12A2*; Na^+ K^+ $2Cl^-$ co-transporter 1) allows chloride to enter cells, while KCC2 (K^+-Cl^- cotransporter 2) allows the efflux of chloride from cells (reviewed by Kaila et al., 2014). Together they maintain a gradient for chloride that determines the effect of $GABA_A$ receptor activation on cell membrane potential. In E17 rat primary cortical neuron cultures, the overexpression of native human APP was found to decrease KCC2 expression by approximately 50%, but had no effect on NKCC1 (Doshina et al., 2017). Consequently, GABA became more excitatory and the human APP-overexpressing neurons displayed a larger calcium increase in response to GABA application (Doshina et al., 2017). KCC2 expression is also reduced in hippocampal CA1 neurons cultured from *APP* knockout mice, producing a depolarising shift in the chloride reversal potential relative to neurons from WT mice (Chen et al., 2017). Relative to cortical neurons, OPCs have a high level of expression of NKCC1 and a low level of expression of KCC2 (Zhang et al., 2014), meaning that the chloride reversal potential in OPCs is depolarised compared with mature neurons, such that activation of $GABA_A$ receptors on OPCs is considered excitatory (Lin and Bergles, 2004); however, APP-

induced changes in KCC2 may still have the capacity to influence $GABA_A$ receptor subunit expression to influence the GABA-mediated current recorded in these cells.

$GABA_A$ receptors are pentameric ion channels made up from a number of different subunit combinations. In *APP* knockout mouse hippocampal cultures have reduced KCC2 expression, but the amplitude of evoked unitary inhibitory post-synaptic currents recorded from glutamatergic neurons was reduced, as was the response of these neurons to the $GABA_A$ receptor agonist, isoguvacine (Chen et al., 2017). This phenotype was associated with an ~50% reduction in expression of the α1 $GABA_A$ receptor subunit in the hippocampus of *APP* knockout mice that could be rescued by potentiating KCC2 function (Chen et al., 2017), suggesting that APP can modulate $GABA_A$ receptor subunit expression in a KCC2-dependent manner. Miniature iPSCs recorded from hippocampal OPCs have slow decay kinetics compared to neurons and are insensitive to zolpidem, suggesting that OPCs have low expression of α1-containing $GABA_A$ receptors (Lin and Bergles, 2004), it is possible that the increased response to GABA detected in OPCs in the hippocampus of P100 *APP* mice could be the result of an APP mediated change in the expression of $GABA_A$ receptor subunits.

A change in the OPC response to GABA may also be an indirect effect, as OPCs adapt to other changes in the *APP* transgenic mouse CNS. Dysfunctional glutamatergic signalling has been demonstrated in AD (reviewed by Findley et al., 2019), and, while $GABA_A$ activation on OPCs is considered to be excitatory (Lin and Bergles, 2004), activation of $GABA_A$ receptors can still negatively modulate the response to glutamate by increasing membrane conductance (shunting) and/or altering intracellular chloride concentration. Indeed, bath application of 5 mM GABA significantly reduced the response to a 4 ms puff application of 200 μM KA in

hippocampal OPCs in acute brain slices prepared from P14 rat brains, an effect which persisted for several minutes after GABA had been washed off and the OPC membrane conductance had returned to baseline levels (Lin and Bergles, 2004), indicating that activation of $GABA_A$ receptors on OPCs could serve to dampen pathological glutamatergic signalling onto OPCs.

It is currently unknown whether the altered response of adult OPCs in the hippocampus of *APP* transgenic mice to GABA could impact the behaviour of OPCs and the oligodendrocytes they produce. Activating $GABA_A$ receptors by applying the agonist muscimol (20 μM) to rat OPC cultures has no effect on OPC differentiation or the expression of myelin proteins (MBP or MAG; Serrano-Regal et al., 2019); however, modulating GABAergic activity *in vivo* and in slice cultures, which preserve neuron and OPC interactions suggest that GABAergic signalling has a significant effect on the behaviour of cells of the oligodendrocyte lineage. During development endogenous GABA acting at $GABA_A$ receptors can regulate oligodendrocyte lineage cell number. For example, when mice were injected with the $GABA_A$ receptor antagonist bicuculline (1mg/kg i.p., daily P5-P11), OPC number doubled, and this was accompanied by an ~40% decrease in the number of mature oligodendrocytes in the cerebellar white matter, while increasing the availability of endogenous GABA decreased OPC number and proliferation but increased the number of mature oligodendrocytes (Zonouzi et al., 2015), suggesting that GABAergic signalling in the cerebellum regulates OPC proliferation and differentiation. The effect of GABAergic signalling on OPCs may differ between CNS region, as applying the $GABA_A$ receptor antagonist, GABAzine, to P8 mouse organotypic cortical slice cultures increased both the number of OPCs and the number of oligodendrocytes present at 6 days *in vitro* (Hamilton et al., 2017). Conversely, exposure of the slice cultures to the $GABA_A$ receptor agonist, muscimol, decreased the number of cells of the oligodendrocyte lineage detected in the cortex.

The effect of endogenous GABA on cell number may be restricted to early development, as OPC density was equivalent in young adult WT and *APP* transgenic mice, despite altered GABAergic signalling in OPCs, and the application of GABAzine to slice cultures was unable to further increase cell number after 14 days *in vitro* (Hamilton et al., 2017). The complex pathology that develops in *APP* mice also makes it difficult to specifically dissect the role of GABAergic signalling, as changes to neuronal signalling can also influence this signalling pathway in OPCs. For example, the effect of GABAzine on oligodendrocyte lineage cell number was prevented by blocking neuronal action potentials with tetrodotoxin, suggesting that the effect of GABAzine was dependent on the release of an activity-dependent factor from neurons (Hamilton et al., 2017). Interestingly, tetrodotoxin alone had no effect on oligodendrocyte lineage cell number, implying an interaction between a direct action at $GABA_A$ receptors on OPCs concomitant with release of an activity-dependent neuronal factor (Hamilton et al., 2017). As neither GABAzine nor muscimol altered node of Ranvier length in mouse cortical organotypic cortical slice cultures (Hamilton et al., 2017), it is likely that the changes detected in node length were independent of the increased responsiveness of OPCs to GABA, and the impact the GABAergic signalling has on myelin thickness has not been explored.

4.3.3. Amyloid accumulation changes myelin ultrastructure

We have shown that paranodes are longer and nodes of Ranvier shorter for axons in the hippocampus of 3-month old *APP* transgenic mice, compared with WT controls. Paranodes form at the end of each myelin internode, flanking the node of Ranvier, facilitated by contact-mediated signalling between proteins in the myelin sheath and the axon to maintain the

clustered voltage gated sodium channels at the nodes of Ranvier; and tether the myelin internode to the axon (reviewed by Pepper et al., 2018). As APP can be found at the nodes of Ranvier (Xu et al., 2014) and can increase NaV1.6-mediated sodium currents (Li et al., 2016), it is possible that pathological human APP could directly induce narrowing of nodes of Ranvier in the hippocampus. In the 3xTg transgenic mouse line, a qualitative decrease was noted in NaV1.6 expression in the CA1 region of the hippocampus and the entorhinal cortex at 6 months of age (Desai et al., 2009); however, this could be the result of myelin degradation and an overall reduction in nodes of Ranvier number, rather than a change in nodal structure. As axon diameter was consistent between WT and *APP* transgenic mice, this is unlikely to be a contributing factor to the node of Ranvier length. The effect of amyloid pathology on the node of Ranvier length is also unlikely to result from changes in axon diameter, as we found no correlation between the node of Ranvier length and node width (a proxy for axon diameter) in WT or *APP* transgenic mice [linear regression node length v node width deviation of slope from 0: WT slope = 0.04, $F(1, 227) = 2.2$, $p = 0.14$; *APP* slope = 0.04, $F(1, 140)$, $p=0.22$], which is consistent with a previous analysis of node of Ranvier length and width in the optic nerve and frontoparietal motor cortex of Sprague-Dawley rats (Arancibia-Cárcamo et al., 2017).

It is likely that the increased paranode length measured for hippocampal axons in the *APP* transgenic mice is the direct result of *APP* transgenic mice having thicker myelin. On average, oligodendrocytes that myelinated axons in the hippocampus of *APP* mice produced an extra myelin lamella, relative to those in WT mice. The extra layer of myelin must be anchored at the paranode, and could readily explain the increased paranode length, and perhaps, if the myelin encroaches on the node of Ranvier, the decrease in nodes of Ranvier length. Increased myelin thickness has also been reported for hippocampal axons in 2-month old

APPSwe/PSEN1dE9 transgenic mice, and was attributed to an upregulation in neuregulin-1 type III (Wu et al., 2017), a known regulator of myelination and myelin thickness (Taveggia et al., 2005, 2008; Velanac et al., 2012), cleaved by the enzyme BACE1 that also cleaves APP (Luo et al., 2011).

While physiological APP was suggested to be a modulator of myelination and remyelination in mice (Truong et al., 2019), it is unclear whether APP regulates myelin thickness. Myelin thickness was unchanged in the sciatic nerve, optic nerve and corpus callosum of *APP* knockout mice at P14 and P77 (Truong et al., 2019); however, pathological overexpression of human $APP695^{Swe}$ increased myelin thickness by 1.3% in the spinal cord of 3 months old Tg2576 mice (Xu et al., 2014), and we found that myelin thickness was increased by ~10% in the hippocampus of *APP* mice overexpressing $APP^{Sw,Ind}$ relative to WT at the same age. The marked increase in myelin thickness in our experiment compared to the change observed in Tg2576 mice could be attributed to higher level of soluble Aβ produced in our model at this age (Hsiao et al., 1996; Mucke et al., 2000). As soluble Aβ induces neuronal hyperactivity in the hippocampus (Busche et al., 2012; Willem et al., 2015), and neuronal activity regulates myelination (Gibson et al., 2014), Aβ could indirectly promote the addition of new myelin layers.

4.3.4. Amyloid accumulation increases oligodendrocyte turnover

OPCs continue to generate new oligodendrocytes in the grey and white matter of the adult mouse brain (Dimou et al., 2008; Rivers et al., 2008; Kang et al., 2010; Hill et al., 2013; Young et al., 2013; Fukushima et al., 2015). While the rate of OPC proliferation and oligodendrocyte addition slows with aging (reviewed by Wang and Young, 2014), OPCs can rapidly proliferate

and differentiate in response to a demyelinating event, to facilitate the replacement of lost oligodendrocytes and enable remyelination (Tripathi et al., 2010; Zawadzka et al., 2010; Assinck et al., 2017; Baxi et al., 2017). By performing Cre-lox lineage tracing using *Pdgfrα-CreER^{T2}::Rosa26-YFP* transgenic mice, we have shown the number of new oligodendrocytes that accumulate in the hippocampus, entorhinal cortex and fimbria of *APP* transgenic mice between P60 and P180 is significantly higher than the number added to these regions in the WT mouse brain. In the hippocampus, oligodendrocyte addition started to deviate between WT and *APP* transgenic mice between 4 and 5 months of age. However, the effect of amyloid pathology on oligodendrogenesis was delayed in the entorhinal cortex and fimbria, being seen between 4 and 6 months of age. Despite the increased number of new oligodendrocytes added to the brain of *APP* transgenic mice, immunolabelling to detect the mature oligodendrocyte marker ASPA revealed that oligodendrocyte density in the hippocampus, entorhinal cortex and fimbria was equivalent between WT and *APP* transgenic mice. However, mature oligodendrocyte addition was significantly increased in the hippocampus and fimbria of *APP* mice relative to controls suggesting that the large number of new cells may serve to replace oligodendrocytes and myelin that are lost. Oligodendrocyte turnover is likely to be enhanced by Aβ toxicity to oligodendrocytes (Xu et al., 2001; Lee et al., 2004), APP accumulation in oligodendrocytes (Bauer et al., 2002), or myelin aberrations (Behrendt et al., 2013); but whether APP or Aβ drives oligodendrocyte replacement remains undefined.

Myelin abnormalities have been reported for a number of animal models of amyloid pathology (Chu et al., 2017; Tse et al., 2018), including focal myelin loss associated with amyloid plaques (Mitew et al., 2010; Schmued et al., 2013). We found that the proportion of hippocampal axons that were myelinated in 3-month old WT and *APP* transgenic mice was equivalent; however, the marked increase in oligodendrogenesis observed between 4 and 6 months of age in the *APP*

transgenic mice may suggest that oligodendrocyte loss and demyelination are a later feature of the pathogenesis. This time line differs significantly from that of *APP*^{Sw} (R1.40) mice in which myelin loss was not reported until 18-months of age (Tse et al., 2018), but would be consistent with the marked reduction in myelinated axon number in the hippocampus of 6-month old 3xTg mice, which occurred prior to plaque deposition (Desai et al., 2009), and the myelin aberrations detected in APP/PS1 mice at 6 months, coincident with plaque detection (Behrendt et al., 2013).

Chapter 5: General discussion and future directions

5.1. Thesis findings summary

The aim of this thesis was to evaluate the impact that overexpressing human pathological variants of *MAPT* or *APP* in neurons had on the behaviour of cells of the oligodendrocyte lineage. Specifically, I aimed to determine whether cells of the oligodendrocyte lineage were affected early in disease, prior to the development of overt cognitive impairment or histopathological hallmarks of disease. By performing cre-lox lineage tracing, immunohistochemistry, electrophysiology and TEM, I found that the cells of the oligodendrocyte lineage respond differently to each pathological protein, with amyloid but not tau pathology influencing the capacity of OPCs to respond to GABAergic signalling and the myelinating capacity of oligodendrocytes. However, both amyloid and tau pathologies resulted in elevated adult oligodendrogenesis, without a coincident increase in total oligodendrocyte number but instead an increase in mature oligodendrocyte addition, perhaps suggesting that both pathologies drive oligodendrocyte and myelin turnover in the brain.

5.2. Does early tau or amyloid pathology drive oligodendrocyte turnover?

By labelling OPCs with YFP in young adulthood, and following their fate over time, I was able to determine that the number of new YFP-labelled oligodendrocytes added to the hippocampus, entorhinal cortex and fimbria was increased in *MAPT* and *APP* transgenic mice when compared with their respective controls. In the *MAPT* mice, this increase in oligodendrogenesis was absent at P60+90, but was first detected at P60+120, which indicates that a large number of new oligodendrocytes are added between 5 and 6 months of age; however, in *APP* mice,

oligodendrogenesis was stimulated earlier, with a significant increase in new oligodendrocyte number first being noted in the hippocampus as P60+90. Nonetheless, by P60+120 the magnitude of the increase was equivalent in the hippocampus, entorhinal cortex and fimbria of *MAPT* mice compared to *APP* mice. Together, this suggests that oligodendrocyte pathology is hastened in *APP* mice, but ultimately reaches similar levels in *APP* and *MAPT* mice by 6 months of age.

New oligodendrocytes produced in adulthood are likely to comprise a combination of premyelinating and myelinating cells. The proportion of premyelinating and myelinating oligodendrocytes could be evaluated in one of two ways. By delivering tamoxifen to *Pdgfrα-CreER^{T2}::Tau-mGFP* transgenic mice (Young et al., 2013; Cullen et al., 2019) that lack or carry the *MAPT* or *APP* transgenes, it would be possible to induce the expression of a membrane-targeted GFP in OPCs and oligodendrocytes produced, and visualise the full oligodendrocyte morphology, to classify them as being premyelinating or myelinating cells. Alternatively, tissue from the control, *MAPT* or *APP* transgenic mice utilised for lineage tracing in this study were stained to detect YFP and the mature oligodendrocyte marker ASPA. If the majority of new oligodendrocytes produced in response to tau or amyloid pathologies were premyelinating oligodendrocytes (YFP$^+$ ASPA-negative), they would be unable to contribute myelin to axons. However, I showed that mature oligodendrocytes were mainly added in the hippocampus and fimbria of *MAPT* and *APP* transgenic mice relative to their respective controls, while the total number of oligodendrocytes was equivalent for control mice and either *MAPT* or *APP* transgenic mice. These data suggest that oligodendrocytes are being lost at the same time that new oligodendrocytes are being added. If the replacement cells were not myelinating oligodendrocytes, the fraction of myelinated axons should go down over time. However, for *MAPT* mice, I noted that the fraction of myelinated axons was the same as that

of control mice at 6 months of age. This was not specifically examined for *APP* mice at the time of increased oligodendrogenesis and yet should be examined to confirm the addition of myelinating cells over time.

For the number of newborn oligodendrocytes to increase significantly, but the total number of oligodendrocytes in the hippocampus, entorhinal cortex and fimbria to remain the same, a significant number of pre-existing, developmentally-born oligodendrocytes must die in response to tau and amyloid pathology. In the developing and mature CNS ~80% of all newborn premyelinating oligodendrocytes die (Barres et al., 1992; Trapp et al., 1997; Hughes et al., 2018), and there is some evidence that mature oligodendrocytes can also die over time (Tripathi et al., 2017). Detecting and quantifying oligodendrocyte cell death is challenging as, once initiated, it occurs rapidly with cells being completely cleared within two days (Hughes et al., 2018). However, it would be valuable to confirm that oligodendrocyte death increases in response to tau and amyloid pathologies produced in the *MAPT* and *APP* mice, respectively. Particularly as myelin protein levels including CNP, MAG, oligodendrocyte myelin glycoprotein and PLP are decreased in late AD suggesting a loss of myelin but also oligodendrocytes (Zhang et al., 2018); however, whether oligodendrocytes are lost in early AD is still unclear. This could be done by evaluating cell death using a TUNEL assay to detect oligodendrocyte death in *MAPT* and *APP* mice at multiple ages between 2 and 6 months of age. This experiment would be necessary to confirm that adult-born oligodendrocytes, generated in response to tau and amyloid pathologies, produce new myelinating cells that act to replace those lost to disease.

As elevated concurrent oligodendrocyte loss and replacement resulting from tau and amyloid pathologies seems the most likely explanation for my data, they suggest that oligodendrogenesis is critical for sustaining myelin on axons in the hippocampus, entorhinal cortex and fimbria of *MAPT* and *APP* mice. Consequently, I hypothesise that in the absence of continued adult oligodendrogenesis I would see a significant loss of oligodendrocytes and a loss of myelin in these regions. It would be possible to determine the importance of adult oligodendrogenesis for myelin maintenance in the face of pathology, by preventing the addition of new oligodendrocytes in adulthood. *Pdgfrα-CreER^{T2}::MyRF$^{flox/flox}$* mice (Mckenzie et al., 2014; Xiao et al., 2016) could be crossed with *MAPT* and *APP* mice, and the addition of tamoxifen would result in the loss of the transcription factor MyRF from OPCs and would ultimately prevent the maturation of OPCs into new oligodendrocytes. I predict that this would result in a demyelination phenotype and ultimately precipitate or aggravate cognitive impairment in these mice.

5.3. Does amyloid pathology alter the balance between inhibition and excitation in the brain?

In *APP* but not *MAPT* transgenic mice, adult OPCs experienced enhanced depolarisation in response to the bath application of GABA; however, their depolarisation in response to the glutamate receptor agonist, KA, was normal. Both GABA and KA exposure are known to depolarise OPCs, due to their low RMP (~-80mV) that results in chloride exiting the cell (Hoppe and Kettenmann, 1989; Lin and Bergles, 2004; Haberlandt et al., 2011; Hamilton et al., 2017), rather than entering the cell, which is the case for neurons. However, these data suggest that between early development (P30) and early adulthood (P100) emerging amyloid pathology, driven by expression of the *PDGFβ-APP^{Sw,Ind}* transgene, either results in a change

in the subunit composition of $GABA_A$ receptors, to allow more chloride efflux, or increases the number of $GABA_A$ receptors expressed on the surface of OPCs.

A single-nucleus RNA sequencing study that compared gene expression in cells from healthy controls and people with AD, suggested that AD resulted in a reduction in GABA receptor subunit expression by OPCs and oligodendrocytes (Grubman et al., 2019). This apparent discrepancy between our functional analysis of OPCs in transgenic *APP* mice and this gene expression analysis, is likely explained by changes that occur in receptor expression and activation susceptibility at different stages of disease. My results could be explained by an increase in $GABA_A$ receptor expression on the surface of OPCs in *APP* transgenic mice.

Under some circumstances, the cell surface expression of neurotransmitter receptors can be influenced by the level of the neurotransmitter expressed in the surrounding environment (Dulcis et al., 2013; Nair et al., 2013; Kwakowsky et al., 2018; Sanderson et al., 2018). For example, a high level of neurotransmitter expression may be associated with the internalisation of receptors or downregulation of their expression by the target cells (Fuhrer et al., 2017; Kwakowsky et al., 2018; Sanderson et al., 2018). Therefore, it may also be possible that a reduction in GABA expression in the brain could be associated with a change in $GABA_A$ receptor expression or composition by OPCs to allow them to respond more robustly to GABA within the environment. Therefore, it would be interesting to determine and compare the level of GABA and glutamate expression within the brain of control, *MAPT* or *APP* transgenic mice by performing a Western blot analysis of glutamate decarboxylase (GAD67; to assess GABA production), glutamate dehydrogenase (GDH1; to measure glutamate production) and glutamine synthase (GLUL; to gauge homeostasis between glutamate and GABA production).

This is particularly interesting as previous reports have presented conflicting results on whether GABA and glutamate levels were increased (Madeira et al., 2018; Snowden et al., 2019) or decreased (Fayed et al., 2011; Gueli and Taibi, 2013; reviewed by Govindpani et al., 2017) in AD; which may result from differences in brain autopsy protocol, brain region variability and individual differences based on disease stage, age and gender (Roy et al., 2018).

Altered GABAergic signalling can directly impact signalling by excitatory glutamatergic neurons in the CNS and there is some evidence that the level of inhibitory vs excitatory signalling is altered in mouse models of amyloidosis (Palop et al., 2007; Sun et al., 2009; Verret et al., 2012). Interestingly, amyloid-induced neuronal overexcitation leads to an increase in aberrant GABAergic interneuron projections in the hippocampus of *APP* mice as a compensation attempt (Palop et al., 2007; Sun et al., 2009). However, $Nav1.1^{+}$ parvalbumin-positive GABAergic interneurons are reduced in *APP* mice, which correlates with gamma oscillation deficits (Verret et al., 2012) and cognitive impairment in *APP* mice (Bender et al., 2016). Nonetheless, rescuing Nav1.1 levels in *APP* mice can restore cognitive function (Verret et al., 2012; Martinez-Losa et al., 2018); while transient enriched environment exposure, associated with cognitive improvement (Balthazar et al., 2018; Prado Lima et al., 2018), restores the number of parvalbumin-positive interneurons with a perineuronal net, which protects the cell integrity, in transgenic mice overexpressing *APP* (Tg2576) (Cattaud et al., 2018). As increased myelin thickness may result from neuronal hyperactivity in *APP* mice, it would be interesting to determine whether reducing glutamate signalling or enhancing GABA signalling in *APP* mice decreases myelin thickness.

Both GABAergic and glutamatergic signalling have been shown to influence oligodendrogenesis and myelination (Gibson et al., 2014; Corell et al., 2015; Gautier et al., 2015; Hamilton et al., 2017; Kougioumtzidou et al., 2017). This is interesting as both inhibitory interneurons and excitatory projection neurons are known to become myelinated (Micheva et al., 2018) and a change in the balance of excitation and inhibition has the capacity to alter myelination in the CNS (Gibson et al., 2014; Gautier et al., 2015; Mitew et al., 2018). While we found no change in the proportion of axons that were myelinated in *APP* mice and their WT littermates at 4 months of age, or the proportion of axons that were myelinated in *MAPT* mice and their WT littermates at 6 months of age, I did note that myelin thickness was increased in the hippocampus of *APP* mice. Aβ-induced increase in neuronal activity (Beraldo et al., 2016; reviewed by Findley et al., 2019) may result in increased myelin thickness (Gibson et al., 2014). Optogenetic stimulation of the mouse premotor cortex results in a rapid increase in new oligodendrocyte addition in this area and the underlying corpus callosum, which was followed by an increase in myelin thickness within 4 weeks post-optogenetic stimulation (Gibson et al., 2014). Furthermore, node length was increased and myelin thickness was decreased during development in the spinal cord and sciatic nerve of *APP* knock-out transgenic mice (Truong et al., 2019), but myelin thickness was increased in the developmental spinal cord of transgenic mice overexpressing human APP_{695} (Xu et al., 2014). It would be interesting to determine whether the decrease in node length and increase in myelin thickness observed in my thesis is partially regulated by APP clustering at the node, and whether this clustering is regulated by neuronal hyperactivity as APP regulate Nav1.6 sodium channel currents (Li et al., 2016), or whether Aβ alone regulates myelin thickness through neuronal hyperactivity.

5.4. How does tau or amyloid pathology influence oligodendrogenesis?

In *APP* and *MAPT* mice, adult oligodendrogenesis was increased by 5 and 6 months of age, respectively. While tau is found to interact with MBP *in vitro* and is required for OPC differentiation and oligodendrocyte process outgrowth (Seiberlich et al., 2015), it is unlikely that *MAPT* overexpression would only promote an increase in adult oligodendrogenesis by 6 months of age if it directly interacted with mature oligodendrocytes via exchange with neurons through the periaxonal space (Fünfschilling et al., 2012; Lee et al., 2012; reviewed by Stassart et al., 2018); or with OPC via synaptic and non-synaptic junctions with neurons (Bergles et al., 2000; Lin and Bergles, 2004; Wake et al., 2015). As a similar effect was observed in *APP* mice, it is possible that enhanced adult oligodendrogenesis occurs in response to the onset of neurodegeneration in both models, rather than an increase in neuronal activity. Indeed, neuronal activity can regulate adult oligodendrogenesis (Gibson et al., 2014; Nagy et al., 2017; Cullen et al., 2019); however, as the increase in adult oligodendrogenesis was not observed at 4 months of age in *APP* mice, it is likely that the increased neuronal activity previously reported in *APP* mice did not trigger new oligodendrocyte addition. Instead, the increase in adult oligodendrogenesis was only observed from 5 months of age in the hippocampus, and only affected the entorhinal cortex and fimbria by 6 months of age coincident with amyloid plaque formation. In close vicinity of amyloid plaques, oligodendrocytes and myelin are lost (Mitew et al., 2010), potentially playing a role in the increasing neuronal hypoactivity observed following amyloid plaque formation (Busche et al., 2012). Interestingly, neuronal hypoactivity is prominent in tau pathology and dominates Aβ-induced neuronal hyperactivity in intercrossed mice expressing both amyloid- and tau-pathology associated mutations (Busche et al., 2019). It was previously suggested that neuronal hypoactivity simply reflects excessive neuronal hyperactivity (reviewed by Zott et al., 2018), which may results in synaptic deficits and neuron loss of function. This is particularly interesting as previous evidences in P301-htau mice

suggest that OPC differentiation is promoted following induced-spinal cord injury causing neuron loss (Ossola et al., 2016). Furthermore, reactive microglia observed in *APP* and *MAPT* mice at 6 months of age may clear dysfunctional synapses in addition to amyloid plaques in *APP* mice (reviewed by Bar and Barak, 2019); and promote oligodendrogenesis and myelination (Miron et al., 2013; Shigemoto-Mogami et al., 2014; Naruse et al., 2018). Consequently, it would be interesting to determine whether new oligodendrocytes are added in *APP* and *MAPT* mice following synaptic deficits and whether reactive microglia promote adult oligodendrogenesis in *APP* and *MAPT* mice.

5.5. Are OPCs potential targets for slowing dementia progression?

In 2019, around 50 million people were diagnosed with dementia worldwide. This figure is expected to reach 152 million by 2050 as reported by the world health organization. AD is the main form of dementia and actually represents 60-70% of dementia cases making AD one of the main health care issues. Most AD treatments include antipsychotic drugs (e.g. risperidone), antidepressants (e.g. sertraline, citalopram) and anticonvulsants (e.g. carbamazepine, valproate), anti-dementia drugs (e.g. memantine, donepezil and rivastigmine) and drugs to treat sleep disturbance. While all treatments delay symptoms onset, they cannot be used as a long-term solution. Therapeutic development to slow down amyloid plaque formation in AD such as Solanezumab (Doody et al., 2014), marijuana (Ramírez et al., 2005) or immunotherapy (Oddo et al., 2004) have failed so far. These multiple pharmaceutical failures show how complex neurodegenerative disease management is, particularly as we do not know what happens first, when and how it happens. Consequently, some of these treatments may have some benefit if given at the right time; however, a proper early AD detection mechanism still needs to be developed and approved.

There are currently two ways to define AD progression: the evaluation of protein levels of $A\beta_{1-42}$, total tau and phosphorylated tau at phosphorylation site 181 in the cerebrospinal fluid as AD biomarkers (Bouwman et al., 2009; Mattsson et al., 2017; Hansson et al., 2018); or a change in brain structure detected using magnetic resonance imaging (deToledo-Morrell et al., 2004; Defrancesco et al., 2014; Kavroulakis et al., 2018). A few compounds have been created to detect amyloid plaques by positron emission tomography or PET scan such as the Pittsburgh Compound B (Klunk et al., 2004; Cohen et al., 2012). Although progress have been made towards better and earlier detection of brain changes in AD and other neurodegenerative diseases, we currently lack appropriate detection and therapy. Consequently, new therapeutic targets should be considered, and it is worth examining the suitability of OPC and oligodendrocyte changes as a biomarker or potential therapeutic target.

OPCs are able to generate large number of oligodendrocytes in the mouse healthy brain, which is increased following demyelination (Baxi et al., 2017) and in AD models (Desai et al., 2010; Behrendt et al., 2013; Ossola et al., 2016; and as shown in this thesis). However, new oligodendrocyte generation does not occur to the same extent in humans as only 1 out of 300 oligodendrocytes is replaced per year (Yeung et al., 2014). While an increase in new oligodendrocyte addition was observed in some patients diagnosed with multiple sclerosis (Yeung et al., 2019), most of the remyelination in the human CNS seems to occur through surviving mature oligodendrocytes generating new myelin internodes following demyelination (Duncan et al., 2018).

However, the expression of genes associated with newly generated and myelinating oligodendrocytes are upregulated in AD patients relative to age-matched controls, suggesting that some attempt is being made at repair (Itoh and Voskuhl, 2017), that could be therapeutically aided. For example, increased *Bridging-Integrator-1 (BIN1)* mRNA (Chapuis et al., 2013; De Rossi et al., 2016) and altered expression of protein isoforms (Holler et al., 2014) represent the second most prevalent risk factor for sporadic late-onset AD (Bertram et al., 2007), yet BIN1 function is still unknown. However, *BIN1* is highly expressed by mature oligodendrocytes (De Rossi et al., 2016) and upregulated in AD (Zhang et al., 2018). Interestingly, downregulation of neuronal BIN1 increases the flux of endosomes, in which tau aggregates, and endosomes are then damaged leaking tau aggregates into the cytoplasm for further seeding and tau pathology propagation (Calafate et al., 2016). Furthermore, LINGO-1 (Leucine rich repeat and Ig domain containing NOGO receptor interacting protein 1) is a negative regulator of neuronal survival, axonal integrity, oligodendrocyte differentiation and myelination, and LINGO-1 blockade was trialled as a remyelination therapy in multiple sclerosis (Biogen; Cadavid et al. 2019). However, as LINGO-1 is significantly upregulated by excitatory neurons and oligodendrocytes in AD (Mathys et al., 2019), and anti-LINGO-1 monoclonal antibodies reduce myelin impairment and improves spatial memory performance in the early phase of AD-like pathology in transgenic mice overexpressing human *APP* (Wu et al., 2018), anti-LINGO-1 may be a valid therapeutic to trial in AD.

The development of novel AD treatment may benefit patients diagnosed with other forms of tauopathy, but clinical and pathological heterogeneity should be carefully considered. Tauopathies are defined by the presence of tau aggregates in neurons, astrocytes or oligodendrocytes (Ikeda et al., 1998; Arai et al., 2001; reviewed by Ferrer, 2018). However, pathological tau strains extracted from post-mortem brains of corticobasal degeneration and

supranuclear palsy spread more rapidly throughout the non-transgenic mouse brain following injection, and targeted different cell populations than tau strains extracted from post-mortem AD brains (Narasimhan et al., 2017). Oligodendrocytes developed tau coiled bodies and participated in tau seeding in a mouse injected with samples from corticobasal degeneration and supranuclear palsy post-mortem brains, while they did not when injected with samples from AD post-mortem brains (Narasimhan et al., 2017), therefore oligodendrocyte and OPC response may differ in other tauopathies. OPC and oligodendrocyte behaviour should be assessed in additional tauopathy models to determine whether oligodendrocyte replacement could be a valid therapeutic target to delay the motor and cognitive deficit onset, if tau clearance is also ensured (Noack et al., 2014; Leyk et al., 2015; Noack and Richter-Landsberg, 2015) to avoid continuous spread of tau aggregates between oligodendrocytes (Ferrer et al., 2019).

By demonstrating that *MAPT* and *APP* overexpression differently alter OPC response to neurotransmitters, oligodendrocyte myelinating capacity and adult oligodendrogenesis, this thesis improves our understanding of the early function of the cells of the oligodendrocyte lineage in AD pathology development. This thesis suggests that OPCs and oligodendrocytes should be considered as potential therapeutic target in AD and other tauopathies. Future studies should determine if enhancing adult oligodendrogenesis or myelination by mature oligodendrocytes and newly added oligodendrocytes can delay pathology onset; and whether changes in neuronal activity observed in AD affect OPCs and regulate adult oligodendrogenesis and myelination.

Appendix 1: Solutions

Common Laboratory Reagents

0.01M Phosphate Buffered Saline (PBS)

MilliQ water	850ml
90.0g/L sodium chloride	100ml
28.0g/L di-sodium hydrogen orthophosphate	40ml
31.2g/L sodium di-hydrogen orthophosphate	10ml

Blocking solution for Immunohistochemistry

	Add	Final Conc.
FCS	1ml	10%
Triton-X100	10µl	1%
PBS	top up to 10ml	-

Solutions for DNA Extraction

DNA Extraction Buffer

1M Tris-HCL (pH 8.5)	12ml
0.5M EDTA (pH 8.0)	1.2ml
5M NaCl	4.8ml
10% SDS	0.2%

NB: Autoclave before adding SDS

Thioflavin-S staining

Thioflavin-S solution

	Add	Final Conc.
Thioflavin-S	0.1g	0.1%
100% ethanol	60 mL	60%
PBS	40 mL	40%

Destain solution

	Add	Final Conc.
100% ethanol	50 mL	50%
PBS	50 mL	50%

Western blot solutions

RIPA buffer (10ml)

	Add	Final Conc.
MQ water	8190µl	-
1M Tris-HCl (pH 7.4)	500µl	50mM
5M NaCl	300µl	150mM
10% NP-40	1mL	1%
Sodium deoxycholate	100mg	1%
10% SDS	10µl	0.1%
Protease inhibitor tablets	1 per 10ml	-

Aliquot and store at -20°C

Tris-buffered saline – Tween 20 (TBS-T)

	Add (per L)	Final Conc.
NaCl	8g	150mM
Tris-Base	3g	25mM
Tween 20	2mL	0.2%

Transfer buffer

	Add	Final Conc.
20X Bolt MES transfer buffer	50ml	1x
Methanol	100ml	10%
Bolt Antioxidant	1ml	1%
MQ water	top up to 1L	-

TEM solutions

0.8% GA 2% PFA in 0.1M sodium cacodylate (200mL)

	Add	Final Conc.
8% glutaraldehyde	20mL	0.8%
16% paraformaldehyde	25mL	2%
0.2M Sodium cacodylate	100mL	0.1%
Calcium chloride	10mL	5mM
Magnesium chloride	10mL	5mM
MQ water	top up to 200mL	-

Osmium tetroxide and potassium ferrycianide (10mL)

	Add	Final Conc.
0.1M Sodium cacodylate	6.5mL	0.065M
4% OsO4	2.5mL	1%
15% K3Fe(III)(CN)6 freshly made	1mL	1.5%

Epon pure

	Add
Embed 812 resin	20 mL
Dodecenyl Succinic Anhydride Specially Distilled (DDSA)	16 mL
Methyl-5-Norbornene-2,3-Dicarboxylic Anhydride (NMA)	8 mL
Benzyldimethylamine (BDMA)	1.1 – 1.3 mL

Appendix 2

Table 1. Transgenic mice

Strains	**Allow to/use as**
C57BL/6	Control, wild type mouse.
PDGFβ-APP^{Sw,Ind}	Induce amyloid pathology (*APP*) or tau pathology (*MAPT*) in the brain. Mutations expressed in neurons.
Prnp-MAPT^{P301S}	
Pdgfrα-CreER^{T2}::Rosa26-YFP	Enable the fluorescent labelling of OPCs in adulthood, and the tracing of their progeny *in vivo*.
Pdgfrα-CreER^{T2}::Rosa26-YFP:: PDGFβ-APP^{Sw,Ind}	Enable the fluorescent labelling of OPCs in adulthood, and the tracing of their progeny *in vivo* in an AD-like environment of amyloid pathology (*APP*) or tau pathology (*MAPT*).
Pdgfrα-CreER^{T2}::Rosa26-YFP::Prnp-MAPT^{P301S}	
Pdgfrα–H2BGFP	Induce fluorescent labelling of OPCs *in vivo*
Pdgfrα–H2BGFP::PDGFβ-APP^{Sw,Ind}	Induce fluorescent labelling of OPCs *in vivo*, in an AD-like environment of amyloid pathology (*APP*) or tau pathology (*MAPT*).
Pdgfrα–H2BGFP:: Prnp-MAPT^{P301S}	

Table 2. PCR reaction for each transgene.

Transgene	Primer pairs	Primer sequences	PCR cycles (94°C-30s, 62°C-45s, 72°C-1min)	PCR cycles (94°C-30s, 57°C-45s, 72°C-1min)
Cre	*Cre 5'*	CAG GTC TCA GGA GCT ATG TCC AAT TTA CTG ACC GTA	34	
	Cre 3'	GGT GTT ATA AGC AAT CCC CAG AA		
Rosa26 WT	*Rosa26 WT 5'*	AAA GTC GCT CTG AGT TGT TAT	37	
	Rosa26 WT 3'	GGA GCG GGA GAA ATG GAT ATG		
Rosa26 MUT	*Rosa26 WT 5'*	AAA GTC GCT CTG AGT TGT TAT	37	
	Rosa26 MUT 5'	GCG AAG AGT TTG TCC TCA ACC		
hMAPT	*hMAPT 5'*	GGG GAC ACG TCT CCA CGG CAT CTC AGC AAT GTC TCC		35
	hMAPT 3'	TCC CCC AGC CTA GAC CAC GAG AAT		
hAPP	*hAPP 5'*	GGT GAG TTT GTA AGT GAT GCC		35
	hAPP 3'	TCT TCT TCT TCC ACC TCA GC		

Appendix 3

Table 3. Antibodies and concentrations used for Western blot analysis.

Primary antibodies		
Antibody	**Concentration**	**Supplier, Cat #**
Mouse anti-6E10	1:500	Covance, SIG-39320
Rabbit anti-E178 (Tau)	1:1000	Abcam, AB32057
Rabbit anti-THR 231 (pTau)	1:1000	Abcam, AB151559
Mouse anti-β-actin	1:5000	Sigma-Aldrich, A1978
Secondary antibodies		
Antibody	**Concentration**	**Supplier, Cat #**
Goat anti-mouse HRP	1:10 000	Dako, P0447
Goat anti-rabbit HRP	1:10 000	Dako, P0448
Rabbit anti-rat HRP	1:10 000	Invitrogen, 61-9520

Table 4. Antibodies and concentrations used for immunohistochemistry.

Primary antibodies		
Antibody	**Concentration**	**Supplier, Cat #**
Goat anti-PDGFRα	1:200	R&D Systems, AF1062
Guinea pig anti-Iba1	1:500	Synaptic Systems, 234 004
Rabbit anti-ASPA	1:200	Merck Millipore, ABN1698
Rat anti-GFP	1:2000	Nacali Tesque, 0440484
Rabbit anti-Ki67	1:200	Abcam, AB15580
Rabbit anti-Nav1.6	1:200	Alomone labs, ASC-009
Rabbit anti-OLIG2	1:400	Merck Millipore, AB9610
Mouse anti-Caspr	1:200	Neuromab, MABN69
Secondary antibodies		
Antibody	**Concentration**	**Supplier, Cat #**
Donkey anti-Rat 488	1:500	Life Technologies, A21208
Goat anti-Guinea pig 488	1:1000	Life Technologies, A-11073
Donkey anti-Rabbit 488	1:1000	Life Technologies, A21206
Donkey anti-Rabbit 568	1:1000	Life Technologies, A10042
Donkey anti-Goat 488	1:1000	Life Technologies, A11055
Donkey anti-Goat 568	1:1000	Life Technologies, A-11057
Donkey anti-Goat 647	1:1000	Life Technologies, A21447
Donkey anti-mouse 647	1:1000	Life Technologies, A31571
Hoechst nuclear stain	1:10 000	Invitrogen, H21492

References

Aggarwal S, Snaidero N, Pähler G, Frey S, Sánchez P, Zweckstetter M, Janshoff A, Schneider A, Weil M-T, Schaap IAT, Görlich D, Simons M (2013) Myelin Membrane Assembly Is Driven by a Phase Transition of Myelin Basic Proteins Into a Cohesive Protein Meshwork Barres BA, ed. PLoS Biol 11:e1001577 Available at: http://dx.plos.org/10.1371/journal.pbio.1001577.

Ainger K, Avossa D, Diana AS, Barry C, Barbarese E, Carson JH (1997) Transport and localization elements in myelin basic protein mRNA. J Cell Biol 138:1077–1087 Available at: http://jcb.rupress.org/content/138/5/1077.abstract.

Ainger K, Avossa D, Morgan F, Hill SJ, Barry C, Barbarese E, Carson JH (1993) Transport and localization of exogenous myelin basic protein mRNA microinjected into oligodendrocytes. J Cell Biol 123:431–441 Available at: http://jcb.rupress.org/content/123/2/431.abstract.

Al-Bassam J, Ozer RS, Safer D, Halpain S, Milligan RA (2002) MAP2 and tau bind longitudinally along the outer ridges of microtubule protofilaments. J Cell Biol 157:1187–1196.

Allen M et al. (2014) Association of MAPT haplotypes with Alzheimer's disease risk and MAPT brain gene expression levels. Alzheimer's Res Ther 6:1–14.

Allinquant B, Staugaitis SM, D'Urso D, Colman DR (1991) The ectopic expression of myelin basic protein isoforms in shiverer oligodendrocytes: Implications for myelinogenesis. J Cell Biol 113:393–403.

Alonso A del C, Grundke-Iqbal I, Iqbal K (1996) Alzheimer's disease hyperphosphorylated tau sequesters normal tau into tangles of filaments and disassembles microtubules. Nat Med 2:783–787 Available at: http://www.ncbi.nlm.nih.gov/pubmed/8673924.

Alonso A del C, Zaidi T, Novak M, Grundke-Iqbal I, Iqbal K (2001) Hyperphosphorylation induces self-assembly of τ into tangles of paired helical filaments/straight filaments. Proc Natl Acad Sci 98:6923–6928 Available at: http://www.pnas.org/content/98/12/6923.short.

Alonso AC, Zaidi T, Grundke-Iqbal I, Iqbal K (1994) Role of abnormally phosphorylated tau in the breakdown of microtubules in Alzheimer disease. Proc Natl Acad Sci 91:5562–5566 Available at: http://www.pnas.org/cgi/doi/10.1073/pnas.91.12.5562.

Amaral DG, Kondo H, Lavenex P (2014) An analysis of entorhinal cortex projections to the dentate gyrus, hippocampus, and subiculum of the neonatal macaque monkey. J Comp Neurol 522:1485–1505.

Amaral RSC, Park MTM, Devenyi GA, Lynn V, Pipitone J, Winterburn J, Chavez S, Schira M, Lobaugh NJ, Voineskos AN, Pruessner JC, Chakravarty MM (2018) Manual segmentation of the fornix, fimbria, and alveus on high-resolution 3T MRI: Application via fully-automated mapping of the human memory circuit white and grey matter in healthy and pathological aging. Neuroimage 170:132–150 Available at: http://dx.doi.org/10.1016/j.neuroimage.2016.10.027.

Amatniek JC, Hauser WA, DelCastillo-Castaneda C, Jacobs DM, Marder K, Bell K, Albert M, Brandt

J, Stern Y (2006) Incidence and predictors of seizures in patients with Alzheimer's disease. Epilepsia 47:867–872.

Andreasen N, Minthon L, Davidsson P, Vanmechelen E, Vanderstichele H, Winblad B, Blennow K (2001) Evaluation of CSF-tau and CSF-Abeta42 as diagnostic markers for Alzheimer disease in clinical practice. Arch Neurol 58:373–379 Available at: http://www.ncbi.nlm.nih.gov/pubmed/11255440.

Arai H, Morikawa Y ichi, Higuchi M, Matsui T, Clark CM, Miura M, Machida N, Lee VMY, Trojanowski JQ, Sasaki H (1997) Cerebrospinal fluid tau levels in neurodegenerative diseases with distinct tau-related pathology. Biochem Biophys Res Commun 236:262–264.

Arai H, Terajima M, Miura M, Higuchi S, Muramatsu T, Machida N, Seiki H, Takase S, Clark CM, Lee VM-Y, others (1995) Tau in cerebrospinal fluid: a potential diagnostic marker in Alzheimer's disease. Ann Neurol 38:649–652 Available at: http://onlinelibrary.wiley.com/doi/10.1002/ana.410380414/full.

Arai T, Ikeda K, Akiyama H, Shikamoto Y, Tsuchiya K, Yagishita S, Beach T, Rogers J, Schwab C, McGeer PL (2001) Distinct isoforms of tau aggregated in neurons and glial cells in brains of patients with Pick's disease, corticobasal degeneration and progressive supranuclear palsy. Acta Neuropathol 101:167–173 Available at: http://www.ncbi.nlm.nih.gov/pubmed/11271372.

Arancibia-Cárcamo IL, Ford MC, Cossell L, Ishida K, Tohyama K, Attwell D (2017) Node of Ranvier length as a potential regulator of myelinated axon conduction speed. Elife 6:1–15.

Arendash GW, King DL, Gordon MN, Morgan D, Hatcher JM, Hope CE, Diamond DM (2001) Progressive, age-related behavioral impairments in transgenic mice carrying both mutant amyloid precursor protein and presenilin-1 transgenes. Brain Res 891:42–53.

Arima K, Nakamura M, Sunohara N, Ogawa M, Anno M, Izumiyama Y, Hirai S, Ikeda K (1997) Ultrastructural characterization of the tau-immunoreactive tubules in the oligodendroglial perikarya and their inner loop processes in progressive supranuclear palsy. Acta Neuropathol 93:558–566.

Assinck P, Duncan GJ, Plemel JR, Lee MJ, Stratton JA, Manesh SB, Liu J, Ramer LM, Kang SH, Bergles DE, Biernaskie J, Tetzlaff W (2017) Myelinogenic Plasticity of Oligodendrocyte Precursor Cells following Spinal Cord Contusion Injury. J Neurosci 37:8635–8654.

Attar A, Liu T, Chan W-TC, Hayes J, Nejad M, Lei K, Bitan G (2013) A Shortened Barnes Maze Protocol Reveals Memory Deficits at 4-Months of Age in the Triple-Transgenic Mouse Model of Alzheimer's Disease Coulson EJ, ed. PLoS One 8:e80355 Available at: http://dx.plos.org/10.1371/journal.pone.0080355.

Auderset L, Cullen CL, Young KM (2016) Low Density Lipoprotein-Receptor Related Protein 1 Is Differentially Expressed by Neuronal and Glial Populations in the Developing and Mature Mouse Central Nervous System. PLoS One 11:e0155878 Available at: http://dx.plos.org/10.1371/journal.pone.0155878.

Auer F, Vagionitis S, Czopka T (2018) Evidence for Myelin Sheath Remodeling in the CNS Revealed by In Vivo Imaging. Curr Biol 28:549-559.e3 Available at: https://doi.org/10.1016/j.cub.2018.01.017.

Ayata P, Badimon A, Strasburger HJ, Duff MK, Montgomery SE, Loh YHE, Ebert A, Pimenova AA, Ramirez BR, Chan AT, Sullivan JM, Purushothaman I, Scarpa JR, Goate AM, Busslinger M, Shen L, Losic B, Schaefer A (2018) Epigenetic regulation of brain region-specific microglia clearance activity. Nat Neurosci 21:1049–1060 Available at: http://dx.doi.org/10.1038/s41593-018-0192-3.

Back SA, Luo NL, Borenstein NS, Levine JM, Volpe JJ, Kinney HC (2001) Late oligodendrocyte progenitors coincide with the developmental window of vulnerability for human perinatal white matter injury. J Neurosci 21:1302–1312.

Back SA, Rosenberg PA (2014) Pathophysiology of glia in perinatal white matter injury. Glia 62:1790–1815 Available at: http://www.ncbi.nlm.nih.gov/pubmed/24687630.

Bailly Y, Haeberlé A-M, Blanquet-Grossard F, Chasserot-Golaz S, Grant N, Schulze T, Bombarde G, Grassi J, Cesbron J-Y, Lemaire-Vieille C (2004) Prion protein (PrP c) immunocytochemistry and expression of the green fluorescent protein reporter gene under control of the bovine PrP gene promoter in the mouse brain. J Comp Neurol 473:244–269 Available at: http://doi.wiley.com/10.1002/cne.20117.

Balthazar J, Schöwe NM, Cipolli GC, Buck HS, Viel TA (2018) Enriched environment significantly reduced senile plaques in a transgenic mice model of Alzheimer's disease, improving memory. Front Aging Neurosci 10:1–10.

Bar E, Barak B (2019) Microglia roles in synaptic plasticity and myelination in homeostatic conditions and neurodevelopmental disorders. Glia:1–17.

Baron JC, Chételat G, Desgranges B, Perchey G, Landeau B, de la Sayette V, Eustache F (2001) In vivo mapping of gray matter loss with voxel-based morphometry in mild Alzheimer's disease. Neuroimage 14:298–309 Available at: http://linkinghub.elsevier.com/retrieve/pii/S1053811901908481.

Barres BA, Hart IK, Coles HSR, Burne JF, Voyvodic JT, Richardson WD, Raff MC (1992) Cell death and control of cell survival in the oligodendrocyte lineage. Cell 70:31–46 Available at: https://linkinghub.elsevier.com/retrieve/pii/009286749290531G.

Bartzokis G (2011) Alzheimer's disease as homeostatic responses to age-related myelin breakdown. Neurobiol Aging 32:1341–1371 Available at: http://linkinghub.elsevier.com/retrieve/pii/S0197458009002711.

Bartzokis G, Sultzer D, Lu PH, Nuechterlein KH, Mintz J, Cummings JL (2004) Heterogeneous age-related breakdown of white matter structural integrity: Implications for cortical 'disconnection' in aging and Alzheimer's disease. Neurobiol Aging 25:843–851.

Bauer J, Bradl M, Klein M, Leisser M, Deckwerth TL, Wekerle H, Lassmann H (2002) Endoplasmic

reticulum stress in PLP-overexpressing transgenic rats: Gray matter oligodendrocytes are more vulnerable than white matter oligodendrocytes. J Neuropathol Exp Neurol 61:12–22 Available at: http://jnen.oxfordjournals.org/.

Baxi EG, DeBruin J, Jin J, Strasburger HJ, Smith MD, Orthmann-Murphy JL, Schott JT, Fairchild AN, Bergles DE, Calabresi PA (2017) Lineage tracing reveals dynamic changes in oligodendrocyte precursor cells following cuprizone-induced demyelination. Glia 65:2087–2098.

Behrendt G, Baer K, Buffo A, Curtis MA, Faull RL, Rees MI, Götz M, Dimou L (2013) Dynamic changes in myelin aberrations and oligodendrocyte generation in chronic amyloidosis in mice and men. Glia 61:273–286 Available at: http://doi.wiley.com/10.1002/glia.22432.

Bender AC, Luikart BW, Lenck-Santini PP (2016) Cognitive deficits associated with Nav1.1 alterations: Involvement of neuronal firing dynamics and oscillations. PLoS One 11:1–19.

Benitez A, Fieremans E, Jensen JH, Falangola MF, Tabesh A, Ferris SH, Helpern JA (2014) White matter tract integrity metrics reflect the vulnerability of late-myelinating tracts in Alzheimer's disease. NeuroImage Clin 4:64–71 Available at: http://linkinghub.elsevier.com/retrieve/pii/S2213158213001496.

Beraldo FH, Ostapchenko VG, Caetano FA, Guimaraes ALS, Ferretti GDS, Daude N, Bertram L, Nogueira KOPC, Silva JL, Westaway D, Cashman NR, Martins VR, Prado VF, Prado MAM (2016) Regulation of amyloid β oligomer binding to neurons and neurotoxicity by the prion protein-mGluR5 complex. J Biol Chem 291:21945–21955.

Berger T, Frotscher M (1994) Distribution and morphological characteristics of oligodendrocytes in the rat hippocampus in situ and in vitro: an immunocytochemical study with the monoclonal Rip antibody. J Neurocytol 23:61–74.

Bergles DE, Roberts JDB, Somogyi P, Jahr CE (2000) Glutamatergic synapses on oligodendrocyte precursor cells in the hippocampus. Nature 405:187–191 Available at: http://www.nature.com/articles/35012083.

Bero AW, Yan P, Roh JH, Cirrito JR, Stewart FR, Raichle ME, Lee JM, Holtzman DM (2011) Neuronal activity regulates the regional vulnerability to amyloid-β 2 deposition. Nat Neurosci 14:750–756.

Billings LM, Oddo S, Green KN, McGaugh JL, LaFerla FM (2005) Intraneuronal Aβ Causes the Onset of Early Alzheimer's Disease-Related Cognitive Deficits in Transgenic Mice. Neuron 45:675–688 Available at: http://linkinghub.elsevier.com/retrieve/pii/S0896627305000784.

Bittner T, Burgold S, Dorostkar MM, Fuhrmann M, Wegenast-Braun BM, Schmidt B, Kretzschmar H, Herms J (2012) Amyloid plaque formation precedes dendritic spine loss. Acta Neuropathol 124:797–807.

Blakemore WF, Murray JA (1981) Quantitative examination of internodal length of remyelinated nerve fibres in the central nervous system.

Blauwendraat C et al. (2019) Genetic analysis of neurodegenerative diseases in a pathology cohort. Neurobiol Aging 76:214.e1-214.e9 Available at: https://doi.org/10.1016/j.neurobiolaging.2018.11.007.

Boda E, Di Maria S, Rosa P, Taylor V, Abbracchio MP, Buffo A (2015) Early phenotypic asymmetry of sister oligodendrocyte progenitor cells after mitosis and its modulation by aging and extrinsic factors. Glia 63:271–286.

Boison D, Stoffel W (1994) Disruption of the compacted myelin sheath of axons of the central nervous system in proteolipid protein-deficient mice. Proc Natl Acad Sci 91:11709–11713 Available at: http://www.pnas.org/content/91/24/11709.short.

Boluda S, Iba M, Zhang B, Raible KM, Lee VM-Y, Trojanowski JQ (2015) Differential induction and spread of tau pathology in young PS19 tau transgenic mice following intracerebral injections of pathological tau from Alzheimer's disease or corticobasal degeneration brains. Acta Neuropathol 129:221–237 Available at: http://link.springer.com/10.1007/s00401-014-1373-0.

Borges K, Kettenmann H (1995) Blockade of K+ channels induced by AMPA/kainate receptor activation in mouse oligodendrocyte precursor cells is mediated by NA+ entry. J Neurosci Res 42:579–593.

Bouwman FH, Schoonenboom NSM, Verwey NA, van Elk EJ, Kok A, Blankenstein MA, Scheltens P, van der Flier WM (2009) CSF biomarker levels in early and late onset Alzheimer's disease. Neurobiol Aging 30:1895–1901 Available at: http://linkinghub.elsevier.com/retrieve/pii/S0197458008000572.

Boyd A, Zhang H, Williams A (2013) Insufficient OPC migration into demyelinated lesions is a cause of poor remyelination in MS and mouse models. Acta Neuropathol 125:841–859 Available at: http://link.springer.com/10.1007/s00401-013-1112-y.

Braak H, Braak E (1996) Development of Alzheimer-related neurofibrillary changes in the neocortex inversely recapitulates cortical myelogenesis. Acta Neuropathol 92:197–201.

Brickman AM, Meier IB, Korgaonkar MS, Provenzano FA, Grieve SM, Siedlecki KL, Wasserman BT, Williams LM, Zimmerman ME (2012) Testing the white matter retrogenesis hypothesis of cognitive aging. Neurobiol Aging 33:1699–1715 Available at: https://linkinghub.elsevier.com/retrieve/pii/S0197458011002077.

Brill MH, Waxman,' SG, Moore JW, Joyner RW (1977) Conduction velocity and spike configuration in myelinated fibres: computed dependence on internode distance.

Brito-Moreira J, Paula-Lima AC, Bomfim TR, Oliveira FF, Sepulveda FJ, De Mello FG, Aguayo LG, Panizzutti R, Ferreira ST (2011) Aβ Oligomers Induce Glutamate Release from Hippocampal Neurons. Curr Alzheimer Res 8:552–562 Available at: http://www.eurekaselect.com/openurl/content.php?genre=article&issn=1567-2050&volume=8&issue=5&spage=552.

Brousse B, Magalon K, Durbec P, Cayre M (2015) Region and dynamic specificities of adult neural

stem cells and oligodendrocyte precursors in myelin regeneration in the mouse brain. Biol Open 4:980–992 Available at: http://bio.biologists.org/cgi/doi/10.1242/bio.012773.

Brueggen K et al. (2019) Structural integrity in subjective cognitive decline, mild cognitive impairment and Alzheimer's disease based on multicenter diffusion tensor imaging. J Neurol Available at: https://doi.org/10.1007/s00415-019-09429-3.

Bugiani O, Murrell JR, Giaccone G, Hasegawa M, Ghigo G, Tabaton M, Morbin M, Primavera A, Carella F, Solaro C, Grisoli M, Savoiardo M, Spillantini MG, Tagliavini F, Goedert M, Ghetti B (1999) Frontotemporal Dementia and Corticobasal Degeneration in a Family with a P301S Mutation in Tau. J Neuropathol Exp Neurol 58:667–677 Available at: https://academic.oup.com/jnen/article-lookup/doi/10.1097/00005072-199906000-00011.

Bujalka H, Koenning M, Jackson S, Perreau VM, Pope B, Hay CM, Mitew S, Hill AF, Lu QR, Wegner M, Srinivasan R, Svaren J, Willingham M, Barres BA, Emery B (2013) MYRF Is a Membrane-Associated Transcription Factor That Autoproteolytically Cleaves to Directly Activate Myelin Genes ffrench-Constant C, ed. PLoS Biol 11:e1001625 Available at: http://dx.plos.org/10.1371/journal.pbio.1001625.

Burgold S, Bittner T, Dorostkar MM, Kieser D, Fuhrmann M, Mitteregger G, Kretzschmar H, Schmidt B, Herms J (2011) In vivo multiphoton imaging reveals gradual growth of newborn amyloid plaques over weeks. Acta Neuropathol 121:327–335.

Busche MA, Chen X, Henning HA, Reichwald J, Staufenbiel M, Sakmann B, Konnerth A (2012) Critical role of soluble amyloid- for early hippocampal hyperactivity in a mouse model of Alzheimer's disease. Proc Natl Acad Sci 109:8740–8745.

Busche MA, Eichhoff G, Adelsberger H, Abramowski D, Wiederhold K-H, Haass C, Staufenbiel M, Konnerth A, Garaschuk O (2008) Clusters of Hyperactive Neurons Near Amyloid Plaques in a Mouse Model of Alzheimer's Disease. Science (80-) 321:1686–1689 Available at: http://www.sciencemag.org/cgi/doi/10.1126/science.1162844.

Busche MA, Wegmann S, Dujardin S, Commins C, Schiantarelli J, Klickstein N, Kamath T V., Carlson GA, Nelken I, Hyman BT (2019) Tau impairs neural circuits, dominating amyloid-β effects, in Alzheimer models in vivo. Nat Neurosci 22:57–64 Available at: http://dx.doi.org/10.1038/s41593-018-0289-8.

Buskila Y, Crowe SE, Ellis-Davies GCR (2013) Synaptic deficits in layer 5 neurons precede overt structural decay in 5xFAD mice. Neuroscience 254:152–159 Available at: https://linkinghub.elsevier.com/retrieve/pii/S0306452213007884.

Bussière T, Bard F, Barbour R, Grajeda H, Guido T, Khan K, Schenk D, Games D, Seubert P, Buttini M (2004) Morphological characterization of Thioflavin-S-positive amyloid plaques in transgenic Alzheimer mice and effect of passive Aβ immunotherapy on their clearance. Am J Pathol 165:987–995.

Butt AM, Ibrahim M, Ruge FM, Berry M (1995) Biochemical subtypes of oligodendrocyte in the

anterior medullary velum of the rat as revealed by the monoclonal antibody rip. Glia 14:185–197.

Cacace R, Sleegers K, Van Broeckhoven C (2016) Molecular genetics of early-onset Alzheimer's disease revisited. Alzheimer's Dement 12:733–748 Available at: http://dx.doi.org/10.1016/j.jalz.2016.01.012.

Cadavid D et al. (2019) Safety and efficacy of opicinumab in patients with relapsing multiple sclerosis (SYNERGY): a randomised, placebo-controlled, phase 2 trial. Lancet Neurol 18:845–856.

Cahoy JD, Emery B, Kaushal A, Foo LC, Zamanian JL, Christopherson KS, Xing Y, Lubischer JL, Krieg PA, Krupenko SA, Thompson WJ, Barres BA (2008) A Transcriptome Database for Astrocytes, Neurons, and Oligodendrocytes: A New Resource for Understanding Brain Development and Function. J Neurosci 28:264–278.

Calafate S, Flavin W, Verstreken P, Moechars D (2016) Loss of Bin1 Promotes the Propagation of Tau Pathology. Cell Rep 17:931–940 Available at: http://dx.doi.org/10.1016/j.celrep.2016.09.063.

Carson JH, Worboys K, Ainger K, Barbarese E (1997) Translocation of myelin basic protein mRNA in oligodendrocytes requires microtubules and kinesin. Cell Motil Cytoskeleton 38:318–328.

Cattaud V, Bezzina C, Rey CC, Lejards C, Dahan L, Verret L (2018) Early disruption of parvalbumin expression and perineuronal nets in the hippocampus of the Tg2576 mouse model of Alzheimer's disease can be rescued by enriched environment. Neurobiol Aging 72:147–158.

Chalermpalanupap T, Schroeder JP, Rorabaugh JM, Liles LC, Lah JJ, Levey AI, Weinshenker D (2017) Locus coeruleus ablation exacerbates cognitive deficits, neuropathology, and lethality in P301S tau transgenic mice. J Neurosci 12:1483–17 Available at: http://www.jneurosci.org/lookup/doi/10.1523/JNEUROSCI.1483-17.2017.

Chang A, Nishiyama A, Peterson J, Prineas J, Trapp BD (2000) NG2-Positive Oligodendrocyte Progenitor Cells in Adult Human Brain and Multiple Sclerosis Lesions. J Neurosci 20:6404–6412 Available at: http://www.jneurosci.org/lookup/doi/10.1523/JNEUROSCI.20-17-06404.2000.

Chang A, Tourtellotte WW, Rudick R, Trapp BD (2002) Premyelinating oligodendrocytes in chronic lesions of multiple sclerosis. N Engl J Med 346:165–173 Available at: http://www.nejm.org/doi/full/10.1056/nejmoa010994.

Chapuis J et al. (2013) Increased expression of BIN1 mediates Alzheimer genetic risk by modulating tau pathology. Mol Psychiatry 18:1225–1234.

Charlton RA, Barrick TR, McIntyre DJ, Shen Y, O'Sullivan M, Howe FA, Clark CA, Morris RG, Markus HS (2006) White matter damage on diffusion tensor imaging correlates with age-related cognitive decline. Neurology 66:217–222 Available at: http://ovidsp.ovid.com/ovidweb.cgi?T=JS&PAGE=reference&D=emed10&NEWS=N&AN=43

970157.

Chen J, Buchanan JB, Sparkman NL, Godbout JP, Freund GG, Johnson RW (2008) Neuroinflammation and disruption in working memory in aged mice after acute stimulation of the peripheral innate immune system. Brain Behav Immun 22:301–311 Available at: http://linkinghub.elsevier.com/retrieve/pii/S0889159107002176.

Chen M, Wang J, Jiang J, Zheng X, Justice NJ, Wang K, Ran X, Li Y, Huo Q, Zhang J, Li H, Lu N, Wang Y, Zheng H, Long C, Yang L (2017) APP modulates KCC2 expression and function in hippocampal GABAergic inhibition. Elife 6:1–26.

Cheng IH, Palop JJ, Esposito LA, Bien-Ly N, Yan F, Mucke L (2004) Aggressive amyloidosis in mice expressing human amyloid peptides with the Arctic mutation. Nat Med 10:1190–1192.

Cheng IH, Scearce-Levie K, Legleiter J, Palop JJ, Gerstein H, Bien-Ly N, Puoliväli J, Lesné S, Ashe KH, Muchowski PJ, Mucke L (2007) Accelerating Amyloid-β Fibrillization Reduces Oligomer Levels and Functional Deficits in Alzheimer Disease Mouse Models. J Biol Chem 282:23818–23828 Available at: http://www.jbc.org/lookup/doi/10.1074/jbc.M701078200.

Cho S, Muthukumar AK, Stork T, Coutinho-Budd JC, Freeman MR (2018) Focal adhesion molecules regulate astrocyte morphology and glutamate transporters to suppress seizure-like behavior. Proc Natl Acad Sci U S A 115:11316–11321.

Choi SJ, Lim KO, Monteiro I, Reisberg B (2005) Diffusion tensor imaging of frontal white matter microstructure in early Alzheimer's disease: A preliminary study. J Geriatr Psychiatry Neurol 18:12–19.

Chong SYCC, Rosenberg SS, Fancy SPJ, Zhao C, Shen YAA, Hahn AT, McGee AW, Xu X, Zheng B, Zhang LI, Rowitch DH, Franklin RJM, Lu QR, Chan JR (2012) Neurite outgrowth inhibitor Nogo-A establishes spatial segregation and extent of oligodendrocyte myelination. Proc Natl Acad Sci U S A 109:1299–1304 Available at: http://www.pnas.org/cgi/doi/10.1073/pnas.1113540109.

Chopra S, Shaw M, Shaw T, Sachdev PS, Anstey KJ, Cherbuin N (2018) More highly myelinated white matter tracts are associated with faster processing speed in healthy adults. Neuroimage 171:332–340 Available at: https://doi.org/10.1016/j.neuroimage.2017.12.069.

Chu TH, Cummins K, Sparling JS, Tsutsui S, Brideau C, Nilsson KPR, Joseph JT, Stys PK (2017) Axonal and myelinic pathology in 5xFAD Alzheimer's mouse spinal cord. PLoS One 12:1–22.

Cissé M, Sanchez PE, Kim DH, Ho K, Yu G-Q, Mucke L (2011) Ablation of Cellular Prion Protein Does Not Ameliorate Abnormal Neural Network Activity or Cognitive Dysfunction in the J20 Line of Human Amyloid Precursor Protein Transgenic Mice. J Neurosci 31:10427–10431 Available at: http://www.jneurosci.org/cgi/doi/10.1523/JNEUROSCI.1459-11.2011.

Citron M, Diehl TS, Gordon G, Biere AL, Seubert P, Selkoe DJ (1996) Evidence that the 42- and 40-amino acid forms of amyloid β protein are generated from the β-amyloid precursor protein by different protease activities. Proc Natl Acad Sci U S A 93:13170–13175.

Citron M, Oltersdorf T, Haass C, McConlogue L, Hung AY, Seubert P, Vigo-Pelfrey C, Lieberburg I, Selkoe DJ (1992) Mutation of the β-amyloid precursor protein in familial Alzheimer's disease increases β-protein production. Nature 360:672–674 Available at: http://www.nature.com/articles/360672a0.

Clarke LE, Young KM, Hamilton NB, Li H, Richardson WD, Attwell D (2012) Properties and Fate of Oligodendrocyte Progenitor Cells in the Corpus Callosum, Motor Cortex, and Piriform Cortex of the Mouse. J Neurosci 32:8173–8185 Available at: http://www.jneurosci.org/cgi/doi/10.1523/JNEUROSCI.0928-12.2012.

Cohen AD, Rabinovici GD, Mathis CA, Jagust WJ, Klunk WE, Ikonomovic MD (2012) Using Pittsburgh Compound B for In Vivo PET Imaging of Fibrillar Amyloid-Beta. In: Bone, pp 27–81 Available at: https://linkinghub.elsevier.com/retrieve/pii/B9780123948168000027.

Copray S, Balasubramaniyan V, Levenga J, de Bruijn J, Liem R, Boddeke E (2006) Olig2 Overexpression Induces the In Vitro Differentiation of Neural Stem Cells into Mature Oligodendrocytes. Stem Cells 24:1001–1010 Available at: http://doi.wiley.com/10.1634/stemcells.2005-0239.

Corell M, Wicher G, Radomska KJ, Dağlikoca ED, Godskesen RE, Fredriksson R, Benedikz E, Magnaghi V, Fex Svenningsen Å (2015) GABA and its B-receptor are present at the node of Ranvier in a small population of sensory fibers, implicating a role in myelination. J Neurosci Res 93:285–295.

Couttas TA, Kain N, Suchowerska AK, Quek L-E, Turner N, Fath T, Garner B, Don AS (2016) Loss of ceramide synthase 2 activity, necessary for myelin biosynthesis, precedes tau pathology in the cortical pathogenesis of Alzheimer's disease. Neurobiol Aging 43:89–100 Available at: http://linkinghub.elsevier.com/retrieve/pii/S0197458016300185.

Cowan N (2009) What are the differences between long-term, short-term, and working memory? Nelson. NIH Public Access 6123:323–338 Available at: http://linkinghub.elsevier.com/retrieve/pii/S0079612307000209.

Cras P, Kawai M, Lowery D, Gonzalez-Dewhitt P, Greenberg B, Perry G (1991) Senile plaque neurites in Alzheimer disease accumulate amyloid precursor protein. Proc Natl Acad Sci 88:7552–7556 Available at: http://www.pnas.org/content/88/17/7552.short.

Crowe SE, Ellis-Davies GCR (2014) Spine pruning in 5xFAD mice starts on basal dendrites of layer 5 pyramidal neurons. Brain Struct Funct 219:571–580 Available at: http://link.springer.com/10.1007/s00429-013-0518-6.

Cruchaga C, Chakraverty S, Mayo K, Vallania FLM, Mitra RD, Faber K, Williamson J, Bird T, Diaz-Arrastia R, Foroud TM, Boeve BF, Graff-Radford NR, St. Jean P, Lawson M, Ehm MG, Mayeux R, Goate AM (2012) Rare Variants in APP, PSEN1 and PSEN2 Increase Risk for AD in Late-Onset Alzheimer's Disease Families Toft M, ed. PLoS One 7:e31039 Available at: http://dx.plos.org/10.1371/journal.pone.0031039.

Cullen CL, Senesi M, Tang AD, Clutterbuck MT, Auderset L, O'Rourke ME, Rodger J, Young KM (2019) Low-intensity transcranial magnetic stimulation promotes the survival and maturation of newborn oligodendrocytes in the adult mouse brain. Glia 67:1462–1477.

Czopka T, Ffrench-Constant C, Lyons DAA (2013) Individual oligodendrocytes have only a few hours in which to generate new myelin sheaths invivo. Dev Cell 25:599–609 Available at: http://linkinghub.elsevier.com/retrieve/pii/S1534580713002876.

D'Orange M et al. (2018) Potentiating tangle formation reduces acute toxicity of soluble tau species in the rat. Brain 141:535–549.

D'Souza I, Poorkaj P, Hong M, Nochlin D, Lee VMY, Bird TD, Schellenberg GD (1999) Missense and silent tau gene mutations cause frontotemporal dementia with parkinsonism-chromosome 17 type, by affecting multiple alternative RNA splicing regulatory elements. Proc Natl Acad Sci 96:5598–5603 Available at: http://www.pnas.org/cgi/doi/10.1073/pnas.96.10.5598.

Dawkins E, Small DH (2014) Insights into the physiological function of the β-amyloid precursor protein: Beyond Alzheimer's disease. J Neurochem 129:756–769.

Dawson MRL, Polito A, Levine JM, Reynolds R (2003) NG2-expressing glial progenitor cells: an abundant and widespread population of cycling cells in the adult rat CNS. Mol Cell Neurosci 24:476–488 Available at: http://linkinghub.elsevier.com/retrieve/pii/S1044743103002100.

De Rossi P, Buggia-Prévot V, Clayton BLLL, Vasquez JB, van Sanford C, Andrew RJ, Lesnick R, Botté A, Deyts C, Salem S, Rao E, Rice RC, Parent A, Kar S, Popko B, Pytel P, Estus S, Thinakaran G (2016) Predominant expression of Alzheimer's disease-associated BIN1 in mature oligodendrocytes and localization to white matter tracts. Mol Neurodegener 11:1–21 Available at: http://molecularneurodegeneration.biomedcentral.com/articles/10.1186/s13024-016-0124-1.

Deacon RMJ, Rawlins JNP (2006) T-maze alternation in the rodent. Nat Protoc 1:7–12.

Dean DC, Kecskemeti SR, Alexander AL, Hurley SA, O'Grady JP, Canda C, Davenport-Sis NJ, Carlsson CM, Asthana S, Sager MA, Johnson SC, Bendlin BB, Zetterberg H, Blennow K (2017) Association of amyloid pathology with myelin alteration in preclinical Alzheimer disease. JAMA Neurol 74:41–49.

Defrancesco M, Egger K, Marksteiner J, Esterhammer R, Hinterhuber H, Deisenhammer EA, Schocke M (2014) Changes in white matter integrity before conversion from mild cognitive impairment to Alzheimer's disease. PLoS One 9.

Dekens DW, Naudé PJW, Keijser JN, Boerema AS, De Deyn PP, Eisel ULM (2018) Lipocalin 2 contributes to brain iron dysregulation but does not affect cognition, plaque load, and glial activation in the J20 Alzheimer mouse model. J Neuroinflammation 15:330 Available at: https://jneuroinflammation.biomedcentral.com/articles/10.1186/s12974-018-1372-5.

Desai MK, Guercio BJ, Narrow WC, Bowers WJ (2011) An Alzheimer's disease-relevant presenilin-1 mutation augments amyloid-beta-induced oligodendrocyte dysfunction. Glia 59:627–640 Available at: http://doi.wiley.com/10.1002/glia.21131.

Desai MK, Mastrangelo MA, Ryan DA, Sudol KL, Narrow WC, Bowers WJ (2010) Early Oligodendrocyte/Myelin Pathology in Alzheimer's Disease Mice Constitutes a Novel Therapeutic Target. Am J Pathol 177:1422–1435 Available at: http://linkinghub.elsevier.com/retrieve/pii/S0002944010601952.

Desai MK, Sudol KL, Janelsins MC, Mastrangelo MA, Frazer ME, Bowers WJ (2009) Triple-transgenic Alzheimer's disease mice exhibit region-specific abnormalities in brain myelination patterns prior to appearance of amyloid and tau pathology. Glia 57:54–65 Available at: http://doi.wiley.com/10.1002/glia.20734.

deToledo-Morrell L, Stoub T., Bulgakova M, Wilson R., Bennett D., Leurgans S, Wuu J, Turner D. (2004) MRI-derived entorhinal volume is a good predictor of conversion from MCI to AD. Neurobiol Aging 25:1197–1203 Available at: http://linkinghub.elsevier.com/retrieve/pii/S0197458004000375.

Devi L, Ohno M (2010) Phospho-eIF2α level is important for determining abilities of BACE1 reduction to rescue cholinergic neurodegeneration and memory defects in 5XFAD mice. PLoS One 5.

Di Paola M, Macaluso E, Carlesimo GA, Tomaiuolo F, Worsley KJ, Fadda L, Caltagirone C (2007) Episodic memory impairment in patients with Alzheimer's disease is correlated with entorhinal cortex atrophy: A voxel-based morphometry study. J Neurol 254:774–781.

Dimou L, Simon C, Kirchhoff F, Takebayashi H, Gotz M (2008) Progeny of Olig2-Expressing Progenitors in the Gray and White Matter of the Adult Mouse Cerebral Cortex. J Neurosci 28:10434–10442 Available at: http://www.jneurosci.org/cgi/doi/10.1523/JNEUROSCI.2831-08.2008.

Dinamarca MC, Raveh A, Schneider A, Fritzius T, Früh S, Rem PD, Stawarski M, Lalanne T, Turecek R, Choo M, Besseyrias V, Bildl W, Bentrop D, Staufenbiel M, Gassmann M, Fakler B, Schwenk J, Bettler B (2019) Complex formation of APP with GABA B receptors links axonal trafficking to amyloidogenic processing. Nat Commun 10:1–17.

Dong YX, Zhang HY, Li HY, Liu PH, Sui Y, Sun XH (2018) Association between Alzheimer's disease pathogenesis and early demyelination and oligodendrocyte dysfunction. Neural Regen Res 13:908–914.

Doody RS, Thomas RG, Farlow M, Iwatsubo T, Vellas B, Joffe S, Kieburtz K, Raman R, Sun X, Aisen PS, Siemers E, Liu-Seifert H, Mohs R (2014) Phase 3 trials of solanezumab for mild-to-moderate alzheimer's disease. N Engl J Med 370:311–321.

Doshina A, Gourgue F, Onizuka M, Opsomer R, Wang P, Ando K, Tasiaux B, Dewachter I, Kienlen-Campard P, Brion J-P, Gailly P, Octave J-N, Pierrot N (2017) Cortical cells reveal APP as a new player in the regulation of GABAergic neurotransmission. Sci Rep 7 Available at: http://www.nature.com/articles/s41598-017-00325-2.

Downes N, Mullins P (2014) The Development of Myelin in the Brain of the Juvenile Rat. Toxicol

Pathol 42:913–922 Available at: http://tpx.sagepub.com/cgi/doi/10.1177/0192623313503518.

Dröge W, Schipper HM (2007) Oxidative stress and aberrant signaling in aging and cognitive decline. Aging Cell 6:361–370 Available at: http://doi.wiley.com/10.1111/j.1474-9726.2007.00294.x.

Du AT, Schuff N, Amend D, Laakso MP, Hsu YY, Jagust WJ, Yaffe K, Kramer JH, Reed B, Norman D, Chui HC, Weiner MW (2001) Magnetic resonance imaging of the entorhinal cortex and hippocampus in mild cognitive impairment and Alzheimer's disease. J Neurol Neurosurg Psychiatry 71:441–447 Available at: https://www.ncbi.nlm.nih.gov/pubmed/11561025.

Dubal DB, Zhu L, Sanchez PE, Worden K, Broestl L, Johnson E, Ho K, Yu GQ, Kim D, Betourne A, Kuro-o M, Masliah E, Abraham CR, Mucke L (2015) Life extension factor klotho prevents mortality and enhances cognition in hAPP transgenic mice. J Neurosci 35:2358–2371.

Dulcis D, Jamshidi P, Leutgeb S, Spitzer NC (2013) Neurotransmitter switching in the adult brain regulates behavior. Science (80-) 340:449–453.

Dumont M, Stack C, Elipenahli C, Jainuddin S, Gerges M, Starkova NN, Yang L, Starkov AA, Beal F (2011) Behavioral deficit, oxidative stress, and mitochondrial dysfunction precede tau pathology in P301S transgenic mice. FASEB J 25:4063–4072.

Duncan ID, Marik RL, Broman AT, Heidari M (2017) Thin myelin sheaths as the hallmark of remyelination persist over time and preserve axon function. Proc Natl Acad Sci 114:E9685–E9691.

Duncan ID, Radcliff AB, Heidari M, Kidd G, August BK, Wierenga LA (2018) The adult oligodendrocyte can participate in remyelination. Proc Natl Acad Sci U S A 115:E11807–E11816.

Eckman CB, Mehta ND, Crook R, Perez-tur J, Prihar G, Pfeiffer E, Graff-Radford N, Hinder P, Yager D, Zenk B, Refolo LM, Prada CM, Younkin SG, Hutton M, Hardy J (1997) A new pathogenic mutation in the APP gene (1716V) increases the relative proportion of Aβ42(43). Hum Mol Genet 6:2087–2089.

Elder GA, Gama Sosa MA, De Gasperi R (2010) Transgenic Mouse Models of Alzheimer's Disease. Mt Sinai J Med A J Transl Pers Med 77:69–81 Available at: http://doi.wiley.com/10.1002/msj.20159.

Emery B, Agalliu D, Cahoy JD, Watkins TA, Dugas JC, Mulinyawe SB, Ibrahim A, Ligon KL, Rowitch DH, Barres BA (2009) Myelin Gene Regulatory Factor Is a Critical Transcriptional Regulator Required for CNS Myelination. Cell 138:172–185 Available at: http://linkinghub.elsevier.com/retrieve/pii/S0092867409004565.

Engels MMA, Hillebrand A, Van Der Flier WM, Stam CJ, Scheltens P, Van Straaten ECW (2016) Slowing of hippocampal activity correlates with cognitive decline in early onset alzheimer's disease. An MEG study with virtual electrodes. Front Hum Neurosci 10:1–13.

Evans C, Beland S-G, Kulaga S, Wolfson C, Kingwell E, Marriott J, Koch M, Makhani N, Morrow S, Fisk J, Dykeman J, Jetté N, Pringsheim T, Marrie RA (2013) Incidence and Prevalence of

Multiple Sclerosis in the Americas: A Systematic Review. Neuroepidemiology 40:195–210 Available at: https://www.karger.com/Article/FullText/342779.

Fan YT, Fang YW, Chen YP, Leshikar ED, Lin CP, Tzeng OJL, Huang HW, Huang CM (2019) Aging, cognition, and the brain: effects of age-related variation in white matter integrity on neuropsychological function. Aging Ment Heal 23:831–839 Available at: https://doi.org/10.1080/13607863.2018.1455804.

Fard MK, van der Meer F, Sánchez P, Cantuti-Castelvetri L, Mandad S, Jäkel S, Fornasiero EF, Schmitt S, Ehrlich M, Starost L, Kuhlmann T, Sergiou C, Schultz V, Wrzos C, Brück W, Urlaub H, Dimou L, Stadelmann C, Simons M (2017) BCAS1 expression defines a population of early myelinating oligodendrocytes in multiple sclerosis lesions. Sci Transl Med 9:eaam7816 Available at: https://stm.sciencemag.org/lookup/doi/10.1126/scitranslmed.aam7816.

Fayed N, Modrego PJ, Rojas-Salinas G, Aguilar K (2011) Brain glutamate levels are decreased in alzheimer's disease: A magnetic resonance spectroscopy study. Am J Alzheimers Dis Other Demen 26:450–456.

Feany MB, Dickson DW (1995) Widespread cytoskeletal pathology characterizes corticobasal degeneration. Am J Pathol 146:1388–1396.

Ferrer I (2018) Oligodendrogliopathy in neurodegenerative diseases with abnormal protein aggregates: The forgotten partner. Prog Neurobiol 169:24–54 Available at: https://doi.org/10.1016/j.pneurobio.2018.07.004.

Ferrer I, Aguiló García M, Carmona M, Andrés-Benito P, Torrejón-Escribano B, Garcia-Esparcia P, del Rio JA (2019) Involvement of Oligodendrocytes in Tau Seeding and Spreading in Tauopathies. Front Aging Neurosci 11:1–16.

Findley CA, Bartke A, Hascup KN, Hascup ER (2019) Amyloid Beta-Related Alterations to Glutamate Signaling Dynamics During Alzheimer's Disease Progression. ASN Neuro 11.

Fitzner D, Schneider A, Kippert A, Möbius W, Willig KI, Hell SW, Bunt G, Gaus K, Simons M (2006) Myelin basic protein-dependent plasma membrane reorganization in the formation of myelin. EMBO J 25:5037–5048 Available at: http://emboj.embopress.org/content/25/21/5037.abstract.

Flores J, Noël A, Foveau B, Lynham J, Lecrux C, LeBlanc AC (2018) Caspase-1 inhibition alleviates cognitive impairment and neuropathology in an Alzheimer's disease mouse model. Nat Commun 9 Available at: http://dx.doi.org/10.1038/s41467-018-06449-x.

Flygt J, Djupsjö A, Lenne F, Marklund N (2013) Myelin loss and oligodendrocyte pathology in white matter tracts following traumatic brain injury in the rat. Eur J Neurosci 38:2153–2165.

Flygt J, Gumucio A, Ingelsson M, Skoglund K, Holm J, Alafuzoff I, Marklund N (2016) Human traumatic brain injury results in oligodendrocyte death and increases the number of Oligodendrocyte progenitor cells. J Neuropathol Exp Neurol 75:503–515.

Franklin KBJ, Paxinos G (2007) The Mouse Brain in Stereotaxic Coordinates, 3. ed. Amsterdam:

Elsevier.

Franklin RJM, Gilson JM, Blakemore WF (1997) Local recruitment of remyelinating cells in the repair of demyelination in the central nervous system. J Neurosci Res 50:337–344.

Fu H, Qi Y, Tan M, Cai J, Takebayashi H, Nakafuku M, Richardson W, Qiu M (2002) Dual origin of spinal oligodendrocyte progenitors and evidence for the cooperative role of Olig2 and Nkx2. 2 in the control of oligodendrocyte differentiation. Development 129:681–693 Available at: http://dev.biologists.org/content/129/3/681.short.

Fuhrer TE, Palpagama TH, Waldvogel HJ, Synek BJL, Turner C, Faull RL, Kwakowsky A (2017) Impaired expression of GABA transporters in the human Alzheimer's disease hippocampus, subiculum, entorhinal cortex and superior temporal gyrus. Neuroscience 351:108–118 Available at: http://dx.doi.org/10.1016/j.neuroscience.2017.03.041.

Fujikawa R, Higuchi S, Nakatsuji M, Yasui M, Ikedo T, Nagata M, Hayashi K, Yokode M, Minami M (2017) Deficiency in EP4 Receptor–Associated Protein Ameliorates Abnormal Anxiety-Like Behavior and Brain Inflammation in a Mouse Model of Alzheimer Disease. Am J Pathol 187:1848–1854 Available at: http://dx.doi.org/10.1016/j.ajpath.2017.04.010.

Fukushima S, Nishikawa K, Furube E, Muneoka S, Ono K, Takebayashi H, Miyata S (2015) Oligodendrogenesis in the fornix of adult mouse brain; The effect of LPS-induced inflammatory stimulation. Brain Res 1627:52–69.

Fünfschilling U, Supplie LM, Mahad D, Boretius S, Saab AS, Edgar J, Brinkmann BG, Kassmann CM, Tzvetanova ID, Möbius W, Diaz F, Meijer D, Suter U, Hamprecht B, Sereda MW, Moraes CT, Frahm J, Goebbels S, Nave K-A (2012) Glycolytic oligodendrocytes maintain myelin and long-term axonal integrity. Nature 485:517–521 Available at: http://www.nature.com/doifinder/10.1038/nature11007.

Gagyi E, Kormos B, Castellanos KJ, Valyi-Nagy K, Korneff D, LoPresti P, Woltjer R, Valyi-Nagy T (2012) Decreased Oligodendrocyte Nuclear Diameter in Alzheimer's Disease and Lewy Body Dementia. Brain Pathol 22:803–810 Available at: http://ovidsp.ovid.com/ovidweb.cgi?T=JS&PAGE=reference&D=emed14&NEWS=N&AN=51963487.

Galvan V, Gorostiza OF, Banwait S, Ataie M, Logvinova A V., Sitaraman S, Carlson E, Sagi SA, Chevallier N, Jin K, Greenberg DA, Bredesen DE (2006) Reversal of Alzheimer's-like pathology and behavior in human APP transgenic mice by mutation of Asp664. Proc Natl Acad Sci U S A 103:7130–7135.

Gao J, Cheung RTF, Lee TMC, Chu LW, Chan YS, Mak HKF, Zhang JX, Qiu D, Fung G, Cheung C (2011) Possible retrogenesis observed with fiber tracking: An anteroposterior pattern of white matter disintegrity in normal aging and alzheimer's disease. J Alzheimer's Dis 26:47–58.

Garcia-Alvarez L, Gomar JJ, Sousa A, Garcia-Portilla MP, Goldberg TE (2019) Breadth and depth of working memory and executive function compromises in mild cognitive impairment and their

relationships to frontal lobe morphometry and functional competence. Alzheimer's Dement Diagnosis, Assess Dis Monit 11:170–179 Available at: https://doi.org/10.1016/j.dadm.2018.12.010.

García-Cáceres C et al. (2016) Astrocytic Insulin Signaling Couples Brain Glucose Uptake with Nutrient Availability. Cell 166:867–880.

Gaser C, Schlaug G (2003) Brain structures differ between musicians and non-musicians. J Neurosci 23:9240–9245 Available at: http://www.jneurosci.org/content/23/27/9240.short.

Gautier HOB, Evans KA, Volbracht K, James R, Sitnikov S, Lundgaard I, James F, Lao-Peregrin C, Reynolds R, Franklin RJM, Káradóttir RT (2015) Neuronal activity regulates remyelination via glutamate signalling to oligodendrocyte progenitors. Nat Commun 6:8518 Available at: http://www.nature.com/doifinder/10.1038/ncomms9518.

Gawel K, Gibula E, Marszalek-Grabska M, Filarowska J, Kotlinska JH (2019) Assessment of spatial learning and memory in the Barnes maze task in rodents—methodological consideration. Naunyn Schmiedebergs Arch Pharmacol 392:1–18.

Ge Y, Grossman RI, Babb JS, Rabin ML, Mannon LJ, Kolson DL (2002) Age-related total gray matter and white matter changes in normal adult brain. Part I: Volumetric MR imaging analysis. Am J Neuroradiol 23:1327–1333.

Gensert JM, Goldman JE (1997) Endogenous progenitors remyelinate demyelinated axons in the adult CNS. Neuron 19:197–203 Available at: http://www.sciencedirect.com/science/article/pii/S0896627300803591.

Giannoni P, Arango-Lievano M, Neves I Das, Rousset MC, Baranger K, Rivera S, Jeanneteau F, Claeysen S, Marchi N (2016) Cerebrovascular pathology during the progression of experimental Alzheimer's disease. Neurobiol Dis 88:107–117 Available at: http://dx.doi.org/10.1016/j.nbd.2016.01.001.

Giau V Van, Bagyinszky E, Yang YS, Youn YC, An SSA, Kim SY (2019) Genetic analyses of early-onset Alzheimer's disease using next generation sequencing. Sci Rep 9:1–10 Available at: http://dx.doi.org/10.1038/s41598-019-44848-2.

Gibson EM, Purger D, Mount CW, Goldstein AK, Lin GL, Wood LS, Inema I, Miller SE, Bieri G, Zuchero JB, Barres BA, Woo PJ, Vogel H, Monje M (2014) Neuronal Activity Promotes Oligodendrogenesis and Adaptive Myelination in the Mammalian Brain. Science (80-) 344:1252304 Available at: http://www.sciencemag.org/cgi/doi/10.1126/science.1252304.

Giorgio A, Santelli L, Tomassini V, Bosnell R, Smith S, De Stefano N, Johansen-Berg H (2010) Age-related changes in grey and white matter structure throughout adulthood. Neuroimage 51:943–951 Available at: http://linkinghub.elsevier.com/retrieve/pii/S1053811910002740.

Girolamo F, Strippoli M, Errede M, Benagiano V, Roncali L, Ambrosi G, Virgintino D (2010) Characterization of oligodendrocyte lineage precursor cells in the mouse cerebral cortex: A confocal microscopy approach to demyelinating diseases. Ital J Anat Embryol 115:95–102.

Gledhill RF, McDonald WI (1977) Morphological characteristics of central demyelination and remyelination: A single-fiber study. Ann Neurol 1:552–560 Available at: http://dx.doi.org/10.1002/ana.410010607.

Goate A et al. (1991) Segregation of a missense mutation in the amyloid precursor protein gene with familial Alzheimer's disease. Nature 349:704–706 Available at: http://www.nature.com/articles/349704a0.

Goedert M, Spillantini MG (2006) A century of Alzheimer's disease. Science (80-) 314:777–781 Available at: http://science.sciencemag.org/content/314/5800/777.short.

Goedert M, Spillantini MG, Jakes R, Rutherford D, Crowther RA (1989) Multiple isoforms of human microtubule-associated protein tau: sequences and localization in neurofibrillary tangles of Alzheimer's disease. Neuron 3:519–526 Available at: https://linkinghub.elsevier.com/retrieve/pii/0896627389902109.

Gogniat MA, Robinson TL, Mewborn CM, Jean KR, Miller LS (2018) Body mass index and its relation to neuropsychological functioning and brain volume in healthy older adults. Behav Brain Res 348:235–240 Available at: https://doi.org/10.1016/j.bbr.2018.04.029.

Gold BT, Zhu Z, Brown CA, Andersen AH, LaDu MJ, Tai L, Jicha GA, Kryscio RJ, Estus S, Nelson PT, Scheff SW, Abner E, Schmitt FA, Van Eldik LJ, Smith CD (2014) White matter integrity is associated with cerebrospinal fluid markers of Alzheimer's disease in normal adults. Neurobiol Aging 35:2263–2271 Available at: http://dx.doi.org/10.1016/j.neurobiolaging.2014.04.030.

Goldenberg MM (2012) Multiple sclerosis review. P T 37:175–184 Available at: http://www.ncbi.nlm.nih.gov/pubmed/22605909%0Ahttp://www.pubmedcentral.nih.gov/articlerender.fcgi?artid=PMC3351877.

Gómez-Ramos A, Díaz-Hernández M, Cuadros R, Hernández F, Avila J (2006) Extracellular tau is toxic to neuronal cells. FEBS Lett 580:4842–4850 Available at: http://doi.wiley.com/10.1016/j.febslet.2006.07.078.

Goode BL, Chau M, Denis PE, Feinstein SC (2000) Structural and functional differences between 3-repeat and 4-repeat tau isoforms: Implications for normal tau function and the onset of neurodegenerative disease. J Biol Chem 275:38182–38189 Available at: http://www.jbc.org/cgi/doi/10.1074/jbc.M007489200.

Govindpani K, Guzmán BCF, Vinnakota C, Waldvogel HJ, Faull RL, Kwakowsky A (2017) Towards a better understanding of GABAergic remodeling in alzheimer's disease. Int J Mol Sci 18.

Graeber MB, Mehraein P (1999) Reanalysis of the first case of Alzheimer's disease. Eur Arch Psychiatry Clin Neurosci 249:S10–S13 Available at: http://link.springer.com/article/10.1007/PL00014167.

Grant MKO, Handoko M, Rozga M, Brinkmalm G, Portelius E, Blennow K, Ashe KH, Zahs KR, Liu P (2019) Human cerebrospinal fluid 6E10- immunoreactive protein species contain amyloid precursor protein fragments. PLoS One 14:1–23.

Gravel M, Peterson J, Yong VW, Kottis V, Trapp B, Braun PE (1996) Overexpression of 2',3'-cyclic nucleotide 3'-phosphodiesterase in transgenic mice alters oligodendrocyte development and produces aberrant myelination. Mol Cell Neurosci 7:453–466 Available at: http://www.sciencedirect.com/science/article/pii/S1044743196900330.

Griffiths I, Klugmann M, Anderson T, Yool D, Thomson C, Schwab MH, Schneider A, Zimmermann F, McCulloch M, Nadon N, Nave KA (1998) Axonal swellings and degeneration in mice lacking the major proteolipid of myelin. Science (80-) 280:1610–1613.

Grimmer T, Henriksen G, Wester H-J, Förstl H, Klunk WE, Mathis CA, Kurz A, Drzezga A (2009) Clinical severity of Alzheimer's disease is associated with PIB uptake in PET. Neurobiol Aging 30:1902–1909 Available at: http://linkinghub.elsevier.com/retrieve/pii/S0197458008000353.

Griner SL, Seidler P, Bowler J, Murray KA, Yang TP, Sahay S, Sawaya MR, Cascio D, Rodriguez JA, Philipp S, Sosna J, Glabe CG, Gonen T, Eisenberg DS (2019) Structure based inhibitors of Amyloid Beta core suggest a common interface with Tau. Elife 8 Available at: http://www.ghbook.ir/index.php?name=فرهنگ و رسانه های نوین&option=com_dbook&task=readonline&book_id=13650&page=73&chkhashk=ED9C9491B4&Itemid=218&lang=fa&tmpl=component.

Grubman A, Chew G, Ouyang JF, Sun G, Choo XY, McLean C, Simmons R, Buckberry S, Landin DV, Pflueger J, Lister R, Rackham OJL, Petretto E, Polo JM (2019) A single cell brain atlas in human Alzheimer's disease. bioRxiv:628347 Available at: https://www.biorxiv.org/content/10.1101/628347v1.

Grundke-Iqbal I, Iqbal K, Tung Y-C, Quinlan M, Wisniewski HM, Binder LI (1986) Abnormal phosphorylation of the microtubule-associated protein tau (tau) in Alzheimer cytoskeletal pathology. Proc Natl Acad Sci 83:4913–4917 Available at: http://www.pnas.org/content/83/13/4913.short.

Gu L, Wu D, Tang X, Qi X, Li X, Bai F, Chen X, Ren Q, Zhang Z (2018) Myelin changes at the early stage of 5XFAD mice. Brain Res Bull 137:285–293.

Gueli MC, Taibi G (2013) Alzheimer's disease: Amino acid levels and brain metabolic status. Neurol Sci 34:1575–1579.

Guo JL, Buist A, Soares A, Callaerts K, Calafate S, Stevenaert F, Daniels JP, Zoll BE, Crowe A, Brunden KR, Moechars D, Lee VMY (2016) The Dynamics and Turnover of Tau Aggregates in Cultured Cells. J Biol Chem 291:13175–13193 Available at: http://www.jbc.org/lookup/doi/10.1074/jbc.M115.712083.

Gutiérrez R, Boison D, Heinemann U, Stoffel W (1995) Decompaction of CNS myelin leads to a reduction of the conduction velocity of action potentials in optic nerve. Neurosci Lett 195:93–96.

Haass C, Lemere CA, Capell A, Citron M, Seubert P, Schenk D, Lannfelt L, Selkoe DJ (1995) The Swedish mutation causes early-onset Alzheimer's disease by β-secretase cleavage within the

secretory pathway. Nat Med 1:1291–1296.

Haberlandt C, Derouiche A, Wyczynski A, Haseleu J, Pohle J, Karram K, Trotter J, Seifert G, Frotscher M, Steinhäuser C, Jabs R (2011) Gray Matter NG2 Cells Display Multiple Ca2+-Signaling Pathways and Highly Motile Processes Degtyar V, ed. PLoS One 6:e17575 Available at: https://dx.plos.org/10.1371/journal.pone.0017575.

Haider L, Zrzavy T, Hametner S, Höftberger R, Bagnato F, Grabner G, Trattnig S, Pfeifenbring S, Brück W, Lassmann H (2016) The topograpy of demyelination and neurodegeneration in the multiple sclerosis brain. Brain 139:807–815 Available at: https://academic.oup.com/brain/article-lookup/doi/10.1093/brain/awv398.

Hamilton NB, Clarke LE, Arancibia-Carcamo IL, Kougioumtzidou E, Matthey M, Káradóttir R, Whiteley L, Bergersen LH, Richardson WD, Attwell D (2017) Endogenous GABA controls oligodendrocyte lineage cell number, myelination, and CNS internode length. Glia 65:309–321 Available at: http://doi.wiley.com/10.1002/glia.23093.

Hamilton TG, Klinghoffer RA, Corrin PD, Soriano P (2003) Evolutionary divergence of platelet-derived growth factor alpha receptor signaling mechanisms. Mol Cell Biol 23:4013–4025 Available at: http://www.ncbi.nlm.nih.gov/pubmed/12748302.

Hampel H, Teipel SJ, Alexander GE, Horwitz B, Teichberg D, Schapiro MB, Rapoport SI (1998) Corpus Callosum Atrophy Is a Possible Indicator of Region– and Cell Type–Specific Neuronal Degeneration in Alzheimer Disease. Arch Neurol 55:193 Available at: http://archneur.jamanetwork.com/article.aspx?doi=10.1001/archneur.55.2.193.

Hansson O, Seibyl J, Stomrud E, Zetterberg H, Trojanowski JQ, Bittner T, Lifke V, Corradini V, Eichenlaub U, Batrla R, Buck K, Zink K, Rabe C, Blennow K, Shaw LM (2018) CSF biomarkers of Alzheimer's disease concord with amyloid-β PET and predict clinical progression: A study of fully automated immunoassays in BioFINDER and ADNI cohorts. Alzheimer's Dement 14:1470–1481.

Harris JA, Devidze N, Halabisky B, Lo I, Thwin MT, Yu G-Q, Bredesen DE, Masliah E, Mucke L (2010) Many Neuronal and Behavioral Impairments in Transgenic Mouse Models of Alzheimer's Disease Are Independent of Caspase Cleavage of the Amyloid Precursor Protein. J Neurosci 30:372–381 Available at: http://www.jneurosci.org/cgi/doi/10.1523/JNEUROSCI.5341-09.2010.

Hashimoto N, Takeuchi T, Ishihara R, Ukai K, Kobayashi H, Iwata H, Iwai K, Mizuno Y, Yamaguchi H, Shibayama H (2003) Glial fibrillary tangles in diffuse neurofibrillary tangles with calcification. Acta Neuropathol 106:150–156.

Hashimoto Y, Matsuoka M (2014) A mutation protective against Alzheimer's disease renders amyloid β precursor protein incapable of mediating neurotoxicity. J Neurochem 130:291–300 Available at: http://doi.wiley.com/10.1111/jnc.12717.

Hatami A, Monjazeb S, Milton S, Glabe CG (2017) Familial Alzheimer's disease mutations within

the amyloid precursor protein alter the aggregation and conformation of the amyloid-β peptide. J Biol Chem 292:3172–3185 Available at: http://www.jbc.org/lookup/doi/10.1074/jbc.M116.755264.

Hefendehl JK, LeDue J, Ko RWY, Mahler J, Murphy TH, MacVicar BA (2016) Mapping synaptic glutamate transporter dysfunction in vivo to regions surrounding Aβ plaques by iGluSnFR two-photon imaging. Nat Commun 7.

Helboe L, Egebjerg J, Barkholt P, Volbracht C (2017) Early depletion of CA1 neurons and late neurodegeneration in a mouse tauopathy model. Brain Res 1665:22–35 Available at: http://dx.doi.org/10.1016/j.brainres.2017.04.002.

Higuchi M, Ishihara T, Zhang B, Hong M, Andreadis A, Trojanowski JQ, Lee VM-Y (2002) Transgenic Mouse Model of Tauopathies with Glial Pathology and Nervous System Degeneration. Neuron 35:433–446 Available at: http://www.sciencedirect.com/science/article/pii/S0896627302007894.

Higuchi M, Zhang B, Forman MS, Yoshiyama Y, Trojanowski JQ, Lee VM-Y (2005) Axonal degeneration induced by targeted expression of mutant human tau in oligodendrocytes of transgenic mice that model glial tauopathies. J Neurosci 25:9434–9443 Available at: http://www.jneurosci.org/cgi/doi/10.1523/JNEUROSCI.2691-05.2005.

Hill RA, Li AM, Grutzendler J (2018) Lifelong cortical myelin plasticity and age-related degeneration in the live mammalian brain. Nat Neurosci 21:683–695 Available at: http://dx.doi.org/10.1038/s41593-018-0120-6.

Hill RA, Patel KD, Goncalves CM, Grutzendler J, Nishiyama A (2014) Modulation of oligodendrocyte generation during a critical temporal window after NG2 cell division. Nat Neurosci 17:1518–1527 Available at: http://www.nature.com/doifinder/10.1038/nn.3815.

Hill RA, Patel KD, Medved J, Reiss AM, Nishiyama A (2013) NG2 cells in white matter but not gray matter proliferate in response to PDGF. J Neurosci 33:14558–14566.

Hirsiger S, Koppelmans V, Mérillat S, Erdin C, Narkhede A, Brickman AM, Jäncke L (2017) Executive Functions in Healthy Older Adults Are Differentially Related to Macro- and Microstructural White Matter Characteristics of the Cerebral Lobes. Front Aging Neurosci 9:1–14 Available at: http://journal.frontiersin.org/article/10.3389/fnagi.2017.00373/full.

Holler CJ, Davis PR, Beckett TL, Platt TL, Webb RL, Head E, Murphy MP (2014) Bridging integrator 1 (BIN1) protein expression increases in the alzheimer's disease brain and correlates with neurofibrillary tangle pathology. J Alzheimer's Dis 42:1221–1227.

Hong S, Beja-Glasser VF, Nfonoyim BM, Frouin A, Li S, Ramakrishnan S, Merry KM, Shi Q, Rosenthal A, Barres BA, Lemere CA, Selkoe DJ, Stevens B (2016) Complement and microglia mediate early synapse loss in Alzheimer mouse models. Science (80-) 352:712–716 Available at: http://www.sciencemag.org/cgi/doi/10.1126/science.aad8373.

Hoos MD, Ahmed M, Smith SO, Van Nostrand WE (2009) Myelin Basic Protein Binds to and

Inhibits the Fibrillar Assembly of Aβ42 in Vitro. Biochemistry 48:4720–4727 Available at: https://pubs.acs.org/doi/10.1021/bi900037s.

Hoppe D, Kettenmann H (1989) GABA triggers a Cl− efflux from cultured mouse oligodendrocytes. Neurosci Lett 97:334–339 Available at: https://linkinghub.elsevier.com/retrieve/pii/0304394089906204.

Horiuchi M, Maezawa I, Itoh A, Wakayama K, Jin L-W, Itoh T, DeCarli C (2012) Amyloid β1–42 oligomer inhibits myelin sheet formation in vitro. Neurobiol Aging 338:499–509 Available at: http://linkinghub.elsevier.com/retrieve/pii/S0197458010002216.

Hornig J, Fröb F, Vogl MR, Hermans-Borgmeyer I, Tamm ER, Wegner M, FrÃ¶b F, Vogl MR, Hermans-Borgmeyer I, Tamm ER, Wegner M (2013) The Transcription Factors Sox10 and Myrf Define an Essential Regulatory Network Module in Differentiating Oligodendrocytes Barres BA, ed. PLoS Genet 9:e1003907 Available at: http://dx.plos.org/10.1371/journal.pgen.1003907.

Howell OW, Palser A, Polito A, Melrose S, Zonta B, Scheiermann C, Vora AJ, Brophy PJ, Reynolds R (2006) Disruption of neurofascin localization reveals early changes preceding demyelination and remyelination in multiple sclerosis. Brain 129:3173–3185.

Hsiao K, Chapman P, Nilsen S, Eckman C, Harigaya Y, Younkin S, Yang F, Cole G (1996) Correlative Memory Deficits, A Elevation, and Amyloid Plaques in Transgenic Mice. Science (80-) 274:99–103 Available at: https://www.sciencemag.org/lookup/doi/10.1126/science.274.5284.99.

Hughes EG, Appel B (2016) The cell biology of CNS myelination. Curr Opin Neurobiol 39:93–100 Available at: http://linkinghub.elsevier.com/retrieve/pii/S0959438816300484.

Hughes EG, Kang SH, Fukaya M, Bergles DE (2013) Oligodendrocyte progenitors balance growth with self-repulsion to achieve homeostasis in the adult brain. Nat Neurosci 16:668–676 Available at: http://www.nature.com/articles/nn.3390.

Hughes EG, Orthmann-Murphy JL, Langseth AJ, Bergles DE (2018) Myelin remodeling through experience-dependent oligodendrogenesis in the adult somatosensory cortex. Nat Neurosci 21:696–706 Available at: http://dx.doi.org/10.1038/s41593-018-0121-5.

Hulst HE, Steenwijk MD, Versteeg A, Pouwels PJW, Vrenken H, Uitdehaag BMJ, Polman CH, Geurts JJG, Barkhof F (2013) Cognitive impairment in MS Impact of white matter integrity, gray matter volume, and lesions. Neurology 80:1025–1032 Available at: http://www.neurology.org/content/80/11/1025.short.

Hutton M et al. (1998) Association of missense and 5'-splice-site mutations in tau with the inherited dementia FTDP-17. Nature 393:702–705 Available at: http://www.nature.com/articles/31508%0Ahttp://www.nature.com/doifinder/10.1038/31508.

Hyman BT, Van Hoesen GW, Damasio AR, Barnes CL (1984) Alzheimer's disease: cell-specific pathology isolates the hippocampal formation. Science 225:1168–1170 Available at:

http://www.ncbi.nlm.nih.gov/pubmed/6474172.

Ihara M, Polvikoski TM, Hall R, Slade JY, Perry RH, Oakley AE, Englund E, O'Brien JT, Ince PG, Kalaria RN, O'brien JT, Ince PG, Kalaria RN, O'Brien JT, Ince PG, Kalaria RN (2010) Quantification of myelin loss in frontal lobe white matter in vascular dementia, Alzheimer's disease, and dementia with Lewy bodies. Acta Neuropathol 119:579–589 Available at: http://link.springer.com/10.1007/s00401-009-0635-8.

Ikeda K, Akiyama H, Arai T, Nishimura T (1998) Glial tau pathology in neurodegenerative diseases: Their nature and comparison with neuronal tangles. Neurobiol Aging 19.

Ikegami S, Harada A, Hirokawa N (2000) Muscle weakness, hyperactivity, and impairment in fear conditioning in tau-deficient mice. Neurosci Lett 279:129–132.

Irish M, Hornberger M, El Wahsh S, Lam BYK, Lah S, Miller L, Hsieh S, Hodges JR, Piguet O (2014) Grey and white matter correlates of recent and remote autobiographical memory retrieval -insights from the dementias. PLoS One 9.

Iseki E, Yamamoto R, Murayama N, Minegishi M, Togo T, Katsuse O, Kosaka K, Akiyama H, Tsuchiya K, Rohan de S, Andrew L, Arai H (2006) Immunohistochemical investigation of neurofibrillary tangles and their tau isoforms in brains of limbic neurofibrillary tangle dementia. Neurosci Lett 405:29–33.

Itoh Y, Voskuhl RR (2017) Cell specificity dictates similarities in gene expression in multiple sclerosis, Parkinson's disease, and Alzheimer's disease. PLoS One 12:1–11.

Jack CR, Wiste HJ, Vemuri P, Weigand SD, Senjem ML, Zeng G, Bernstein MA, Gunter JL, Pankratz VS, Aisen PS, Weiner MW, Petersen RC, Shaw LM, Trojanowski JQ, Knopman DS, Initiative the ADN (2010) Brain beta-amyloid measures and magnetic resonance imaging atrophy both predict time-to-progression from mild cognitive impairment to Alzheimer's disease. Brain 133:3336–3348 Available at: https://academic.oup.com/brain/article-lookup/doi/10.1093/brain/awq277.

Jackson J, Bianco G, Rosa AO, Cowan K, Bond P, Anichtchik O, Fern R (2018) White matter tauopathy: Transient functional loss and novel myelin remodeling. Glia 66:813–827 Available at: http://doi.wiley.com/10.1002/glia.23286.

Jakovcevski I, Filipovic R, Mo Z, Rakic S, Zecevic N (2009) Oligodendrocyte development and the onset of myelination in the human fetal brain. Front Neuroanat 3:5 Available at: http://journal.frontiersin.org/article/10.3389/neuro.05.005.2009/abstract.

Jakovcevski I, Mo Z, Zecevic N (2007) Down-regulation of the axonal polysialic acid-neural cell adhesion molecule expression coincides with the onset of myelination in the human fetal forebrain. Neuroscience 149:328–337.

Jakovcevski I, Zecevic N (2005) Olig transcription factors are expressed in oligodendrocyte and neuronal cells in human fetal CNS. J Neurosci 25:10064–10073 Available at: http://www.jneurosci.org/cgi/doi/10.1523/JNEUROSCI.2324-05.2005.

Jankowsky JL, Fadale DJ, Anderson J, Xu GM, Gonzales V, Jenkins NA, Copeland NG, Lee MK, Younkin LH, Wagner SL, Younkin SG, Borchelt DR (2004) Mutant presenilins specifically elevate the levels of the 42 residue β-amyloid peptide in vivo: Evidence for augmentation of a 42-specific γ secretase. Hum Mol Genet 13:159–170.

Jawhar S, Trawicka A, Jenneckens C, Bayer TA, Wirths O (2012) Motor deficits, neuron loss, and reduced anxiety coinciding with axonal degeneration and intraneuronal Aβ aggregation in the 5XFAD mouse model of Alzheimer's disease. Neurobiol Aging 33:196.e29-196.e40 Available at: http://dx.doi.org/10.1016/j.neurobiolaging.2010.05.027.

Jiang L, Cao X, Li T, Tang Y, Li W, Wang J, Chan RC, Li C (2016) Cortical Thickness Changes Correlate with Cognition Changes after Cognitive Training: Evidence from a Chinese Community Study. Front Aging Neurosci 8 Available at: http://journal.frontiersin.org/Article/10.3389/fnagi.2016.00118/abstract.

Jin C, Katayama S, Hiji M, Watanabe C, Noda K, Nakamura S, Matsumoto M (2006) Relationship between neuronal loss and tangle formation in neurons and oligodendroglia in progressive supranuclear palsy. Neuropathology 26:50–56.

Jin SC, Pastor P, Cooper B, Cervantes S, Benitez BA, Razquin C, Goate A, Cruchaga C (2012) Pooled-DNA sequencing identifies novel causative variants in PSEN1, GRN and MAPT in a clinical early-onset and familial Alzheimer's disease Ibero-American cohort. Alzheimer's Res Ther 4:1–9.

Joachim C, Games D, Morris J, Ward P, Frenkel D, Selkoe D (1991) Antibodies to non-beta regions of the beta-amyloid precursor protein detect a subset of senile plaques. Am J Pathol 138:373–384 Available at: http://www.ncbi.nlm.nih.gov/pubmed/1704190%0Ahttp://www.pubmedcentral.nih.gov/articlerender.fcgi?artid=PMC1886178.

Kadavath H, Hofele R V., Biernat J, Kumar S, Tepper K, Urlaub H, Mandelkow E, Zweckstetter M (2015) Tau stabilizes microtubules by binding at the interface between tubulin heterodimers. Proc Natl Acad Sci U S A 112:7501–7506.

Kagawa T, Ikenaka K, Inoue Y, Kuriyama S, Tsujii T, Nakao J, Nakajima K, Aruga J, Okano H, Mikoshiba K (1994) Glial cell degeneration and hypomyelination caused by overexpression of myelin proteolipid protein gene. Neuron 13:427–442.

Kaila K, Price TJ, Payne JA, Puskarjov M, Voipio J (2014) Cation-chloride cotransporters in neuronal development, plasticity and disease. Nat Rev Neurosci 15:637–654 Available at: http://dx.doi.org/10.1038/nrn3819.

Kalani A, Chaturvedi P, Maldonado C, Bauer P, Joshua IG, Tyagi SC, Tyagi N (2017) Dementia-like pathology in type-2 diabetes: A novel microRNA mechanism. Mol Cell Neurosci 80:58–65 Available at: https://linkinghub.elsevier.com/retrieve/pii/S104474311730057X.

Kang J, Lemaire HG, Unterbeck A, Salbaum JM, Masters CL, Grzeschik KH, Multhaup G,

Beyreuther K, Müller-Hill B (1987) The precursor of Alzheimer's disease amyloid A4 protein resembles a cell-surface receptor. Nature 325:733–736.

Kang SH, Fukaya M, Yang JK, Rothstein JD, Bergles DE (2010) NG2+ CNS Glial Progenitors Remain Committed to the Oligodendrocyte Lineage in Postnatal Life and following Neurodegeneration. Neuron 68:668–681 Available at: http://linkinghub.elsevier.com/retrieve/pii/S0896627310007269.

Kashyap G, Bapat D, Das D, Gowaikar R, Amritkar RE, Rangarajan G, Ravindranath V, Ambika G (2019) Synapse loss and progress of Alzheimer's disease -A network model. Sci Rep 9:1–9.

Kassubek J, Müller H-P, Del Tredici K, Hornberger M, Schroeter ML, Müller K, Anderl-Straub S, Uttner I, Grossman M, Braak H, Hodges JR, Piguet O, Otto M, Ludolph AC (2018) Longitudinal Diffusion Tensor Imaging Resembles Patterns of Pathology Progression in Behavioral Variant Frontotemporal Dementia (bvFTD). Front Aging Neurosci 10:47 Available at: http://www.ncbi.nlm.nih.gov/pubmed/29559904.

Kato D, Wake H, Lee PR, Tachibana Y, Ono R, Sugio S, Tsuji Y, Tanaka YH, Tanaka YR, Masamizu Y, Hira R, Moorhouse AJ, Tamamaki N, Ikenaka K, Fields RD (2019) Motor learning requires myelination to reduce asynchrony and spontaneity in neural activity. :1–18.

Kavroulakis E, Simos PG, Kalaitzakis G, Maris TG, Karageorgou D, Zaganas I, Panagiotakis S, Basta M, Vgontzas A, Papadaki E (2018) Myelin content changes in probable Alzheimer's disease and mild cognitive impairment: Associations with age and severity of neuropsychiatric impairment. J Magn Reson Imaging 47:1359–1372.

Keirstead HS, Levine JM, Blakemore WF (1998) Response of the oligodendrocyte progenitor cell population (Defined by NG2 labelling) to demyelination of the adult spinal cord. Glia 22:161–170.

Kesner RP, Rolls ET (2015) A computational theory of hippocampal function, and tests of the theory: New developments. Neurosci Biobehav Rev 48:92–147 Available at: http://dx.doi.org/10.1016/j.neubiorev.2014.11.009.

Kessaris N, Fogarty M, Iannarelli P, Grist M, Wegner M, Richardson WD (2006) Competing waves of oligodendrocytes in the forebrain and postnatal elimination of an embryonic lineage. Nat Neurosci 9:173–179 Available at: http://www.nature.com/doifinder/10.1038/nn1620.

Khatoon S, Grundke-Iqbal I, Iqbal K (1992) Brain Levels of Microtubule-Associated Protein τ Are Elevated in Alzheimer's Disease: A Radioimmuno-Slot-Blot Assay for Nanograms of the Protein. J Neurochem 59:750–753.

Kim YS, Woo J, Lee CJ, Yoon BE (2017) Decreased Glial GABA and tonic inhibition in cerebellum of mouse model for Attention-Deficit/ Hyperactivity Disorder (ADHD). Exp Neurobiol 26:206–212.

Kitchigina VF (2018) Alterations of Coherent Theta and Gamma Network Oscillations as an Early Biomarker of Temporal Lobe Epilepsy and Alzheimer's Disease. Front Integr Neurosci 12:1–15

Available at: https://www.frontiersin.org/article/10.3389/fnint.2018.00036/full.

Klugmann M, Schwab MH, Pühlhofer A, Schneider A, Zimmermann F, Griffiths IR, Nave K-A (1997) Assembly of CNS Myelin in the Absence of Proteolipid Protein. Neuron 18:59–70 Available at: https://linkinghub.elsevier.com/retrieve/pii/S0896627301800465.

Klunk WE et al. (2004) Imaging brain amyloid in Alzheimer's disease with Pittsburgh Compound-B. Ann Neurol 55:306–319 Available at: http://onlinelibrary.wiley.com/doi/10.1002/ana.20009/full.

Knapp PE, Skoff RP, Redstone DW (1986) Oligodendroglial cell death in jimpy mice: an explanation for the myelin deficit. J Neurosci 6:2813–2822 Available at: http://www.ncbi.nlm.nih.gov/pubmed/3760936.

Komori T (1999) Tau-positive glial inclusions in progressive supranuclear palsy, corticobasal degeneration and Pick's disease. Brain Pathol 9:663–679.

Köpke E, Tung YC, Shaikh S, Alonso AC, Iqbal K, Grundke-Iqbal I (1993) Microtubule-associated protein tau. Abnormal phosphorylation of a non-paired helical filament pool in Alzheimer disease. J Biol Chem 268:24374–24384 Available at: http://www.ncbi.nlm.nih.gov/pubmed/8226987.

Kotarba AE, Aucoin D, Hoos MD, Smith SO, Van Nostrand WE (2013) Fine mapping of the amyloid β-protein binding site on myelin basic protein. Biochemistry 52:2565–2573.

Kougioumtzidou E, Shimizu T, Hamilton NB, Tohyama K, Sprengel R, Monyer H, Attwell D, Richardson WD (2017) Signalling through AMPA receptors on oligodendrocyte precursors promotes myelination by enhancing oligodendrocyte survival. Elife 6.

Kovacs GG, Majtenyi K, Spina S, Murrell JR, Gelpi E, Hoftberger R, Fraser G, Crowther RA, Goedert M, Budka H, Ghetti B (2008) White Matter Tauopathy With Globular Glial Inclusions: A Distinct Sporadic Frontotemporal Lobar Degeneration. J Neuropathol Exp Neurol 67:963–975 Available at: https://academic.oup.com/jnen/article-lookup/doi/10.1097/NEN.0b013e318187a80f.

Krishnamurthy PK, Deng Y, Sigurdsson EM (2011) Mechanistic studies of antibody-mediated clearance of tau aggregates using an ex vivo brain slice model. Front Psychiatry 2:1–6.

Kuhlmann T, Miron V, Cuo Q, Wegner C, Antel J, Brück W, Bruck W (2008) Differentiation block of oligodendroglial progenitor cells as a cause for remyelination failure in chronic multiple sclerosis. Brain 131:1749–1758 Available at: http://brain.oxfordjournals.org/cgi/doi/10.1093/brain/awn096.

Kujuro Y, Suzuki N, Kondo T (2010) Esophageal cancer-related gene 4 is a secreted inducer of cell senescence expressed by aged CNS precursor cells. Proc Natl Acad Sci 107:8259–8264 Available at: http://www.pnas.org/cgi/doi/10.1073/pnas.0911446107.

Kwakowsky A, Calvo-Flores Guzmán B, Pandya M, Turner C, Waldvogel HJ, Faull RL (2018) GABA A receptor subunit expression changes in the human Alzheimer's disease hippocampus,

subiculum, entorhinal cortex and superior temporal gyrus. J Neurochem 145:374–392.

Lalonde R, Kim HD, Maxwell JA, Fukuchi K (2005) Exploratory activity and spatial learning in 12-month-old APP 695 SWE/co + PS1/ΔE9 mice with amyloid plaques. Neurosci Lett 390:87–92.

Lappe-Siefke C, Goebbels S, Gravel M, Nicksch E, Lee J, Braun PE, Griffiths IR, Nave K-A (2003) Disruption of Cnp1 uncouples oligodendroglial functions in axonal support and myelination. Nat Genet 33:366–374 Available at: http://www.nature.com/doifinder/10.1038/ng1095.

Larson VA, Zhang Y, Bergles DE (2016) Electrophysiological properties of NG2 + cells: Matching physiological studies with gene expression profiles. Brain Res 1638:138–160 Available at: http://linkinghub.elsevier.com/retrieve/pii/S0006899315007088.

Lasagna-Reeves CAA et al. (2016) Reduction of Nuak1 Decreases Tau and Reverses Phenotypes in a Tauopathy Mouse Model. Neuron 92:407–418 Available at: http://linkinghub.elsevier.com/retrieve/pii/S0896627316305815.

Lasiene J, Matsui A, Sawa Y, Wong F, Horner PJ (2009) Age-related myelin dynamics revealed by increased oligodendrogenesis and short internodes. Aging Cell 8:201–213 Available at: http://doi.wiley.com/10.1111/j.1474-9726.2009.00462.x.

Laws SM, Friedrich P, Diehl-Schmid J, Müller J, Eisele T, Bäuml J, Förstl H, Kurz A, Riemenschneider M (2007) Fine mapping of the MAPT locus using quantitative trait analysis identifies possible causal variants in Alzheimer's disease. Mol Psychiatry 12:510–517.

Lee J-T, Xu J, Lee J-M, Ku G, Han X, Yang D-I, Chen S, Hsu CY (2004) Amyloid-β peptide induces oligodendrocyte death by activating the neutral sphingomyelinase–ceramide pathway. J Cell Biol 164:123–131 Available at: http://www.jcb.org/lookup/doi/10.1083/jcb.200307017.

Lee J, Gravel M, Zhang R, Thibault P, Braun PE (2005) Process outgrowth in oligodendrocytes is mediated by CNP, a novel microtubule assembly myelin protein. J Cell Biol 170:661–673 Available at: http://www.jcb.org/lookup/doi/10.1083/jcb.200411047.

Lee S et al. (2016) White matter hyperintensities are a core feature of Alzheimer's disease: Evidence from the dominantly inherited Alzheimer network. Ann Neurol 79:929–939.

Lee Y, Morrison BM, Li Y, Lengacher S, Farah MH, Hoffman PN, Liu Y, Tsingalia A, Jin L, Zhang P-W, Pellerin L, Magistretti PJ, Rothstein JD (2012) Oligodendroglia metabolically support axons and contribute to neurodegeneration. Nature 487:443–448 Available at: http://www.nature.com/doifinder/10.1038/nature11314.

Lei P, Ayton S, Finkelstein DI, Spoerri L, Ciccotosto GD, Wright DK, Wong BXW, Adlard PA, Cherny RA, Lam LQ, Roberts BR, Volitakis I, Egan GF, McLean CA, Cappai R, Duce JA, Bush AI (2012) Tau deficiency induces parkinsonism with dementia by impairing APP-mediated iron export. Nat Med 18:291–295 Available at: http://dx.doi.org/10.1038/nm.2613.

Lemere CA, Lopera F, Kosik KS, Lendon CL, Ossa J, Saido TC, Yamaguchi H, Ruiz A, Martinez A, Madrigal L, Hincapie L, Arango JC, Anthony DC, Koo EH, Goate AM, Selkoe DJ, Arango JC (1996) The E280A presenilin 1 Alzheimer mutation produces increased A beta 42 deposition

and severe cerebellar pathology. Nat Med 2:1146–1150 Available at: http://www.ncbi.nlm.nih.gov/pubmed/8837617.

Leone DP, Genoud S, Atanasoski S, Grausenburger R, Berger P, Metzger D, Macklin WB, Chambon P, Suter U (2003) Tamoxifen-inducible glia-specific Cre mice for somatic mutagenesis in oligodendrocytes and Schwann cells. Mol Cell Neurosci 22:430–440 Available at: http://linkinghub.elsevier.com/retrieve/pii/S1044743103000290.

Lerdkrai C, Asavapanumas N, Brawek B, Kovalchuk Y, Mojtahedi N, Olmedillas del Moral M, Garaschuk O (2018) Intracellular Ca 2+ stores control in vivo neuronal hyperactivity in a mouse model of Alzheimer's disease. Proc Natl Acad Sci 115:E1279–E1288 Available at: http://www.pnas.org/lookup/doi/10.1073/pnas.1714409115.

Levy E, Carman M, Fernandez-Madrid I, Power M, Lieberburg I, van Duinen S, Bots G, Luyendijk W, Frangione B (1990) Mutation of the Alzheimer's disease amyloid gene in hereditary cerebral hemorrhage, Dutch type. Science (80-) 248:1124–1126 Available at: http://www.sciencemag.org/cgi/doi/10.1126/science.2111584.

Lewis J, McGowan E, Rockwood J, Melrose H, Nacharaju P, Van Slegtenhorst M, Gwinn-Hardy K, Murphy MP, Baker M, Yu X, Duff K, Hardy J, Corral A, Lin W-L, Yen S-H, Dickson DW, Davies P, Hutton M (2000) Neurofibrillary tangles, amyotrophy and progressive motor disturbance in mice expressing mutant (P301L) tau protein. Nat Genet 25:402–405 Available at: http://www.nature.com/ng/journal/v25/n4/abs/ng0800_402.html.

Leyk J, Goldbaum O, Noack M, Richter-Landsberg C (2015) Inhibition of HDAC6 Modifies Tau Inclusion Body Formation and Impairs Autophagic Clearance. J Mol Neurosci 55:1031–1046.

Li S, Wang X, Ma Q-H, Yang W, Zhang X-G, Dawe GS, Xiao Z-C (2016) Amyloid precursor protein modulates Nav1.6 sodium channel currents through a Go-coupled JNK pathway. Sci Rep 6 Available at: http://www.nature.com/articles/srep39320.

Li W, Tang Y, Fan Z, Meng Y, Yang G, Luo J, Ke Z-JJ (2013) Autophagy is involved in oligodendroglial precursor-mediated clearance of amyloid peptide. Mol Neurodegener 8:1 Available at: http://molecularneurodegeneration.biomedcentral.com/articles/10.1186/1750-1326-8-27.

Liao M-C, Ahmed M, Smith SO, Van Nostrand WE (2009) Degradation of Amyloid Protein by Purified Myelin Basic Protein. J Biol Chem 284:28917–28925 Available at: http://www.jbc.org/cgi/doi/10.1074/jbc.M109.050856.

Liao MC, Hoos MD, Aucoin D, Ahmed M, Davis J, Smith SO, Van Nostrand WE (2010) N-terminal domain of myelin basic protein inhibits amyloid β-protein fibril assembly. J Biol Chem 285:35590–35598.

Ligon KL, Alberta JA, Kho AT, Weiss J, Kwaan MR, Nutt CL, Louis DN, Stiles CD, Rowitch DH (2004) The oligodendroglial lineage marker OLIG2 is universally expressed in diffuse gliomas. J Neuropathol Exp Neurol 63:499–509.

Ligon KL, Kesari S, Kitada M, Sun T, Arnett HA, Alberta JA, Anderson DJ, Stiles CD, Rowitch DH (2006) Development of NG2 neural progenitor cells requires Olig gene function. Proc Natl Acad Sci U S A 103:7853–7858.

Lin SC, Bergles DE (2004) Synaptic signaling between GABAergic interneurons and oligodendrocyte precursor cells in the hippocampus. Nat Neurosci 7:24–32.

Lin W-L, Lewis J, Yen S-H, Hutton M, Dickson DW (2003a) Filamentous Tau in Oligodendrocytes and Astrocytes of Transgenic Mice Expressing the Human Tau Isoform with the P301L Mutation. Am J Pathol 162:213–218 Available at: http://www.sciencedirect.com/science/article/pii/S0002944010638126.

Lin WL, Lewis J, Yen SH, Hutton M, Dickson DW (2003b) Ultrastructural neuronal pathology in transgenic mice expressing mutant (P301L) human tau. J Neurocytol 32:1091–1105.

LoPresti P, Konat GW (2001) Hydrogen peroxide induces transient dephosphorylation of tau protein in cultured rat oligodendrocytes. Neurosci Lett 311:142–144.

Lou F, Luo X, Li M, Ren Y, He Z (2017) Very early–onset sporadic Alzheimer's disease with a de novo mutation in the PSEN1 gene. Neurobiol Aging 53:193.e1-193.e5 Available at: http://linkinghub.elsevier.com/retrieve/pii/S0197458016303396.

Lu PH, Lee GJ, Shapira J, Jimenez E, Mather MJ, Thompson PM, Bartzokis G, Mendez MF (2014) Regional differences in white matter breakdown between frontotemporal dementia and early-onset Alzheimer's disease. J Alzheimer's Dis 39:261–269.

Lu QR, Sun T, Zhu Z, Ma N, Garcia M, Stiles CD, Rowitch DH (2002) Common developmental requirement for Olig function indicates a motor neuron/oligodendrocyte connection. Cell 109:75–86 Available at: http://www.sciencedirect.com/science/article/pii/S0092867402006785.

Lüders KA, Nessler S, Kusch K, Patzig J, Jung RB, Möbius W, Nave KA, Werner HB (2019) Maintenance of high proteolipid protein level in adult central nervous system myelin is required to preserve the integrity of myelin and axons. Glia 67:634–649.

Lundgaard I, Luzhynskaya A, Stockley JH, Wang Z, Evans KA, Swire M, Volbracht K, Gautier HOB, Franklin RJM, ffrench-Constant C, Attwell D, Káradóttir RT (2013) Neuregulin and BDNF Induce a Switch to NMDA Receptor-Dependent Myelination by Oligodendrocytes. PLoS Biol 11.

Luo X, Prior M, He W, Hu X, Tang X, Shen W, Yadav S, Kiryu-Seo S, Miller R, Trapp BD, Yan R (2011) Cleavage of neuregulin-1 by BACE1 or ADAM10 protein produces differential effects on myelination. J Biol Chem 286:23967–23974.

Luyt K, Slade TP, Dorward JJ, Durant CF, Wu Y, Shigemoto R, Mundell SJ, Váradi A, Molnár E (2007) Developing oligodendrocytes express functional GABA B receptors that stimulate cell proliferation and migration. J Neurochem 100:822–840 Available at: http://doi.wiley.com/10.1111/j.1471-4159.2006.04255.x.

Luyt K, Varadi A, Molnar E (2003) Functional metabotropic glutamate receptors are expressed in

oligodendrocyte progenitor cells. J Neurochem 84:1452–1464 Available at: http://doi.wiley.com/10.1046/j.1471-4159.2003.01661.x.

Mably AJ, Liu W, Mc Donald JM, Dodart JC, Bard F, Lemere CA, O'Nuallain B, Walsh DM (2015) Anti-Aβ antibodies incapable of reducing cerebral Aβ oligomers fail to attenuate spatial reference memory deficits in J20 mice. Neurobiol Dis 82:372–384 Available at: http://dx.doi.org/10.1016/j.nbd.2015.07.008.

Madeira C, Vargas-Lopes C, Brandão CO, Reis T, Laks J, Panizzutti R, Ferreira ST (2018) Elevated Glutamate and Glutamine Levels in the Cerebrospinal Fluid of Patients With Probable Alzheimer's Disease and Depression. Front Psychiatry 9:1–8 Available at: https://www.frontiersin.org/article/10.3389/fpsyt.2018.00561/full.

Maire CL, Wegener A, Kerninon C, Oumesmar BN, Nait Oumesmar B (2010) Gain-of-Function of Olig Transcription Factors Enhances Oligodendrogenesis and Myelination. Stem Cells 28:1611–1622 Available at: http://doi.wiley.com/10.1002/stem.480.

Makinodan M, Rosen KM, Ito S, Corfas G (2012) A Critical Period for Social Experience-Dependent Oligodendrocyte Maturation and Myelination. Science (80-) 337:1357–1360 Available at: http://www.sciencemag.org/cgi/doi/10.1126/science.1220845.

Mander BA, Marks SM, Vogel JW, Rao V, Lu B, Saletin JM, Ancoli-Israel S, Jagust WJ, Walker MP (2015) β-amyloid disrupts human NREM slow waves and related hippocampus-dependent memory consolidation. Nat Neurosci 18:1051–1057 Available at: http://dx.doi.org/10.1038/nn.4035.

Manrique-Hoyos N, Jürgens T, Grønborg M, Kreutzfeldt M, Schedensack M, Kuhlmann T, Schrick C, Brück W, Urlaub H, Simons M, Merkler D (2012) Late motor decline after accomplished remyelination: Impact for progressive multiple sclerosis. Ann Neurol 71:227–244 Available at: http://doi.wiley.com/10.1002/ana.22681.

Marques S et al. (2016) Oligodendrocyte heterogeneity in the mouse juvenile and adult central nervous system. Science 352:1326–1329 Available at: http://www.sciencemag.org/cgi/doi/10.1126/science.aaf0784.

Martinez-Losa M, Tracy TE, Ma K, Verret L, Clemente-Perez A, Khan AS, Cobos I, Ho K, Gan L, Mucke L, Alvarez-Dolado M, Palop JJ (2018) Nav1.1-Overexpressing Interneuron Transplants Restore Brain Rhythms and Cognition in a Mouse Model of Alzheimer's Disease. Neuron 98:75-89.e5.

Masahira N, Takebayashi H, Ono K, Watanabe K, Ding L, Furusho M, Ogawa Y, Nabeshima Y ichi, Alvarez-Buylla A, Shimizu K, Ikenaka K (2006) Olig2-positive progenitors in the embryonic spinal cord give rise not only to motoneurons and oligodendrocytes, but also to a subset of astrocytes and ependymal cells. Dev Biol 293:358–369.

Masliah E, Alford M, DeTeresa R, Mallory M, Hansen L (1996) Deficient glutamate transport is associated with neurodegeneration in Alzheimer's disease. Ann Neurol 40:759–766.

Mathys H, Davila-Velderrain J, Peng Z, Gao F, Mohammadi S, Young JZ, Menon M, He L, Abdurrob F, Jiang X, Martorell AJ, Ransohoff RM, Hafler BP, Bennett DA, Kellis M, Tsai LH (2019) Single-cell transcriptomic analysis of Alzheimer's disease. Nature 570:332–337 Available at: http://dx.doi.org/10.1038/s41586-019-1195-2.

Matthews MA, Duncan D (1971) A quantitative study of morphological changes accompanying the initiation and progress of myelin production in the dorsal funiculus of the rat spinal cord. J Comp Neurol 142:1–22.

Mattsson N, Schöll M, Strandberg O, Smith R, Palmqvist S, Insel PS, Hägerström D, Ohlsson T, Zetterberg H, Jögi J, Blennow K, Hansson O (2017) 18 F-AV-1451 and CSF T-tau and P-tau as biomarkers in Alzheimer's disease . EMBO Mol Med 9:1212–1223.

Mazurek R, Dave JM, Chandran RR, Misra A, Sheikh AQ, Greif DM (2017) Vascular Cells in Blood Vessel Wall Development and Disease, 1st ed. Elsevier Inc. Available at: http://dx.doi.org/10.1016/bs.apha.2016.08.001.

Mckenzie IA, Ohayon D, Li H, Faria JP De, Emery B, Tohyama K, Richardson WD, Paes De Faria J, Emery † Ben, Tohyama K, Richardson WD (2014) Motor skill learning requires active central myelination. Science (80-) 346:318–322 Available at: http://science.sciencemag.org/.

McKhann G, Drachman D, Folstein M, Katzman R, Price D, Stadlan EM (1984) Clinical diagnosis of Alzheimer's disease: report of the NINCDS-ADRDA Work Group under the auspices of Department of Health and Human Services Task Force on Alzheimer's Disease. Neurology 34:939–944 Available at: http://www.ncbi.nlm.nih.gov/pubmed/6610841.

McMillan PJ, Leverenz JB, Dorsa DM (2000) Specific downregulation of presenilin 2 gene expression is prominent during early stages of sporadic late-onset Alzheimer's disease. Mol Brain Res 78:138–145.

McTigue DM, Horner PJ, Stokes BT, Gage FH (2018) Neurotrophin-3 and Brain-Derived Neurotrophic Factor Induce Oligodendrocyte Proliferation and Myelination of Regenerating Axons in the Contused Adult Rat Spinal Cord. J Neurosci 18:5354–5365.

Mecha M, Torrao AS, Mestre L, Carrillo-Salinas FJ, Mechoulam R, Guaza C (2012) Cannabidiol protects oligodendrocyte progenitor cells from inflammation-induced apoptosis by attenuating endoplasmic reticulum stress. Cell Death Dis 3:2–9.

Meilandt WJ, Cisse M, Ho K, Wu T, Esposito LA, Scearce-Levie K, Cheng IH, Yu G-Q, Mucke L (2009) Neprilysin Overexpression Inhibits Plaque Formation But Fails to Reduce Pathogenic A Oligomers and Associated Cognitive Deficits in Human Amyloid Precursor Protein Transgenic Mice. J Neurosci 29:1977–1986 Available at: http://www.jneurosci.org/cgi/doi/10.1523/JNEUROSCI.2984-08.2009.

Menn B, Garcia-Verdugo JM, Yaschine C, Gonzalez-Perez O, Rowitch D, Alvarez-Buylla A (2006) Origin of Oligodendrocytes in the Subventricular Zone of the Adult Brain. J Neurosci 26:7907–7918 Available at: http://www.jneurosci.org/cgi/doi/10.1523/JNEUROSCI.1299-06.2006.

Merchán-Rubira J, Sebastián-Serrano Á, Díaz-Hernández M, Avila J, Hernández F (2019) Peripheral nervous system effects in the PS19 tau transgenic mouse model of tauopathy. Neurosci Lett 698:204–208 Available at: https://doi.org/10.1016/j.neulet.2019.01.031.

Mesquita SD, Ferreira AC, Gao F, Coppola G, Geschwind DH, Sousa JC, Correia-Neves M, Sousa N, Palha JA, Marques F (2015) The choroid plexus transcriptome reveals changes in type I and II interferon responses in a mouse model of Alzheimer's disease. Brain Behav Immun 49:280–292 Available at: http://dx.doi.org/10.1016/j.bbi.2015.06.008.

Metzger D, Clifford J, Chiba H, Chambon P (1995) Conditional site-specific recombination in mammalian cells using a ligand-dependent chimeric Cre recombinase. Proc Natl Acad Sci 92:6991–6995 Available at: http://www.pnas.org/content/92/15/6991.short.

Meyer N, Richter N, Fan Z, Siemonsmeier G, Pivneva T, Jordan P, Steinhäuser C, Semtner M, Nolte C, Kettenmann H (2018) Oligodendrocytes in the Mouse Corpus Callosum Maintain Axonal Function by Delivery of Glucose. Cell Rep 22:2383–2394.

Micheva KD, Chang EF, Nana AL, Seeley WW, Ting JT, Cobbs C, Lein E, Smith SJ, Weinberg RJ, Madison D V. (2018) Distinctive structural and molecular features of myelinated inhibitory axons in human neocortex. eNeuro 5:1–12.

Miller DL, Papayannopoulos IA, Styles J, Bobin SA, Lin YY, Biemann K, Iqbal K (1993) Peptide Compositions of the Cerebrovascular and Senile Plaque Core Amyloid Deposits of Alzheimer′s Disease. Arch Biochem Biophys 301:41–52.

Milner B, Squire LR, Kandel ER (1998) Cognitive neuroscience and the study of memory. Neuron 20:445–468 Available at: http://www.sciencedirect.com/science/article/pii/S0896627300809873.

Mimuro M, Yoshida M, Miyao S, Harada T, Ishiguro K, Hashizume Y (2010) Neuronal and glial tau pathology in early frontotemporal lobar degeneration-tau, Pick's disease subtype. J Neurol Sci 290:177–182 Available at: http://dx.doi.org/10.1016/j.jns.2009.11.002.

Miron VE, Boyd A, Zhao JW, Yuen TJ, Ruckh JM, Shadrach JL, Van Wijngaarden P, Wagers AJ, Williams A, Franklin RJM, Ffrench-Constant C (2013) M2 microglia and macrophages drive oligodendrocyte differentiation during CNS remyelination. Nat Neurosci 16:1211–1218.

Mitew S, Gobius I, Fenlon LR, McDougall SJ, Hawkes D, Xing YL, Bujalka H, Gundlach AL, Richards LJ, Kilpatrick TJ, Merson TD, Emery B (2018) Pharmacogenetic stimulation of neuronal activity increases myelination in an axon-specific manner. Nat Commun 9:1–16 Available at: http://dx.doi.org/10.1038/s41467-017-02719-2.

Mitew S, Kirkcaldie MTK, Halliday GM, Shepherd CE, Vickers JC, Dickson TC (2010) Focal demyelination in Alzheimer's disease and transgenic mouse models. Acta Neuropathol 119:567–577.

Montarolo F, Martire S, Perga S, Spadaro M, Brescia I, Allegra S, De Francia S, Bertolotto A (2019) NURR1 deficiency is associated to ADHD-like phenotypes in mice. Transl Psychiatry 9

Available at: http://dx.doi.org/10.1038/s41398-019-0544-0.

Montez T, Poil SS, Jones BF, Manshanden I, Verbunt JPA, Van Dijk BW, Brussaard AB, Van Ooyen A, Stam CJ, Scheltens P, Linkenkaer-Hansen K (2009) Altered temporal correlations in parietal alpha and prefrontal theta oscillations in early-stage Alzheimer disease. Proc Natl Acad Sci U S A 106:1614–1619.

Morris M, Hamto P, Adame A, Devidze N, Masliah E, Mucke L (2013) Age-appropriate cognition and subtle dopamine-independent motor deficits in aged Tau knockout mice. Neurobiol Aging 34:1523–1529 Available at: http://dx.doi.org/10.1016/j.neurobiolaging.2012.12.003.

Mucke L, Masliah E, Yu G-Q, Mallory M, Rockenstein EM, Tatsuno G, Hu K, Kholodenko D, Johnson-Wood K, McConlogue L (2000) High-Level Neuronal Expression of Aβ 1–42 in Wild-Type Human Amyloid Protein Precursor Transgenic Mice: Synaptotoxicity without Plaque Formation. J Neurosci 20:4050–4058 Available at: http://www.jneurosci.org/lookup/doi/10.1523/JNEUROSCI.20-11-04050.2000.

Mullan M, Crawford F, Axelman K, Houlden H, Lilius L, Winblad B, Lannfelt L (1992) A pathogenic mutation for probable Alzheimer's disease in the APP gene at the N–terminus of β–amyloid. Nat Genet 1:345–347.

Müller R, Heinrich M, Heck S, Blohm D, Richter-Landsberg C (1997) Expression of microtubule-associated proteins MAP2 and tau in cultured rat brain oligodendrocytes. Cell Tissue Res 288:239–249 Available at: http://link.springer.com/article/10.1007/s004410050809.

Murakami K, Yokoyama S ichi, Murata N, Ozawa Y, Irie K, Shirasawa T, Shimizu T (2011) Insulin receptor mutation results in insulin resistance and hyperinsulinemia but does not exacerbate Alzheimer's-like phenotypes in mice. Biochem Biophys Res Commun 409:34–39 Available at: http://dx.doi.org/10.1016/j.bbrc.2011.04.101.

Murrell J, Farlow M, Ghetti B, Benson MD (1991) A mutation in the amyloid precursor protein associated with hereditary Alzheimer's disease. Science 254:97–99 Available at: http://www.ncbi.nlm.nih.gov/pubmed/1925564.

Myers AJ, Kaleem M, Marlowe L, Pittman AM, Lees AJ, Fung HC, Duckworth J, Leung D, Gibson A, Morris CM, de Silva R, Hardy J (2005) The H1c haplotype at the MAPT locus is associated with Alzheimer's disease. Hum Mol Genet 14:2399–2404.

Nagy B, Hovhannisyan A, Barzan R, Chen TJ, Kukley M (2017) Different patterns of neuronal activity trigger distinct responses of oligodendrocyte precursor cells in the corpus callosum.

Nair R, Lauks J, Jung SY, Cooke NE, de Wit H, Brose N, Kilimann MW, Verhage M, Rhee JS (2013) Neurobeachin regulates neurotransmitter receptor trafficking to synapses. J Cell Biol 200:61–80.

Nait-Oumesmar B, Decker L, Lachapelle F, Avellana-Adalid V, Bachelin C, Baron-Van Evercooren A, Evercooren V, Baron A (1999) Progenitor cells of the adult mouse subventricular zone proliferate, migrate and differentiate into oligodendrocytes after demyelination. Eur J Neurosci 11:4357–4366 Available at: http://onlinelibrary.wiley.com/doi/10.1046/j.1460-

9568.1999.00873.x/full.

Narasimhan S, Guo JL, Changolkar L, Stieber A, McBride JD, Silva L V., He Z, Zhang B, Gathagan RJ, Trojanowski JQ, Lee VMY (2017) Pathological Tau Strains from Human Brains Recapitulate the Diversity of Tauopathies in Nontransgenic Mouse Brain. J Neurosci 37:11406–11423.

Naruse M, Shibasaki K, Shimauchi-Ohtaki H, Ishizaki Y (2018) Microglial Activation Induces Generation of Oligodendrocyte Progenitor Cells from the Subventricular Zone after Focal Demyelination in the Corpus Callosum. Dev Neurosci 40:54–63.

Nasrabady SE, Rizvi B, Goldman JE, Brickman AM (2018) White matter changes in Alzheimer's disease: a focus on myelin and oligodendrocytes. Acta Neuropathol Commun 6:22.

Neve RL, Harris P, Kosik KS, Kurnit DM, Donlon TA (1986) Identification of cDNA clones for the human microtubule-associated protein tau and chromosomal localization of the genes for tau and microtubule-associated protein 2. Mol Brain Res 1:271–280 Available at: http://www.sciencedirect.com/science/article/pii/0169328X86900331.

Nielsen HM, Ek D, Avdic U, Orbjörn C, Hansson O, Veerhuis R, Rozemuller AJM, Brun A, Minthon L, Wennström M (2013) NG2 cells, a new trail for Alzheimer's disease mechanisms? Acta Neuropathol Commun 1:1 Available at: https://actaneurocomms.biomedcentral.com/articles/10.1186/2051-5960-1-7.

Nielsen HM, Hall S, Surova Y, Nägga K, Nilsson C, Londos E, Minthon L, Hansson O, Wennström M (2014) Low levels of soluble NG2 in cerebrospinal fluid from patients with dementia with lewy bodies. J Alzheimer's Dis 40:343–350.

Nishimura M, Tomimoto H, Suenaga T, Namba Y, Ikeda K, Akiguchi I, Kimura J (1995a) Immunocytochemical characterization of glial fibrillary tangles in Alzheimer's disease brain. Am J Pathol 146:1052–1058 Available at: http://www.ncbi.nlm.nih.gov/pubmed/7747799.

Nishimura T, Ikeda K, Akiyama H, Kondo H, Kato M, Li F, Iseki E, Kosaka K (1995b) Immunohistochemical investigation of tau-positive structures in the cerebral cortex of patients with progressive supranuclear palsy. Neurosci Lett 201:123–126.

Nishiyama A, Lin XH, Giese N, Heldin CH, Stallcup WB (1996) Co-localization of NG2 proteoglycan and PDGF α-receptor on O2A progenitor cells in the developing rat brain. J Neurosci Res 43:299–314.

Noack M, Leyk J, Richter-Landsberg C (2014) HDAC6 inhibition results in tau acetylation and modulates tau phosphorylation and degradation in oligodendrocytes. Glia 62:535–547.

Noack M, Richter-Landsberg C (2015) Activation of Autophagy by Rapamycin Does Not Protect Oligodendrocytes Against Protein Aggregate Formation and Cell Death Induced by Proteasomal Inhibition. J Mol Neurosci 55:99–108 Available at: http://link.springer.com/10.1007/s12031-014-0380-x.

Nunes MA, Schöwe NM, Monteiro-Silva KC, Baraldi-Tornisielo T, Souza SIG, Balthazar J,

Albuquerque MS, Caetano AL, Viel TA, Buck HS (2015) Chronic microdose lithium treatment prevented memory loss and neurohistopathological changes in a transgenic mouse model of Alzheimer's disease. PLoS One 10:1–26.

O'Brien JS, Sampson EL (1965) Lipid composition of the normal human brain: gray matter, white matter, and myelin. J Lipid Res 6:537–544 Available at: http://www.jlr.org/content/6/4/537.short.

O'Dwyer L, Lamberton F, Bokde ALW, Ewers M, Faluyi YO, Tanner C, Mazoyer B, O'Neill D, Bartley M, Collins DR, Coughlan T, Prvulovic D, Hampel H (2011) Multiple Indices of Diffusion Identifies White Matter Damage in Mild Cognitive Impairment and Alzheimer's Disease Ginsberg SD, ed. PLoS One 6:e21745 Available at: http://dx.plos.org/10.1371/journal.pone.0021745.

O'Leary TP, Robertson A, Chipman PH, Rafuse VF, Brown RE (2018) Motor function deficits in the 12 month-old female 5xFAD mouse model of Alzheimer's disease. Behav Brain Res 337:256–263 Available at: http://dx.doi.org/10.1016/j.bbr.2017.09.009.

O'Rourke M, Cullen CL, Auderset L, Pitman KA, Achatz D, Gasperini R, Young KM (2016) Evaluating tissue-specific recombination in a Pdgfra-CreER T2 transgenic mouse line. PLoS One 11:1–19.

Oakley H, Cole SL, Logan S, Maus E, Shao P, Craft J, Guillozet-Bongaarts A, Ohno M, Disterhoft J, Van Eldik L, Berry R, Vassar R (2006) Intraneuronal beta-Amyloid Aggregates, Neurodegeneration, and Neuron Loss in Transgenic Mice with Five Familial Alzheimer's Disease Mutations: Potential Factors in Amyloid Plaque Formation. J Neurosci 26:10129–10140 Available at: http://www.jneurosci.org/cgi/doi/10.1523/JNEUROSCI.1202-06.2006.

Oddo S, Billings L, Kesslak JP, Cribbs DH, LaFerla FM (2004) Aβ Immunotherapy Leads to Clearance of Early, but Not Late, Hyperphosphorylated Tau Aggregates via the Proteasome. Neuron 43:321–332 Available at: https://linkinghub.elsevier.com/retrieve/pii/S0896627304004246.

Ong WY, Tanaka K, Dawe GS, Ittner LM, Farooqui AA (2013) Slow excitotoxicity in alzheimer's disease. J Alzheimer's Dis 35:643–668.

Ossola B, Zhao C, Compston A, Pluchino S, Franklin RJMM, Spillantini MG (2016) Neuronal expression of pathological tau accelerates oligodendrocyte progenitor cell differentiation. Glia 64:457–471.

Ota M, Sato N, Kimura Y, Shigemoto Y, Kunugi H, Matsuda H (2019) Changes of Myelin Organization in Patients with Alzheimer's Disease Shown by q-Space Myelin Map Imaging. Dement Geriatr Cogn Dis Extra 9:24–33.

Ou-Yang MH, Xu F, Liao MC, Davis J, Robinson JK, Van Nostrand WE (2015) The N-terminal region of myelin basic protein reduces fibrillar amyloid-β deposition in Tg-5xFAD mice. Neurobiol Aging 36:801–811 Available at:

http://dx.doi.org/10.1016/j.neurobiolaging.2014.10.006.

Palop JJ, Chin J, Roberson ED, Wang J, Thwin MT, Bien-Ly N, Yoo J, Ho KO, Yu G-Q, Kreitzer A, Finkbeiner S, Noebels JL, Mucke L (2007) Aberrant Excitatory Neuronal Activity and Compensatory Remodeling of Inhibitory Hippocampal Circuits in Mouse Models of Alzheimer's Disease. Neuron 55:697–711 Available at: http://linkinghub.elsevier.com/retrieve/pii/S0896627307005703.

Palop JJ, Jones B, Kekonius L, Chin J, Yu G-Q, Raber J, Masliah E, Mucke L (2003) Neuronal depletion of calcium-dependent proteins in the dentate gyrus is tightly linked to Alzheimer's disease-related cognitive deficits. Proc Natl Acad Sci 100:9572–9577 Available at: http://www.pnas.org/content/100/16/9572.short.

Panda D, Samuel JC, Massie M, Feinstein SC, Wilson L (2003) Differential regulation of microtubule dynamics by three- and four-repeat tau: Implications for the onset of neurodegenerative disease. Proc Natl Acad Sci U S A 100:9548–9553.

Paolicelli RC, Bolasco G, Pagani F, Maggi L, Scianni M, Panzanelli P, Giustetto M, Ferreira TA, Guiducci E, Dumas L, Ragozzino D, Gross CT (2011) Synaptic Pruning by Microglia Is Necessary for Normal Brain Development. 333:1456–1459.

Paula-Lima AC, De Felice FG, Brito-Moreira J, Ferreira ST (2005) Activation of GABAA receptors by taurine and muscimol blocks the neurotoxicity of β-amyloid in rat hippocampal and cortical neurons. Neuropharmacology 49:1140–1148.

Pennanen C, Kivipelto M, Tuomainen S, Hartikainen P, Hänninen T, Laakso MP, Hallikainen M, Vanhanen M, Nissinen A, Helkala E-L, Vainio P, Vanninen R, Partanen K, Soininen H (2004) Hippocampus and entorhinal cortex in mild cognitive impairment and early AD. Neurobiol Aging 25:303–310 Available at: http://linkinghub.elsevier.com/retrieve/pii/S0197458003000848.

Pepper RE, Pitman KA, Cullen CL, Young KM (2018) How Do Cells of the Oligodendrocyte Lineage Affect Neuronal Circuits to Influence Motor Function, Memory and Mood? Front Cell Neurosci 12:399 Available at: https://www.frontiersin.org/article/10.3389/fncel.2018.00399/full.

Pervolaraki E, Hall SP, Foresteire D, Saito T, Saido TC, Whittington MA, Lever C, Dachtler J (2019) Insoluble Aβ overexpression in an App knock-in mouse model alters microstructure and gamma oscillations in the prefrontal cortex, affecting anxiety-related behaviours . Dis Model Mech 12:dmm040550.

Peters A (2004) Oligodendrocytes, their Progenitors and other Neuroglial Cells in the Aging Primate Cerebral Cortex. Cereb Cortex 14:995–1007 Available at: http://cercor.oxfordjournals.org/cgi/doi/10.1093/cercor/bhh060.

Philips T, Bento-Abreu A, Nonneman A, Haeck W, Staats K, Geelen V, Hersmus N, Kusters B, Van Den Bosch L, Van Damme P, Richardson WD, Robberecht W (2013) Oligodendrocyte dysfunction in the pathogenesis of amyotrophic lateral sclerosis. Brain 136:471–482 Available

at: http://www.brain.oxfordjournals.org/cgi/doi/10.1093/brain/aws339.

Picard-Riera N, Decker L, Delarasse C, Goude K, Nait-Oumesmar B, Liblau R, Pham-Dinh D, Baron-Van Evercooren A, Evercooren AB-V (2002) Experimental autoimmune encephalomyelitis mobilizes neural progenitors from the subventricular zone to undergo oligodendrogenesis in adult mice. Proc Natl Acad Sci 99:13211–13216 Available at: http://www.pnas.org/content/99/20/13211.short.

Potier B, Billard JM, Rivière S, Sinet PM, Denis I, Champeil-Potokar G, Grintal B, Jouvenceau A, Kollen M, Dutar P (2010) Reduction in glutamate uptake is associated with extrasynaptic NMDA and metabotropic glutamate receptor activation at the hippocampal CA1 synapse of aged rats. Aging Cell 9:722–735.

Potter H, Granic A, Caneus J (2016) Role of trisomy 21 mosaicism in sporadic and familial Alzheimer's disease. Curr Alzheimer Res 13:7–17 Available at: http://www.ingentaconnect.com/content/ben/car/2016/00000013/00000001/art00003.

Powers BE, Sellers DL, Lovelett EA, Cheung W, Aalami SP, Zapertov N, Maris DO, Horner PJ (2013) Remyelination reporter reveals prolonged refinement of spontaneously regenerated myelin. Proc Natl Acad Sci 110:4075–4080 Available at: http://www.pubmedcentral.nih.gov/articlerender.fcgi?artid=3593891&tool=pmcentrez&rendertype=abstract.

Prado Lima MG, Schimidt HL, Garcia A, Daré LR, Carpes FP, Izquierdo I, Mello-Carpes PB (2018) Environmental enrichment and exercise are better than social enrichment to reduce memory deficits in amyloid beta neurotoxicity. Proc Natl Acad Sci U S A 115:E2403–E2409.

Prineas JW, Connell F (1979) Remyelination in multiple sclerosis. Ann Neurol 5:22–31 Available at: http://onlinelibrary.wiley.com/doi/10.1002/ana.410050105/full.

Pringle NP, Mudhar HS, Collarini EJ, Richardson WD (1992) PDGF receptors in the rat CNS: during late neurogenesis, PDGF alpha-receptor expression appears to be restricted to glial cells of the oligodendrocyte lineage. Development 115:535–551 Available at: http://www.ncbi.nlm.nih.gov/pubmed/1425339.

Psachoulia K, Jamen F, Young KM, Richardson WD (2009) Cell cycle dynamics of NG2 cells in the postnatal and ageing brain. Neuron Glia Biol 5:57 Available at: http://www.journals.cambridge.org/abstract_S1740925X09990354.

Pu D, Zhao Y, Chen J, Sun Y, Lv A, Zhu S, Luo C, Zhao K, Xiao Q (2018) Protective Effects of Sulforaphane on Cognitive Impairments and AD-like Lesions in Diabetic Mice are Associated with the Upregulation of Nrf2 Transcription Activity. Neuroscience 381:35–45 Available at: https://doi.org/10.1016/j.neuroscience.2018.04.017.

Qiang L, Sun X, Austin TO, Muralidharan H, Jean DC, Liu M, Yu W, Baas PW (2018) Tau Does Not Stabilize Axonal Microtubules but Rather Enables Them to Have Long Labile Domains. Curr Biol 28:2181-2189.e4 Available at: https://doi.org/10.1016/j.cub.2018.05.045.

Qiang W, Yau W-MM, Lu J-XX, Collinge J, Tycko R (2017) Structural variation in amyloid-β fibrils from Alzheimer's disease clinical subtypes. Nature 541:217–221 Available at: http://dx.doi.org/10.1038/nature20814.

Racine AM, Adluru N, Alexander AL, Christian BT, Okonkwo OC, Oh J, Cleary CA, Birdsill A, Hillmer AT, Murali D, Barnhart TE, Gallagher CL, Carlsson CM, Rowley HA, Dowling NM, Asthana S, Sager MA, Bendlin BB, Johnson SC (2014) Associations between white matter microstructure and amyloid burden in preclinical Alzheimer's disease: A multimodal imaging investigation. NeuroImage Clin 4:604–614 Available at: http://dx.doi.org/10.1016/j.nicl.2014.02.001.

Radde R, Bolmont T, Kaeser SA, Coomaraswamy J, Lindau D, Stoltze L, Calhoun ME, Jäggi F, Wolburg H, Gengler S, Haass C, Ghetti B, Czech C, Hölscher C, Mathews PM, Jucker M (2006) Aβ42-driven cerebral amyloidosis in transgenic mice reveals early and robust pathology. EMBO Rep 7:940–946 Available at: http://embor.embopress.org/cgi/doi/10.1038/sj.embor.7400784.

Raff MC, Miller RH, Noble M (1983) A glial progenitor cell that develops in vitro into an astrocyte or an oligodendrocyte depending on culture medium. Nature 303:390–396 Available at: http://www.nature.com/nature/journal/v303/n5916/pdf/303390a0.pdf%5Cnpapers2://publication/uuid/921DEA33-1577-409F-B703-F8000C1C0AEA.

Raff MC, Mirsky R, Fields KL, Lisak RP, Dorfman SH, Silberberg DH, Gregson NA, Leibowitz S, Kennedy MC (1978) Galactocerebroside is a specific cell-surface antigenic marker for oligodendrocytes in culture. Nature 274:813–816.

Ramírez BG, Blázquez C, Gómez del Pulgar T, Guzmán M, de Ceballos ML (2005) Prevention of Alzheimer's disease pathology by cannabinoids: neuroprotection mediated by blockade of microglial activation. J Neurosci 25:1904–1913 Available at: http://www.jneurosci.org/cgi/doi/10.1523/JNEUROSCI.4540-04.2005.

Ramsden M, Kotilinek L, Forster C, Paulson J, McGowan E, SantaCruz K, Guimaraes A, Yue M, Lewis J, Carlson G, Hutton M, Ashe KH (2005) Age-dependent neurofibrillary tangle formation, neuron loss, and memory impairment in a mouse model of human tauopathy (P301L). J Neurosci 25:10637–10647.

Reisberg B, Franssen EH, Hasan SM, Monteiro I, Boksay I, Souren LEM, Kenowsky S, Auer SR, Elahi S, Kluger A (1999) Retrogenesis: Clinical, physiologic, and pathologic mechanisms in brain aging, Alzheimer's and other dementing processes. Eur Arch Psychiatry Clin Neurosci 249:28–36.

Rémy F, Vayssière N, Saint-Aubert L, Barbeau E, Pariente J (2015) White matter disruption at the prodromal stage of Alzheimer's disease: Relationships with hippocampal atrophy and episodic memory performance. NeuroImage Clin 7:482–492 Available at: http://dx.doi.org/10.1016/j.nicl.2015.01.014.

Ren Y, Lin WL, Sanchez L, Ceballos C, Polydoro M, Spires-Jones TL, Hyman BT, Dickson DW,

Sahara N (2014) Endogenous tau aggregates in oligodendrocytes of rTg4510 mice induced by human P301L tau. J Alzheimer's Dis 38:589–600.

Reynolds ES (1963) THE USE OF LEAD CITRATE AT HIGH pH AS AN ELECTRON-OPAQUE STAIN IN ELECTRON MICROSCOPY. J Cell Biol 17:208–212 Available at: https://rupress.org/jcb/article/17/1/208/1220/THE-USE-OF-LEAD-CITRATE-AT-HIGH-pH-AS-AN.

Rice HC, de Malmazet D, Schreurs A, Frere S, Van Molle I, Volkov AN, Creemers E, Vertkin I, Nys J, Ranaivoson FM, Comoletti D, Savas JN, Remaut H, Balschun D, Wierda KD, Slutsky I, Farrow K, De Strooper B, de Wit J (2019) Secreted amyloid-β precursor protein functions as a GABA B R1a ligand to modulate synaptic transmission. Science (80-) 363:eaao4827 Available at: https://www.sciencemag.org/lookup/doi/10.1126/science.aao4827.

Richter-Landsberg C (2016) Protein aggregate formation in oligodendrocytes: tau and the cytoskeleton at the intersection of neuroprotection and neurodegeneration. Biol Chem 397:185–194 Available at: http://www.degruyter.com/view/j/bchm.2016.397.issue-3/hsz-2015-0157/hsz-2015-0157.xml.

Richter-Landsberg C, Gorath M (1999) Developmental regulation of alternatively spliced isoforms of mRNA encoding MAP2 and tau in rat brain oligodendrocytes during culture maturation. J Neurosci Res 56:259–270.

Rivers LE, Young KM, Rizzi M, Jamen F, Psachoulia K, Wade A, Kessaris N, Richardson WD (2008) PDGFRA/NG2 glia generate myelinating oligodendrocytes and piriform projection neurons in adult mice. Nat Neurosci 11:1392–1401 Available at: http://www.nature.com/doifinder/10.1038/nn.2220.

Roher AE et al. (2009) Amyloid beta peptides in human plasma and tissues and their significance for Alzheimer's disease. Alzheimer's Dement 5:18–29 Available at: http://linkinghub.elsevier.com/retrieve/pii/S1552526008028963.

Roher AE, Lowenson JD, Clarke S, Wolkow C, Wang R, Cotter RJ, Reardon IM, Zurcher-Neely HA, Heinrikson RL, Ball MJ, Greenberg BD (1993) Structural alterations in the peptide backbone of β-amyloid core protein may account for its deposition and stability in Alzheimer's disease. J Biol Chem 268:3072–3083.

Roher AE, Weiss N, Kokjohn TA, Kuo Y-MM, Kalback W, Anthony J, Watson D, Luehrs DC, Sue L, Walker D, Emmerling M, Goux W, Beach T (2002) Increased Aβ peptides and reduced cholesterol and myelin proteins characterize white matter degeneration in Alzheimer's disease. Biochemistry 41:11080–11090 Available at: http://pubs.acs.org/doi/abs/10.1021/bi026173d.

Rone MB, Cui QL, Fang J, Wang LC, Zhang J, Khan D, Bedard M, Almazan G, Ludwin SK, Jones R, Kennedy TE, Antel JP (2016) Oligodendrogliopathy in multiple sclerosis: Low glycolytic metabolic rate promotes oligodendrocyte survival. J Neurosci 36:4698–4707.

Rose SE, Chen F, Chalk JB, Zelaya FO, Strugnell WE, Benson M, Semple J, Doddrell DM (2000)

Loss of connectivity in Alzheimer's disease: an evaluation of white matter tract integrity with colour coded MR diffusion tensor imaging. J Neurol Neurosurg Psychiatry 69:528–530 Available at: http://jnnp.bmj.com/content/69/4/528.short.

Rosenbluth J, Nave K-A, Mierzwa A, Schiff R (2006) Subtle myelin defects in PLP-null mice. Glia 54:172–182 Available at: http://www.ncbi.nlm.nih.gov/pubmed/17659524.

Roy U, Stute L, Höfling C, Hartlage-Rübsamen M, Matysik J, Roβner S, Alia A (2018) Sex- and age-specific modulation of brain GABA levels in a mouse model of Alzheimer's disease. Neurobiol Aging 62:168–179 Available at: https://doi.org/10.1016/j.neurobiolaging.2017.10.015.

Saher G, Brügger B, Lappe-Siefke C, Möbius W, Tozawa R, Wehr MC, Wieland F, Ishibashi S, Nave K-A (2005) High cholesterol level is essential for myelin membrane growth. Nat Neurosci 8:468–475 Available at: http://www.nature.com/doifinder/10.1038/nn1426.

Sampaio-Baptista C, Khrapitchev AA, Foxley S, Schlagheck T, Scholz J, Jbabdi S, DeLuca GC, Miller KL, Taylor A, Thomas N, Kleim J, Sibson NR, Bannerman D, Johansen-Berg H (2013) Motor Skill Learning Induces Changes in White Matter Microstructure and Myelination. J Neurosci 33:19499–19503 Available at: http://www.jneurosci.org/cgi/doi/10.1523/JNEUROSCI.3048-13.2013.

Sanchez PE, Zhu L, Verret L, Vossel KA, Orr AG, Cirrito JR, Devidze N, Ho K, Yu G-Q, Palop JJ, Mucke L (2012) Levetiracetam suppresses neuronal network dysfunction and reverses synaptic and cognitive deficits in an Alzheimer's disease model. Proc Natl Acad Sci 109:E2895–E2903 Available at: http://www.pnas.org/cgi/doi/10.1073/pnas.1121081109.

Sanderson TM, Bradley CA, Georgiou J, Hong YH, Ng AN, Lee Y, Kim HD, Kim D, Amici M, Son GH, Zhuo M, Kim K, Kaang BK, Kim SJ, Collingridge GL (2018) The Probability of Neurotransmitter Release Governs AMPA Receptor Trafficking via Activity-Dependent Regulation of mGluR1 Surface Expression. Cell Rep 25:3631-3646.e3.

Santacruz K et al. (2005) Tau suppression in a neurodegenerative mouse model improves memory function. Science 309:476–481 Available at: http://www.sciencemag.org/cgi/doi/10.1126/science.1113694.

Sbardella E, Petsas N, Tona F, Prosperini L, Raz E, Pace G, Pozzilli C, Pantano P (2013) Assessing the Correlation between Grey and White Matter Damage with Motor and Cognitive Impairment in Multiple Sclerosis Patients Villoslada P, ed. PLoS One 8:e63250 Available at: http://dx.plos.org/10.1371/journal.pone.0063250.

Scheuner D et al. (1996) Secreted amyloid β–protein similar to that in the senile plaques of Alzheimer's disease is increased in vivo by the presenilin 1 and 2 and APP mutations linked to familial Alzheimer's disease. Nat Med 2:864–870 Available at: http://www.nature.com/articles/nm0896-864.

Schirmer L et al. (2019) Neuronal vulnerability and multilineage diversity in multiple sclerosis. Nature 573:75–82 Available at: http://dx.doi.org/10.1038/s41586-019-1404-z.

Schmidt ML, Lee VM-Y, Trojanowski JQ (1990) Relative abundance of tau and neurofilament epitopes in hippocampal neurofibrillary tangles. Am J Pathol 136:1069–1075 Available at: http://www.ncbi.nlm.nih.gov/pubmed/1693468.

Schmued LC, Raymick J, Paule MG, Dumas M, Sarkar S (2013) Characterization of myelin pathology in the hippocampal complex of a transgenic mouse model of Alzheimer's disease. Curr Alzheimer Res 10:30–37 Available at: http://www.ingentaconnect.com/content/ben/car/2013/00000010/00000001/art00005.

Schneider A, Biernat J, von Bergen M, Mandelkow E-M, Mandelkow E-M (1999) Phosphorylation that Detaches Tau Protein from Microtubules (Ser262, Ser214) Also Protects It against Aggregation into Alzheimer Paired Helical Filaments †. Biochemistry 38:3549–3558 Available at: http://pubs.acs.org/doi/abs/10.1021/bi981874p.

Scholz J, Klein MC, Behrens TEJ, Johansen-Berg H (2009) Training induces changes in white-matter architecture. Nat Neurosci 12:1370–1371 Available at: http://www.nature.com/articles/nn.2412.

Scolding NJ, Frith S, Linington C, Morgan BP, Campbell AK, Compston DAS (1989) Myelin-oligodendrocyte glycoprotein (MOG) is a surface marker of oligodendrocyte maturation. J Neuroimmunol 22:169–176 Available at: https://linkinghub.elsevier.com/retrieve/pii/0165572889900143.

Scott HL, Pow D V, Tannenberg AEG, Dodd PR (2002) Aberrant expression of the glutamate transporter excitatory amino acid transporter 1 (EAAT1) in Alzheimer's disease. J Neurosci 22:RC206–1 Available at: https://espace.library.uq.edu.au/view/UQ:115033.

Scott JA, Braskie MN, Tosun D, Thompson PM, Weiner M, DeCarli C, Carmichael OT (2015) Cerebral Amyloid and Hypertension are Independently Associated with White Matter Lesions in Elderly. Front Aging Neurosci 7:1–9 Available at: http://journal.frontiersin.org/article/10.3389/fnagi.2015.00221.

Seiberlich V, Bauer NG, Schwarz L, Ffrench-Constant C, Goldbaum O, Richter-Landsberg C (2015) Downregulation of the microtubule associated protein Tau impairs process outgrowth and myelin basic protein mRNA transport in oligodendrocytes. Glia 63:1621–1635.

Selkoe DJ (2001) Alzheimer's disease: genes, proteins, and therapy. Physiol Rev 81:741–766 Available at: http://physrev.physiology.org/.

Selkoe DJ, Hardy J (2016) The amyloid hypothesis of Alzheimer's disease at 25 years. EMBO Mol Med 8:595–608 Available at: http://embomolmed.embopress.org/lookup/doi/10.15252/emmm.201606210.

Serneels L et al. (2009) γ-Secretase heterogeneity in the aph1 subunit: Relevance for alzheimer's disease. Science (80-) 324:639–642.

Serrano-Regal MP, Luengas-Escuza I, Bayón-Cordero L, Ibarra-Aizpurua N, Alberdi E, Pérez-Samartín A, Matute C, Sánchez-Gómez MV (2019) Oligodendrocyte Differentiation and Myelination Is Potentiated via GABAB Receptor Activation. Neuroscience.

Serwanski D, Rasmussen A, Brunquell C, Perkins S, Nishiyama A (2018) Sequential Contribution of Parenchymal and Neural Stem Cell-Derived Oligodendrocyte Precursor Cells toward Remyelination. Neuroglia 1:8 Available at: http://www.mdpi.com/2571-6980/1/1/8.

Shi L, Zhao L, Wong A, Wang D, Mok V (2015) Mapping the Relationship of Contributing Factors for Preclinical Alzheimer's Disease. Sci Rep 5:1–9 Available at: http://dx.doi.org/10.1038/srep11259.

Shigematsu H, Imasaki T, Doki C, Sumi T, Aoki M, Uchikubo-Kamo T, Sakamoto A, Tokuraku K, Shirouzu M, Nitta R (2018) Structural insight into microtubule stabilization and kinesin inhibition by Tau family MAPs. J Cell Biol 217:4155–4163.

Shigemoto-Mogami Y, Hoshikawa K, Goldman JE, Sekino Y, Sato K (2014) Microglia Enhance Neurogenesis and Oligodendrogenesis in the Early Postnatal Subventricular Zone. J Neurosci 34:2231–2243 Available at: http://www.jneurosci.org/cgi/doi/10.1523/JNEUROSCI.1619-13.2014.

Sibille J, Dao Duc K, Holcman D, Rouach N (2015) The Neuroglial Potassium Cycle during Neurotransmission: Role of Kir4.1 Channels. PLoS Comput Biol 11:1–22.

Simons M, Nave K-A (2016) Oligodendrocytes: Myelination and Axonal Support. Cold Spring Harb Perspect Biol 8:a020479 Available at: http://cshperspectives.cshlp.org/lookup/doi/10.1101/cshperspect.a020479.

Sindou P, Lesort M, Couratier P, Yardin C, Esclaire F, Hugon J (1994) Glutamate increases tau phosphorylation in primary neuronal cultures from fetal rat cerebral cortex. Brain Res 646:124–128.

Smith R (2004) Moving Molecules: mRNA Trafficking in Mammalian Oligodendrocytes and Neurons. Neurosci 10:495–500 Available at: http://nro.sagepub.com/cgi/doi/10.1177/1073858404266759.

Snaidero N, Möbius W, Czopka T, Hekking LHP, Mathisen C, Verkleij D, Goebbels S, Edgar J, Merkler D, Lyons DA, Nave K-A, Simons M (2014) Myelin Membrane Wrapping of CNS Axons by PI(3,4,5)P3-Dependent Polarized Growth at the Inner Tongue. Cell 156:277–290 Available at: http://linkinghub.elsevier.com/retrieve/pii/S0092867413015304.

Snaidero N, Velte C, Myllykoski M, Raasakka A, Ignatev A, Werner HB, Erwig MS, Möbius W, Kursula P, Nave KA, Simons M (2017) Antagonistic Functions of MBP and CNP Establish Cytosolic Channels in CNS Myelin. Cell Rep 18:314–323.

Snowden SG, Ebshiana AA, Hye A, Pletnikova O, O'Brien R, Yang A, Troncoso J, Legido-Quigley C, Thambisetty M (2019) Neurotransmitter Imbalance in the Brain and Alzheimer's Disease Pathology. J Alzheimer's Dis:1–9.

Spillantini MG, Crowther RA, Kamphorst W, Heutink P, Van Swieten JC (1998) Tau pathology in two Dutch families with mutations in the microtubule- binding region of tau. Am J Pathol 153:1359–1363 Available at: http://dx.doi.org/10.1016/S0002-9440(10)65721-5.

Squire LR, Zola SM (1996) Structure and function of declarative and nondeclarative memory systems. Proc Natl Acad Sci 93:13515–13522 Available at: http://www.pnas.org/cgi/doi/10.1073/pnas.93.24.13515.

Srinivas S, Watanabe T, Lin C-S, William CM, Tanabe Y, Jessell TM, Costantini F (2001) Cre reporter strains produced by targeted insertion of EYFP and ECFP into the ROSA26 locus. BMC Dev Biol 1:1 Available at: http://bmcdevbiol.biomedcentral.com/articles/10.1186/1471-213X-1-4.

Stassart RM, Möbius W, Nave K-A, Edgar JM (2018) The Axon-Myelin Unit in Development and Degenerative Disease. Front Neurosci 12:467 Available at: https://www.frontiersin.org/article/10.3389/fnins.2018.00467/full.

Steiner H, Capell A, Pesold B, Keck S, Baader M, Haass C, Duff K, Picciano M, Romig H, Fechteler K, Grim MG, Baumeister R, Lincoln S, Hardy J, Yu X, Citron M, Kopan R, Tomita T, Iwatsubo T (1999) A loss of function mutation of presenilin-2 interferes with amyloid β- peptide production and Notch signaling. J Biol Chem 274:28669–28673.

Stelzmann RA, Norman Schnitzlein H, Reed Murtagh F (1995) An english translation of Alzheimer's 1907 paper. Clin Anat 8:429–431.

Stidworthy MF, Genoud S, Suter U, Mantei N, Franklin RJM (2003) Quantifying the Early Stages of Remyelination Following Cuprizone-induced Demyelination. Brain Pathol 13:329–339 Available at: http://onlinelibrary.wiley.com/doi/10.1111/j.1750-3639.2003.tb00032.x/full.

Stojic A, Bojcevski J, Williams SK, Diem R, Fairless R (2018) Early nodal and paranodal disruption in autoimmune optic neuritis. J Neuropathol Exp Neurol 77:361–373.

Stricker NH, Schweinsburg BC, Delano-Wood L, Wierenga CE, Bangen KJ, Haaland KY, Frank LR, Salmon DP, Bondi MW (2009) Decreased white matter integrity in late-myelinating fiber pathways in Alzheimer's disease supports retrogenesis. Neuroimage 45:10–16 Available at: http://linkinghub.elsevier.com/retrieve/pii/S1053811908012317.

Sugiarto S, Persson AI, Munoz EG, Waldhuber M, Lamagna C, Andor N, Hanecker P, Ayers-Ringler J, Phillips J, Siu J, Lim DA, Vandenberg S, Stallcup W, Berger MS, Bergers G, Weiss WA, Petritsch C (2011) Asymmetry-Defective Oligodendrocyte Progenitors Are Glioma Precursors. Cancer Cell 20:328–340 Available at: http://linkinghub.elsevier.com/retrieve/pii/S1535610811003084.

Sun A, Nguyen X V., Bing G (2002) Comparative analysis of an improved thioflavin-S stain, Gallyas silver stain, and immunohistochemistry for neurofibrillary tangle demonstration on the same sections. J Histochem Cytochem 50:463–472.

Sun B, Halabisky B, Zhou Y, Palop JJ, Yu G, Mucke L, Gan L (2009) Imbalance between GABAergic and Glutamatergic Transmission Impairs Adult Neurogenesis in an Animal Model of Alzheimer's Disease. Cell Stem Cell 5:624–633 Available at: http://linkinghub.elsevier.com/retrieve/pii/S1934590909005141.

Takasugi N, Tomita T, Hayashi I, Tsuruoka M, Niimura M, Takahashi Y, Thinakaran G, Iwatsubo T (2003) The role of presenilin cofactors in the gamma-secretase complex. Nature 422:438–441 Available at: http://www.ncbi.nlm.nih.gov/pubmed/12660785.

Takeuchi H, Iba M, Inoue H, Higuchi M, Takao K, Tsukita K, Karatsu Y, Iwamoto Y, Miyakawa T, Suhara T, Trojanowski JQ, Lee VM-Y, Takahashi R (2011) P301S Mutant Human Tau Transgenic Mice Manifest Early Symptoms of Human Tauopathies with Dementia and Altered Sensorimotor Gating Bush AI, ed. PLoS One 6:e21050 Available at: http://dx.plos.org/10.1371/journal.pone.0021050.

Talantova M et al. (2013) Aβ induces astrocytic glutamate release, extrasynaptic NMDA receptor activation, and synaptic loss. Proc Natl Acad Sci U S A 110.

Tan DCS, Yao S, Ittner A, Bertz J, Ke YD, Ittner LM, Delerue F (2018) Generation of a New Tau Knockout (tau Δex1) Line Using CRISPR/Cas9 Genome Editing in Mice. J Alzheimer's Dis 62:571–578.

Tanaka J, Okuma Y, Tomobe K, Nomura Y (2005) The age-related degeneration of oligodendrocytes in the hippocampus of the senescence-accelerated mouse (SAM) P8: A quantitative immunohistochemical study. Biol Pharm Bull 28:615–618.

Tang BL (2019) Amyloid Precursor Protein (APP) and GABAergic Neurotransmission. Cells 8:550.

Tang X, Wu D, Gu LH, Nie B Bin, Qi XY, Wang YJ, Wu FF, Li XL, Bai F, Chen XC, Xu L, Ren QG, Zhang ZJ (2016) Spatial learning and memory impairments are associated with increased neuronal activity in 5XFAD mouse as measured by manganese-enhanced magnetic resonance imaging. Oncotarget 7:57556–57570.

Taveggia C, Thaker P, Petrylak A, Caporaso GL, Toews A, Falls DL, Einheber S, Salzer JL (2008) Type III neuregulin-1 promotes oligodendrocyte myelination. Glia 56:284–293 Available at: http://doi.wiley.com/10.1002/glia.20612.

Taveggia C, Zanazzi G, Petrylak A, Yano H, Rosenbluth J, Einheber S, Xu X, Esper RM, Loeb JA, Shrager P, Chao M V., Falls DL, Role L, Salzer JL (2005) Neuregulin-1 Type III Determines the Ensheathment Fate of Axons. Neuron 47:681–694 Available at: http://www.sciencedirect.com/science/article/pii/S0896627305006926.

Tkachev D, Mimmack ML, Ryan MM, Wayland M, Freeman T, Jones PB, Starkey M, Webster MJ, Yolken RH, Bahn S (2003) Oligodendrocyte dysfunction in schizophrenia and bipolar disorder. Lancet 362:798–805 Available at: https://linkinghub.elsevier.com/retrieve/pii/S0140673603142894.

Traka M, Podojil JR, Mccarthy DP, Miller SD, Popko B (2015) Oligodendrocyte death results in immune-mediated CNS demyelination. Nat Neurosci 19:65–74.

Trapp BD, Nishiyama A, Cheng D, Macklin W (1997) Differentiation and death of premyelinating oligodendrocytes in developing rodent brain. J Cell Biol 137:459–468 Available at: http://jcb.rupress.org/content/137/2/459.abstract.

Tremblay P, Bouzamondo-Bernstein E, Heinrich C, Prusiner SB, DeArmond SJ (2007) Developmental expression of PrP in the post-implantation embryo. Brain Res 1139:60–67 Available at: https://linkinghub.elsevier.com/retrieve/pii/S0006899306035803.

Tripathi RB, Jackiewicz M, McKenzie IA, Kougioumtzidou E, Grist M, Richardson WD (2017) Remarkable Stability of Myelinating Oligodendrocytes in Mice. Cell Rep 21:316–323.

Tripathi RB, Rivers LE, Young KM, Jamen F, Richardson WD (2010) NG2 Glia Generate New Oligodendrocytes But Few Astrocytes in a Murine Experimental Autoimmune Encephalomyelitis Model of Demyelinating Disease. J Neurosci 30:16383–16390 Available at: http://www.jneurosci.org/cgi/doi/10.1523/JNEUROSCI.3411-10.2010.

Truong PH, Ciccotosto GD, Merson TD, Spoerri L, Chuei MJ, Ayers M, Xing YL, Emery B, Cappai R (2019) Amyloid precursor protein and amyloid precursor-like protein 2 have distinct roles in modulating myelination, demyelination, and remyelination of axons. Glia 67:525–538 Available at: http://doi.wiley.com/10.1002/glia.23561.

Tse K-H, Cheng A, Ma F, Herrup K (2018) DNA damage-associated oligodendrocyte degeneration precedes amyloid pathology and contributes to Alzheimer's disease and dementia. Alzheimer's Dement 14:664–679 Available at: https://linkinghub.elsevier.com/retrieve/pii/S1552526017338530.

Utton MA, Vandecandelaere A, Wagner U, Reynolds CH, Gibb GM, Miller CCJ, Bayley PM, Anderton BH (1997) Phosphorylation of tau by glycogen synthase kinase 3β affects the ability of tau to promote microtubule self-assembly. Biochem J 323:741–747.

Van Der Flier WM, Van Den Heuvel DMJ, Weverling-Rijnsburger AWE, Bollen ELEM, Westendorp RGJ, Van Buchem MA, Middelkoop HAM (2002) Magnetization transfer imaging in normal aging, mild cognitive impairment, and Alzheimer's disease. Ann Neurol 52:62–67 Available at: http://doi.wiley.com/10.1002/ana.10244.

Van Groen T, Miettinen P, Kadish I (2014) Axonal tract tracing for delineating interacting brain regions: Implications for Alzheimer's disease-associated memory. Future Neurol 9:89–98.

Van Hummel A, Bi M, Ippati S, Van Der Hoven J, Volkerling A, Lee WS, Tan DCS, Bongers A, Ittner A, Ke YD, Ittner LM (2016) No overt deficits in aged tau-deficient C57Bl/6.Mapttm1(EGFP)kit GFP knockin mice. PLoS One 11:1–14.

Vassar R et al. (1999) Beta-secretase cleavage of Alzheimer's amyloid precursor protein by the transmembrane aspartic protease BACE. Science 286:735–741 Available at: http://science.sciencemag.org/.

Velanac V, Unterbarnscheidt T, Hinrichs W, Gummert MN, Fischer TM, Rossner MJ, Trimarco A, Brivio V, Taveggia C, Willem M, Haass C, Möbius W, Nave KA, Schwab MH (2012) Bace1 processing of NRG1 type III produces a myelin-inducing signal but is not essential for the stimulation of myelination. Glia 60:203–217.

Velasco I, Tapia R (2002) High extracellular γ-aminobutyric acid protects cultured neurons against

damage induced by the accumulation of endogenous extracellular glutamate. J Neurosci Res 67:406–410.

Venkatramani A, Panda D (2019) Regulation of neuronal microtubule dynamics by tau: Implications for tauopathies. Int J Biol Macromol 133:473–483 Available at: https://doi.org/10.1016/j.ijbiomac.2019.04.120.

Verret L, Mann EO, Hang GB, Barth AMI, Cobos I, Ho K, Devidze N, Masliah E, Kreitzer AC, Mody I, Mucke L, Palop JJ (2012) Inhibitory Interneuron Deficit Links Altered Network Activity and Cognitive Dysfunction in Alzheimer Model. Cell 149:708–721 Available at: https://linkinghub.elsevier.com/retrieve/pii/S009286741200284X.

Villani A, Benjaminsen J, Moritz C, Henke K, Hartmann J, Norlin N, Richter K, Schieber NL, Franke T, Schwab Y, Peri F (2019) Clearance by Microglia Depends on Packaging of Phagosomes into a Unique Cellular Compartment. Dev Cell 49:77-88.e7 Available at: https://doi.org/10.1016/j.devcel.2019.02.014.

Vlkolinský R, Cairns N, Fountoulakis M, Lubec G (2001) Decreased brain levels of 2',3'-cyclic nucleotide-3'-phosphodiesterase in Down syndrome and Alzheimer's disease. Neurobiol Aging 22:547–553 Available at: www.elsevier.com/locate/neuaging.

Vondran MW, Singh H, Honeywell JZ, Dreyfus CF (2011) Levels of BDNF impact oligodendrocyte lineage cells following a cuprizone lesion. J Neurosci 31:14182–14190.

Voutsinos-Porche B, Bonvento G, Tanaka K, Steiner P, Welker E, Chatton JY, Magistretti PJ, Pellerin L (2003) Glial glutamate transporters mediate a functional metabolic crosstalk between neurons and astrocytes in the mouse developing cortex. Neuron 37:275–286.

Wakabayashi K, Ikeuchi T, Ishikawa A, Takahashi H (1998) Multiple system atrophy with severe involvement of the motor cortical areas and cerebral white matter. J Neurol Sci 156:114–117.

Wakabayashi K, Oyanagi K, Makifuchi T, Ikuta F, Homma A, Homma Y, Horikawa Y, Tokiguchi S (1994) Corticobasal degeneration: etiopathological significance of the cytoskeletal alterations. Acta Neuropathol 87:545–553 Available at: http://link.springer.com/10.1007/BF00293314.

Wake H, Ortiz FC, Woo DH, Lee PR, Angulo MC, Fields RD (2015) Nonsynaptic junctions on myelinating glia promote preferential myelination of electrically active axons. Nat Commun 6:7844 Available at: http://www.nature.com/doifinder/10.1038/ncomms8844.

Wang H, Li C, Wang H, Mei F, Liu Z, Shen HY, Xiao L (2013) Cuprizone-induced demyelination in mice: Age-related vulnerability and exploratory behavior deficit. Neurosci Bull 29:251–259.

Wang S, Young KM (2014) White matter plasticity in adulthood. Neuroscience 276:148–160 Available at: http://linkinghub.elsevier.com/retrieve/pii/S0306452213008713.

Watanabe M, Sakurai Y, Ichinose T, Aikawa Y, Kotani M, Itoh K (2006) Monoclonal antibody Rip specifically recognizes 2′,3′-cyclic nucleotide 3′-phosphodiesterase in oligodendrocytes. J Neurosci Res 84:525–533 Available at: http://doi.wiley.com/10.1002/jnr.20950.

Way SW, Podojil JR, Clayton BL, Zaremba A, Collins TL, Kunjamma RB, Robinson AP, Brugarolas

P, Miller RH, Miller SD, Popko B (2015) Pharmaceutical integrated stress response enhancement protects oligodendrocytes and provides a potential multiple sclerosis therapeutic. Nat Commun 6:1–13 Available at: http://www.nature.com/doifinder/10.1038/ncomms7532.

Weil MT, Möbius W, Winkler A, Ruhwedel T, Wrzos C, Romanelli E, Bennett JL, Enz L, Goebels N, Nave KA, Kerschensteiner M, Schaeren-Wiemers N, Stadelmann C, Simons M (2016) Loss of Myelin Basic Protein Function Triggers Myelin Breakdown in Models of Demyelinating Diseases. Cell Rep 16:314–322.

Weingarten MD, Lockwood AH, Hwo S-Y, Kirschner MW (1975) A protein factor essential for microtubule assembly. Proc Natl Acad Sci 72:1858–1862 Available at: http://www.pnas.org/content/72/5/1858.short.

Willem M et al. (2015) σ-Secretase processing of APP inhibits neuronal activity in the hippocampus. Nature 526:443–447.

Wilson R, Brophy PJ (1989) Role for the oligodendrocyte cytoskeleton in myelination. J Neurosci Res 22:439–448 Available at: http://onlinelibrary.wiley.com/doi/10.1002/jnr.490220409/full.

Wisco JJ, Killiany RJ, Guttmann CRG, Warfield SK, Moss MB, Rosene DL (2008) An MRI study of age-related white and gray matter volume changes in the rhesus monkey. Neurobiol Aging 29:1563–1575 Available at: http://linkinghub.elsevier.com/retrieve/pii/S0197458007001303.

Wolswijk G, Noble M, Wren D, Munro P, Noble M (1989) Identification of an adult-specific glial progenitor cell. Development 27:387–400 Available at: http://dev.biologists.org/content/develop/105/2/387.full.pdf.

Wolswijk G, Riddle PN, Noble M (1990) Coexistence of perinatal and adult forms of a glial progenitor cell during development of the rat optic nerve.

Wong AW, Xiao J, Kemper D, Kilpatrick TJ, Murray SS (2013) Oligodendroglial expression of TrkB independently regulates myelination and progenitor cell proliferation. J Neurosci 33:4947–4957.

Wren D, Wolswijk G, Noble M (1992) In vitro analysis of the origin and maintenance of O-2Aadult progenitor cells. J Cell Biol 116:167–176 Available at: http://jcb.rupress.org/content/116/1/167.abstract.

Wright AL, Zinn R, Hohensinn B, Konen LM, Beynon SB, Tan RP, Clark IA, Abdipranoto A, Vissel B (2013) Neuroinflammation and Neuronal Loss Precede Aβ Plaque Deposition in the hAPP-J20 Mouse Model of Alzheimer's Disease Guillemin GJ, ed. PLoS One 8:e59586 Available at: http://dx.plos.org/10.1371/journal.pone.0059586.

Wu D, Tang X, Gu LH, Li XL, Qi XY, Bai F, Chen XC, Wang JZ, Ren QG, Zhang ZJ (2018) LINGO-1 antibody ameliorates myelin impairment and spatial memory deficits in the early stage of 5XFAD mice. CNS Neurosci Ther 24:381–393.

Wu Y, Ma Y, Liu Z, Geng Q, Chen Z, Zhang Y (2017) Alterations of myelin morphology and oligodendrocyte development in early stage of Alzheimer's disease mouse model. Neurosci Lett 642:102–106 Available at: http://linkinghub.elsevier.com/retrieve/pii/S0304394017301131.

Wyss JM, Swanson LW, Cowan WM (1980) The organization of the fimbria, dorsal fornix and ventral hippocampal commissure in the rat. Anat Embryol (Berl) 158:303–316.

Xiao L, Ohayon D, McKenzie IA, Sinclair-Wilson A, Wright JL, Fudge AD, Emery B, Li H, Richardson WD (2016) Rapid production of new oligodendrocytes is required in the earliest stages of motor-skill learning. Nat Neurosci 19:1210–1217 Available at: http://dx.doi.org/10.1038/nn.4351.

Xiao L, Xu H, Zhang Y, Wei Z, He J, Jiang W, Li X, Dyck LE, Devon RM, Deng Y, Li XM (2008) Quetiapine facilitates oligodendrocyte development and prevents mice from myelin breakdown and behavioral changes. Mol Psychiatry 13:697–708.

Xing YL, Roth PT, Stratton JAS, Chuang BHA, Danne J, Ellis SL, Ng SW, Kilpatrick TJ, Merson TD (2014) Adult Neural Precursor Cells from the Subventricular Zone Contribute Significantly to Oligodendrocyte Regeneration and Remyelination. J Neurosci 34:14128–14146.

Xu X Bin, Fan SJ, He Y, Ke X, Song C, Xiao Y, Zhang WH, Zhang JY, Yin XP, Kato N, Pan BX (2017) Loss of Hippocampal Oligodendrocytes Contributes to the Deficit of Contextual Fear Learning in Adult Rats Experiencing Early Bisphenol A Exposure. Mol Neurobiol 54:4524–4536.

Xu D-E, Zhang W-M, Yang ZZ, Zhu H-M, Yan K, Li S, Bagnard D, Dawe GS, Ma Q-H, Xiao Z-C (2014) Amyloid precursor protein at node of Ranvier modulates nodal formation. Cell Adh Migr 8:396–403 Available at: http://www.tandfonline.com/doi/full/10.4161/cam.28802.

Xu H, Yang HJ, McConomy B, Browning R, Li XM (2010) Behavioral and neurobiological changes in C57BL/6 mouse exposed to cuprizone: Effects of antipsychotics. Front Behav Neurosci 4:1–10.

Xu J, Chen S, Ahmed SH, Chen H, Ku G, Goldberg MP, Hsu CY (2001) Amyloid-β Peptides Are Cytotoxic to Oligodendrocytes. J Neurosci 21:RC118–RC118 Available at: http://www.ncbi.nlm.nih.gov/pubmed/11150354.

Xu Y, Jack CR, O'brien PC, Kokmen E, Smith GE, Ivnik RJ, Boeve BF, Tangalos RG, Petersen RC (2000) Usefulness of MRI measures of entorhinal cortex versus hippocampus in AD. Neurology 54:1760–1767 Available at: http://www.neurology.org/content/54/9/1760.short.

Yamada K, Holth JK, Liao F, Stewart FR, Mahan TE, Jiang H, Cirrito JR, Patel TK, Hochgräfe K, Mandelkow EM, Holtzman DM (2014) Neuronal activity regulates extracellular tau in vivo. J Exp Med 211:387–393.

Yang Y, Cheng Z, Tang H, Jiao H, Sun X, Cui Q, Luo F, Pan H, Ma C, Li B (2017) Neonatal Maternal Separation Impairs Prefrontal Cortical Myelination and Cognitive Functions in Rats Through Activation of Wnt Signaling. Cereb Cortex 27:2871–2884.

Yasuhara O, Kawamata T, Aimi Y, McGeer EG, McGeer PL (1994) Two types of dystrophic neurites in senile plaques of alzheimer disease and elderly non-demented cases. Neurosci Lett 171:73–76.

Yeung MSY, Djelloul M, Steiner E, Bernard S, Salehpour M, Possnert G, Brundin L, Frisén J (2019) Dynamics of oligodendrocyte generation in multiple sclerosis. Nature 566:538–542 Available at: http://dx.doi.org/10.1038/s41586-018-0842-3.

Yeung MSY, Zdunek S, Bergmann O, Bernard S, Salehpour M, Alkass K, Perl S, Tisdale J, Possnert G, Brundin L, Druid H, Frisén J (2014) Dynamics of Oligodendrocyte Generation and Myelination in the Human Brain. Cell 159:766–774 Available at: http://linkinghub.elsevier.com/retrieve/pii/S0092867414012987.

Yin X, Crawford TO, Griffin JW, Tu PH, Lee VMY, Li C, Roder J, Trapp BD (1998) Myelin-associated glycoprotein is a myelin signal that modulates the caliber of myelinated axons. J Neurosci 18:1953–1962.

Yin X, Kidd GJ, Ohno N, Perkins GA, Ellisman MH, Bastian C, Brunet S, Baltan S, Trapp BD (2016a) Proteolipid protein-deficient myelin promotes axonal mitochondrial dysfunction via altered metabolic coupling. J Cell Biol 215:531–542 Available at: http://www.jcb.org/lookup/doi/10.1083/jcb.201607099.

Yin X, Peterson J, Gravel M, Braun PE, Trapp BD (1997) CNP overexpression induces aberrant oligodendrocyte membranes and inhibits MBP accumulation and myelin compaction. J Neurosci Res 50:238–247.

Yin Y, Gao D, Wang Y, Wang Z-H, Wang X, Ye J, Wu D, Fang L, Pi G, Yang Y, Wang X-C, Lu C, Ye K, Wang J-Z (2016b) Tau accumulation induces synaptic impairment and memory deficit by calcineurin-mediated inactivation of nuclear CaMKIV/CREB signaling. Proc Natl Acad Sci U S A 113:E3773-81 Available at: http://www.pnas.org/lookup/doi/10.1073/pnas.1604519113.

Yoshiyama Y, Higuchi M, Zhang B, Huang S-M, Iwata N, Saido TC, Maeda J, Suhara T, Trojanowski JQ, Lee VM-Y (2007) Synapse Loss and Microglial Activation Precede Tangles in a P301S Tauopathy Mouse Model. Neuron 53:337–351 Available at: http://linkinghub.elsevier.com/retrieve/pii/S089662730700030X.

Young KM, Psachoulia K, Tripathi RB, Dunn S-J, Cossell L, Attwell D, Tohyama K, Richardson WD (2013) Oligodendrocyte Dynamics in the Healthy Adult CNS: Evidence for Myelin Remodeling. Neuron 77:873–885 Available at: http://linkinghub.elsevier.com/retrieve/pii/S0896627313000500.

Yuste R (2015) From the neuron doctrine to neural networks. Nat Rev Neurosci 16:487–497 Available at: http://dx.doi.org/10.1038/nrn3962.

Zalc B, Monge M, Dupouey P, Hauw JJ, Baumann NA (1981) Immunohistochemical localization of galactosyl and sulfogalactosyl ceramide in the brain of the 30-day-old mouse. Brain Res 211:341–354 Available at: https://linkinghub.elsevier.com/retrieve/pii/000689938190706X.

Zawadzka M, Rivers LE, Fancy SPJ, Zhao C, Tripathi R, Jamen F, Young K, Goncharevich A, Pohl H, Rizzi M, Rowitch DH, Kessaris N, Suter U, Richardson WD, Franklin RJM (2010) CNS-Resident Glial Progenitor/Stem Cells Produce Schwann Cells as well as Oligodendrocytes

during Repair of CNS Demyelination. Cell Stem Cell 6:578–590 Available at: http://linkinghub.elsevier.com/retrieve/pii/S1934590910001578.

Zehr C, Lewis J, McGowan E, Crook J, Lin W-L, Godwin K, Knight J, Dickson DW, Hutton M (2004) Apoptosis in oligodendrocytes is associated with axonal degeneration in P301L tau mice. Neurobiol Dis 15:553–562 Available at: http://linkinghub.elsevier.com/retrieve/pii/S0969996103002857.

Zhan X, Jickling G, Ander B, Liu D, Stamova B, Cox C, Jin L-W, DeCarli C, Sharp F (2014) Myelin Injury and Degraded Myelin Vesicles in Alzheimer's Disease. Curr Alzheimer Res 11:232–238.

Zhan X, Jickling GC, Ander BP, Stamova B, Liu D, Kao PF, Zelin MA, Jin LW, Decarli C, Sharp FR (2015) Myelin basic protein associates with AβPP, Aβ1-42, and Amyloid plaques in cortex of Alzheimer's disease brain. J Alzheimer's Dis 44:1213–1229.

Zhang L, Chen C, Mak MSH, Lu J, Wu Z, Chen Q, Han Y, Li Y, Pi R (2020) Advance of sporadic Alzheimer's disease animal models. Med Res Rev 40:431–458 Available at: https://onlinelibrary.wiley.com/doi/abs/10.1002/med.21624.

Zhang Q, Ma C, Gearing M, Wang PG, Chin L-S, Li L (2018) Integrated proteomics and network analysis identifies protein hubs and network alterations in Alzheimer's disease. Acta Neuropathol Commun 6:19 Available at: http://www.ncbi.nlm.nih.gov/pubmed/29490708.

Zhang Y, Chen K, Sloan SA, Bennett ML, Scholze AR, O'Keeffe S, Phatnani HP, Guarnieri P, Caneda C, Ruderisch N, Deng S, Liddelow SA, Zhang C, Daneman R, Maniatis T, Barres BA, Wu JQ (2014) An RNA-sequencing transcriptome and splicing database of glia, neurons, and vascular cells of the cerebral cortex. J Neurosci 34:11929–11947.

Zhang Y, Schuff N, Du A-T, Rosen HJ, Kramer JH, Gorno-Tempini ML, Miller BL, Weiner MW (2009) White matter damage in frontotemporal dementia and Alzheimer's disease measured by diffusion MRI. Brain 132:2579–2592 Available at: http://brain.oxfordjournals.org/cgi/doi/10.1093/brain/awp071.

Zhen J, Qian Y, Weng X, Su W, Zhang J, Cai L, Dong L, An H, Su R, Wang J, Zheng Y, Wang X (2017) Gamma rhythm low field magnetic stimulation alleviates neuropathologic changes and rescues memory and cognitive impairments in a mouse model of Alzheimer's disease. Alzheimer's Dement Transl Res Clin Interv 3:487–497 Available at: https://doi.org/10.1016/j.trci.2017.07.002.

Zhou Q, Anderson DJ (2002) The bHLH transcription factors OLIG2 and OLIG1 couple neuronal and glial subtype specification. Cell 109:61–73 Available at: http://www.sciencedirect.com/science/article/pii/S0092867402006773.

Zhou Q, Choi G, Anderson DJ (2001) The bHLH Transcription Factor Olig2 Promotes Oligodendrocyte Differentiation in Collaboration with Nkx2.2 less is known, however, about the corresponding mech-anisms that underlie temporal switches in the generation of particular cell types from a common .

Zhou Q, Wang S, Anderson DJ (2000) Identification of a novel family of oligodendrocyte lineage-specific basic helix–loop–helix transcription factors. Neuron 25:331–343 Available at: http://www.sciencedirect.com/science/article/pii/S0896627300808983.

Zhu Q, Zhao X, Zheng K, Li H, Huang H, Zhang Z, Mastracci T, Wegner M, Chen Y, Sussel L, Qiu M (2014) Genetic evidence that Nkx2.2 and Pdgfra are major determinants of the timing of oligodendrocyte differentiation in the developing CNS. Development 141:548–555 Available at: http://dev.biologists.org/cgi/doi/10.1242/dev.095323.

Zhu X, Bergles DE, Nishiyama A (2007) NG2 cells generate both oligodendrocytes and gray matter astrocytes. Development 135:145–157 Available at: http://dev.biologists.org/cgi/doi/10.1242/dev.004895.

Zhu X, Hill RA, Dietrich D, Komitova M, Suzuki R, Nishiyama A (2011) Age-dependent fate and lineage restriction of single NG2 cells. Development 138:745–753.

Zhu X, Hill RA, Nishiyama A (2008) NG2 cells generate oligodendrocytes and gray matter astrocytes in the spinal cord. Neuron Glia Biol 4:19–26 Available at: http://www.journals.cambridge.org/abstract_S1740925X09000015.

Zonouzi M, Scafidi J, Li P, McEllin B, Edwards J, Dupree JL, Harvey L, Sun D, Hübner CA, Cull-Candy SG, Farrant M, Gallo V (2015) GABAergic regulation of cerebellar NG2 cell development is altered in perinatal white matter injury. Nat Neurosci 18:674–682 Available at: http://www.nature.com/doifinder/10.1038/nn.3990.

Zott B, Busche MA, Sperling RA, Konnerth A (2018) What Happens with the Circuit in Alzheimer's Disease in Mice and Humans? Annu Rev Neurosci 41:277–297 Available at: https://www.annualreviews.org/doi/10.1146/annurev-neuro-080317-061725.